UNIVERSITY OF SOUTHAMPTON

FACULTY OF ENGINEERING, SCIENCE AND MATHEMATICS

INSTITUTE OF SOUND AND VIBRATION RESEARCH

Modelling approaches for the low-frequency analysis of built-up structures with non-deterministic properties

by

Lars Hinke

Thesis for the degree of Doctor of Philosophy

April 2008

UNIVERSITY OF SOUTHAMPTON

ABSTRACT

FACULTY OF ENGINEERING, SCIENCE AND MATHEMATICS
INSTITUTE OF SOUND AND VIBRATION RESEARCH

Doctor of Philosophy

Modelling approaches for the low-frequency analysis of built-up structures with non-deterministic properties

by Lars Hinke

Virtual simulations of the behaviour of mechanical systems are of widespread use in academia and industry. Mechanical structures are often analysed using the finite element method, where deterministic models with one particular set of physical parameters are employed. However, the underlying assumption that the input data is precisely known is in general not valid, because there are uncertainties about the parameters, often until the last stage of the design cycle and even when the product is in service. Furthermore, every manufacturing process naturally introduces some product variability, which is inevitable. These effects can be compensated for by the application of safety factors. However, with the increasing requirements towards product performance, the effects of non-deterministic properties are of growing concern and advanced methods are needed that properly take them into account. In this context, it is often more important to predict the variation in the response than attempt to further improve the accuracy of a deterministic model. A number of viable methods to take non-deterministic properties into account already exist, but their computational efficiency and applicability have to be increased.

In this thesis, a framework for the non-deterministic analysis of built-up structures using component mode synthesis (CMS) is presented. It is shown how several coordinate systems in CMS can be used advantageously for the quantification and propagation of non-deterministic data. A specific approach, based on considering the variation in component natural frequencies only, is introduced and its efficiency and accuracy investigated. The application of perturbational relations for uncertainty propagation in CMS is discussed. The framework of CMS is also used to combine qualitatively different uncertain data and the inclusion of experimental data is addressed. Overall, CMS methods can be used to reduce the numerical costs, improve the applicability of the approaches and also gain some physical insight for a structural dynamic problem with non-deterministic properties. Furthermore, several

contributions are made to simulation methods that are usually applied in connection with the CMS approach. Different concepts for non-deterministic modal superposition are presented, which can be used to estimate the variation in frequency response functions from uncertain modal data. The application of the Line-Sampling simulation method, as an advanced Monte Carlo approach, to structural dynamic problems is shown. Finally, the modelling of spatial variations in components using random fields and the implementation in existing finite element models are addressed. Numerical examples are presented throughout.

To my family.

Contents

List of Figures

List of Tables

Declaration of Authorship

I, Lars Hinke, declare that the thesis entitled 'Modelling approaches for the low-frequency analysis of built-up structures with non-deterministic properties' and the work presented in the thesis are both my own, and have been generated by me as the result of my own original research.

I confirm that this work was done wholly or mainly while in candidature for a research degree at this university; where I have consulted the published work of others, this is always clearly attributed; I have acknowledged all main sources of help; parts of this work have been published in references [3–8].

Lars Hinke

April 2008

Acknowledgments

I would like to thank my supervisors Brian Mace and Tim Waters for their support and encouragement during the past years. I feel very privileged to have been working with them. Further, I would like to thank Neil Ferguson, Prasanth Nair and Fadi Dohnal for their helpful comments and suggestions for this thesis.

I acknowledge the financial support by the European Commission in the framework of the Marie-Curie Research Training Network 'MADUSE'. The activities and the time spent with colleagues and friends in the 'MADUSE' community has benefited me greatly. I am also grateful to The Royal Academy of Engineering and the British Council for funding my research exchanges.

Many thanks to all staff and colleagues at the Institute of Sound and Vibration Research, and especially those in the Dynamics Group, who have made my time in Southampton an enjoyable experience.

This thesis is dedicated to my family. They have always supported me during my studies including the associated travel around the world.

Abbreviations

cdf	Cumulative density function
$COV(p)$	Covariance matrix of p
CV	Coefficient of variation
CMS	Component mode synthesis
diag	Diagonal matrix
DOF	Degree of freedom
FE	Finite element
FRF	Frequency response function
KL	Karhunen-Loève
LS	Line-Sampling
MC	Monte Carlo
pdf	Probability density function
SEA	Statistical energy analysis

List of Symbols

Latin letters

A	Receptance matrix $[m/N]$
A	Area of the cross-section $[m^2]$
b	Width of beam $[m]$
B	Component modal matrix
C	Transformation matrix, damping matrix
D	Global modal matrix
E	Young's modulus $[N/m^2]$
f	Frequency $[Hz]$, force $[N]$
F	Force magnitude$[N]$
G	Flexibility matrix
G	Shear modulus $[N/m^2]$
h	Thickness $[m]$
H	Constraint matrix
I	Second moment of area $[m^4]$
K	Stiffness matrix
L	Global modal matrix
L	Length $[m]$
M	Mass matrix
M	Modal overlap
n	Number of a quantity
p	Physical parameter

q Modal coordinate

$\mathbf{R}$ Sensitivity matrix

$\mathbf{S}$ Sensitivity matrix, stochastic overlap

$\mathbf{T}$ Sensitivity matrix

u Displacement $[m]$

v Independent component modal coordinates

w Global modal coordinates

x Location

Greek letters

α Receptance, level of membership

δ Kronecker delta

ζ Standard normal random variable

η Modal loss factor

$\boldsymbol{\kappa}$ Modal stiffness matrix

λ Eigenvalue

$\boldsymbol{\mu}$ Modal mass matrix

ν Poisson's ratio

ρ Mass density $[kg/m^3]$

σ Standard deviation

$\boldsymbol{\upsilon}$ Characteristic constraint modes

$\boldsymbol{\phi}$ Normal modes in CMS

$\boldsymbol{\Psi}$ Static constraint modes in CMS

ω Angular frequency $[2\pi f]$

Vector and matrix quantities are denoted in lower and upper case bold font respectively.

Superscripts and subscripts

B	Boundary DOF
fi	Fixed
fr	Free
gl	Global
I	Internal DOF
L	Lower limit
M	Master DOF
R	Reduced vector or matrix
S	Slave DOF
U	Upper limit
α	Component α
β	Component β

Chapter 1

Introduction and background

1.1 Preface and motivation

All industrial sectors face the challenge of improving the performance and quality of their products and, at the same time, reducing the development time and cost. This can be achieved by employing virtual prototyping and simulation, i.e. using numerical models. In this way, the optimal product design can be found at an early stage in the product development cycle, where the cost associated with changes and modifications is small, and the number and range of necessary practical tests can be reduced. Hence, there is a constant need for appropriate modelling and simulation methods and tools. In this context, the effects of non-deterministic properties are of growing concern and advanced approaches are needed to take them into account.

1.1.1 Virtual simulation and non-deterministic effects

Figure 1.1 shows the outline of a typical computer simulation. Input data is specified for the numerical model of a real system and the response is calculated. Mechanical structures are often analysed using the finite element method (FEM) [9, 10]. In a structural dynamic analysis [11, 12], the input parameters are mass, stiffness and damping properties and the response quantities of interest can be frequency response functions (FRFs), eigenfrequencies etc. If a physical realisation of the structure is available, response measurements can be performed and compared with the calculated response to validate the numerical model.

In general, methods for the analysis of mechanical structures employ deterministic models with one particular set of physical input parameters. However, the underlying assumption that the input data is precisely known is in general not valid, because there are uncertainties about the parameters, often until the last stage of the design cycle and even when the product is in service. There are also uncertain-

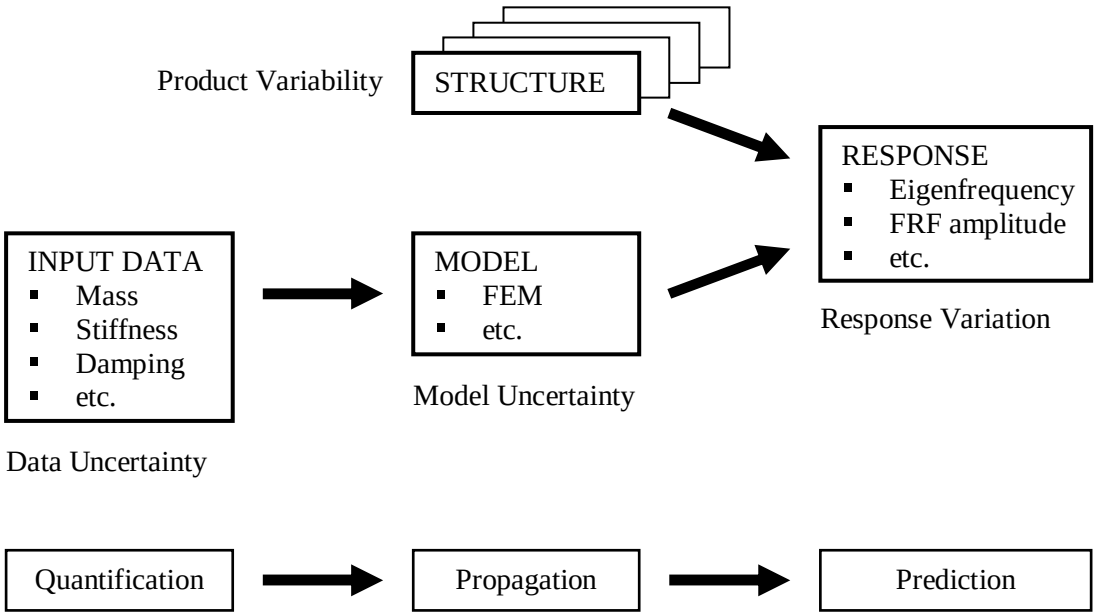

Figure 1.1: *Outline of a numerical simulation with non-deterministic effects.*

ties about the model, because it is always an idealisation of the real system, based on assumptions and approximations. Furthermore, every manufacturing process naturally introduces some product variability, which is inevitable. These sources of uncertainty and variability are indicated in Figure 1.1, and lead to variation in the response. The non-deterministic effects can be compensated for by the application of safety factors. However, with the increasing requirements towards product performance, advanced methods are needed that properly take these aspects into account. In this context, it is often more important to predict the variations in the response than attempt to further improve the accuracy of a deterministic model. This forward analysis concerns the quantification of uncertainties and variabilities, their numerical propagation through the model and the prediction of variations in the system response (see Figure 1.1).

Considering non-deterministic effects also implies changes to the objective of inverse analyses, such as optimisation and model updating [13]. Instead of optimising the value of a certain response quantity, it might be important to minimise its sensitivity with respect to changes in the input parameters and the model. In the context of product variability, sometimes an ensemble of different measurements for nominally identical products is available. The model should then be updated such that it predicts the mean response and its variations. The overall objective of all non-deterministic analyses is to achieve a more robust design.

The work presented in this thesis concerns modelling approaches for the dynamic analysis of mechanical structures based on the finite element method. It is

confined to the forward analysis, addressing the quantification of non-deterministic properties in the structure and their subsequent propagation through the model. Non-determinism in the excitation is not considered.

1.1.2 Types of non-determinism

There are many different classifications for non-deterministic effects. In the following, three complementary definitions based on the origin and cause of the variations, the way they are described in the modelling process and the point at which they are quantified in the numerical model will be presented.

The sources of non-determinism can be distinguished into two fundamentally different categories [14]. **Reducible uncertainty**, also known as epistemic uncertainty, is due to a lack of knowledge, especially in the early stages of the design process and even when a product is in service. It can be removed by gathering more information. The uncertainty associated with a development process can be purely man-made, for example if input parameters of an initial design are expected to change over time and the resulting variations in the response are to be predicted. When a product is in service, there is often incomplete information about the accuracy of the model, for example the damping properties. However, this means that the data might be either correct by chance or incorrect. **Irreducible uncertainty or variability**, also known as aleatory uncertainty, describes inherent, naturally introduced variation that cannot be removed. It can be further separated into intra-variability and inter-variability, concerning the variation of the properties of one product with time and the variation of the properties of more than one realisation of a product, respectively. Intra-variability is due to environmental effects (e.g. temperature), operating conditions, wear, fatigue and so on. Inter-variability describes differences between individual realisations of a product, which can be due to variations in the material and geometric properties and the manufacturing process (tolerances etc.). A comprehensive survey of sources of uncertainty and variability in general FE analysis is given by Alvin [15]. Although the definition of these two categories is widely accepted in the literature, the use of the terminology is not unambiguous. The term 'uncertainty' alone is often used to describe all non-deterministic effects.

From an engineering and design point of view, it is important to understand the source of the uncertainties. However, when it comes to numerical simulation, the variation has to be quantified to make it accessible for the modelling. In general this step is of crucial importance for the analysis, because it determines the calculation approaches that can be applied and the quality of the results that can be achieved.

Two different classes of a non-deterministic analysis, based on the quantification of the uncertainty, can be defined. In **possibilistic approaches** the variation of a parameter is specified by a range of possible values, given by a lower and an upper bound for example. It is only known that there are possible realisations within the interval, but no information about their likelihood are given. Similarly, the output of any possibilistic analysis in general can not provide any information about the probability of events and only intervals of response quantities, such as FRF envelopes, can be obtained. On the other hand, in **probabilistic approaches** information about the probability of events is included. The variation of a parameter is typically specified by a probability density function (pdf), for example by assuming a common distribution, such as a normal distribution. Therefore, distribution functions and statistics of the response, such as a probability of failure, can be calculated. In general, product variability has an underlying probability distribution that can be quantified by observations. If there is not enough data available however, it might be reasonable to use a possibilistic description instead. Epistemic uncertainties in general can not be associated with distinct probabilities and a possibilistic approach is often applied.

Finally, a separation can be made into **parametric and non-parametric uncertainties**, the former directly related to given parameters and the latter often associated with all other effects, such as the accuracy of the model. The numerical model of a real system, including the specified parameters, is always an idealisation. It is therefore impossible to cover all non-deterministic effects by considering parametric uncertainties only. However, in many cases it is reasonable to quantify variation in the input parameters only, especially in a low-frequency analysis and when the model has been validated. Product variability can often be appropriately quantified using parametric approaches. Additionally, by quantifying uncertainties numerically or experimentally in non-physical parameters, such as modal properties, some of the model uncertainties can be included. It is often observed that the statistics of various quantities are asymptotic, especially for higher frequencies. The natural frequency spacing, for example, can then be described by the Gaussian orthogonal ensemble [16]. Furthermore, response levels often have a normal or log-normal distribution. Therefore, it is possible to predict the response variations inherent in the design without the need to quantify specific variations in input parameters. Other non-parametric approaches focus on the random structure of the system matrices, utilising for example random matrix theory [17] and matrix variate distributions [18]. Methods have been proposed that are based on the direct construction of a probabilistic model for the mass, damping and stiffness matrices of a FE model [19, 20]. Furthermore, a unified approach [21] to model both paramet-

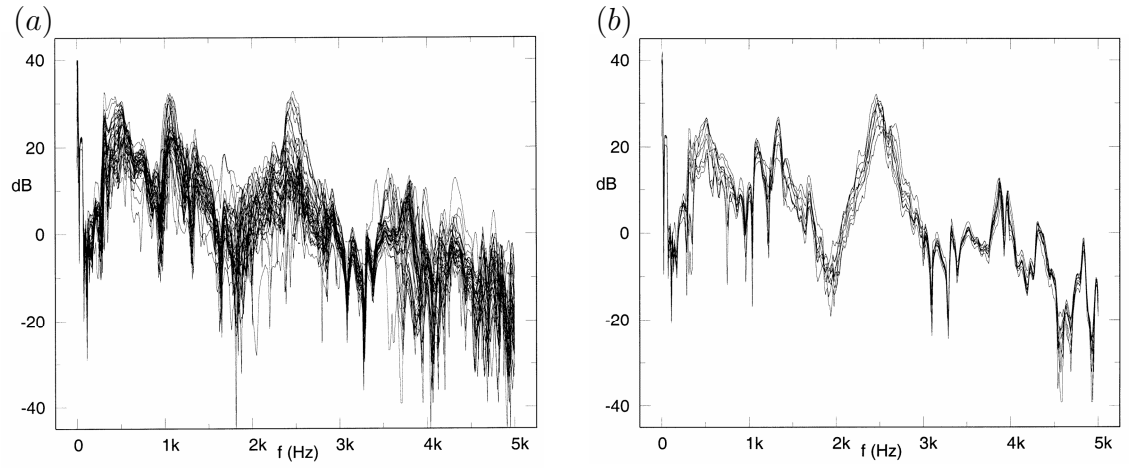

Figure 1.2: *Measured FRFs of beer cans: (a) variability in nominal identical structures, (b) repeatability [1].*

ric and non-parametric uncertainties simultaneously has been proposed. Random matrix theory also gives rise to asymptotic statistics.

Various types of non-determinism will be considered in this work, with a focus on parametric uncertainties. Both probabilistic and possibilistic approaches will be addressed and some emphasis is placed on combining them, which can be a realistic approach in some industrial applications.

1.1.3 Uncertainty assessment - experimental measurements

The inherent variations between nominally identical products are often of interest in experimental investigations. Fahy [1] took 41 nominal identical mechanical structures (cans) and measured the FRFs for acoustic excitation. Figure 1.2a shows the ensemble of 41 FRFs. There is a large variation over the whole frequency range and only a few resonance peaks can be matched between the realisations. Figure 1.2b shows a test of the repeatability of the measurements, where the same structure has been measured, removed and replaced 8 times. There is some variation between the 8 FRFs, which is due to differences and errors in the measurement set-up and procedure. Therefore, it can be assumed that the higher variations in Figure 1.2a are due to differences in the structural properties of the 41 cans.

Kompella and Bernhard [2] carried out an extensive experimental campaign measuring structure-borne noise on a large number of nominally identical vehicles. The ensemble of 98 FRFs is shown in Figure 1.3. The variations are considerable, but resonance peaks can be identified at lower frequencies. A comprehensive analysis of measured variability data for this, and other experimental campaigns, has been performed in [22, 23]. The work focused on the FRF magnitude distribution at a

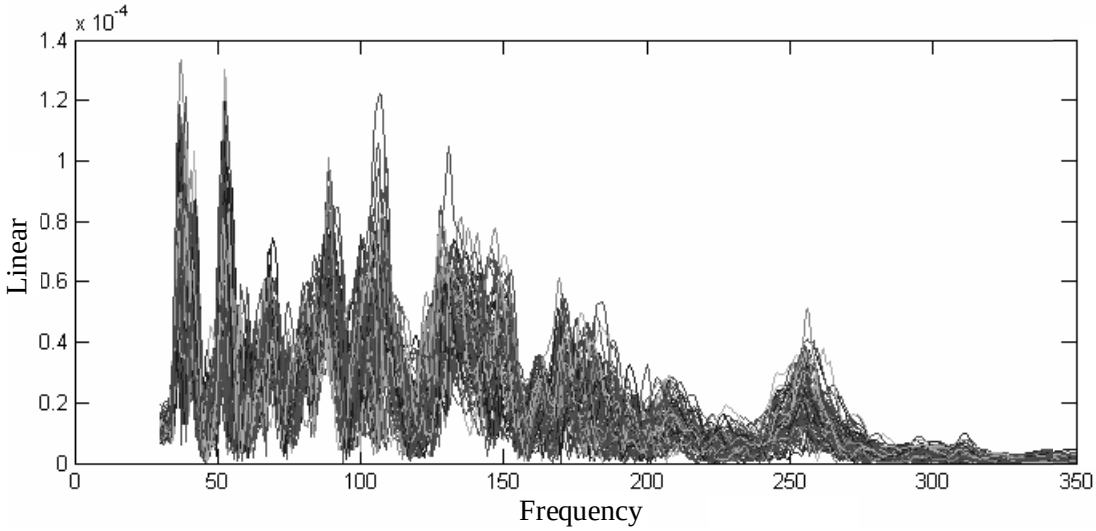

Figure 1.3: *Ensemble of measured FRFs for 98 nominal identical vehicles [2].*

fixed frequency and the change of the distribution with frequency. It has been found that a normal distribution is a reasonably good fit to the variations. In general, if an assumption about the probability distribution of a input parameter has to be made, a normal distribution seems to be most appropriate. It reflects the expected behaviour that there is a concentration of realisations around the mean and fewer realisations far away from the mean. Other works on the variations within nominally identical product lines include that of Brown and Gear [24].

This thesis focuses on numerical methods for non-deterministic modelling and no new experimental results will be presented. Newly proposed computationally efficient approaches will be compared with numerical reference solutions and virtual experiments are conducted. However, theoretical concepts that have the purpose of improving the quantification of experimental data will be discussed.

1.1.4 Frequency range

In structural dynamics, the modelling requirements and objectives depend on the frequency of vibration [25]. Many modelling approaches, such as FEM, are based on domain discretisation, where the mesh size has to be refined for higher frequencies in order to obtain results of similar detail and accuracy. Therefore, the model size and the required computing resources increase with frequency and an analysis becomes numerically more expensive. On the other hand, the required level of detail of an analysis can differ depending on the frequency range of interest. Figure 1.4 shows a typical ensemble of FRFs for a non-deterministic mechanical system, where the FRF of one realisation is highlighted. The entirety of all possible FRFs (dark area) can

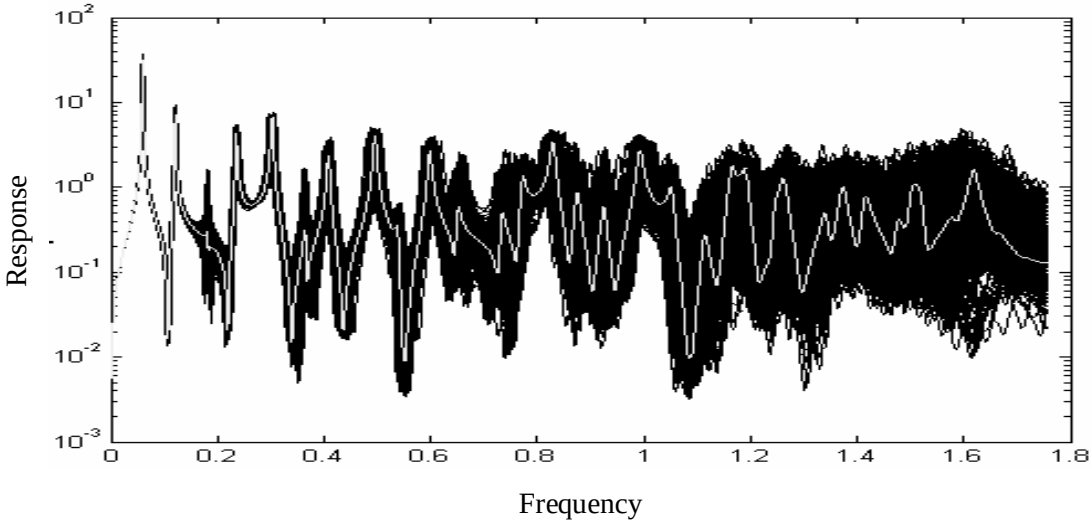

Figure 1.4: *Ensemble of FRFs and an individual FRF realisation.*

be described by a lower and upper FRF envelope. Some frequency characteristics of a deterministic FRF realisation can be described by the modal overlap $M(f)$, quantifying the number of modes that are significantly excited in a system at any one frequency f. It is a dimensionless parameter, defined by $M(f) = n(f)\,\Delta(f)$, where $n(f)$ is the modal density, defined as the expected value of the number of modes per unit frequency, and $\Delta(f)$ is the half-power bandwidth, which is the difference between the frequencies where the FRF magnitude of a mode falls to $1/\sqrt{2}$ of the peak value. Furthermore, if the whole ensemble of FRFs is considered, there is a degree of overlap due to the spread of individual natural frequencies. It can be quantified by the stochastic overlap $S(f)$, defined by $S(f) = 2\,n(f)\,\sigma(f)$, where $\sigma(f)$ is the standard deviation of a natural frequency. In general, the modal density, the half-power bandwidth and the standard deviation of natural frequencies increase with frequency and so do the modal and stochastic overlaps. These parameters can also be used as criteria to determine the required level of detail.

At low frequencies, both the modal and stochastic overlaps are typically small and typically only one or two modes of vibration contribute to the response of the structure at any one frequency. The individual resonance peaks are distinct and do not overlap, even when their variation is considered. Therefore, detailed structural results for modal properties and the FRF are of interest. These can be calculated using standard finite element techniques and modal analysis. However, FE methods in general might require a very large model size and therefore be numerically costly. In connection with non-deterministic approaches, which often require that a deterministic problem is solved repeatedly, the numerical cost becomes a major factor. In the high frequency range, the modal and stochastic overlaps are typically greater

than unity and many modes of vibration contribute to the structural response at a given frequency. Individual resonance peaks cannot be recognised within the FRF envelope. Therefore, the required level of detail for modal properties is low and average quantities of the FRF are of interest. For this case, energy methods, such as statistical energy analysis (SEA) [26, 27], are often employed. The models are in general relatively small and the numerical cost does not pose a problem. In the mid-frequency region, neither FEM nor SEA alone seem appropriate. A detailed FE analysis is not necessary and also becomes unfeasible, because of the increase in numerical cost with frequency. On the other hand, high frequency energy methods do not provide the required level of detail. Therefore hybrid methods combining both approaches have been suggested [28]. Within a built-up structure, the contributions of components to the overall dynamic characteristics can be quite different. Some components require a detailed FE analysis and others can be appropriately modelled by energy methods [29].

This thesis will focus on low-frequency modal approaches for cases when relatively large finite element models are required to obtain detailed structural responses.

1.2 Approaches for a non-deterministic analysis

It is appropriate to classify methods for an uncertainty analysis into probabilistic and possibilistic approaches. In general, this determines the quantification and propagation of non-deterministic data and the form of output response.

1.2.1 Possibilistic approach

In possibilistic approaches [30], the basic quantification of a parameter variation is an interval, where only knowledge about a lower and upper bound is required. As shown in Figure 1.5, a lower and an upper limit (x_L, x_U) of the parameter x are given. There is no information about the probability of a realisation within the interval, i.e. there is no difference in the importance of a value near the middle of the interval compared to one near the bounds. In general, a baseline value within the interval is assumed for the deterministic problem. The difficulty lies in quantifying the bounds, which are in general taken to be conservative. However, the specification of a bound can easily be too conservative and unrealistic, especially if used to describe physical variability.

If the variation in input parameters is defined by an interval, the variation in the output can in general only be predicted as an interval. In Figure 1.6, the baseline frequency response function (FRF) and conservative estimates for the lower and

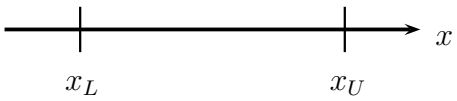

Figure 1.5: *Interval of random variable* x*:* x_L*,* x_U *- lower and upper bounds.*

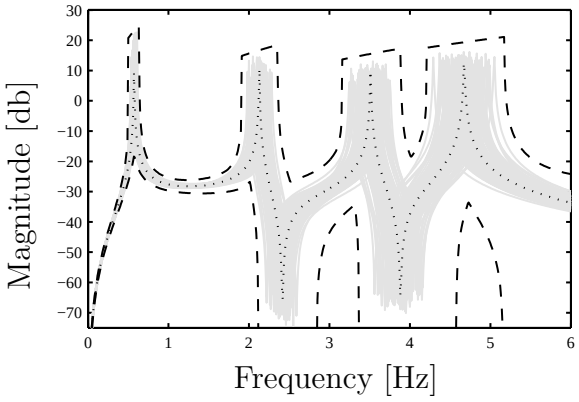

Figure 1.6: *Example FRF:* ——— *100 realisations;* ····· *baseline FRF;* – – – *lower and upper envelopes.*

upper FRF envelopes are shown. The goal of a possibilistic propagation approach [31] is to calculate the bounds on the response quantity of interest. If the problem is monotonic, i.e. the output depends monotonically on every input parameter, it is sufficient to consider all combinations of the bounds of the input parameters only, which is referred to as the vertex method [32]. The numerical cost of this approach is 2^n solutions of the deterministic problem, where n is the number of random variables. The results are conservative, because correlations between several interval variables and intermediate response calculations are neglected. If the conservatism is unreasonably high, advanced interval methods, such as affine analysis [33], can be applied to improve results. If the problem is non-monotonic, the vertex method does not necessarily lead to conservative results, because any parameter value within an interval may contribute to an extreme system response. In an approximate numerical approach, additional points within the interval can be considered to cover some of the non-monotonicity. The design of experiments (DOE) [34] methodology provides a framework to facilitate the selection of a set of points in the uncertain input parameter space. DOE methods apply to both experimental and numerical tests, where only a limited number of parameter realisations can be considered and an optimal selection has to be found.

There are approaches that extend the basic possibilistic concept by including additional information within the interval. Fuzzy sets, for example, have been used to represent incomplete information [35, 36]. Figure 1.7 shows a triangular fuzzy membership function, where a level of membership μ between 0 and 1 is indicated.

If $\mu(x) = 0$ then x is definitely not a member of the set, if $\mu(x) = 1$ then x is definitely a member of the set. For all $0 < \mu < 1$ the membership is not certain. This approach to uncertainty quantification is intended to be used for special types of uncertain data, where neither a pdf nor an interval are appropriate, such as lin-

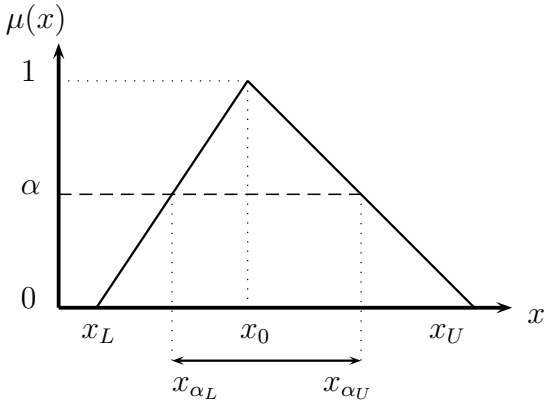

Figure 1.7: *Fuzzy membership function of random variable x: x_{α_L}, x_{α_U} - lower and upper bounds at membership level α, x_0 - crisp value at $\alpha = 1$.*

guistic data from expert opinion. In order to make the fuzzy membership function accessible for numerical propagation methods, it can be represented by a number of intervals [37]. At predefined levels of membership α, the fuzzy membership function is intersected to find an interval for this α-cut. Subsequently, general interval methods can be used and the output membership function can be reassembled from the output intervals. This approach can also be seen as a framework for combining several interval analyses, controlled by the shape of the fuzzy membership functions and the parameter α. Specific interval propagation techniques, such as the transformation method [38], have been developed for fuzzy membership functions. A review of possibilistic uncertainties in finite element analysis, with a focus on fuzzy methods, is given by Moens [30].

1.2.2 Probabilistic approach

In probabilistic approaches [39, 40], information about the likelihood and probability of events are included. In Figure 1.8 the variation in the parameter y is specified by a probability density function (pdf), with mean value y_0 and standard deviation σ_y. Similarly, the variation in the response can be quantified in terms of distribution functions or statistics. For example, Figure 1.9 shows percentiles for the FRF distribution. In practice there is often not enough data to quantify a distribution exactly and a standard pdf, such as a normal distribution, is assumed. The mean value can be taken as the deterministic value and only the variance has to be quantified. A normal distribution is often a reasonable assumption to model product variability in physical processes. In statistics, this is also supported by the Central Limit Theorem [41], which states that any sum of many independent and identically distributed variables with finite variance is approximately normally distributed. The unbounded tails of the normal distribution are often inconsistent with reality, which

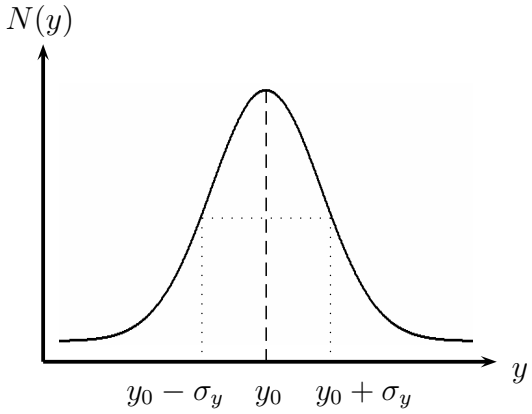

Figure 1.8: *Probability density function (pdf) of random variable y:* y_0 *- mean value,* σ_y *- standard deviation.*

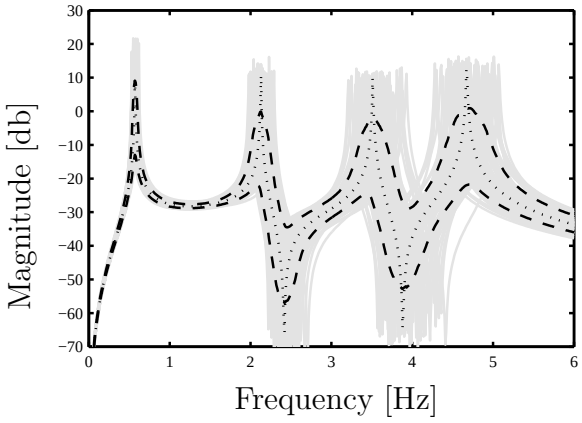

Figure 1.9: *Example FRF;* ▬ *100 realisations;* ····· *baseline FRF;* - - - 10 *and* 90 *percentiles.*

has to be taken into account.

Uncertain mechanical structures often have spatially varying properties, such as the thickness of metal panels, which can be represented by random fields [42]. In stochastic finite element methods [43], the continuous random fields are first discretised and represented in terms of a finite number of random variables, i.e. the number of degrees of freedom (DOFs) of the system. Subsequent decomposition schemes, such as the Karhunen-Loève (KL) expansion [44], lead to a system of random algebraic equations, which are accessible by uncertainty propagation methods.

The standard method for propagating probabilistic data is the Monte Carlo (MC) method [45–47]. In standard MC sampling, parameter values are randomly drawn according to their probability distributions and a deterministic problem is solved for each sample. The results are analysed to estimate response statistics and distribution functions. The method is very robust and converges to the exact solution as the sample size tends to infinity. It makes no approximations and considers all effects modelled in the deterministic problem. In general, a sample size of the order of 10 is sufficient to estimate the mean of a distribution function and a sample size of the order of 100 is required to obtain a reasonable estimate of the variance. However, the numerical cost to estimate a small probability of failure can be in the order of thousands of deterministic solutions.

In contrast to sampling approaches, there are various subspace projection schemes [48], such as polynomial chaos expansion [43] and stochastic reduced basis methods [49]. Other approaches for uncertainty quantification include Dempster-Shafer theory (DST), which is an evidence based approach [50, 51]. It allows one to consider a level of confidence in the probabilities of certain events. Similarities with fuzzy approaches and probability distributions have been shown [52].

1.3 Challenges for and solutions of a non-deterministic analysis

Virtual simulations of the behaviour of mechanical systems are of widespread use in academia and industry. There are well-established commercial software packages for the finite element analysis of mechanical structures. However, in general a deterministic model with one particular set of physical parameters is employed. The effects of non-deterministic properties are of growing concern in the design of engineering structures and a number of viable methods to take them into account already exist. In order for them to become of widespread use in industry, the additional challenges of a non-deterministic analysis have to be addressed. These are in general the increased numerical cost and the applicability and practicality of the approaches.

1.3.1 Numerical cost

For the analysis of a structure with non-deterministic properties, most approaches require that the deterministic problem is solved repeatedly and are therefore numerically expensive. Probabilistic methods, such as Monte Carlo sampling, may require a large sample size. The numerical cost of possibilistic approaches, such as interval methods, increases exponentially with the number of uncertain parameters. Therefore, research has focused on reducing both the number of necessary deterministic solutions and the calculation time for one deterministic run.

Reducing the number of necessary deterministic solutions. In a Monte Carlo analysis, the number of necessary evaluations can be reduced by using advanced sampling techniques [53]. These reduce the variance of the sampling estimator and achieve the same accuracy with a lower number of samples. The most common techniques are importance sampling [54], directional sampling [55], subset simulation [56] and Line-Sampling [57].

The DOE methodology can also be applied to create advanced MC methods to estimate the mean and variance of a distribution using a very low number of samples. Latin Hypercube sampling [58] is a version of stratified sampling, where it is ensured that the samples are taken more evenly from the input parameter distribution.

In a possibilistic interval analysis the number of required solutions mainly depends on the number of independent variables. Therefore a reduction in the number of variables or the inclusion of assumptions regarding their interdependence can reduce the numerical cost. In the case of non-monotonic possibilistic problems, the accuracy of the results is related to the number of simulations performed. The DOE

methodology provides a systematic approach to get the best results from a minimum number of deterministic runs. In this context, advanced transformation methods are available for the propagation of fuzzy membership functions [38]. Furthermore, hybrid exact/approximate techniques have been developed for the fuzzy finite element method [59].

Reducing the calculation time for one deterministic solution. In general, a smaller model can be solved faster and therefore most model reduction techniques, such as Guyan reduction [60] or component mode synthesis (CMS) [61], are appropriate to be applied in a non-deterministic analysis.

The calculation cost for one solution can also be reduced drastically, if numerically expensive operations, such as solving the eigenvalue problem, are replaced with numerically cheap formulations. First order perturbation methods using response sensitivities [62] are appropriate for low levels of uncertainty. For larger uncertainties, higher order perturbation or interpolation can be used. A systematic approach to select the reference solutions for an interpolation is given by the design of experiments methodology. It can also be used to construct an approximate response surface model (RSM) [63], which replaces the original model to provide a relationship between input parameters and response quantities. Although a replacement of the original model is often associated with errors due to approximations, these can often be neglected with respect to the level of uncertainty in the input data.

1.3.2 Applicability and practicality

The other main challenge to achieve a successful and beneficial use of non-deterministic simulation approaches is to increase their applicability and practicality. This concerns the quantification of uncertainties using available experimental or numerical data, and the combination of qualitatively and quantitatively different data, amongst others.

In order to increase the applicability, the requirements for industrial applications have to be considered. Approaches should support the use of standard finite element software and not be limited by the size and complexity of the model. In industrial applications, there can be a large number of uncertain parameters (> 100) with a considerable magnitude of variation. These could include physical, geometrical and material properties as well as loads and boundary conditions. Some approaches, such as Monte Carlo sampling, are independent of the number of uncertain parameters. Substructuring and model reduction techniques become more useful for larger models.

Empirical data should be used for uncertainty quantification wherever possible.

It is therefore important to assess what experimental data are likely to be obtained. Some theories and models for the quantification of non-deterministic effects (e.g. random fields) have been around for many decades, but the experimental data required to define them is often not available. In this context, the quantification of uncertainties in modal properties can be more practical.

In practice it is most likely that both probabilistic and possibilistic uncertainty descriptions are given within a built-up structure or an individual component. Therefore, the modelling has to consider their practical combination, i.e. defining some data probabilistically and some possibilistically.

The modelling of damping in structural dynamic models is a difficult problem. However, for some cases the variation in damping might be the most decisive factor for the variation in the response. In a modal analysis, it can be assumed that a change in damping only causes a change in response magnitude. Therefore, variability and uncertainty in damping can be considered independent of variations in eigenfrequencies and modeshapes.

Most mechanical structures comprise some sort of joints and often the effects of the uncertainty in joints can be more important than other sources of uncertainty in a structure. There is a wide range of dynamic characteristics between different joints and the behaviour of joints often differs greatly from the behaviour of the rest of the structure.

A promising approach to address several of these challenges is substructuring, which will be addressed in this thesis.

1.4 Scope of the thesis

The thesis concerns the dynamic analysis of mechanical structures that are modelled by the finite element method. The vibrations of multi-degree-of-freedom, viscously-damped linear systems is described by the differential equation

$$\mathbf{M}\ddot{\mathbf{u}} + \mathbf{C}\dot{\mathbf{u}} + \mathbf{K}\mathbf{u} = \mathbf{f} \tag{1.1}$$

where $\mathbf{M}$, $\mathbf{C}$ and $\mathbf{K}$ are the mass, damping and stiffness matrices, respectively, $\mathbf{u}$ is a vector of displacements and $\mathbf{f}$ a vector of forces. For free vibration ($\mathbf{f} = \mathbf{0}$), the undamped eigenvalue problem

$$[\mathbf{K} - \lambda_i \mathbf{M}]\, \boldsymbol{\phi}_i = \mathbf{0} \tag{1.2}$$

gives the ith eigenvalue and eigenvector λ_i and $\boldsymbol{\phi}_i$ respectively. If damping is assumed to be proportional (Rayleigh damping) then these eigenvectors are also eigenvectors of the damped system. This work considers low-frequency modal approaches for the forward analysis concerning eigenvalues, eigenvectors and frequency response functions. Parametric uncertainty in both physical and modal properties is considered. The excitation is deterministic and all properties are time-invariant.

At low-frequencies, the modal and stochastic overlaps are small and detailed information about the structural response is desired. The frequency response can be expressed in terms of modes of vibration, obtained from solving the eigenvalue problem. It is appropriate to first estimate the variation in the eigenvalues and eigenvectors and subsequently propagate these effects to the FRF. The thesis will present a framework for the non-deterministic analysis of built-up structures using component mode synthesis (CMS). First, the variation in modal properties at component level is estimated. Subsequently, it is propagated to the global modal level and to the global physical frequency response. In this context, it is shown how CMS is suitable to address several of the challenges of a non-deterministic analysis. Overall, CMS methods can be used to drastically reduce numerical costs, improve the applicability of the approaches and also gain some physical insight of the underlying problem. In addition, several advanced uncertainty propagation methods are presented that can be used in conjunction with a CMS model.

The next chapter reviews some of the basic concepts for a numerically efficient reanalysis of the eigenvalue problem, which is fundamental to linear modal analysis, but usually associated with high numerical costs. **Chapter 3** addresses the modelling of spatial variations in components using random fields and their implementation in existing finite element models. The concept of a random field model with a possibilistic parameter variation will be presented. Subsequently, **Chapter 4** focuses on model reduction techniques and the deterministic component mode synthesis method. **Chapter 5** discusses the advantages of substructuring and CMS for a non-deterministic analysis. These arise from that fact that each substructure can be treated independently regarding the quantification and propagation of non-deterministic data. For each component a qualitatively and quantitatively different analysis method can be chosen. A specific approach, based on considering the variation in component natural frequencies only, is introduced and its efficiency and accuracy investigated. The application of perturbational relations for uncertainty propagation is presented. The framework of CMS is also used to combine possibilistic and probabilistic data. Subsequently, free and fixed-interface methodologies in CMS are discussed in **Chapter 6**. In low-frequency approaches, the global frequency response can be expressed in terms of modal responses. **Chapter 7** discusses

various aspects of non-deterministic model superposition. A new approach to the estimation of frequency response function envelopes from possibilistic or probabilistic data is presented. The Monte Carlo method will be used to propagate all probabilistic uncertainties and especially to estimate percentiles of modal properties. Advanced Monte Carlo methods are essential for reducing the cost of the analysis and will be discussed in **Chapter 8**. Novel contributions will be made to the Line-Sampling technique, including its application to the estimation of distribution functions and its use in conjunction with random field models. The application case of an automotive windshield is presented in **Chapter 9**. The creation of an appropriate non-deterministic model, implementation within the finite element model and processing using commercial software are discussed.

In summary, the original contributions of this thesis are:

- CMS as a framework for the low-frequency analysis of built-up structures with non-deterministic properties (Chapters 5 and 6)
  - Advantages of substructuring and multi-level quantification and propagation of uncertainties
  - Application of perturbational methods within CMS
  - Assessment of approaches regarding efficiency, sources of inaccuracies and error
  - Combination of probabilistic and possibilistic approaches

- Uncertainty quantification (Chapters 3 and 6)
  - Possibilistic parameter variation in random field models
  - Free and fixed-interface methodologies in CMS

- Non-deterministic modal superposition (Chapter 7)
  - Proposal of new parameter set for the modal space
  - Combination of possibilistic and probabilistic approaches

- Application of Line-Sampling (Chapters 8 and 9)
  - Estimation of distribution functions and other statistics
  - Efficient combination of Line-Sampling and random field models

- Industrial application case (Chapter 9)
  - Implementation of random field in existing FE model
  - Automated analysis using a PERL script, MATLAB and NASTRAN software

Chapter 2

Eigensolution reanalysis

2.1 Introduction

This chapter concerns the numerically efficient reanalysis of the eigenvalue problem in the context of a non-deterministic analysis. The eigenvalue problem is one of the most important equations in structural dynamics and many other fields. It is essential for linear modal analysis and modal superposition. The eigenvalues correspond to resonance frequencies of the system and the eigenvectors can be used to perform a transformation from physical to modal coordinates. In general, the eigenvalue problem also involves the highest numerical cost in an analysis. Therefore, reducing the numerical cost and resources that are associated with the eigenvalue problem has a significant effect on making a non-deterministic analysis more efficient. This chapter reviews some basic concepts to replace the eigenvalue problem with numerically cheap algebraic equations. These are based on the fact that the reanalysis of the eigenvalue problem in a non-deterministic analysis often occurs only with small changes in the governing parameters. Some of the expressions will be used in later chapters, for example in combination with component mode synthesis.

2.2 Eigenvalue problem

Consider a multi-degree-of-freedom damped linear dynamic system with mass ($\mathbf{M}$), stiffness ($\mathbf{K}$) and damping ($\mathbf{C}$) matrices of size $n \times n$. The eigenvalue problem of the undamped system is given by

$$(\mathbf{K} - \lambda_i \mathbf{M})\, \boldsymbol{\phi}_i = \mathbf{0} \tag{2.1}$$

where λ_i and $\boldsymbol{\phi}_i$ are the eigenvalues and eigenvectors, respectively, $i = 1, 2, \ldots n$ and n is the number of degrees of freedom (DOFs).

Assuming that the system matrices are symmetric, real-valued and positive definite, the eigensolutions are real and the eigenvalues non-negative. As a consequence, the eigenvalue and eigenvector sensitivities are also real. In the case of a proportionally damped system (Rayleigh damping), the damping matrix can be diagonalised by the eigenvectors. Furthermore, the eigenvalue problem is self-adjoint and can also be written as

$$\boldsymbol{\phi}_i^T \left(\mathbf{K} - \lambda_i \mathbf{M}\right) = \mathbf{0} \tag{2.2}$$

because the right eigenvector coincides with the left eigenvector. The orthogonality conditions for mass-normalised eigenvectors are

$$\boldsymbol{\phi}_k^T \mathbf{M} \boldsymbol{\phi}_i = \delta_{ki} \tag{2.3}$$

$$\boldsymbol{\phi}_k^T \mathbf{K} \boldsymbol{\phi}_i = \lambda_k \delta_{ki} \tag{2.4}$$

where δ is the Kronecker Delta.

Changes in the stiffness or mass matrices lead to changes in the modal properties and therefore a reanalysis of the eigenvalue problem is required. However, an exact reanalysis, solving Equation 2.1, is often not feasible due to the high numerical cost associated with the eigenvalue problem. In the following, numerically cheap approximate reanalysis methods based on perturbation and interpolation will be reviewed.

2.3 First order modal sensitivities

A change in the ith eigenvalue ($\Delta\lambda_i$) due to changes in parameters (Δp_j) can be approximated using first order sensitivities in the form

$$\Delta\lambda_i \approx \sum_j \frac{\partial \lambda_i}{\partial p_j} \Delta p_j \tag{2.5}$$

where $\frac{\partial \lambda_i}{\partial p_j}$ is the derivative of the ith eigenvalue λ with respect to the jth parameter p evaluated when $\Delta p = 0$. A similar expression can be used for the variation in eigenvectors. The rate of change of eigenvalues and eigenvectors has been studied extensively [64–67]. Differentiation of Equation 2.1 with respect to a parameter p_j yields

$$\left(\frac{\partial \mathbf{K}}{\partial p_j} - \lambda_i \frac{\partial \mathbf{M}}{\partial p_j}\right) \boldsymbol{\phi}_i - \frac{\partial \lambda_i}{\partial p_j} \mathbf{M} \boldsymbol{\phi}_i + \left(\mathbf{K} - \lambda_i \mathbf{M}\right) \frac{\partial \boldsymbol{\phi}_i}{\partial p_j} = \mathbf{0} \tag{2.6}$$

Premultiplying by $\boldsymbol{\phi}_i^T$ and some manipulation leads to

$$\frac{\partial \lambda_i}{\partial p_j} = \boldsymbol{\phi}_i^T \left(\frac{\partial \mathbf{K}}{\partial p_j} - \lambda_i \frac{\partial \mathbf{M}}{\partial p_j} \right) \boldsymbol{\phi}_i \tag{2.7}$$

which involves derivatives of the mass and stiffness matrices as well as the baseline eigenvalues and eigenvectors.

The rate of change of an eigenvector with respect to a parameter p_j can be expressed as the sum of contributions from all eigenvectors with factors γ in the form

$$\frac{\partial \boldsymbol{\phi}_i}{\partial p_j} = \sum_l \gamma_{il} \boldsymbol{\phi}_l \tag{2.8}$$

Substituting this expression in Equation 2.6 and premultiplying by $\boldsymbol{\phi}_k^T$ gives

$$\boldsymbol{\phi}_k^T \left(\mathbf{K} - \lambda_i \mathbf{M} \right) \sum_{l=1}^{N} \gamma_{il} \boldsymbol{\phi}_l + \boldsymbol{\phi}_k^T \left(\frac{\partial \mathbf{K}}{\partial p_j} - \lambda_i \frac{\partial \mathbf{M}}{\partial p_j} \right) \boldsymbol{\phi}_i - \boldsymbol{\phi}_k^T \frac{\partial \lambda_i}{\partial p_j} \mathbf{M} \boldsymbol{\phi}_i = \mathbf{0} \tag{2.9}$$

which can be simplified to

$$\left(\lambda_k - \lambda_i \right) \gamma_{ik} + \boldsymbol{\phi}_k^T \left(\frac{\partial \mathbf{K}}{\partial p_j} - \lambda_i \frac{\partial \mathbf{M}}{\partial p_j} \right) \boldsymbol{\phi}_i - \frac{\partial \lambda_i}{\partial p_j} \delta_{ki} = \mathbf{0} \tag{2.10}$$

It follows that

$$\gamma_{ik} = - \frac{\boldsymbol{\phi}_k^T \left(\frac{\partial \mathbf{K}}{\partial p_j} - \lambda_i \frac{\partial \mathbf{M}}{\partial p_j} \right) \boldsymbol{\phi}_i}{\left(\lambda_k - \lambda_i \right)} \qquad k \neq i \tag{2.11}$$

Differentiation of Equation 2.3 with respect to a parameter p_j yields

$$\frac{\partial \boldsymbol{\phi}_i^T}{\partial p_j} \mathbf{M} \boldsymbol{\phi}_i + \boldsymbol{\phi}_i^T \frac{\partial \mathbf{M}}{\partial p_j} \boldsymbol{\phi}_i + \boldsymbol{\phi}_i^T \mathbf{M} \frac{\partial \boldsymbol{\phi}_i}{\partial p_j} = 0 \tag{2.12}$$

Substituting Equation 2.8 into Equation 2.12 and some manipulation leads to

$$\gamma_{ii} = - \frac{1}{2} \boldsymbol{\phi}_i^T \frac{\partial \mathbf{M}}{\partial p_j} \boldsymbol{\phi}_i \tag{2.13}$$

Therefore the eigenvector sensitivity is found as

$$\frac{\partial \boldsymbol{\phi}_i}{\partial p_j} = \sum_{k \neq i} - \frac{\boldsymbol{\phi}_k^T \left(\frac{\partial \mathbf{K}}{\partial p_j} - \lambda_i \frac{\partial \mathbf{M}}{\partial p_j} \right) \boldsymbol{\phi}_i}{\left(\lambda_k - \lambda_i \right)} \boldsymbol{\phi}_k - \frac{1}{2} \left(\boldsymbol{\phi}_i^T \frac{\partial \mathbf{M}}{\partial p_j} \boldsymbol{\phi}_i \right) \boldsymbol{\phi}_i \tag{2.14}$$

2.4 Perturbation of eigenvalue problem

If a change Δp in a parameter p changes the mass and stiffness matrices by $\Delta\mathbf{M}$ and $\Delta\mathbf{K}$, respectively, defined as

$$\Delta\mathbf{K} = \mathbf{K}(p + \Delta p) - \mathbf{K}(p) \qquad \Delta\mathbf{M} = \mathbf{M}(p + \Delta p) - \mathbf{M}(p) \tag{2.15}$$

then Equation 2.1 can be written as

$$(\mathbf{K} + \Delta\mathbf{K})(\boldsymbol{\phi}_i + \Delta\boldsymbol{\phi}_i) = (\lambda_i + \Delta\lambda_i)(\mathbf{M} + \Delta\mathbf{M})(\boldsymbol{\phi}_i + \Delta\boldsymbol{\phi}_i) \tag{2.16}$$

where $\Delta\boldsymbol{\phi}_i$ and $\Delta\lambda_i$ denote the resulting change of the ith eigenvector and eigenvalue, respectively. Expanding this equation and ignoring higher order terms gives

$$(\mathbf{K}\boldsymbol{\phi}_i + \mathbf{K}\Delta\boldsymbol{\phi}_i + \Delta\mathbf{K}\boldsymbol{\phi}_i) \approx (\lambda_i\mathbf{M}\boldsymbol{\phi}_i + \lambda_i\mathbf{M}\Delta\boldsymbol{\phi}_i + \lambda_i\Delta\mathbf{M}\boldsymbol{\phi}_i + \Delta\lambda_i\mathbf{M}\boldsymbol{\phi}_i) \tag{2.17}$$

Premultiplying by $\boldsymbol{\phi}_i^T$ and some manipulation leads to

$$\Delta\lambda_i \approx \boldsymbol{\phi}_i^T(\Delta\mathbf{K} - \lambda_i\Delta\mathbf{M})\boldsymbol{\phi}_i \tag{2.18}$$

which approximates the change in eigenvalue due to a change in the physical matrices to first order. It is equivalent to Equation 2.7 in the limit $\Delta p \to 0$.

The perturbation in the ith eigenvectors can be expressed as

$$\Delta\boldsymbol{\phi}_i = \sum_{i \neq k} \gamma_{il}\boldsymbol{\phi}_l \tag{2.19}$$

where γ_{ik} are first order quantities. By substituting Equation 2.19 into Equation 2.17, multiplying by $\boldsymbol{\phi}_k^T$ and some manipulations, it can be shown that

$$\Delta\boldsymbol{\phi}_i = -\sum_{k \neq i} \frac{\boldsymbol{\phi}_k^T\left(\Delta\mathbf{K} - \lambda_i\Delta\mathbf{M}\right)\boldsymbol{\phi}_i}{(\lambda_k - \lambda_i)}\boldsymbol{\phi}_k - \frac{1}{2}\left(\boldsymbol{\phi}_i^T\Delta\mathbf{M}\boldsymbol{\phi}_i\right)\boldsymbol{\phi}_i \tag{2.20}$$

which can be compared to Equation 2.14. The approaches reviewed in this and the last section are based on the assumption that there are no repeated eigenvalues, which can be seen in the denominators of Equations 2.14 and 2.20. There are advanced approaches that can cope with repeated eigenvalues [68, 69] or consider damped dynamic systems [70, 71].

2.4.1 Example

A single-degree-of-freedom model of a cantilever beam is considered, where the mass is proportional to the length ($m \sim L$) and the stiffness is inverse proportional to the length cubed ($k \sim 1/L^3$). All other variables are equal to one and the length is the parameter to be modified ($p = L$). The baseline value p_0 and the change Δp are specified as follows

$$p = p_0 + \Delta p \qquad p_0 = 1 \qquad -0.5 \leq \Delta p \leq 0.5 \tag{2.21}$$

The eigenvalue is given as

$$\lambda = \frac{k}{m} = \frac{1}{p^4} \tag{2.22}$$

In Figure 2.1 the approximations of the eigenvalue from Equation 2.7 and Equation 2.18 are compared with the exact solution. Whereas the sensitivity approach results in a straight line with the same gradient as the exact solution at p_0, the perturbation of the eigenvalue problem gives a nonlinear approximation, which compares much better to the exact solution. Although the perturbation only considers first order terms, the approximation can be nonlinear, because the differences $\Delta\mathbf{K}$ and $\Delta\mathbf{M}$ are nonlinear if the mass and stiffness matrices are nonlinear functions of the parameter p. If the conditions

$$\frac{\partial \mathbf{K}}{\partial p_j}\Delta p_j = \Delta\mathbf{K} \qquad \text{and} \qquad \frac{\partial \mathbf{M}}{\partial p_j}\Delta p_j = \Delta\mathbf{M} \tag{2.23}$$

hold, then the perturbation and the sensitivity approach yield the same results.

The perturbation and linear sensitivity approaches are useful techniques if the change in a parameter is small and the change in the quantity of interest is small as well. In general, except for periodic structures or if two eigenvalues are equal or close, a small change in a physical parameter results in a relatively small change in the eigensolutions.

2.5 Interpolation of eigenvectors

The perturbation and linear sensitivity approach both approximate a new evaluation based on the change from the baseline solution. In contrast, there are interpolation approaches, which use more than one exact solution to approximate a new evaluation. The basic concept of these is reviewed next.

If Equation 2.16 is multiplied by $(\boldsymbol{\phi}_i + \Delta\boldsymbol{\phi}_i)^T$ it follows after some rearrangement

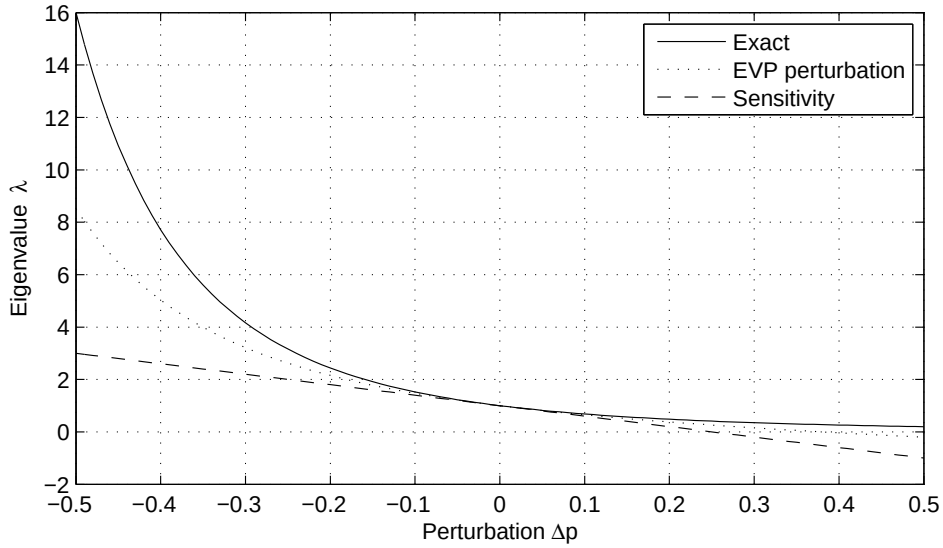

Figure 2.1: *Approximation of an eigenvalue by perturbation of the eigenvalue problem and linear sensitivity approach for a nonlinear function.*

that

$$\lambda_i + \Delta\lambda_i = \frac{(\boldsymbol{\phi}_i + \Delta\boldsymbol{\phi}_i)^T(\mathbf{K} + \Delta\mathbf{K})(\boldsymbol{\phi}_i + \Delta\boldsymbol{\phi}_i)}{(\boldsymbol{\phi}_i + \Delta\boldsymbol{\phi}_i)^T(\mathbf{M} + \Delta\mathbf{M})(\boldsymbol{\phi}_i + \Delta\boldsymbol{\phi}_i)} \tag{2.24}$$

which is also referred to as the Rayleigh quotient. The computationally expensive part of this equation is to calculate a new eigenvector for any change in parameter p. Bhaskar [72] suggested to solve the eigenvalue problem only for the smallest and largest values of the parameter p and interpolate the eigenvectors for intermediate values of p. Equation 2.24 becomes

$$\lambda_i + \Delta\lambda_i = \frac{\bar{\boldsymbol{\phi}}_i^T(\mathbf{K} + \Delta\mathbf{K})\bar{\boldsymbol{\phi}}_i}{\bar{\boldsymbol{\phi}}_i^T(\mathbf{M} + \Delta\mathbf{M})\bar{\boldsymbol{\phi}}_i} \tag{2.25}$$

where $\bar{\boldsymbol{\phi}}$ denotes the interpolated eigenvector. Considering the lower and upper limits in the space of parameter p as

$$p_L \leq p \leq p_R \tag{2.26}$$

two eigenvalue problems at $p = p_L$ and $p = p_R$ have to be solved, which are given as

$$\mathbf{K}_L\boldsymbol{\phi}_L = \lambda_L\mathbf{M}_L\boldsymbol{\phi}_L \qquad \mathbf{K}_R\boldsymbol{\phi}_R = \lambda_R\mathbf{M}_R\boldsymbol{\phi}_R \tag{2.27}$$

The exact eigenvectors $\boldsymbol{\phi}_L$ and $\boldsymbol{\phi}_R$ are then combined using a varying weight by

$$\bar{\boldsymbol{\phi}} = (1-t)\boldsymbol{\phi}_L + t\boldsymbol{\phi}_R \tag{2.28}$$

The weight t depends on the point of interest in the parameter space and is defined by

$$t = \frac{p - p_L}{p_R - p_L} \tag{2.29}$$

This approach can be extended to any number of parameters. The parameter space of two variable parameters p^a and p^b is shown in Figure 2.2. The eigenvalue problem has to be solved for the parameter combinations in each of the four corners. The normalised weights are defined as

$$t^a = \frac{p^a - p^a_L}{p^a_R - p^a_L} \qquad t^b = \frac{p^b - p^b_L}{p^b_R - p^b_L} \tag{2.30}$$

and the eigenvector for any combination of p^a and p^b within the parameter space can be estimated by

$$\bar{\boldsymbol{\phi}} = (1-t^a)(1-t^b)\boldsymbol{\phi}_{LL} + t^a(1-t^b)\boldsymbol{\phi}_{RL} + t^b(1-t^a)\boldsymbol{\phi}_{LR} + t^a t^b \boldsymbol{\phi}_{RR} \tag{2.31}$$

which is a bilinear interpolation using the four exact solutions at the corners. The number of eigenvalue problems to be solved increases exponentially with the number of parameters, which makes this method computationally expensive.

An alternative approach would be to calculate the exact eigenvectors in two opposite corners $(\boldsymbol{\phi}_{LL}, \boldsymbol{\phi}_{RR})$ only. The interpolation is then given by

$$\bar{\boldsymbol{\phi}} = (1-t^d)\boldsymbol{\phi}_{LL} + t^d\boldsymbol{\phi}_{RR} \tag{2.32}$$

where the weight is

$$t^d = (t^a + t^b)/2 \tag{2.33}$$

2.6 Interpolation of eigenvalues

The interpolation technique can also be applied to estimate eigenvalues. In [73] an approach is presented where several approximate solutions of an eigenvalue, based on perturbations about different points, are combined to one approximate eigenvalue solution.

Equation 2.18 can be used to find the approximate solutions $\tilde{\lambda}^L$ and $\tilde{\lambda}^R$ based on a perturbation about $p = p_L$ and $p = p_R$, respectively. Alternatively, Rayleigh's

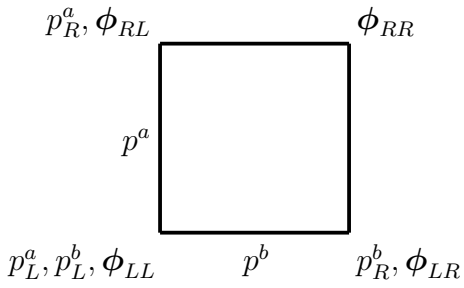

Figure 2.2: *Two-dimensional parameter space.*

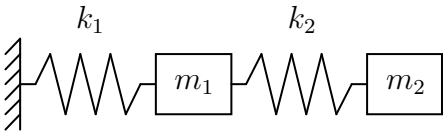

Figure 2.3: *Two-DOF system.*

quotient, Equation 2.25, can be used with eigenvectors from the corner points in the form of

$$\tilde{\lambda}^L = \frac{\bar{\boldsymbol{\phi}}_L^T(\mathbf{K}+\Delta\mathbf{K})\bar{\boldsymbol{\phi}}_L}{\bar{\boldsymbol{\phi}}_L^T(\mathbf{M}+\Delta\mathbf{M})\bar{\boldsymbol{\phi}}_L} \qquad \tilde{\lambda}^R = \frac{\bar{\boldsymbol{\phi}}_R^T(\mathbf{K}+\Delta\mathbf{K})\bar{\boldsymbol{\phi}}_R}{\bar{\boldsymbol{\phi}}_R^T(\mathbf{M}+\Delta\mathbf{M})\bar{\boldsymbol{\phi}}_R} \tag{2.34}$$

Both methods give an approximation of the eigenvalue from the left and from the right side, which can be combined to one estimate based on the position in the parameter space by

$$\tilde{\lambda} = \frac{p_R - p}{p_R - p_L}\tilde{\lambda}^L + \frac{p - p_L}{p_R - p_L}\tilde{\lambda}^R \tag{2.35}$$

Furthermore, since each approximation is exact in one corner, the error of the other approximation can be evaluated, which can be used to change the weights and improve the combined approximation. The values obtained using the Rayleigh quotient are always larger than the exact solution, due to the nature of this approximation [73].

The response surface methodology (RSM) [63] can be seen as an extension of the interpolation approaches. It is used to construct an approximate meta-model, which replaces the original model to provide a relationship between input parameters and response quantities.

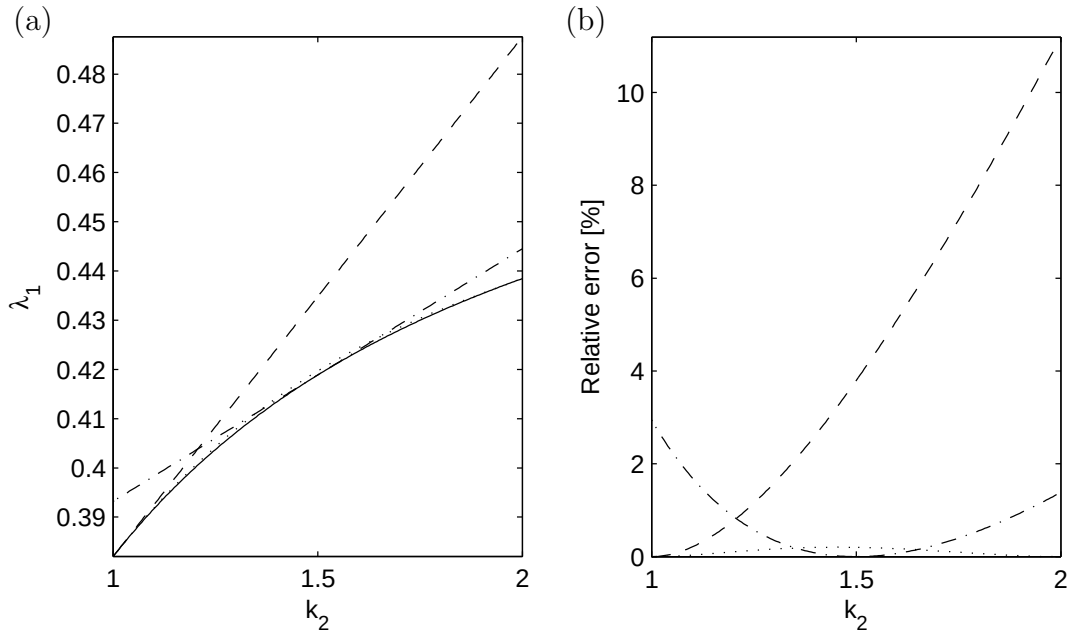

Figure 2.4: *Change of eigenvalue λ_1 due to changes in parameter k_2: absolute values (a) and relative errors (b);* ___ *exact;* _ _ _ *perturbation about $k_2 = 1$;* _.._. *perturbation about $k_2 = 1.5$;* . . . . *interpolation approach.*

2.6.1 Numerical example

A two-DOF mass-spring chain (Figure 2.3) is considered, where the stiffness k_2 can vary as $1 < k_2 < 2$ and the other properties have a deterministic value of one. The mass and stiffness matrices are thus given as

$$\mathbf{M} = \begin{bmatrix} 1 & 0 \\ 0 & 1 \end{bmatrix} \qquad \mathbf{K} = \begin{bmatrix} (1+k_2) & -k_2 \\ -k_2 & k_2 \end{bmatrix} \tag{2.36}$$

The fundamental eigenvalue is calculated using an exact approach and several approximations. The interpolated eigenvector method (Equation 2.25) is applied based on exact solutions for $k_2 = 1$ and $k_2 = 2$. Results for the interpolation of eigenvalues (Equation 2.35) are not shown. The perturbation approach (Equation 2.18) around a baseline value of $k_2 = 1$ and $k_2 = 1.5$, respectively, is realised. The results for the eigenvalues are shown in Figure 2.4a and the relative errors are shown in Figure 2.4b.

In all cases the differences increase for values of k_2 that are further away from an exact deterministic solution. The perturbation approach about the lower limit of the interval of k_2 results in the largest errors of about 10% at the upper limit. The perturbation about the centre point of the interval causes considerable errors of

up to 3%. The interpolated eigenvector approach gives good results over the whole interval with the maximum error of about 0.2%.

2.7 Discussion and concluding remarks

The basic concepts of modal perturbation and interpolation approaches have been presented. The perturbation and linear sensitivity approaches are useful techniques if the change in a parameter is small and the change in the quantity of interest is small as well. In general, except for periodic structures or if two eigenvalues are equal or close together, a small change in a physical parameter results in a relatively small change in the eigensolutions. The interpolation approaches give good results for the system discussed here. There are some constraints in addition to the ones above in that eigenvalues must not change order when a parameter varies. The effects of veering and crossing of eigenvalues have to be considered. The computational cost of solving the eigenvalue problem at a number of points can become quite large. In non-deterministic modelling, usually the baseline properties are known exactly but lower and upper limits are difficult to define. There are many variations of these approaches considering more complex systems and a larger number of uncertain variables.

Chapter 3

Modelling of spatial variations by random fields

3.1 Introduction

This chapter concerns the modelling of spatial variations, which is a common type of uncertainty in mechanical structures. Many physical parameters, such as material and geometric properties, vary locally and spatially, which can be modelled by probabilistic random fields [42]. The Karhunen-Loève (KL) expansion [40] is well suited to represent random fields. It can be used to transform correlated random variables into uncorrelated random variables. In the following sections, first the theory of discretised random fields and the KL expansion are reviewed. The implementation of random fields within existing finite element models and the relation between correlation length and finite element size are discussed. Perturbational approaches are considered in order to reduce the numerical cost. Finally, a new concept to model spatial variations is presented in Section 3.4, which incorporates possibilistic bounds for the local physical parameter variations and probabilistic parameters to include the spatial variations.

3.2 Theory

3.2.1 Random field and Karhunen-Loève expansion

A simple model for a random field is a homogenous isotropic Gaussian field, where the random variables have a Gaussian distribution that does not change with direction or location. Therefore, the interdependency between two random variables defined at two points depends only on the distance between them. The correlation r

between two Gaussian random variables can be modelled by an exponential function of the form

$$r(d, L_c, \sigma) = \sigma^2 \exp\left(-\left|\frac{d}{L_c}\right|\right) \tag{3.1}$$

where σ is the standard deviation, L_c is the correlation length and $d = |\mathbf{x}^1 - \mathbf{x}^2|$ is the distance between two positions $\mathbf{x}^1$ and $\mathbf{x}^2$.

A Gaussian random field $P(x)$ can be represented by the KL expansion in the form [40]

$$P(x) = \overline{P(x)} + \sum_{j=1}^{\infty} \boldsymbol{\psi}(x)_j \sqrt{\mu_j}\zeta_j \tag{3.2}$$

where ζ_j are uncorrelated standard normal random variables, independent of x. The deterministic terms μ_j and $\boldsymbol{\psi}_j$ are the eigenvalues and eigenvectors, respectively, of the covariance function C of the continuous random field. The integral eigenvalue problem is given in the form

$$\int C(\mathbf{x}^1, \mathbf{x}^2)\boldsymbol{\psi}_j(\mathbf{x}^1)d\mathbf{x}^1 = \mu_j \boldsymbol{\psi}_j(\mathbf{x}^2) \tag{3.3}$$

There are several approaches to the solution of Equation 3.3, for example by means of a Galerkin procedure [43]. Similarly, there are several procedures for the discretisation of the continuous random field for a FE analysis, for example spatial averaging methods, shape function methods and point discretisation methods [74]. Following the discretisation the covariance function can be replaced by a nxn covariance matrix $\mathbf{C}$, for which the (k, l)th element is given by

$$c_{kl} = R(d_{kl}, L_c, \sigma) \qquad k, l = 1 \ldots n \tag{3.4}$$

where n is the number of finite elements and where $d_{kl} = |\mathbf{x}^k - \mathbf{x}^l|$, $\mathbf{x}^k$ being the centre of the kth element. The matrix $\mathbf{C}$ is a symmetric completely positive matrix and the values on the diagonal refer to the autocorrelation and are equal to the variance of the Gaussian variable. The eigenvalue problem of the covariance matrix is

$$\mathbf{C}\boldsymbol{\psi}_j = \mu_j \boldsymbol{\psi}_j \tag{3.5}$$

A discretised random field in one dimension, given by a vector $\mathbf{p}$ of length n, can be represented by the KL expansion in the form [40]

$$\mathbf{p} = \bar{\mathbf{p}} + \sum_{j=1}^{r \leq n} \boldsymbol{\psi}_j \sqrt{\mu_j}\zeta_j \tag{3.6}$$

where $\bar{\mathbf{p}}$ denotes the mean, ζ_j are uncorrelated standard normal (zero mean and unit variance) random variables. The mean $\bar{\mathbf{p}}$ and the eigensolutions μ_j and $\boldsymbol{\psi}_j$ are deterministic. The randomness of the field is only included in ζ. There are n eigensolutions, but in general it is sufficient to consider only the $r < n$ eigenfunctions with the largest eigenvalues, which give a good approximation of the random field. The parameters of the Gaussian random field are the mean value $\overline{p}$, the standard deviation σ and the correlation length L_c.

3.2.2 Finite element methods

In the finite element (FE) method [9], the structure is divided into a number n_e of elements of finite size. The element mass- and stiffness matrices $\mathbf{M}_e$ and $\mathbf{K}_e$ are assembled to give the global mass- and stiffness matrices $\mathbf{M}$ and $\mathbf{K}$ of the complete structure. For simplicity, only the stiffness matrix will be considered in the following derivations, but all expressions are equally valid for the mass matrix as well. The global stiffness matrix can be written as

$$\mathbf{K} = \sum_{e=1}^{n_e} \mathbf{A}_e^T \mathbf{K}_e \mathbf{A}_e \tag{3.7}$$

where $\mathbf{A}_e$ are transformation matrices given by

$$\mathbf{u}_e = \mathbf{A}_e \mathbf{u} \tag{3.8}$$

where $\mathbf{u}_e$ and $\mathbf{u}$ are the element and global coordinates, respectively.

In order to model uncertainty, that is given by a probabilistic random field model, point discretisation methods are often appropriate. These are known for their easy and efficient implementation, because the value of the random field at location $\mathbf{x}^i$ is given by $p_i = P(x^i)$. If the random field is discretised using the finite element mesh, one value of the random field has to be assigned to each finite element, which can be expressed as

$$\mathbf{K}_e = \mathbf{K}_e(p_e) \tag{3.9}$$

This can be done using the midpoint method, where the random field is evaluated at the geometric midpoint of the element. Other approaches use a combination of the random field values that are evaluated at the node points of an element [74]. It has to be noted that the modelling of the random field using point discretisation methods depends on the finite element mesh. However, this approximation is justified, if the correlation length is large compared to the element size.

The global eigenvalue problem is then given by

$$\left(\mathbf{K}(\mathbf{p}) - \lambda_i(\mathbf{p})\mathbf{M}(\mathbf{p})\right)\boldsymbol{\phi}_i(\mathbf{p}) = \mathbf{0} \tag{3.10}$$

where λ_i and $\boldsymbol{\phi}_i$ are the eigenfrequencies and mode shapes of the structure, respectively, that depend on the vector $\mathbf{p}$.

The statistics of the variation of these properties are usually estimated by a Monte Carlo simulation approach, where the problem is solved repeatedly to obtain a number of samples. In each run, first the element matrices $\mathbf{K}_e(p_e)$ and $\mathbf{M}_e(p_e)$ are updated according to a realisation of the random field vector $\mathbf{p}$ (Equation 3.6). Subsequently the global system matrices $\mathbf{K}(\mathbf{p}), \mathbf{M}(\mathbf{p})$ are assembled and finally the eigenvalue problem 3.10 is solved. Alternative approaches include polynomial chaos expansion [43] and stochastic reduced basis methods [49].

If the stiffness matrix $\mathbf{K}(\mathbf{p})$ is linearly dependent on $\mathbf{p}$, then Equations 3.6, 3.7 and 3.9 can be combined to give

$$\mathbf{K}(\mathbf{p}) = \mathbf{K}_0 + \sum_{j=1}^{r} \mathbf{K}^j \zeta_j \tag{3.11}$$

where $\mathbf{K_0}$ is the baseline stiffness matrix and the deterministic matrices $\mathbf{K}^j$ are given by

$$\mathbf{K}^j = \mathbf{K}(\mathbf{p}^j) \qquad \mathbf{p}^j = \boldsymbol{\psi}_j\sqrt{\mu_j} \tag{3.12}$$

3.2.3 Perturbation

Expressions for modal sensitivities have been introduced in the previous chapter. The rate of change of an eigenvalue with respect to a parameter v was found to be [64]

$$\frac{\partial \lambda_i}{\partial v} = \boldsymbol{\phi}_i^T \left(\frac{\partial \mathbf{K}}{\partial v} - \lambda_i \frac{\partial \mathbf{M}}{\partial v}\right)\boldsymbol{\phi}_i \tag{3.13}$$

Therefore, the derivatives of the stiffness and mass matrices with respect to the parameter v are needed. For the application of random fields, these parameters are the random variables ζ. The derivative of the stiffness matrix with respect to a random variable ζ_j can be written using Equation 3.7 as

$$\frac{\partial \mathbf{K}}{\partial \zeta_j} = \sum_{e=1}^{n_e} \mathbf{A}_e^T \frac{\partial \mathbf{K}_e}{\partial p_e}\frac{\partial p_e}{\partial \zeta_j}\mathbf{A}_e \tag{3.14}$$

where $\frac{\partial \mathbf{K}_e}{\partial p_e}$ is the derivative of the eth element stiffness matrix with respect to parameter p_e and

$$\frac{\partial p_e}{\partial \zeta_j} = \psi_{ej}\sqrt{\mu_j} \tag{3.15}$$

is the derivative of the parameter p_e with respect to the random variable ζ_j. Equation 3.13 then becomes

$$\frac{\partial \lambda_i}{\partial \zeta_j} = \boldsymbol{\phi}_i^T \left[\sum_{e=1}^{n_e} \mathbf{A}_e^T \left(\frac{\partial \mathbf{K_e}}{\partial p_e} - \lambda_i \frac{\partial \mathbf{M_e}}{\partial p_e} \right) \mathbf{A}_e \psi_{ej} \sqrt{\mu_j} \right] \boldsymbol{\phi}_i \tag{3.16}$$

which can be written as

$$\frac{\partial \lambda_i}{\partial \zeta_j} = \boldsymbol{\phi}_i^T \left[\sum_{e=1}^{n_e} \mathbf{A}_e^T \tilde{\mathbf{D}}_{ei} \mathbf{A}_e \psi_{ej} \right] \boldsymbol{\phi}_i \sqrt{\mu_j} \tag{3.17}$$

where

$$\tilde{D}_{ei} = \frac{\partial \mathbf{K_e}}{\partial p_e} - \lambda_i \frac{\partial \mathbf{M_e}}{\partial p_e} \tag{3.18}$$

Finally the change in eigenvalue λ_i due to changes in the KL variables $\boldsymbol{\zeta}$ can be approximated by

$$\lambda_i(\boldsymbol{\zeta}) = \bar{\lambda_i} + \sum_{j=1}^{r \leq n_j} \frac{\partial \lambda_i}{\partial \zeta_j} \zeta_j \tag{3.19}$$

3.3 Example

A cantilever beam as shown in Figure 3.1 is used as a numerical example. The element stiffness and mass matrices for Euler-Bernoulli beam theory and transverse and rotational nodal DOFs are [9]

$$\mathbf{M}_e = \frac{\rho A a}{105} \begin{bmatrix} 78 & 22a & 27 & -13a \\ 22a & 8a^2 & 13a & -6a^2 \\ 27 & 13a & 78 & -22a \\ -13a & -6a^2 & -22a & 8a^2 \end{bmatrix} \quad \mathbf{K}_e = \frac{EI}{2a^3} \begin{bmatrix} 3 & 3a & -3 & 3a \\ 3a & 4a^2 & -3a & 2a^2 \\ -3 & -3a & 3 & -3a \\ 3a & 2a^2 & -3a & 4a^2 \end{bmatrix} \tag{3.20}$$

where ρ is the density, E is Young's modulus and a is half the element length. The second moment of area I and the cross-sectional area A for a rectangular cross-section with thickness h and width b are given by

$$I = \frac{bh^3}{12} \qquad A = bh \tag{3.21}$$

l $[m]$	h $[m]$	b $[m]$	ρ $[kg]$	E $[N/m^2]$
1	0.01	0.1	7850	$2.1e11$

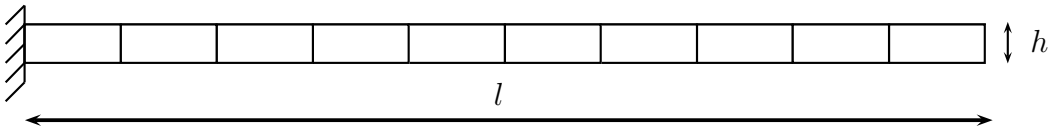

Figure 3.1: *Uniform cantilever beam with rectangular cross section, baseline parameters.*

The uniform beam is divided into 20 elements. The left end is fixed and the length of the beam is $l = 1m$.

3.3.1 Random field for Young's modulus

In this analysis, the Young's modulus E is modelled by a random field and a Monte Carlo simulation with 10^4 realisations is performed. The pseudo-exact numerical solution is compared with approximate solutions: first, a reduction in the number of random variables ζ_j from 20 to 5 in Equation 3.6 is considered ($r < n$). Second, the perturbation (3.19) is applied to both the complete and the reduced set of random variables ζ_j. The criterion for comparison is the probability that the first eigenfrequency is lower than a certain limit. This limit was calculated for a probability of 10% from the exact numerical solution.

In Figure 3.2 the results are shown with reference to the exact solution. The correlation length is $L_c = 0.5m$ and the coefficient of variation ($CV = \sigma/\overline{E}$) is varied from 5% to 20%. The error introduced by discretising the random field is very small and can be neglected, because the correlation length is 10 times the element length. It can be seen that all approximate solutions underestimate the probability of occurrence and that the error increases for higher CV. The reduced exact solution gives the best results, followed by the full perturbation and the reduced perturbation, although there is little difference between the last two.

In Figure 3.3 the CV is 10% and the correlation length is varied. All approximate solutions converge to the exact solution for a correlation length larger than $L_c = 10m$. In this case, only the first few random variables ζ_j are important. For very large correlation lengths, the random field models a constant distribution of Young's modulus, which corresponds to a linear relation between the eigenfrequencies and the first random variable ζ_1.

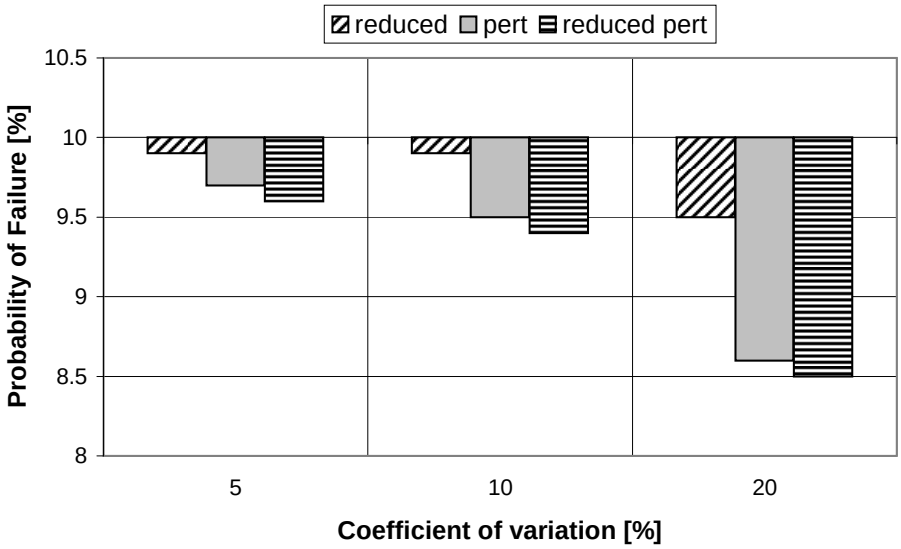

Figure 3.2: *Variation in the fundamental eigenfrequency of a beam due to spatial variation in Young's modulus, different coefficient of variation, approximate results by reduction in number of random variables and perturbation,* $L_c = 0.5m$.

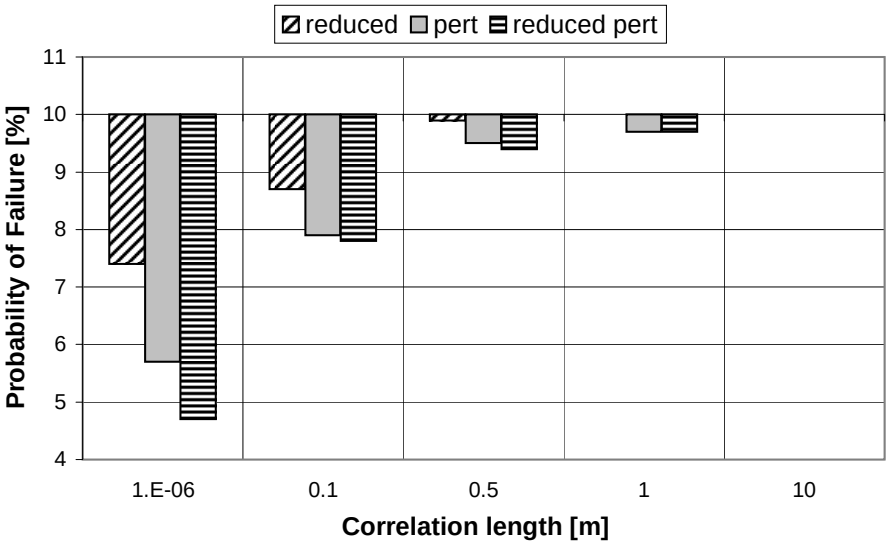

Figure 3.3: *Variation in the fundamental eigenfrequency of a beam due to spatial variation in Young's modulus, different correlation lengths, approximate results by reduction in number of random variables and perturbation.*

3.3.2 Random field for beam thickness

In this analysis, the variation of the beam thickness h is modelled by a random field. This parameter appears linearly in the mass matrix and with a cubic term in the stiffness matrix. In Figure 3.4 the correlation length is $0.5m$ and the CV is varied from 5% to 20%. The error in the approximations increases with higher CV. The reduced solution underestimates the exact results, because some contributions to the variation are neglected. However, the perturbation overestimates the probability, because there is a shift to lower values for the fundamental eigenfrequencies.

In Figure 3.5, the CV is 10% and the correlation length is varied. The reduced exact solution always underestimates the exact result and converges to it for larger correlation lengths. The perturbation underestimates the exact result for low correlation lengths and overestimates it for large correlation lengths.

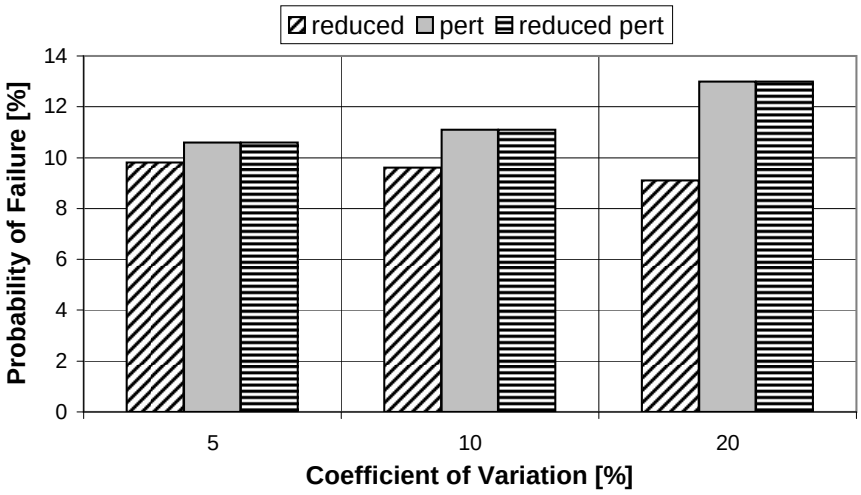

Figure 3.4: *Variation in the fundamental eigenfrequency of a beam due to spatial variation in thickness, different coefficient of variation, approximate results by reduction in number of random variables and perturbation.*

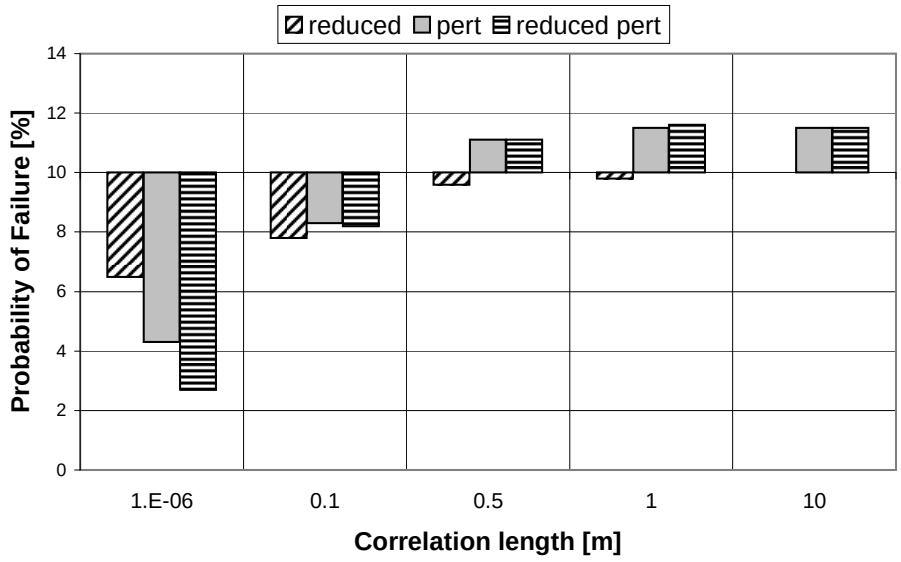

Figure 3.5: *Variation in the fundamental eigenfrequency of a beam due to spatial variation in thickness, different correlations lengths, approximate results by reduction in number of random variables and perturbation.*

3.4 Possibilistic approach for spatial variations

In this section, the combination of the KL expansion with a possibilistic concept is investigated. The basic idea is that the uncorrelated standard normal random variables in the probabilistic approach are allowed to vary within a range where the limits refer to possibilistic bounds of the physical variables. The KL expansion in Equation 3.6 can be rewritten in the form

$$\mathbf{p} = \bar{\mathbf{p}} + \sum_{j=1}^{r \leq n} \quad \boldsymbol{\psi}_j \sqrt{\overline{\mu_j}} \quad v_j \tag{3.22}$$

where $v_j = \sigma\zeta_j$ and the eigenvalues $\overline{\mu_j}$ are independent of the standard deviation σ. In this case, the correlation function

$$R(d, L_c) = \exp\left(-\left|\frac{d}{L_c}\right|\right) \tag{3.23}$$

depends only on the distance d and the correlation length L_c. In the standard probabilistic random field approach, v_j are uncorrelated random variables with zero mean and variance σ ($v_j = N(0, \sigma)$). In the proposed possibilistic approach, v_j are given by intervals with lower and upper limits referring to the given physical limits

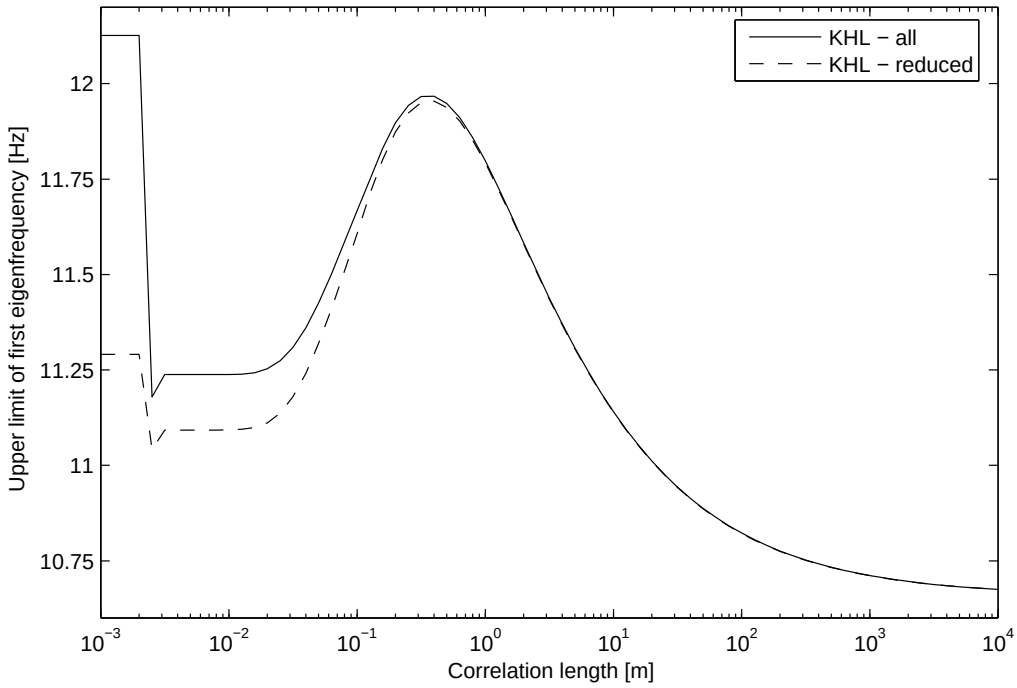

Figure 3.6: *Variation of the upper limit of the fundamental eigenfrequency over correlation length; possibilistic approach using KL eigenvectors; results for complete and reduced set of variables.*

($v_j = [\underline{v_j}, \overline{v_j}]$).

There are n independent variables v_j and a vertex approach [32] with 2^n combinations can be performed. If only the r eigenvectors with the largest eigenvalues $\overline{\mu_j}$ are considered, the number of vertices reduces to 2^r.

The numerical example of Section 3.3 is used to obtain results. The beam is modelled by 12 finite elements and the thickness of each element can vary by $\pm 10\%$. The upper limit of the first eigenfrequency has been computed for correlation lengths from $L_c = 10^{-3}$ up to $L_c = 10^4$. In Figure 3.6 the results are shown for the cases that all 12 eigenvectors of the covariance matrix and a reduced set of the first 6 eigenvectors are used in the KL expansion.

There is a maximum in the upper limit of the fundamental frequency for a correlation length of about 1/3 of the length of the beam ($L_c = 0.3m$). In this case the contributions from the eigenvectors in the KL expansion are related to the characteristic spatial variation of the thickness that results in a high upper limit for the first eigenfrequency. For a higher correlation length, the upper limit of the first eigenfrequency decreases and converges to the value for the case of a constant but random thickness ($f_1 = 10.66Hz$). In this region, the reduced set of eigenvectors yields accurate results. For correlation lengths $L_c < 1/3m$, the upper limit decreases

and converges to a value around $f_1 = 11.25Hz$. This corresponds to a solution where all eigenvectors in the KL expansion contribute the same. However, in this region, the correlation length is down to about one tenth of the element length and the model is not valid, because the finite element mesh has an influence on the results. Below a correlation length of about $L_c = 2 \times 10^{-3}$, the correlation is numerical zero and all elements vary independently. In this case, the results shift to a larger value of about $f_1 = 12.1Hz$. The solution with the reduced set of eigenvectors approximates a lower value.

The standard possibilistic vertex approach requires that $m = 2^n$ combinations are considered, where n is the number of uncertain parameters. However, only one of these combinations corresponds to the upper limit of a response parameter. It would be a computational advantage, if a reduced number of vertices can be identified such that a smaller number of combinations ($m < 2^n$) has to be considered. In this context, the eigenvectors of the covariance matrix can be used to select vertex combinations. If the signs of the elements of the n eigenvectors are considered, $2n$ vertices are described out of the complete set of $m = 2^n$. These selected vertices are related to characteristic spatial variations of physical properties. For the one-dimensional beam, these shapes are similar to the natural modes, which could also be used to identify $2n$ vertices. In Figure 3.7 the results are compared for the cases that all elements are independent ($m = 2^n$) or dependent ($m = 2$), and where $2n$ vertices are found from KL eigenvectors and mode shapes, respectively. The results for the upper limit of the first five eigenfrequencies are given in percent of the maximum values from the exact vertex method. If a constant but random variation is modelled for all elements, the results give much lower values for the first modes. For higher modes the results from this approach improve continuously. The vertices obtained from the KL eigenvectors give the best approximation for the fundamental eigenfrequency. For higher frequency, there is no improvement compared to the constant variation. This however seems normal for this simple beam model and more complicated structures should be investigated.

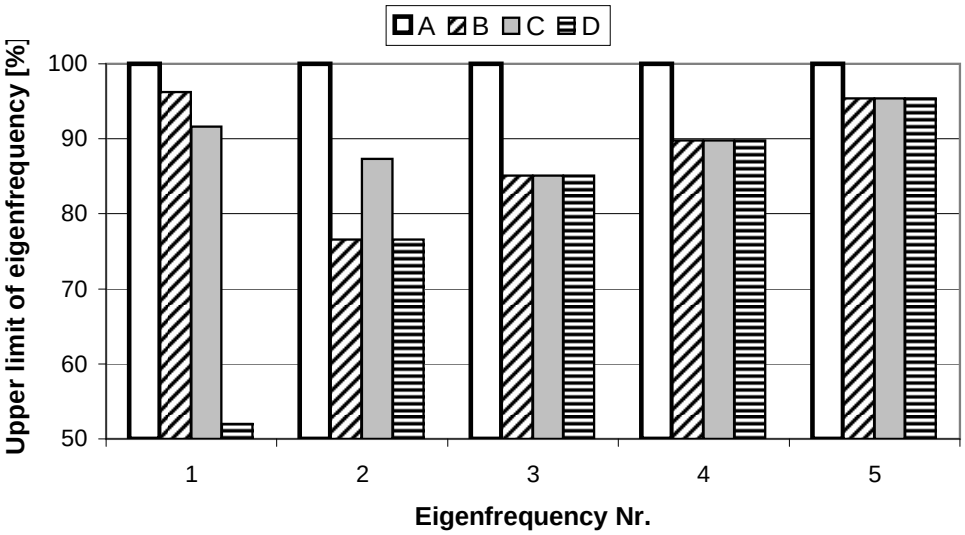

Figure 3.7: *Upper limit of first five eigenfrequency. A - vertices from all elements* $m = 2^n$*, B - vertices from KL eigenvectors* $m = 2n$*, C - vertices from natural modes* $m = 2n$*, D - constant variation* $m = 2$

3.5 Discussion and concluding remarks

Spatial variations of properties in mechanical structures occur often and should be considered. Random field models and the KL representation are appropriate to model spatial variations. A discretisation of the continuous random field at the element mesh using point discretisation methods is convenient for implementation within existing FE models and software. However, the dependency on the mesh size has to be considered. If the correlation length is large compared to the finite element size, then errors due to the approximation can be neglected. A perturbation method is straightforward to implement, because the sensitivities of the random field vector with respect to the KL variables are already given. The KL expansion can be used to drastically reduce the number of random variables. The random field model can be used to estimate the extreme cases of total correlation or no correlation between the random variables by selecting a very large or very small correlation length, respectively. However, in most practical cases, no data about the correlation length is available. It has been shown [75] that the correlation length is more important than the shape of the correlation function.

In this chapter a numerical example with spatially varying properties has been considered. The efficient application of a random field model based on the KL ex-

pansion was shown. The effects of a reduction in the number of DOFs and the use of approximate perturbation methods were investigated. The introduced errors depend on the correlation length. The truncation of terms in the KL expansion leads to an underestimation of the variation. The number of required terms in the KL expansion to achieve a certain accuracy can be calculated from the magnitudes of the eigenvalues of the covariance matrix. The errors due to perturbation are less predictable with both under- and overestimation of results possible, depending on the correlation length and the uncertain parameters. In general perturbation also leads to a shift in the mean value of response parameters. However, it is often appropriate to use perturbational relations to reduce the numerical costs. The idea of a random field model with a possibilistic parameter variation has been presented. Although some physical interpretation of the results is possible, it remains a theoretical approach.

Chapter 4

Model reduction and substructuring for built-up structures

4.1 Introduction

This chapter addresses the use of deterministic model reduction and substructuring methods for the analysis of built-up structures. The calculation time of most mathematical operations increases nonlinearly with the size of the model and the storage of large amounts of data is a problem as well. Model reduction techniques can be used to reduce the computational cost drastically. This effect is even more important in the context of repeated solutions of a deterministic model in a non-deterministic analysis. Additionally, the concept of substructuring offers possibilities to include uncertainties and variabilities at the component level in an appropriate way. All methods introduced in this chapter are independent of the non-deterministic data. There are some model reduction and substructuring methods that take the uncertainty in properties into account directly [76]. However, for most cases, the differences are small and negligible in the context of other sources of inaccuracies.

A reduction in model size can imply a loss of information and the reduced model then only gives an approximation to the solution provided by the full model. Therefore a reduction method should be case-specific and truncate only unwanted, unimportant or redundant information. The finite element model of a vibrating structure is often defined by a mass and a stiffness matrix. Solving for dynamic properties or responses generally involves an inverse matrix operation or an eigenvalue problem, which has a computational cost associated with it that is disproportionately high compared to the number of DOFs. Therefore, reduction techniques have been

specifically developed for static and dynamic FE problems. It is often appropriate to perform a coordinate transformation and apply the reduction in a different coordinate space than the original physical space.

An approach that goes hand in hand with reduction techniques is substructuring [77]. If a structure is divided into several components, the computational cost of solving all smaller problems independently is in general less than solving the original large problem. In practice many complex structures already consist of several components which are assembled in the final stage of production. They could be manufactured by different companies and independent numerical models or solutions already exist for each of them. In this case it is advisable to use the predefined substructuring. It is then normally the case that uncertainties in each component are statistically independent. It is also often appropriate and physically meaningful to reduce the size of models at the component level. While here, the substructuring is applied to the physical components, in general a structure could be divided into substructures arbitrarily. Components can be defined according to mathematical properties rather than physical or geometric criteria. One such method is Automated Multi-Level Substructuring (AMLS) [78], where a finite element model is repeatedly divided into substructures based on the sparsity of the system matrices.

In Section 4.2.1 static and dynamic reduction methods, including Guyan reduction [60] are presented. These approaches are, in general, exact only for one particular frequency. Section 4.2.2 describes the modal reduction approach, where the model is transformed into modal space and some of the higher frequency modes are neglected. Section 4.2.3 demonstrates a combination of the static and dynamic reduction to make use of the advantages of both with respect to substructuring. The main focus of this chapter is on component mode synthesis (CMS) methods [9, 61, 79–87], which are described in detail in Section 4.3. These methods have been developed mainly to improve the modelling of coupled substructures to get improved accuracy of the assembled model, which is of a reduced size. The reduction in size is done at the component level in the modal space.

In this chapter, deterministic model reduction and component synthesis will be reviewed. In Chapters 5 and 6, the fixed-interface CMS method, which is reviewed in Section 4.3.4, will be used as a framework for a non-deterministic analysis. In order to follow the flow of the thesis, it is suggested to focus on Section 4.3.4 of this chapter only.

4.2 Model reduction methods

4.2.1 Static and dynamic reduction

The Guyan reduction method [60] is based on the reduction of the stiffness matrix and is therefore also known as static condensation. The governing equation in static analysis is given by

$$\mathbf{F} = \mathbf{K}\mathbf{u} \tag{4.1}$$

where $\mathbf{F}$ and $\mathbf{u}$ are vectors of force and DOFs respectively and $\mathbf{K}$ is the stiffness matrix. This equation can be partitioned in the form

$$\begin{bmatrix} \mathbf{F}_S \\ \mathbf{F}_M \end{bmatrix} = \begin{bmatrix} \mathbf{K}_{SS} & \mathbf{K}_{SM} \\ \mathbf{K}_{MS} & \mathbf{K}_{MM} \end{bmatrix} \begin{bmatrix} \mathbf{u}_S \\ \mathbf{u}_M \end{bmatrix} \tag{4.2}$$

where the coordinates are divided into two sets S and M, which are referred to as slave and master coordinates. If the forces $\mathbf{F}_S$ are zero then the first line of Equation 4.2 gives

$$\mathbf{u}_S = -\mathbf{K}_{SS}^{-1}\mathbf{K}_{SM}\mathbf{u}_M \tag{4.3}$$

which can be used to eliminate the coordinates where no forces are applied. Substituting Equation 4.3 into the first line of Equation 4.2 gives the governing equation of the reduced system in the form

$$\mathbf{F}_M = \mathbf{K}_M\mathbf{u}_M \tag{4.4}$$

with

$$\mathbf{K}_M = \left[\mathbf{K}_{MM} - \mathbf{K}_{MS}\mathbf{K}_{SS}^{-1}\mathbf{K}_{SM}\right] \tag{4.5}$$

This reduced static equation yields the exact solutions for $\mathbf{u}_M$, and $\mathbf{u}_S$ are then calculated from Equation 4.3.

In a dynamic analysis the undamped equation of motion is given as

$$\mathbf{M}\ddot{\mathbf{u}} + \mathbf{K}\mathbf{u} = \mathbf{f} \tag{4.6}$$

where $\mathbf{M}$ is the mass matrix and $\ddot{\mathbf{u}}$ denotes acceleration. Assuming time harmonic motion $\mathbf{u} = \mathbf{U}e^{i\omega t}$ with magnitudes $\mathbf{U}$ and frequency ω due to forces $\mathbf{f} = \mathbf{F}e^{i\omega t}$, Equation 4.6 can be written as

$$\left[\mathbf{K} - \omega^2\mathbf{M}\right]\mathbf{U} = \mathbf{F} \tag{4.7}$$

which may be partitioned into two sets of coordinates S and M in the form

$$\begin{bmatrix} \mathbf{K}_{SS} - \omega^2 \mathbf{M}_{SS} & \mathbf{K}_{SM} - \omega^2 \mathbf{M}_{SM} \\ \mathbf{K}_{MS} - \omega^2 \mathbf{M}_{MS} & \mathbf{K}_{MM} - \omega^2 \mathbf{M}_{MM} \end{bmatrix} \begin{bmatrix} \mathbf{U}_S \\ \mathbf{U}_M \end{bmatrix} = \begin{bmatrix} \mathbf{F}_S \\ \mathbf{F}_M \end{bmatrix} \tag{4.8}$$

Assuming that $\mathbf{F}_S = 0$, the first line of Equation 4.8 gives

$$\mathbf{U}_S = - \left[\mathbf{K}_{SS} - \omega^2 \mathbf{M}_{SS} \right]^{-1} \left[\mathbf{K}_{SM} - \omega^2 \mathbf{M}_{SM} \right] \mathbf{U}_M \tag{4.9}$$

In contrast to a static analysis, Equation 4.9 depends on the angular frequency ω. In order to perform the model reduction, a fixed value for the frequency can be chosen. This approach is referred to as dynamic reduction, which is exact for the chosen frequency only.

If the terms including mass and frequency in Equation 4.9 are small or zero, this expression can be approximated by

$$\mathbf{U}_S = -\mathbf{K}_{SS}^{-1} \mathbf{K}_{SM} \mathbf{U}_M \tag{4.10}$$

which conforms to the Guyan reduction method (Equation 4.3) where effectively a frequency $\omega = 0$ is chosen. The transformation matrix $\mathbf{\Psi}$ is then given by

$$\begin{bmatrix} \mathbf{U}_S \\ \mathbf{U}_M \end{bmatrix} = \begin{bmatrix} -\mathbf{K}_{SS}^{-1} \mathbf{K}_{SM} \\ \mathbf{I} \end{bmatrix} \mathbf{U}_M = \mathbf{\Psi} \mathbf{U}_M \tag{4.11}$$

and the mass, stiffness and force matrices of the reduced system are calculated by

$$\begin{aligned} \mathbf{K}_R &= \mathbf{\Psi}^T \mathbf{K} \mathbf{\Psi} \\ \mathbf{M}_R &= \mathbf{\Psi}^T \mathbf{M} \mathbf{\Psi} \\ \mathbf{f}_R &= \mathbf{\Psi}^T \mathbf{f} \end{aligned} \tag{4.12}$$

The equation of motion

$$\mathbf{M}_R \ddot{\mathbf{u}}_M + \mathbf{K}_R \mathbf{u}_M = \mathbf{f}_R \tag{4.13}$$

and the eigenvalue problem

$$\left[\mathbf{K}_R - \lambda_j \mathbf{M}_R \right] \boldsymbol{\phi}_j = \mathbf{0} \tag{4.14}$$

are now reduced to the size of the set of master coordinates M. The solutions for the set of slave coordinates S are calculated using the transformation matrix (4.11). The static response is exact and the reduced stiffness matrix $\mathbf{K}_R$ preserves all information. The reduced mass matrix however is not exact since approximations

have been made to Equation 4.9. The eigenvalues and eigenvectors found from Equation 4.14 are thus close approximations to the exact solutions [60]. These are justified if low frequencies are considered or if the mass is small compared to the stiffness at coordinates S [77]. Additionally the off-diagonal terms $\mathbf{M}_{SM}$ are zero in diagonal mass-matrices or there may be no mass associated with some coordinates in a lumped-mass parameter model.

In practice often only a few coordinates have forces acting on them and the majority of coordinates could be reduced. The partitioning depends on the application and should comply with the approximations made in Equation 4.10. In substructuring the coordinates at the boundaries are retained and the interior coordinates can be eliminated.

A numerical example for the Guyan reduction method will be given for the system shown in Figure 4.1. It is a mass-spring chain consisting of four masses and

N/m	k_1 1025	k_2 1575	k_3 3025	k_4 2325
kg	m_1 5.5	m_2 13	m_3 9.5	m_4 17

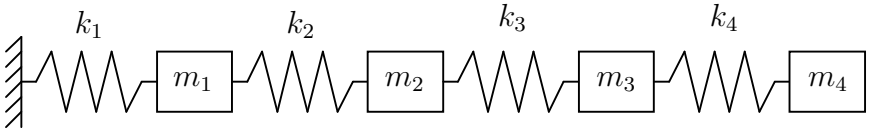

Figure 4.1: *Four degree of freedom model for analysis*

four springs, where at the left end spring k_1 is fixed and at the right end mass m_4 is free. The eigenfrequencies range from $0.58Hz$ to $4.55Hz$. The system is treated as one subsystem and mass 4 at the right boundary will be retained as a master DOF in all cases.

In Figure 4.2 the receptance frequency response function (FRF) $|\alpha_{14}|$ is plotted. This gives the response at DOF 1 for a time harmonic force applied at DOF 4. The exact solution and solutions of reduced systems with different sets of master and slave coordinates are shown. In Figure 4.2a, results are shown where coordinate 4 and one other coordinate at a time were chosen as master coordinates with the remaining two coordinates being condensed. The size of the reduced system is half the size of the original system and therefore two resonances are calculated. It can

be seen that the first resonance matches the exact solution very well in all cases. The second natural frequency however differs for the three cases. The accuracy depends on the approximation made as describe in the previous section. In general, the mass associated with the condensed coordinates and the contributions to the modal masses, which depend on the mode shapes, are determining factors. The fundamental frequency is predicted well, because the fundamental mode shape is similar to the static mode shape. In Figure 4.2b, results are shown for the cases where coordinate 4 and two other coordinates are retained, and hence only one coordinate is condensed. If mass 3 is condensed, the approximation of the second natural frequency is good, but the third frequency is in error. If mass 2 is condensed, the results improve for the third frequency but worsen for the second.

The Guyan reduction method is correct for a static analysis, but in a dynamic analysis a general error is introduced to the reduced mass matrix and therefore to the modal properties. In general all natural frequencies and modes shapes are affected because a modal mass depends on many physical masses. If the stated assumptions are met then the approximations are valid and Guyan reduction can also be used for dynamic analysis. However, the computational cost associated with calculating the inverse of $\mathbf{K}_{SS}$ in Equation 4.3 can be high. In substructuring, some or all of the interior DOFs can be condensed. The DOFs at the boundaries are retained so that the physical coupling of components is simple.

4.2.2 Modal reduction

The eigenvalue problem of a structure is given by

$$[\mathbf{K} - \lambda_j \mathbf{M}]\, \boldsymbol{\phi}_j = \mathbf{0} \tag{4.15}$$

where $\mathbf{K}$ and $\mathbf{M}$ are nxn matrices. A modal transformation from the physical coordinates u to the modal coordinates q can be done by the transformation

$$\mathbf{u} = \mathbf{\Phi q} \tag{4.16}$$

where the natural modes $\boldsymbol{\phi}$ are the columns of the modal matrix $\mathbf{\Phi}$. If only k modes are retained, this matrix reduces to $\mathbf{\Phi}_k$ and the transformation

$$\mathbf{u} = \mathbf{\Phi}_k \mathbf{q}_k \tag{4.17}$$

becomes a modal reduction from physical coordinates $\mathbf{u}$ to a smaller number of modal coordinates $\mathbf{q}_k$. The reduced mass and stiffness matrices and the force vector

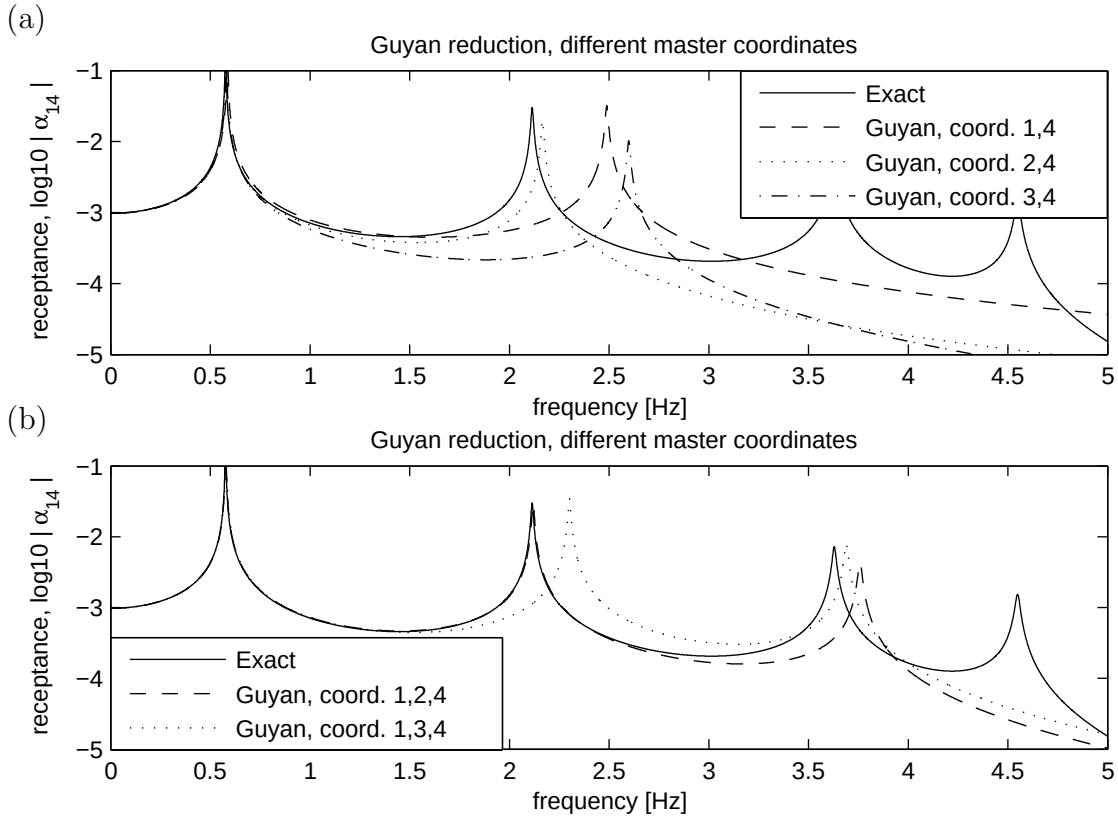

Figure 4.2: *Guyan reduction: comparison of implementations with different master coordinates.*

are given by

$$\mathbf{M}_R = \mathbf{\Phi}_k^T \mathbf{M} \mathbf{\Phi}_k \tag{4.18}$$

$$\mathbf{K}_R = \mathbf{\Phi}_k^T \mathbf{K} \mathbf{\Phi}_k \tag{4.19}$$

$$\mathbf{f}_R = \mathbf{\Phi}_k^T \mathbf{f} \tag{4.20}$$

and the reduced equation of motion is

$$\mathbf{M}_R \ddot{\mathbf{q}}_k + \mathbf{K}_R \mathbf{q} = \mathbf{f}_R \tag{4.21}$$

where $\mathbf{K}_R$ and $\mathbf{M}_R$ are now of size kxk.

Such a reduction has been applied to the system in Figure 4.1. In Figure 4.3 the FRF of the reduced system is shown and compared with the exact solution. Different sets of modes were used for the modal transformation. Figures 4.3a and 4.3b show the results if sets of two and three modes are used, respectively. It can be seen that each mode dominates the FRF around its associated resonance frequency, which is true if the damping is small. For a finite frequency range, only modes with resonance frequencies close to that range are needed to obtain the exact solution within limits.

In practice higher frequency modes are often neglected to reduce the size of the system. Since the modal coordinates are independent, other natural frequencies and mode shapes are not affected. Compared to static condensation the reduction takes place in the frequency domain rather than in the geometrical domain. This is most appropriate since only unneeded information is deleted and the effects are clear. However, the full eigenvalue problem has to be solved to obtain the required modes. The approach would be worthwhile though, if the reduced system can be used for a number of subsequent calculations. Another advantage arises in substructuring where it may be cheaper to solve the eigenvalue problem of a number of the components and of the assembled reduced global system compared to solving the complete global eigenvalue problem. The drawback of this approach is that all physical DOFs are transformed into modal DOFs and therefore the synthesis of components is not straightforward. Additionally the reduced equation of motion is not statically exact.

4.2.3 Modal reduction including static modes

Consider a modal transformation of a set of physical coordinates S in the form

$$\mathbf{u}_S = \mathbf{\Phi}^S \mathbf{q}_S \tag{4.22}$$

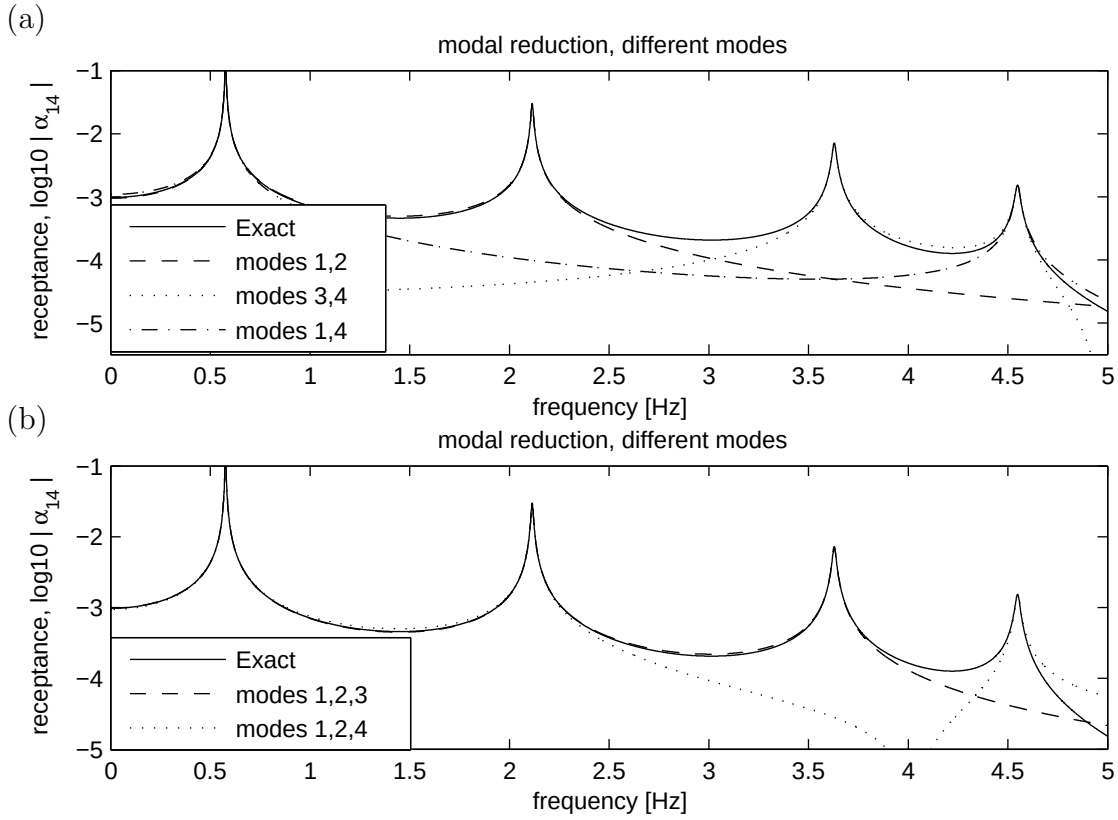

Figure 4.3: *Modal reduction: comparison of implementations with different modes retained.*

where $\mathbf{\Phi}^S$ is a set of the natural modes of the structure. Alternatively, the static reduction from Equation 4.3 can be included to get

$$\mathbf{u}_S = \mathbf{\Phi}^S \mathbf{q}_S - \mathbf{K}_{SS}^{-1} \mathbf{K}_{SM} \mathbf{u}_M \tag{4.23}$$

and the transformation matrix follows as

$$\begin{bmatrix} \mathbf{u}_S \\ \mathbf{u}_M \end{bmatrix} = \begin{bmatrix} \mathbf{\Phi}^S & -\mathbf{K}_{SS}^{-1} \mathbf{K}_{SM} \\ \mathbf{0} & \mathbf{I} \end{bmatrix} \begin{bmatrix} \mathbf{q}_S \\ \mathbf{u}_M \end{bmatrix} \tag{4.24}$$

In Equation 4.24 the natural modes $\mathbf{\Phi}^S$ and the static modes are used to relate the set of slave coordinates S to modal coordinates and master coordinates M. The transformation 4.24 is exact, if the natural modes and the static modes are linearly independent. A static mode is the displacement of all nodes due to a unit displacement applied at one coordinate of the M set and all other coordinates M fixed. Therefore, the modes $\mathbf{\Phi}^S$ can be defined as the natural modes of the structure with all DOFs $\mathbf{u}_M$ fixed. The eigenvalue problem for this case is given by

$$\left[\mathbf{K}_{SS} - \lambda_j \mathbf{M}_{SS}\right] \boldsymbol{\phi}_j^S = \mathbf{0} \tag{4.25}$$

If none of the natural modes are used, this approach equals the Guyan reduction presented in Section 4.2.1. If all nodes are considered as slave coordinates S, this becomes the modal reduction method described in Section 4.2.2.

In order to achieve a reduction in the size of the equation of motion, only some of the natural modes will be kept in $\mathbf{\Phi}_k^S$ and the transformation matrix becomes

$$\mathbf{B} = \begin{bmatrix} \mathbf{\Phi}_k^S & -\mathbf{K}_{SS}^{-1} \mathbf{K}_{SM} \\ \mathbf{0} & \mathbf{I} \end{bmatrix} \tag{4.26}$$

which reduces the mass and stiffness matrices by

$$\begin{aligned} \mathbf{K}_R &= \mathbf{B}^T \mathbf{K} \mathbf{B} \\ \mathbf{M}_R &= \mathbf{B}^T \mathbf{M} \mathbf{B} \\ \mathbf{f}_R &= \mathbf{B}^T \mathbf{f} \end{aligned} \tag{4.27}$$

The transformation presented here is used in one method of component mode synthesis, where a component is modelled with fixed-interface normal modes and static constraint modes to account for the fixed interfaces. The boundary DOFs, which are shared with other components, are selected for the set of coordinates M, while all interior DOFs form the set S of coordinates. The physical boundary coordi-

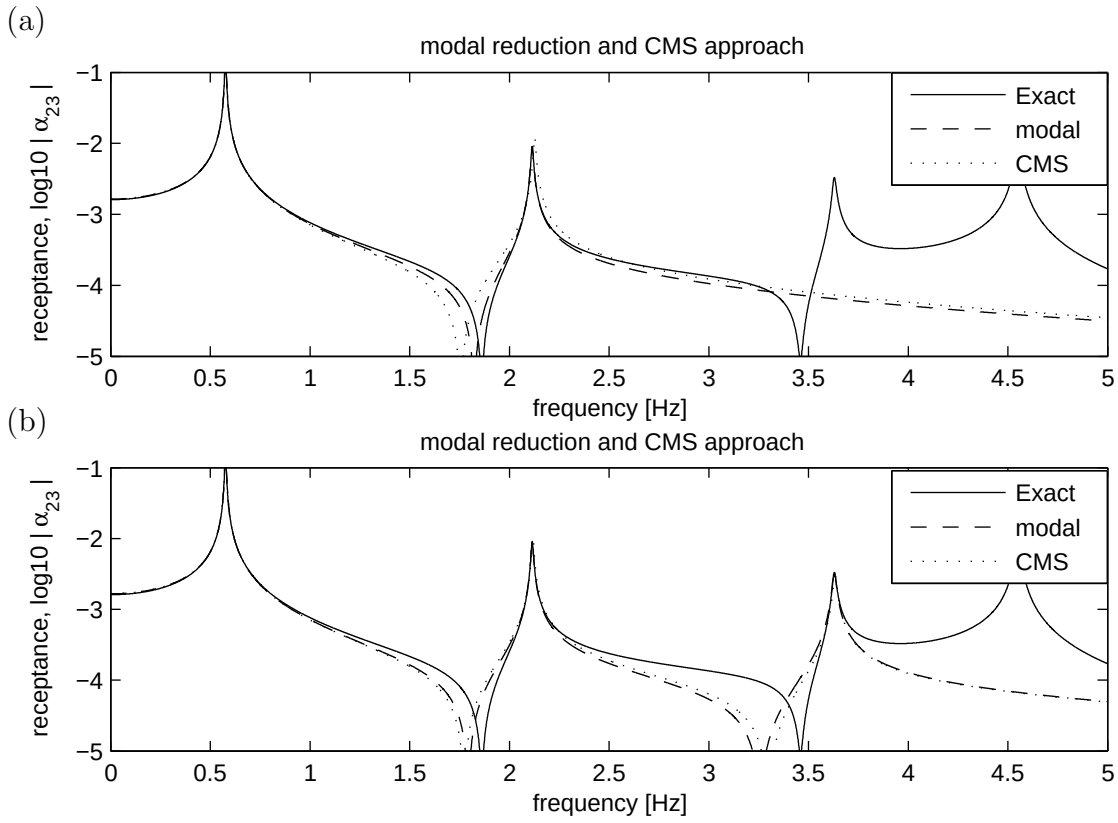

Figure 4.4: *Comparison of modal reduction and CMS approach. Approximation of first two and three modes, respectively.*

nates are retained and the assembly of components is straightforward. The size of the component model can be reduced by neglecting some of the higher frequency fixed-interface normal modes. Additionally the reduced equation of motion is statically exact due to the constraint modes. The advantages of modal reduction and Guyan reduction are combined. Guyan reduction, modal reduction and component mode synthesis belong to the class of Rayleigh-Ritz methods with certain Ritz basis vectors [77].

For the example in Figure 4.1, this fixed-interface CMS approach will be compared with the modal reduction approach. Mass 4 at the right end will be considered the boundary DOF where other components may be attached. Three natural modes are found for masses 1 to 3 when mass 4 is fixed. Some of these will be used in addition to the static constraint mode for the transformation into modal space. The results for different cases, where one or two of the natural modes are retained are plotted in Figure 4.4a and 4.4b, respectively. The static mode is a good approximation to the fundamental mode and therefore the fundamental frequency is predicted well. The first, second and third mode of the constrained system correspond to the

second, third and fourth mode of the original system. The resonance frequencies are predicted very well with a small difference in the magnitude for the CMS solution. If more natural modes are taken into account, as in Figure 4.4b, the approximation of all modes improves.

4.3 Component Mode Synthesis

The component mode synthesis method will be described in detail in this section. Component mode synthesis (CMS) is a technique to assemble models of several components. The static and dynamic behaviour of each component is described in terms of a set of basis functions, e.g. the modes of the component. These include normal modes found from solving a component eigenvalue problem and additional static constraint or attachment modes. The reduction in size is achieved by truncating higher frequency modes at the component level.

CMS methods originated in the 1960's and 70's, starting with a publication by Hurty in 1965 [79]. Since then, numerous CMS methods have been presented, with major contributions by Craig et al. [61, 85, 88]. Books on structural dynamics with chapters dedicated to CMS are [9, 82, 83]. A general review of CMS methods can be found in [81, 84, 86, 87].

In the following sections, first, different types of common component modes are defined and a generalised approach for the coupling of components is presented. Subsequently, the two most common CMS methods, the fixed-interface Craig-Bampton method [61] and the free-interface Craig-Chang method [85, 88] are discussed in detail and compared by numerical examples.

4.3.1 Modes in Component Mode Synthesis

In this section, component modes of different types will be derived. The undamped equation of motion of a component is given by

$$\mathbf{M}\ddot{\mathbf{u}} + \mathbf{K}\mathbf{u} = \mathbf{f} \tag{4.28}$$

where $\mathbf{u}$ are the physical DOFs and $\mathbf{M}$ and $\mathbf{K}$ are the mass and stiffness matrices, respectively. The physical DOFs can be partitioned into a set of interior DOFs $\mathbf{u}_I$ and a set of interface, or boundary, DOFs $\mathbf{u}_B$. The interface coordinates are those coordinates where two or more components are joined together. Each component alone can be unconstrained or constrained (no rigid body freedom). Equation 4.28

can be written as

$$\begin{bmatrix} \mathbf{M}_{II} & \mathbf{M}_{IB} \\ \mathbf{M}_{BI} & \mathbf{M}_{BB} \end{bmatrix} \begin{bmatrix} \ddot{\mathbf{u}}_I \\ \ddot{\mathbf{u}}_B \end{bmatrix} + \begin{bmatrix} \mathbf{K}_{II} & \mathbf{K}_{IB} \\ \mathbf{K}_{BI} & \mathbf{K}_{BB} \end{bmatrix} \begin{bmatrix} \mathbf{u}_I \\ \mathbf{u}_B \end{bmatrix} = \begin{bmatrix} \mathbf{f}_I \\ \mathbf{f}_B \end{bmatrix} \tag{4.29}$$

where $\mathbf{f}_B = \mathbf{0}$ if the interface is free and $\mathbf{u}_B = \mathbf{0}$ if the interface is fixed. There are no forces acting on the interior DOFs ($\mathbf{f}_I = \mathbf{0}$).

Free-interface normal modes

The free-interface normal modes of a component are the eigenvectors of the component with the boundary DOFs free. They are found from solving the eigenvalue problem

$$(\mathbf{K} - \lambda_j^{fr}\mathbf{M})\boldsymbol{\phi}_j^{fr} = \mathbf{0} \tag{4.30}$$

and can be combined as columns to give the normal mode matrix $\boldsymbol{\Phi}_n^{fr}$. The normal modes may be divided into a set of modes k to be kept for further calculations and a complementary set of modes d that will be deleted, i.e.

$$\boldsymbol{\Phi}^{fr} = \begin{bmatrix} \boldsymbol{\Phi}_k^{fr} & \boldsymbol{\Phi}_d^{fr} \end{bmatrix} \tag{4.31}$$

Similarly, the eigenvalues λ are arranged on the diagonal of the eigenvalue matrix $\boldsymbol{\Lambda}$ and can be divided into sets k and d to give

$$\boldsymbol{\Lambda}^{fr} = \begin{bmatrix} \boldsymbol{\Lambda}_k^{fr} & \mathbf{0} \\ \mathbf{0} & \boldsymbol{\Lambda}_d^{fr} \end{bmatrix} \tag{4.32}$$

If a component is unconstrained, the normal mode set contains rigid body modes with zero-valued eigenvalues.

Fixed-interface normal modes

The fixed-interface normal modes of a component are the eigenvectors of the component with the interface DOFs fixed. The size of the eigenvalue problem is therefore reduced by the number of interface DOFs. It is governed by the elements of the mass and stiffness matrices associated with the interior DOFs only and given as

$$(\mathbf{K}_{II} - \lambda_j^{fi}\mathbf{M}_{II})\boldsymbol{\phi}_{I_j}^{fi} = \mathbf{0} \tag{4.33}$$

where λ_j^{fi} are the fixed-interface eigenvalues. The eigenvectors $\boldsymbol{\phi}_{I_j}^{fi}$ form the columns of the normal mode matrix $\boldsymbol{\Phi}^{fi}$, which can be divided into a matrix with kept (k)

and deleted (d) modes, respectively. The normal mode matrix is then

$$\mathbf{\Phi}^{fi} = \begin{bmatrix} \mathbf{\Phi}_k^{fi} & \mathbf{\Phi}_d^{fi} \end{bmatrix} = \begin{bmatrix} \mathbf{\Phi}_{Ik}^{fi} & \mathbf{\Phi}_{Id}^{fi} \\ \mathbf{0}_{Bk} & \mathbf{0}_{Bd} \end{bmatrix} \tag{4.34}$$

where $\mathbf{0}_B$ relate to the DOFs of the fixed boundary. There are no rigid body modes in Equation 4.34 if the set of fixed boundary DOFs is sufficient to constrain all rigid body modes of the unconstrained component.

Constraint modes

Static constraint modes will be defined with respect to the interface DOFs and denoted by the subscript c. A constraint mode is the static displacement of all nodes due to a unit displacement applied to one interface coordinate and with all other interface coordinates fixed. This can be written in matrix form as

$$\begin{bmatrix} \mathbf{K}_{II} & \mathbf{K}_{Ic} \\ \mathbf{K}_{cI} & \mathbf{K}_{cc} \end{bmatrix} \begin{bmatrix} \mathbf{\Psi}_{Ic} \\ \mathbf{I}_{cc} \end{bmatrix} = \begin{bmatrix} \mathbf{0}_{Ic} \\ \mathbf{F}_{cc} \end{bmatrix} \tag{4.35}$$

where $\mathbf{\Psi}_{Ic}$ is a matrix of displacements of the interior DOFs and $\mathbf{I}_{cc}$ is an identity matrix, which defines zero and unit displacements for all constraint modes. $\mathbf{F}_{cc}$ are the force reactions at the nodes with prescribed displacements and the interior nodes are force-free. From the first line of Equation 4.35 it follows that

$$\mathbf{\Psi}_{Ic} = -\mathbf{K}_{II}^{-1}\mathbf{K}_{Ic} \tag{4.36}$$

and the complete matrix of constraint modes is given by

$$\mathbf{\Psi}_c = \begin{bmatrix} -\mathbf{K}_{II}^{-1}\mathbf{K}_{Ic} \\ \mathbf{I}_{cc} \end{bmatrix} \tag{4.37}$$

To make the structure of the previous matrix expressions more clear, they are rewritten for the case of two boundary DOFs. Equation 4.35 becomes

$$\begin{bmatrix} \mathbf{K}_{II} & \mathbf{K}_{Ic_1} & \mathbf{K}_{Ic_2} \\ \mathbf{K}_{c_1I} & K_{c_1c_1} & K_{c_1c_2} \\ \mathbf{K}_{c_2I} & K_{c_2c_1} & K_{c_2c_2} \end{bmatrix} \begin{bmatrix} \mathbf{\Psi}_{Ic_1} & \mathbf{\Psi}_{Ic_2} \\ 1 & 0 \\ 0 & 1 \end{bmatrix} = \begin{bmatrix} \mathbf{0}_{Ic_1} & \mathbf{0}_{Ic_2} \\ R_{c_1c_1} & R_{c_1c_2} \\ R_{c_2c_1} & R_{c_2c_2} \end{bmatrix} \tag{4.38}$$

where the constraint modes are given by

$$\boldsymbol{\Psi}_c = \begin{bmatrix} -\mathbf{K}_{II}^{-1}\mathbf{K}_{Ic_1} & -\mathbf{K}_{II}^{-1}\mathbf{K}_{Ic_2} \\ 1 & 0 \\ 0 & 1 \end{bmatrix} \tag{4.39}$$

Rigid body modes

Rigid body modes appear if a component is unconstrained. They are obtained either as free-interface normal modes (Equation 4.31) from the eigenvalue problem or recovered from constraint modes (Equation 4.37). However they are often regarded as a separate class of component modes and will be denoted by $\boldsymbol{\Psi}_r$.

Attachment Modes

Static attachment modes will be defined with respect to the boundary DOFs and will be denoted by the subscript a. An attachment mode is the static displacement of all nodes due to a unit force applied to one boundary coordinate and with all other boundary coordinates a force-free. Since forces are applied, the cases of a constrained and an unconstrained component have to be distinguished. If the component is constrained the governing static equation is given by

$$\begin{bmatrix} \mathbf{K}_{II} & \mathbf{K}_{Ia} \\ \mathbf{K}_{aI} & \mathbf{K}_{aa} \end{bmatrix} \begin{bmatrix} \boldsymbol{\Psi}_{Ia} \\ \boldsymbol{\Psi}_{aa} \end{bmatrix} = \begin{bmatrix} \mathbf{0}_{Ia} \\ \mathbf{I}_{aa} \end{bmatrix} \tag{4.40}$$

where $\boldsymbol{\Psi}_{Ia}$ and $\boldsymbol{\Psi}_{aa}$ are the unknown nodal displacements. The identity matrix $\mathbf{I}_{aa}$ arises from the forces at the boundary DOFs. All interior DOFs are force-free. A solution can be found by inverting the stiffness matrix $\mathbf{K}$, where $\mathbf{G} = \mathbf{K}^{-1}$ is the flexibility matrix, assuming the inverse exists, to give

$$\begin{bmatrix} \boldsymbol{\Psi}_{Ia} \\ \boldsymbol{\Psi}_{aa} \end{bmatrix} = \begin{bmatrix} \mathbf{K}_{II} & \mathbf{K}_{Ia} \\ \mathbf{K}_{aI} & \mathbf{K}_{aa} \end{bmatrix}^{-1} \begin{bmatrix} \mathbf{0}_{Ia} \\ \mathbf{I}_{aa} \end{bmatrix} = \begin{bmatrix} \mathbf{G}_{II} & \mathbf{G}_{Ia} \\ \mathbf{G}_{aI} & \mathbf{G}_{aa} \end{bmatrix} \begin{bmatrix} \mathbf{0}_{Ia} \\ \mathbf{I}_{aa} \end{bmatrix} \tag{4.41}$$

The attachment modes are then found to be

$$\boldsymbol{\Psi}_a = \begin{bmatrix} \mathbf{G}_{Ia} \\ \mathbf{G}_{aa} \end{bmatrix} \tag{4.42}$$

If the component is not constrained there is no solution for the displacement due to an applied force. The stiffness matrix is singular and cannot be inverted. Therefore, the component must be sufficiently restrained against rigid body motion at a set of coordinates r, normally a subset of the interior DOFs. Rigid body modes

are then added separately. The attachment modes with respect to the boundary coordinates a and relative to the restraint coordinates are described by

$$\begin{bmatrix} \mathbf{K}_{\hat{I}\hat{I}} & \mathbf{K}_{\hat{I}a} & \mathbf{K}_{\hat{I}r} \\ \mathbf{K}_{a\hat{I}} & \mathbf{K}_{aa} & \mathbf{K}_{ar} \\ \mathbf{K}_{r\hat{I}} & \mathbf{K}_{ra} & \mathbf{K}_{rr} \end{bmatrix} \begin{bmatrix} \boldsymbol{\Psi}_{\hat{I}a} \\ \boldsymbol{\Psi}_{aa} \\ \mathbf{0}_{ra} \end{bmatrix} = \begin{bmatrix} \mathbf{0}_{\hat{I}a} \\ \mathbf{I}_{aa} \\ \mathbf{F}_{ra} \end{bmatrix} \tag{4.43}$$

where $\boldsymbol{\Psi}_{\hat{I}a}$ and $\boldsymbol{\Psi}_{aa}$ are the unknown displacements and $\mathbf{0}_{ra}$ correspond to the fixed restraint coordinates. The forces acting on the boundary DOFs are $\mathbf{I}_{aa}$, while the unrestrained interior DOFs are force-free and the restrained coordinates have reactive forces $\mathbf{F}_{ra}$ acting on them. The static equation can be reduced to

$$\begin{bmatrix} \mathbf{K}_{\hat{I}\hat{I}} & \mathbf{K}_{\hat{I}a} \\ \mathbf{K}_{a\hat{I}} & \mathbf{K}_{aa} \end{bmatrix} \begin{bmatrix} \boldsymbol{\Psi}_{\hat{I}a} \\ \boldsymbol{\Psi}_{aa} \end{bmatrix} = \begin{bmatrix} \mathbf{0}_{\hat{I}a} \\ \mathbf{I}_{aa} \end{bmatrix} \tag{4.44}$$

and the resulting stiffness matrix can be inverted. The attachment modes are found as columns of the flexibility matrix with zeros added for the fixed displacements.

$$\boldsymbol{\Psi}_a = \begin{bmatrix} \mathbf{G}_{\hat{I}a} \\ \mathbf{G}_{aa} \\ \mathbf{0}_{ra} \end{bmatrix} \tag{4.45}$$

Residual attachment modes

The flexibility matrix of a system without rigid body modes can be written in terms of free-interface properties as

$$\mathbf{G} = \boldsymbol{\Phi}\boldsymbol{\Lambda}^{-1}\boldsymbol{\Phi}^T \tag{4.46}$$

where $\boldsymbol{\Phi}$ is the free-interface normal mode matrix and $\boldsymbol{\Lambda}$ are the free-interface eigenvalues. Equation 4.46 can be rewritten as

$$\mathbf{G} = \boldsymbol{\Phi}\boldsymbol{\Lambda}^{-1}\boldsymbol{\Phi}^T = \boldsymbol{\Phi}_k\boldsymbol{\Lambda}_k^{-1}\boldsymbol{\Phi}_k^T + \boldsymbol{\Phi}_d\boldsymbol{\Lambda}_d^{-1}\boldsymbol{\Phi}_d^T \tag{4.47}$$

where subscripts k and d denote the kept and deleted modes, respectively.

$$\mathbf{G}_d = \boldsymbol{\Phi}_d\boldsymbol{\Lambda}_d^{-1}\boldsymbol{\Phi}_d^T \tag{4.48}$$

is the residual flexibility matrix associated with the deleted modes. The matrix of

forces is given in Equation 4.40 as

$$\mathbf{F}_a = \begin{bmatrix} \mathbf{0}_{Ia} \\ \mathbf{I}_{aa} \end{bmatrix} \tag{4.49}$$

where a unit force is a applied to one of the boundary DOFs at a time with all other DOFs force-free. A set of residual attachment modes is then defined by

$$\mathbf{\Psi}_{a_R} = \mathbf{G}_d \mathbf{F}_a \tag{4.50}$$

By using the residual flexibility matrix the residual attachment modes are a linear combination of the deleted normal modes and therefore linearly independent of the kept normal modes. Another advantage is that this approach also holds for components with rigid body freedom.

For an unconstrained system, the response in the rigid body modes can be represented by inertia relief attachment modes. In one approach these are defined as the static displacement of all nodes due to d'Alembert forces resulting from a rigid body motion. Another approach is to apply both unit forces and d'Alembert forces, which would result from the rigid body motion due to the unit forces alone, to the set of boundary DOFs. In both cases the component has to be sufficiently constrained. There are also residual inertia relief attachment modes, which are independent of the kept normal modes. An equivalent to the modal space is the Krylov space, which is described by Krylov vectors instead of eigenvectors. These Krylov modes are also used in CMS. Details on these other component modes can be found in the review papers [81, 84, 86, 87].

4.3.2 Synthesis of Components

A selection of component modes described in the previous section is arranged in a component modal matrix $\mathbf{B}$. Usually these are one of two general types: kept fixed-interface modes and constraint modes; kept free-interface modes and attachment modes. The physical coordinates $\mathbf{u}^\alpha$ of a component α can be transformed into the component modal coordinates $\mathbf{q}^\alpha$ by

$$\mathbf{u}^\alpha = \mathbf{B}^\alpha \mathbf{q}^\alpha \tag{4.51}$$

where the columns of $\mathbf{B}$ correspond to the appropriate mode shapes. The component modal mass and stiffness matrices $\boldsymbol{\mu}$ and $\boldsymbol{\kappa}$ are calculated by

$$\boldsymbol{\mu}^\alpha = \mathbf{B}^{\alpha T} \mathbf{M}^\alpha \mathbf{B}^\alpha \quad \text{and} \quad \boldsymbol{\kappa}^\alpha = \mathbf{B}^{\alpha T} \mathbf{K}^\alpha \mathbf{B}^\alpha \tag{4.52}$$

respectively, which are diagonal matrices if the modes used in $\mathbf{B}^\alpha$ are linearly independent. If two components α and β are considered, a global modal vector $\mathbf{q}$ can be formed as

$$\mathbf{q} = \begin{bmatrix} \mathbf{q}^\alpha \\ \mathbf{q}^\beta \end{bmatrix} \tag{4.53}$$

and the modal mass and stiffness matrices of the components are assembled as

$$\boldsymbol{\mu} = \begin{bmatrix} \boldsymbol{\mu}^\alpha & \mathbf{0} \\ \mathbf{0} & \boldsymbol{\mu}^\beta \end{bmatrix} \quad \text{and} \quad \boldsymbol{\kappa} = \begin{bmatrix} \boldsymbol{\kappa}^\alpha & \mathbf{0} \\ \mathbf{0} & \boldsymbol{\kappa}^\beta \end{bmatrix} \tag{4.54}$$

Let n be the number of DOFs of the global structure. Then

$$n = n^\alpha + n^\beta - n_B^{\alpha\beta} \tag{4.55}$$

where n^α and n^β are the numbers of modal DOFs of component α and β, respectively, and $n_B^{\alpha\beta}$ is the number of common interface DOFs. The number of modal DOFs in Equation 4.53 is given by

$$n_q = n_k^\alpha + n_k^\beta + n_{c,a}^\alpha + n_{c,a}^\beta \tag{4.56}$$

where n_k^α and n_k^β are the numbers of kept modes and $n_{c,a}^\alpha$ and $n_{c,a}^\beta$ are the numbers of constraint or attachment modes used for each component.

The constraints at the component interface are continuity of displacement, $\mathbf{u}_B^\alpha = \mathbf{u}_B^\beta$, and equilibrium of forces, $\mathbf{f}_B^\alpha + \mathbf{f}_B^\beta = \mathbf{0}$. The constraint equations of the conditions to be satisfied can be expressed in terms of the modal coordinates $\mathbf{q}$ and written in matrix form as

$$\mathbf{H}\mathbf{q} = \mathbf{0} \tag{4.57}$$

where $\mathbf{H}$ is the constraint matrix. This equation can be partitioned into linearly independent coordinates l and dependent coordinates d which will be condensed and whose number equals the number of constraint equations considered. Thus

$$\begin{bmatrix} \mathbf{H}_{dd} & \mathbf{H}_{dl} \end{bmatrix} \begin{bmatrix} \mathbf{q}_d \\ \mathbf{q}_l \end{bmatrix} = \mathbf{0} \tag{4.58}$$

The dependent coordinates are related to the linearly independent coordinates by

$$\mathbf{q}_d = -\mathbf{H}_{dd}^{-1}\mathbf{H}_{dl}\mathbf{q}_l \tag{4.59}$$

and a linear transformation can be defined as

$$\mathbf{q} = \begin{bmatrix} \mathbf{q}_d \\ \mathbf{q}_l \end{bmatrix} = \mathbf{C}\mathbf{q}_l = \mathbf{C}\mathbf{v} \tag{4.60}$$

where $\mathbf{v}$ is the new set of independent modal coordinates and

$$\mathbf{C} = \begin{bmatrix} -\mathbf{H}_{dd}^{-1}\mathbf{H}_{dl} \\ \mathbf{I}_{ll} \end{bmatrix} \tag{4.61}$$

is the transformation matrix. The mass and stiffness matrices of the global system are then found by

$$\mathbf{M}_R^{gl} = \mathbf{C}^T\boldsymbol{\mu}\mathbf{C} \quad \text{and} \quad \mathbf{K}_R^{gl} = \mathbf{C}^T\boldsymbol{\kappa}\mathbf{C} \tag{4.62}$$

which are reduced in size compared to the original system if not all of the natural modes of the components are kept in Equation 4.51.

If the component mass, stiffness and modal matrices are assembled in the form

$$\mathbf{M}^{\alpha\beta} = \begin{bmatrix} \mathbf{M}^{\alpha} & \mathbf{0} \\ \mathbf{0} & \mathbf{M}^{\beta} \end{bmatrix}, \quad \mathbf{K}^{\alpha\beta} = \begin{bmatrix} \mathbf{K}^{\alpha} & \mathbf{0} \\ \mathbf{0} & \mathbf{K}^{\beta} \end{bmatrix}, \quad \mathbf{B} = \begin{bmatrix} B^{\alpha} & \mathbf{0} \\ \mathbf{0} & \mathbf{B}^{\beta} \end{bmatrix} \tag{4.63}$$

then the mass and stiffness matrices of the global system are determined by two consecutive transformations in the form

$$\mathbf{M}_R^{gl} = \mathbf{C}^T\mathbf{B}^T\mathbf{M}^{\alpha\beta}\mathbf{B}\mathbf{C} \tag{4.64}$$

and

$$\mathbf{K}_R^{gl} = \mathbf{C}^T\mathbf{B}^T\mathbf{K}^{\alpha\beta}\mathbf{B}\mathbf{C} \tag{4.65}$$

where the transformation $\mathbf{B}$ into modal coordinates may imply a reduction in size and the transformation $\mathbf{C}$ imposes the selected interface conditions.

4.3.3 Global modes and frequency response function

The free vibration equation of motion of the global system in terms of coordinates $\mathbf{v}$ is given by

$$\mathbf{M}_R^{gl}\ddot{\mathbf{v}} + \mathbf{K}_R^{gl}\mathbf{v} = \mathbf{0} \tag{4.66}$$

A transformation into global modal coordinates $\mathbf{w}$ can be done by

$$\mathbf{v} = \mathbf{D}\mathbf{w} \tag{4.67}$$

where $\mathbf{D}$ is the matrix of global eigenvectors, which are found from the global eigenvalue problem

$$\left(\mathbf{K}_R^{gl} - \lambda_j^{gl}\mathbf{M}_R^{gl}\right)\boldsymbol{\phi}_j^{gl} = \mathbf{0} \tag{4.68}$$

Provided these modes are mass-normalised, the global modal mass and stiffness matrices are given by

$$\boldsymbol{\mu}_R^{gl} = \mathbf{D}^T\mathbf{M}_R^{gl}\mathbf{D} = \mathbf{I} \tag{4.69}$$

and

$$\boldsymbol{\kappa}_R^{gl} = \mathbf{D}^T\mathbf{K}_R^{gl}\mathbf{D} = \boldsymbol{\Lambda}^{gl} \tag{4.70}$$

which are uncoupled diagonal matrices.

To summarise, the transformation from the physical coordinates $\mathbf{u}$ to the global modal coordinates $\mathbf{w}$ involves the following transformations and coordinates:

$\mathbf{u}$		physical coordinates
	$\mathbf{u} = \mathbf{Bq}$	modal transformation at component level
$\mathbf{q}$		component modal coordinates
	$\mathbf{q} = \mathbf{Cv}$	transformation to impose coupling conditions
$\mathbf{v}$		linearly independent component modal coordinates
	$\mathbf{v} = \mathbf{Dw}$	modal transformation at global level
$\mathbf{w}$		global modal coordinates

Initially, each component and its properties are defined in terms of the physical coordinates $\mathbf{u}$. Depending on the particular method, appropriate modes are selected to form the modal matrix $\mathbf{B}$. Usually these include free or fixed-interface modes and additional component modes. The synthesis of components is done at the component modal level and is represented by the linear transformation $\mathbf{C}$. The modal coordinates $\mathbf{q}$, which include dependencies between different components, are transformed into an independent set of component modal coordinates $\mathbf{v}$. The equation of motion of the whole structure is given in terms of coordinates $\mathbf{v}$ and the modal properties of the whole structure can be found by the transformation $\mathbf{D}$ into global modal coordinates $\mathbf{w}$.

The relation between global modal coordinates $\mathbf{w}$ and physical coordinates $\mathbf{u}$ can be expressed as

$$\mathbf{u} = \mathbf{Lw} \quad ; \qquad \mathbf{L} = \mathbf{BCD} \tag{4.71}$$

where $\mathbf{L}$ is the global modal matrix that contains the global modes in terms of the physical coordinates.

The equation of motion for forced vibration in terms of the global modal coordinates is given as

$$\boldsymbol{\mu}_R^{gl}\ddot{\mathbf{w}} + \boldsymbol{\kappa}_R^{gl}\mathbf{w} = \mathbf{f} \tag{4.72}$$

where

$$\mathbf{f} = \mathbf{L}^T\mathbf{f}^{\alpha\beta} \quad \text{and} \quad \mathbf{f}^{\alpha\beta} = \begin{bmatrix} \mathbf{f}^{\alpha} & 0 \\ 0 & \mathbf{f}^{\beta} \end{bmatrix} \tag{4.73}$$

Assuming time harmonic motion $\mathbf{u} = \mathbf{U}e^{i\omega t}$, $\mathbf{w} = \mathbf{W}e^{i\omega t}$ and forces $\mathbf{f} = \mathbf{F}e^{i\omega t}$, the frequency response in global modal coordinates follows as

$$\mathbf{W} = diag\left(\frac{1}{\lambda_j^{gl} - \omega^2}\right)\mathbf{F} \tag{4.74}$$

and the receptance matrix $\mathbf{A}$ in terms of the physical coordinates and forces is given such that

$$\mathbf{U} = \mathbf{A}\mathbf{F}^{\alpha\beta} = \left[\mathbf{L} \quad diag\left(\frac{1}{\lambda_j^{gl} - \omega^2}\right)\mathbf{L}^T\right]\mathbf{F}^{\alpha\beta} \tag{4.75}$$

The two most common approaches in CMS are the fixed-interface method with constraint modes and the free-interface method with attachment modes. These will be described in more detail in the remaining sections of this chapter.

4.3.4 Fixed-interface method with constraint modes

In the fixed-interface method of CMS, fixed normal modes $\boldsymbol{\Phi}^{fi}$ of a component are found with the boundaries fixed. To account for that condition, Craig and Bampton [61] add static constraint modes $\boldsymbol{\Psi}_c$ to the component modal matrix $\mathbf{B}$. These assure the compatibility of the components, improve convergence and also yield the exact static solution. A reduction in the size of the component model can be achieved by keeping only some of the fixed-interface normal modes in $\boldsymbol{\Phi}_k^{fi}$. The component modal matrix of a component α is then defined as

$$\mathbf{B}^{\alpha} = \begin{bmatrix} \boldsymbol{\Phi}_k^{fi} & \boldsymbol{\Psi}_c \end{bmatrix}^{\alpha} \tag{4.76}$$

and the transformation from physical coordinates $\mathbf{u}^{\alpha}$ to component modal coordinates $\mathbf{q}^{\alpha}$ is given by

$$\mathbf{u}^{\alpha} = \mathbf{B}^{\alpha}\mathbf{q}^{\alpha} = \begin{bmatrix} \mathbf{u}_I^{\alpha} \\ \mathbf{u}_B^{\alpha} \end{bmatrix} = \begin{bmatrix} \boldsymbol{\Phi}_{Ik}^{fi} & -\mathbf{K}_{II}^{-1}\mathbf{K}_{Ic} \\ \mathbf{0} & \mathbf{I}_{cc} \end{bmatrix}^{\alpha} \begin{bmatrix} \mathbf{q}_k^{\alpha} \\ \mathbf{q}_c^{\alpha} \end{bmatrix} \tag{4.77}$$

The interior physical coordinates $\mathbf{u}_I$ are transformed into modal coordinates $\mathbf{q}_k$. The physical boundary coordinates $\mathbf{u}_B$ are retained, but will be denoted as constraint coordinates $\mathbf{q}_c$. The component modal mass matrix follows in the form

$$\boldsymbol{\mu}^\alpha = \begin{bmatrix} \mathbf{I}_{kk} & \mathbf{m}_{kc} \\ \mathbf{m}_{kc}^T & \mathbf{m}_{cc} \end{bmatrix}^\alpha \tag{4.78}$$

where $\mathbf{I}_{kk}$ is a identity matrix if the normal modes are mass-normalised. The matrix $\mathbf{m}_{cc}$ contains the modal constraint masses and $\mathbf{m}_{kc}$ are coupling matrices between the modal coordinates $\mathbf{q}_k$ and the constraint coordinates $\mathbf{q}_c$. The component modal stiffness matrix is given by

$$\boldsymbol{\kappa}^\alpha = \begin{bmatrix} \boldsymbol{\Lambda}_{kk} & \mathbf{0} \\ \mathbf{0} & \mathbf{k}_{cc} \end{bmatrix}^\alpha \tag{4.79}$$

where $\boldsymbol{\Lambda}_{kk}$ is a diagonal matrix of eigenvalues and $\mathbf{k}_{cc}$ is the constraint modal stiffness matrix. If two components α and β are considered, the vector of modal coordinates $\mathbf{q}$ can be written as

$$\mathbf{q} = \begin{bmatrix} \mathbf{q}_k^{\alpha^T} & \mathbf{q}_c^{\alpha^T} & \mathbf{q}_k^{\beta^T} & \mathbf{q}_c^{\beta^T} \end{bmatrix}^T \tag{4.80}$$

At the interface of components α and β, the boundary condition of continuity of displacements is given by

$$\mathbf{u}_B^\alpha = \mathbf{u}_B^\beta \tag{4.81}$$

which can be transformed into modal space by Equation 4.77 to become

$$\mathbf{q}_c^\alpha = \mathbf{q}_c^\beta = \mathbf{q}_c \tag{4.82}$$

if $\mathbf{q}_c^\alpha$ and $\mathbf{q}_c^\beta$ are consistent. The matrix constraint equation now takes the form

$$\mathbf{H}\mathbf{q} = \begin{bmatrix} \mathbf{0} & \mathbf{I} & \mathbf{0} & -\mathbf{I} \end{bmatrix} \begin{bmatrix} \mathbf{q}_k^{\alpha^T} & \mathbf{q}_c^{\alpha^T} & \mathbf{q}_k^{\beta^T} & \mathbf{q}_c^{\beta^T} \end{bmatrix}^T = \mathbf{0} \tag{4.83}$$

and the transformation to impose the coupling conditions follows from Equation 4.61 as

$$\mathbf{q} = \begin{bmatrix} \mathbf{q}_k^\alpha \\ \mathbf{q}_c^\alpha \\ \mathbf{q}_k^\beta \\ \mathbf{q}_c^\beta \end{bmatrix} = \begin{bmatrix} \mathbf{I} & \mathbf{0} & \mathbf{0} \\ \mathbf{0} & \mathbf{0} & \mathbf{I} \\ \mathbf{0} & \mathbf{I} & \mathbf{0} \\ \mathbf{0} & \mathbf{0} & \mathbf{I} \end{bmatrix} \begin{bmatrix} \mathbf{q}_k^\alpha \\ \mathbf{q}_k^\beta \\ \mathbf{q}_c \end{bmatrix} = \mathbf{C}\mathbf{v} \tag{4.84}$$

where $\mathbf{C}$ is the transformation matrix and $\mathbf{v}$ are linearly independent modal coordinates. The reduced global system matrices are found by Equation 4.63. Their

structure is similar to the component modal matrices, so that

$$\mathbf{M}_R^{gl} = \begin{bmatrix} \mathbf{I}_{kk}^{\alpha} & \mathbf{0} & \mathbf{m}_{kc}^{\alpha} \\ \mathbf{0} & \mathbf{I}_{kk}^{\beta} & \mathbf{m}_{kc}^{\beta} \\ \mathbf{m}_{kc}^{\alpha\,T} & \mathbf{m}_{kc}^{\beta\,T} & \mathbf{m}_{cc}^{\alpha} + \mathbf{m}_{cc}^{\beta} \end{bmatrix} \tag{4.85}$$

and

$$\mathbf{K}_R^{gl} = \begin{bmatrix} \mathbf{\Lambda}_{kk}^{\alpha} & \mathbf{0} & \mathbf{0} \\ \mathbf{0} & \mathbf{\Lambda}_{kk}^{\beta} & \mathbf{0} \\ \mathbf{0} & \mathbf{0} & \mathbf{k}_{cc}^{\alpha} + \mathbf{k}_{cc}^{\beta} \end{bmatrix} \tag{4.86}$$

Due to the simplicity of the transformation matrix $\mathbf{C}$ in the fixed-interface CMS method, the component synthesis is straightforward and the global system matrices have the same structure as the component matrices. The global matrices are reduced in size based on the number of modes deleted in the component mode matrix $\mathbf{B}$. The special structure of the global matrices, especially the fact that the component eigenvalues appear uncoupled, has many advantageous also for uncertainty propagation, which will be the subject of investigation in the following chapters.

4.3.5 Interface DOF reduction

The size of the constraint matrices in Equations 4.85 and 4.86 depends on the number of interface DOFs. In applications involving line and surface coupling of components, the number of interface DOFs can be considerable compared to the overall number of DOFs. Therefore it might be desirable to reduce the number of interface DOFs as well. An appealing approach using characteristic constraint modes has been presented in [89]. An eigenanalysis of the form

$$[\mathbf{K}_{cc} - \lambda_j \mathbf{M}_{cc}]\, \boldsymbol{\upsilon}_j = \mathbf{0} \tag{4.87}$$

is performed where $\mathbf{M}_{cc}$ and $\mathbf{K}_{cc}$ are constraint matrices given as

$$\mathbf{M}_{cc} = \mathbf{m}_{cc}^{\alpha} + \mathbf{m}_{cc}^{\beta} \quad \textit{and} \quad \mathbf{K}_{cc} = \mathbf{k}_{cc}^{\alpha} + \mathbf{k}_{cc}^{\beta} \tag{4.88}$$

The eigenvectors $\boldsymbol{\upsilon}_j$ are referred to as characteristic constraint modes. They can be used to transform the interface DOFs into a reduced set of characteristic interface DOFs by

$$\mathbf{q}_c = \mathbf{\Upsilon}\mathbf{q}_c^* \tag{4.89}$$

where $\boldsymbol{\Upsilon}$ contains a few kept characteristic constraint modes that are associated with the largest eigenvalues. Finally, the constraint matrices can be reduced by

$$\mathbf{K}_{cc}^{*} = \boldsymbol{\Upsilon}^{T}\mathbf{K}_{cc}\boldsymbol{\Upsilon} \quad and \quad \mathbf{M}_{cc}^{*} = \boldsymbol{\Upsilon}^{T}\mathbf{M}_{cc}\boldsymbol{\Upsilon} \tag{4.90}$$

If the characteristic constraint modes are mass normalised, the constraint stiffness matrix is given by the characteristic constraint eigenvalues on the diagonal. Therefore, the complete CMS stiffness matrix in the fixed-interface method is diagonal and all terms are uncoupled.

Similar interface reduction methods have been proposed for free-interface and hybrid-interface CMS methods in [90, 91].

4.3.6 Free-interface method

In this section a free-interface method is presented where no additional modes are used. The modal matrix $\mathbf{B}^{\alpha}$ for a component α consists only of the kept free-interface modes

$$\mathbf{B}^{\alpha} = \left[\begin{array}{c} \boldsymbol{\Phi}_{k}^{fr} \end{array} \right]^{\alpha} \tag{4.91}$$

The superscript fr will be omitted for the remainder of this section. The physical coordinates are transformed into the modal space by

$$\left[\begin{array}{c} \mathbf{u}_{I}^{\alpha} \\ \mathbf{u}_{B}^{\alpha} \end{array} \right] = \left[\begin{array}{c} \boldsymbol{\Phi}_{Ik} \\ \boldsymbol{\Phi}_{Bk} \end{array} \right]^{\alpha} \left[\begin{array}{c} \mathbf{q}_{k}^{\alpha} \end{array} \right] \tag{4.92}$$

This approach is the same as that discussed in Section 4.2.2. The component modal mass and stiffness matrices are diagonal matrices of the form

$$\boldsymbol{\mu}^{\alpha} = [\mathbf{I}_{kk}]^{\alpha} \tag{4.93}$$

and

$$\boldsymbol{\kappa}^{\alpha} = [\boldsymbol{\Lambda}_{kk}]^{\alpha} \tag{4.94}$$

If two components are considered the vector of modal coordinates becomes

$$\mathbf{q} = \left[\begin{array}{cc} \mathbf{q}_{k}^{\alpha^{T}} & \mathbf{q}_{k}^{\beta^{T}} \end{array} \right]^{T} \tag{4.95}$$

The coupling condition of continuity of displacements is given by

$$\mathbf{u}_{B}^{\alpha} = \mathbf{u}_{B}^{\beta} \tag{4.96}$$

which can be written in terms of the modal coordinates using Equation 4.92 as

$$\mathbf{\Phi}^{\alpha}_{Bk}\mathbf{q}^{\alpha}_{k} = \mathbf{\Phi}^{\beta}_{Bk}\mathbf{q}^{\beta}_{k} \tag{4.97}$$

If there are a number n_B of constraint equations, n_B modal coordinates in Equation 4.95 are dependent and can be condensed. Therefore the set of coordinates of component α is divided into linear independent and dependent coordinates in the form

$$\left[\begin{array}{cc} \mathbf{q}^{\alpha^T}_{k} & \mathbf{q}^{\beta^T}_{k} \end{array} \right]^T = \left[\begin{array}{ccc} \mathbf{q}^{\alpha^T}_{kd} & \mathbf{q}^{\alpha^T}_{kl} & \mathbf{q}^{\beta^T}_{k} \end{array} \right]^T \tag{4.98}$$

The constraint equations can now be written as

$$\left[\begin{array}{cc} \mathbf{\Phi}^{\alpha}_{Bd} & \mathbf{\Phi}^{\alpha}_{Bl} \end{array} \right] \left[\begin{array}{c} \mathbf{q}^{\alpha}_{kd} \\ \mathbf{q}^{\alpha}_{kl} \end{array} \right] = \mathbf{\Phi}^{\beta}_{Bk}\mathbf{q}^{\beta}_{k} \tag{4.99}$$

and the constraint matrix equation follows as

$$\mathbf{Hq} = \left[\begin{array}{ccc} \mathbf{\Phi}^{\alpha}_{Bd} & \mathbf{\Phi}^{\alpha}_{Bl} & -\mathbf{\Phi}^{\beta}_{Bk} \end{array} \right] \left[\begin{array}{ccc} \mathbf{q}^{\alpha^T}_{kd} & \mathbf{q}^{\alpha^T}_{kl} & \mathbf{q}^{\beta^T}_{k} \end{array} \right]^T = \mathbf{0} \tag{4.100}$$

Using Equation 4.61 the matrix $\mathbf{C}$ is found and the transformation is given by

$$\mathbf{q} = \left[\begin{array}{c} \mathbf{q}^{\alpha}_{kd} \\ \mathbf{q}^{\alpha}_{kl} \\ \mathbf{q}^{\beta}_{k} \end{array} \right] = \left[\begin{array}{cc} -{\mathbf{\Phi}^{\alpha}_{Bd}}^{-1}\mathbf{\Phi}^{\alpha}_{Bl} & {\mathbf{\Phi}^{\alpha}_{Bd}}^{-1}\mathbf{\Phi}^{\beta}_{Bk} \\ \mathbf{I} & \mathbf{0} \\ \mathbf{0} & \mathbf{I} \end{array} \right] \left[\begin{array}{c} \mathbf{q}^{\alpha}_{kl} \\ \mathbf{q}^{\beta}_{k} \end{array} \right] = \mathbf{Cv} \tag{4.101}$$

The reduced global mass and stiffness matrices $\mathbf{M}^{gl}_{R}$ and $\mathbf{K}^{gl}_{R}$, which follow from Equations 4.62, are fully populated and do not have any special structure. This is due to the complex form of the transformation matrix $\mathbf{C}$. Another disadvantage is that the reduced global equation of motion is not statically correct.

4.3.7 Free-interface method with residual attachment modes

The use of free-interface normal modes is sometimes preferred because these can be measured more easily than fixed-interface modes. In this section residual attachment modes will be added to the set of free-interface normal modes to improve the accuracy of the free-interface CMS method, as described by Craig and Chang [85, 88]. The component modal matrix $\mathbf{B}$ is then given as

$$\mathbf{B}^{\alpha} = \left[\begin{array}{cc} \mathbf{\Phi}^{\alpha}_{k} & \mathbf{\Psi}^{\alpha}_{a_R} \end{array} \right] \tag{4.102}$$

and the transformation into modal space follows as

$$\begin{bmatrix} \mathbf{u}_I^\alpha \\ \mathbf{u}_B^\alpha \end{bmatrix} = \begin{bmatrix} \boldsymbol{\Phi}_{Ik} & \boldsymbol{\Psi}_{Ia_R} \\ \boldsymbol{\Phi}_{Bk} & \boldsymbol{\Psi}_{Ba_R} \end{bmatrix}^\alpha \begin{bmatrix} \mathbf{q}_k^\alpha \\ \mathbf{q}_a^\alpha \end{bmatrix} \tag{4.103}$$

If the component is constrained and only some of the normal modes are kept it is best to use residual attachment modes. These are linearly independent of the normal modes and therefore the equations of motion will be uncoupled and the component modal mass and stiffness matrices become

$$\boldsymbol{\mu}^\alpha = \begin{bmatrix} \mathbf{I}_{kk} & \mathbf{0} \\ \mathbf{0} & \mathbf{m}_{aa} \end{bmatrix}^\alpha \tag{4.104}$$

and

$$\boldsymbol{\kappa}^\alpha = \begin{bmatrix} \boldsymbol{\Lambda}_{kk} & \mathbf{0} \\ \mathbf{0} & \boldsymbol{\Psi}_{Ba} \end{bmatrix}^\alpha \tag{4.105}$$

The vector of modal coordinates is given by

$$\mathbf{q} = \begin{bmatrix} \mathbf{q}_k^{\alpha^T} & \mathbf{q}_a^{\alpha^T} & \mathbf{q}_k^{\beta^T} & \mathbf{q}_a^{\beta^T} \end{bmatrix}^T \tag{4.106}$$

The coupling condition of continuity of displacements

$$\mathbf{u}_B^\alpha = \mathbf{u}_B^\beta \tag{4.107}$$

can be written in terms of the modal coordinates as

$$\begin{bmatrix} \boldsymbol{\Phi}_{Bk}^\alpha & \boldsymbol{\Psi}_{Ba}^\alpha \end{bmatrix} \begin{bmatrix} \mathbf{q}_k^\alpha \\ \mathbf{q}_a^\alpha \end{bmatrix} = \begin{bmatrix} \boldsymbol{\Phi}_{Bk}^\beta & \boldsymbol{\Psi}_{Ba}^\beta \end{bmatrix} \begin{bmatrix} \mathbf{q}_k^\beta \\ \mathbf{q}_a^\beta \end{bmatrix} \tag{4.108}$$

Due to the use of attachment modes the conditions of equilibrium of forces

$$\mathbf{f}_B^\alpha = -\mathbf{f}_B^\beta \tag{4.109}$$

can be imposed as well. The static equation of component α in terms of modal coordinates is given by

$$\begin{bmatrix} \boldsymbol{\Lambda}_{kk} & \mathbf{0} \\ \mathbf{0} & \boldsymbol{\Psi}_{Ba} \end{bmatrix}^\alpha \begin{bmatrix} \mathbf{q}_k^\alpha \\ \mathbf{q}_a^\alpha \end{bmatrix} = \begin{bmatrix} \boldsymbol{\Phi}_k^T \\ \boldsymbol{\Psi}_a^T \end{bmatrix}^\alpha \begin{bmatrix} \mathbf{0} \\ \mathbf{f}_B^\alpha \end{bmatrix} \tag{4.110}$$

where $\mathbf{f}_B^\alpha$ are the forces at the boundary. The second line of this equation can be written as

$$\mathbf{\Psi}_{Ba}^\alpha \mathbf{q}_a^\alpha = \mathbf{\Psi}_{Ba}^\alpha \mathbf{f}_B^\alpha \tag{4.111}$$

and it follows that

$$\mathbf{q}_a^\alpha = \mathbf{f}_B^\alpha \tag{4.112}$$

Because of the special structure of the modal stiffness matrix, which is due to the attachment modes, the forces at the boundary are simply the modal constraint coordinates in a pseudostatic approximation. The equilibrium of forces can therefore be replaced by

$$\mathbf{q}_a^\alpha + \mathbf{q}_a^\beta = \mathbf{0} \tag{4.113}$$

The constraint equations in matrix form become

$$\mathbf{Hq} = \begin{bmatrix} \mathbf{\Psi}_{Ba}^\alpha & -\mathbf{\Psi}_{Ba}^\beta & \mathbf{\Phi}_{Bk}^\alpha & -\mathbf{\Phi}_{Bk}^\beta \\ \mathbf{I} & \mathbf{I} & \mathbf{0} & \mathbf{0} \end{bmatrix} \begin{bmatrix} \mathbf{q}_a^\alpha \\ \mathbf{q}_a^\beta \\ \mathbf{q}_k^\alpha \\ \mathbf{q}_k^\beta \end{bmatrix} = \mathbf{0} \tag{4.114}$$

where the submatrices of the dependent and linearly independent coordinates are given by

$$\mathbf{H}_{dd} = \begin{bmatrix} \mathbf{\Psi}_{Ba}^\alpha & -\mathbf{\Psi}_{Ba}^\beta \\ \mathbf{I} & \mathbf{I} \end{bmatrix}, \qquad \mathbf{H}_{dl} = \begin{bmatrix} \mathbf{\Phi}_{Bk}^\alpha & -\mathbf{\Phi}_{Bk}^\beta \\ \mathbf{0} & \mathbf{0} \end{bmatrix} \tag{4.115}$$

The transformation imposing the displacement and force boundary conditions is then obtained by Equation 4.62 as

$$\mathbf{q} = \begin{bmatrix} \mathbf{q}_a^\alpha \\ \mathbf{q}_a^\beta \\ \mathbf{q}_k^\alpha \\ \mathbf{q}_k^\beta \end{bmatrix} = \begin{bmatrix} -\mathbf{m}\mathbf{\Phi}_{Bk}^\alpha & \mathbf{m}\mathbf{\Phi}_{Bk}^\beta \\ \mathbf{m}\mathbf{\Phi}_{Bk}^\alpha & -\mathbf{m}\mathbf{\Phi}_{Bk}^\beta \\ \mathbf{I} & \mathbf{0} \\ \mathbf{0} & \mathbf{I} \end{bmatrix} \begin{bmatrix} \mathbf{q}_k^\alpha \\ \mathbf{q}_k^\beta \end{bmatrix} = \mathbf{Cv} \tag{4.116}$$

where

$$\mathbf{m} = \left(\mathbf{\Psi}_{Bd}^\alpha + \mathbf{\Psi}_{Bd}^\beta \right)^{-1} \tag{4.117}$$

The reduced global mass and stiffness matrices $\mathbf{M}_R^{gl}$ and $\mathbf{K}_R^{gl}$, found by Equation 4.63, are fully populated and do not have any special structure. The reduced equation of motion is statically correct because of the static attachment modes. The accuracy of this approach is in general better compared to the fixed-interface and simple free-interface CMS approaches because both the continuity of displacements and the equilibrium of forces are ensured.

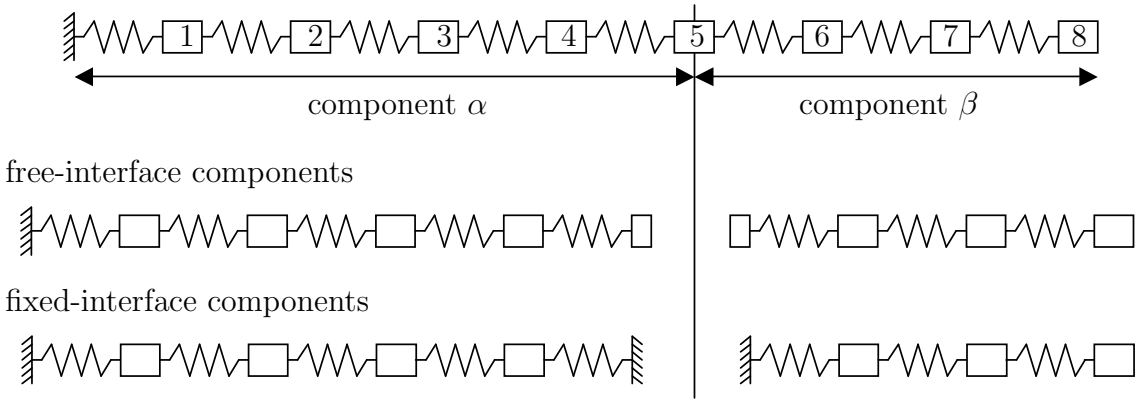

Figure 4.5: *8-DOF mass-spring chain divided into two CMS components.*

4.3.8 Numerical example of CMS for two components

In this section a numerical example of the implementation of the fixed-interface Craig-Bampton method [61] and the free-interface Craig-Chang method [85, 88] is presented. Consider the mass-spring chain in Figure 4.5 that has 8 DOFs and is fixed at the left end and free at the right end. This structure will be divided into two components α and β at coordinate 5. Mass number 5 will be assigned with half of its physical mass to each component. In theory it is possible to make any division, including creating a massless DOF. However, in such cases, numerical problems can arise that require special attention. Figure 4.5 also shows the realisation of free-interface and fixed-interface components. The free-interface components α and β have five and four DOFs, respectively. In total they have one more DOF than the original structure, because one additional DOF was created when dividing mass number 5. It has to be noted that component β is now unconstrained and has rigid body freedom, whereas the whole structure is sufficiently constrained. The fixed-interface components have the boundary DOF number 5 fixed. Therefore the components have four and three internal DOFs, respectively, and in total one DOF less than the original structure. Component β is now constrained at the boundary and does not have rigid body freedom.

The objective is to couple the components, by using different CMS methods, to obtain an exact equation of motion and a reduced equation of motion. The total number of DOFs is to be reduced from 8 to 4 and therefore each component will be reduced by two DOFs. In Table 4.1, the type and number of component modes used are listed for each CMS method. The simple free-interface method with normal modes only, the free-interface method with attachment modes (Craig-Chang) and

		Component modes and DOFs component α		component β		boundary condition	total DOFs
		normal	other	normal	other		
Free	no red.	5	0	3	1 r.(n.)	−1	8
	red.	$5-2=3$	0	$3-2=1$	1 r.(n.)	−1	4
Free + a.	red.[a]	$5-2=3$	1 a.	$3-2=1$	1 r.(n.)+1 a.	−2	5
	red.[b]	$5-3=2$	1 a.	$3-2=1$	1 r.(n.)+1 a.	−2	4
Fixed + c.	no red.	4	1 c.	3	1 r.(c.)	−1	8
	red.	$4-2=2$	1 c.	$3-2=1$	1 r.(c.)	−1	4
Abbr. of modes: n. - normal ; a. - attachment ; c. - constraint ; r. - rigid body							

Table 4.1: *Component modes and number of DOFs for two components in different CMS methods.*

the fixed-interface method with constraint modes (Craig-Bampton) are considered. There are the cases where there is no reduction, and hence all modes are kept (no. red.), and where higher frequency normal modes are deleted (red.). For each component, the resulting number of normal modes and other modes (attachment, constraint, rigid body) is stated. The number of DOFs that are removed if the boundary conditions are imposed are noted with a minus sign. The total number of DOFs of the assembled structure is given in the last column and can be calculated by a summation over the row.

With the interfaces free, the eigenvalue problem gives five normal modes for component α and three normal modes and one rigid body mode for component β. In the simple free-interface CMS method, the boundary condition of continuity of displacements removes one DOF. Therefore the original size of eight DOFs is retained and the equation of motion yields the exact results. If two normal modes are deleted, respectively, component α is described by three normal modes and component β is described by one normal mode and one rigid body mode. The assembled structure then has a total of four DOFs and yields an approximate result compared to the full model.

In the Craig-Chang method, one residual attachment mode is added to each component. Because these modes include the effects of the deleted modes, this method is only meaningful if a component model is reduced. If this is not the case, the DOFs are not independent. Since also the equilibrium of forces is ensured, two DOFs are removed due to the boundary conditions. However, if two normal modes are truncated in each component, the total number of DOFs is only reduced

by 3 (case a). In order to achieve the desired reduction by 4 DOFs, three normal modes will be deleted in component α (case b). Because component β has rigid body freedom, it would have to be restrained before an attachment mode due to a force could be defined. However, the residual attachment mode is determined by the residual flexibility matrix, which depends on the higher frequency modes, and therefore the rigid body freedom is not relevant.

In the fixed-interface method, the number of DOFs is reduced to 4 and 3 for components α and β, respectively, because the boundary coordinate 5 is fixed. The fixed-interface components are sufficiently constrained and only normal modes are obtained from the eigenvalue problem. Additional constraint modes are necessary to carry out the coupling and to preserve the exact result. For component β the constraint mode, where a unit displacement is applied at the boundary, is a rigid body mode. One DOF is removed by the coupling condition at the boundary.

In summary, all CMS methods preserve the exact result of the full model if the number of independent modal component coordinates is the same as the total number of physical DOFs and if the component modes are linearly independent. The normal modes found from an eigenvalue problem are linearly independent by definition and the residual attachment modes are independent of the kept normal modes. The constraint modes of a fixed-interface component are independent of each other and independent of the fixed normal modes, because if a unit displacement is described at one coordinate all other coordinates are fixed.

For a reduced component model, the simple free-interface method is not statically correct. The use of additional attachment modes ensures the correct static result and improves the approximation, but also increases the size of the model. In the fixed-interface method, some of the dynamical information is lost compared to the free-interface method, because the mode set comprises static constraint modes and a reduced number of normal modes. However, the result is statically correct and the size of the assembled model is unchanged.

In Table 4.2, the estimates of the natural frequencies by the different CMS methods are shown. The number of DOFs was reduced for all cases from 8 to 4. The first five natural frequencies of the exact system range from 0.38 Hz to 3.599 Hz and the errors in the estimated values are given in percent.

The fixed-interface method gives accurate results for the lower modes but approximations get worse for higher frequency. The free-interface method with attachment modes behaves in the same manner, but gives an accurate result also for the third natural frequency and is less in error for the fourth. The simple free-interface method achieves the best result for the third natural frequency but shows unsystematic errors for the others. In Figure 4.6, a transfer FRF and a point FRF are plotted to

Mode	Exact	Fixed+Constr.		Free		Free+Attach.[b]		Free+Attach.[a]	
	Hz	Hz	err. %	Hz	err. %	Hz	err. %	Hz	err. %
1	0.380	0.380	0	0.385	1.3	0.380	0	0.380	0
2	1.105	1.105	0	1.192	7.9	1.105	0	1.105	0
3	2.018	2.029	0.5	2.021	0.2	2.018	0	2.018	0
4	3.086	3.372	9.2	3.433	11.2	3.112	0.8	3.099	0.4
5	3.599							3.628	0.8

Table 4.2: *Natural frequencies of a mass-spring chain modelled by different CMS methods.*

show the qualitative variations in the different approximations.

This numerical example was used to demonstrate some of the basic characteristics of different CMS approaches. The specific performance of these methods depends on the properties of the structure and the objective of the application. However, it is indicated in the literature that the free-interface method with residual attachment modes gives the best results of the three approaches illustrated. The fixed-interface method with constraint modes is accurate for lower modes and at the same time is the most simple to implement.

4.4 Discussion and concluding remarks

The static reduction by Guyan is most appropriate for static problems. For linear dynamic problems, the modal reduction approach should be used, if some of the lower frequency modes can be neglected. In the context of built-up structures, CMS methods combine the benefits of modal reduction with the capability to couple different component models. The accuracy of both the free and fixed-interface CMS methods is sufficient, if the frequency of the highest mode considered is relatively large compared to the highest frequency of interest. The substructuring approaches considered in this chapter were based on the system matrices. However, there are also other techniques, which consider response data, for example FRF based substructuring [92–94].

This thesis concerns the low-frequency analysis of built-up structures with non-deterministic properties, focusing on the first few modes of vibration where the modal and stochastic overlaps are low. The possible reduction in model size, without loss of accuracy, can be substantial depending on the overall number of DOFs. Therefore, model reduction is an essential step in a low-frequency non-deterministic analysis in order to reduce the computational cost and make it more applicable.

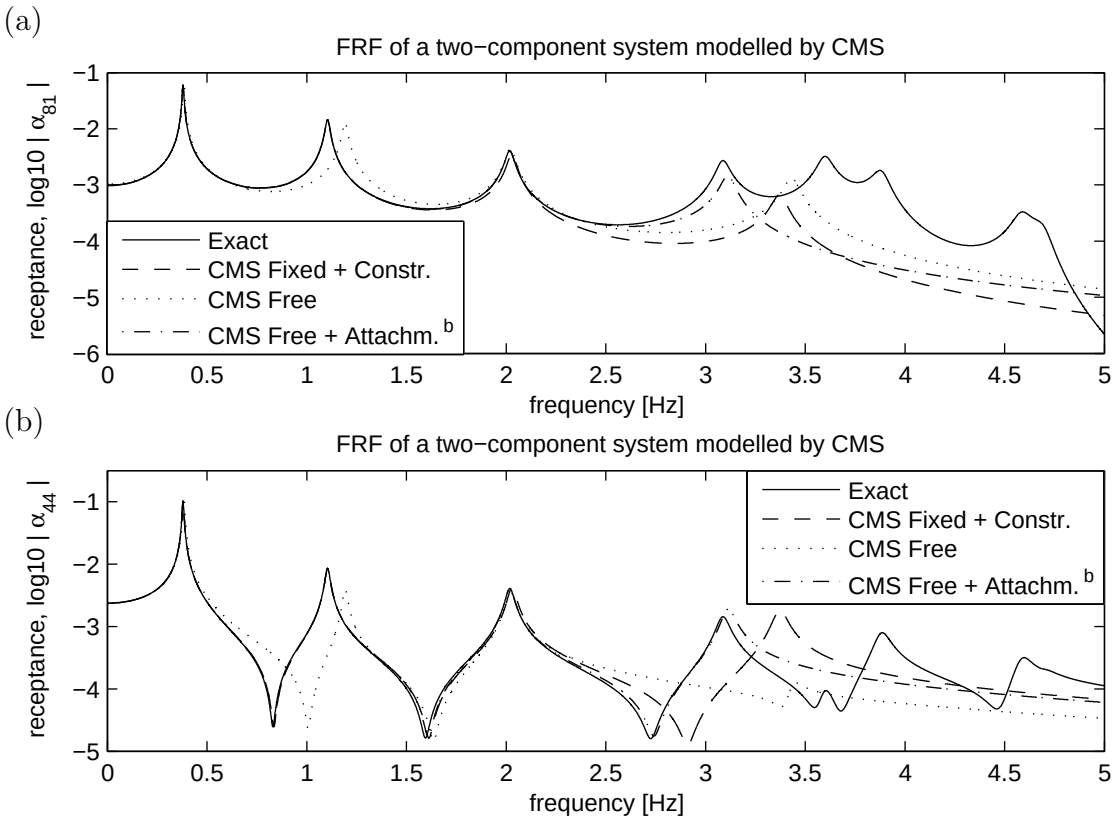

Figure 4.6: *Frequency response of a mass-spring chain modelled by different CMS methods.*

Chapter 5

CMS and non-deterministic data

5.1 Introduction

A promising methodology to address several of the challenges in the modelling of the dynamics of non-deterministic properties in complex structures is substructuring. The component modes synthesis (CMS) method combines the benefits of substructuring with the benefits of modal approaches. The application of CMS methods for the deterministic analysis of structures that are built-up of several components, as is generally the case in industrial applications, has been reviewed in the previous chapter.

In the analysis of structures with non-deterministic properties, a deterministic problem often has to be solved repeatedly, which is numerically expensive. In this context, deterministic model reduction by CMS is especially important because the benefits accurre multiple times. Reanalysis is required of only those components of the structure which are uncertain or where uncertainty is significant. The individual components and the joints are typically statistically independent, being made up by different manufacturing processes. The advantage of CMS that it can deal with quantitatively and qualitatively different deterministic FE component models can be extended to a non-deterministic analysis as well.

Other benefits concern how uncertain data is quantified and propagated. Uncertainties in properties can be naturally and straightforwardly introduced at the component level, either in terms of the component physical properties or the component modal properties. The former typically require quantification of a random field for each physical property, while the latter involve component natural frequencies - a discrete set of data of low order - and eigenfunctions. This enables possibilities for substantial reduction in the quantity of uncertain data that must be included in the model. It is therefore possible to estimate uncertainties in response using a rel-

atively small set of uncertain input data, further reducing computational cost. The propagation of uncertainties in CMS can be treated in several independent steps using four different coordinate systems in CMS.

CMS methods are amenable to the inclusion of experimentally measured variability data. Theories and models for the representation of variation in properties (e.g. random fields for spatial variation) have been in existence for many years, but the experimental data required to quantify them is often not available. In this context, it is much easier to measure the variation in modal properties of a component than quantifying the spatial distribution of physical properties. A simple hammer test can be sufficient to determine the statistics of component modal properties. Finally, advantages arise from the fact that each substructure can be treated independently regarding the quantification and propagation of non-deterministic data. For example, a hybrid description can be adopted, with different parts of a built-up structure perhaps being described by possibilistic and probabilistic concepts. Overall, CMS offers more physical insight into the analysis of structures with uncertain properties than other methods.

Numerical models are most easily constructed using the fixed-interface (Craig-Bampton) method, which has been reviewed in the previous chapter. In this case, advantages arise from the special structure of the CMS equations that can be exploited. This chapter addresses the quantification and propagation of non-deterministic properties with a focus on the fixed-interface CMS method. First, the various possibilities for uncertainty quantification and propagation as well as the influence of modal parameters are discussed. Subsequently, Section 5.4 concerns the combination of possibilistic and probabilistic approaches in one analysis. This is followed by a presentation of the use of perturbational relations for forward propagation within the CMS framework.

5.2 Uncertainty quantification and propagation in CMS

The fixed-interface CMS method has been reviewed in detail and in the context of other CMS methods in the previous chapter. The main equations will be summarised in this section for easier reference. The undamped equation of motion of a component α is

$$\mathbf{M}\ddot{\mathbf{u}} + \mathbf{K}\mathbf{u} = \mathbf{f} \tag{5.1}$$

At component level, the fixed-interface eigenvalue problem

$$\left(\mathbf{K}_{II} - \lambda_j^{fi}\mathbf{M}_{II}\right)\mathbf{\Phi}_{I,j} = \mathbf{0} \tag{5.2}$$

has to be solved. The modal matrix $\mathbf{B}^\alpha$ is given as

$$\mathbf{B} = \begin{bmatrix} \mathbf{\Phi}_{Ik} & -\mathbf{K}_{II}^{-1}\mathbf{K}_{Ic} \\ \mathbf{0} & \mathbf{I}_{cc} \end{bmatrix}^\alpha \tag{5.3}$$

where constraint modes have been added to improve convergence. The modal matrix $\mathbf{B}^\alpha$ is then used to transform the component matrices from physical to component modal coordinates. Following the synthesis of components the global mass and stiffness matrices are found as

$$\mathbf{M}^{gl} = \begin{bmatrix} \mathbf{I}_{kk}^\alpha & \mathbf{0} & \mathbf{m}_{kc}^\alpha \\ \mathbf{0} & \mathbf{I}_{kk}^\beta & \mathbf{m}_{kc}^\beta \\ \mathbf{m}_{kc}^{\alpha\,T} & \mathbf{m}_{kc}^{\beta\,T} & \mathbf{m}_{cc}^\alpha + \mathbf{m}_{cc}^\beta \end{bmatrix} \qquad \mathbf{K}^{gl} = \begin{bmatrix} \mathbf{\Lambda}_{kk}^\alpha & \mathbf{0} & \mathbf{0} \\ \mathbf{0} & \mathbf{\Lambda}_{kk}^\beta & \mathbf{0} \\ \mathbf{0} & \mathbf{0} & \mathbf{k}_{cc}^\alpha + \mathbf{k}_{cc}^\beta \end{bmatrix} \tag{5.4}$$

These constitute the global eigenvalue problem

$$\left(\mathbf{K}^{gl} - \lambda_i^{gl}\mathbf{M}^{gl}\right)\mathbf{\Phi}_i^{gl} = \mathbf{0} \tag{5.5}$$

which yields the global eigenvalues and eigenvectors. Finally, the global eigenvectors can be related to global physical coordinates by the transformation

$$\mathbf{V} = \mathbf{BCD} \tag{5.6}$$

which is required to calculate the FRF by modal summation.

5.2.1 Quantification of uncertainties

There are four different coordinate systems in the CMS framework, given by component and global, physical and modal coordinates as shown in Figure 5.1. Parametric uncertainties can be introduced at the component physical level in terms of mass and stiffness properties. In practice, many of these properties vary spatially and random field models (Chapter 3) are required to represent them. However, the quantification of these models is often difficult or impossible, due to a lack of data and the effort and expense of acquiring it. For example, there is almost no data available for the correlation length that is a parameter in random field models. In most cases, experimental quantification at the physical level is difficult and expensive. Quantification in a numerical model is therefore an approximation. Alternatively, uncertainties

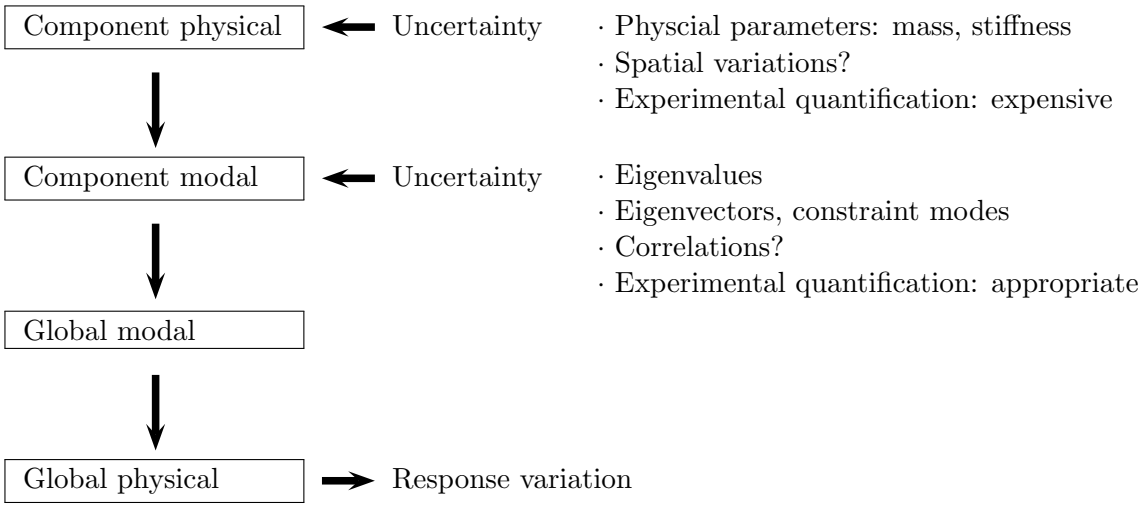

Figure 5.1: *Outline of uncertainty quantification in CMS.*

can be introduced at the component modal level in terms of the modal parameters: the fixed-interface component eigenfrequencies, mode shapes and constraint modes. The special structure of the global matrices (Equation 5.4), where the component eigenvalues appear uncoupled on the diagonal of the stiffness matrix, is most advantageous for this purpose. Experimental quantification of the eigenvalues in particular is straightforward using a simple hammer test, for example. However, in practice it might be simplest to perform this with a free rather than fixed interface. The quantification of uncertainty in the mode shapes and in the constraint terms is not so straightforward. A simple and practical approximate approach is therefore to consider variation in component eigenfrequencies only. The inaccuracies and errors caused by this approach will be investigated in the next section. In contrast to physical properties, quantification in modal properties takes account of all sources of uncertainty, including non-parametric effects. Finally it should be noted that it is possible to describe uncertainty in different subsystems in a different qualitative manner, some possibilistically and some probabilistically.

5.2.2 Propagation of uncertainties

The different strategies for uncertainty propagation are outlined in Figure 5.2. In a classical analysis, the variation in physical properties can be propagated directly to the global physical level, e.g. the frequency response function (FRF). In a modal approach, first the variations in global modal properties are calculated, which are subsequently propagated to the global physical level. Within the CMS framework,

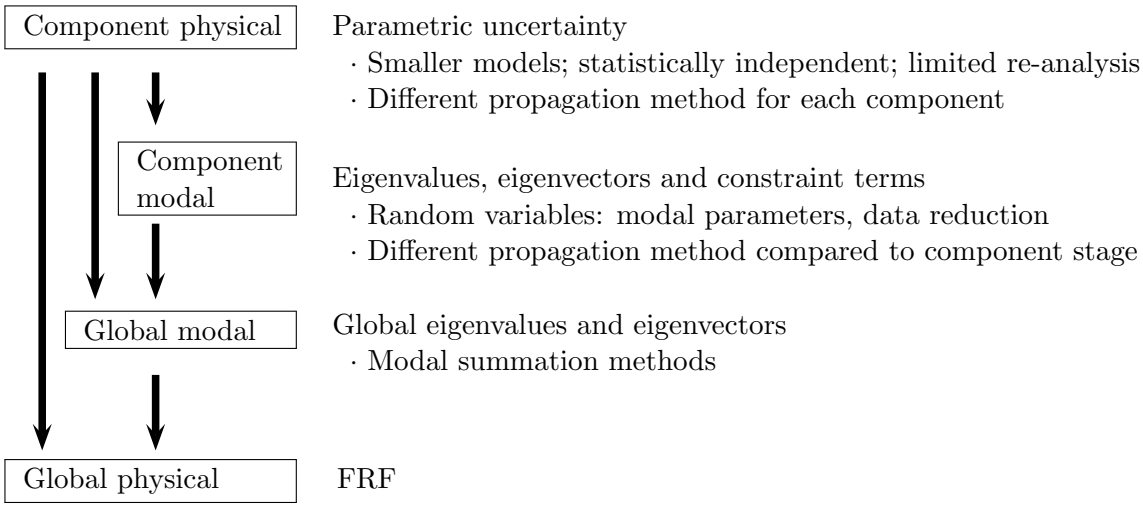

Figure 5.2: *Outline of uncertainty propagation in CMS.*

a further coordinate level is introduced. Therefore, a total of three different and independent propagation steps can be considered. At component level, only those components where uncertainty is significant have to be considered. The component model size is much smaller than the original global problem and the computational cost is less. If components are considered to be statistically independent, the number of random variables is also smaller, which makes interval analyses more feasible. Therefore, it is often reasonable to use an exact propagation method, such as MC simulation, at this stage. A further advantage is that for each component a different propagation approach can be applied. Therefore, exact and approximate, as well as probabilistic and possibilistic concepts, can be applied as appropriate. The second step of propagation, associated with the component synthesis, is independent of the previous propagation approaches. It is based on a different and reduced set of random variables, which can be selected according to the frequency range of interest. In general, the modal properties of different components are uncorrelated. At this stage, all quantitatively and qualitatively different approaches are combined. Probabilistic and possibilistic descriptions can be unified by putting bounds on the distributions of modal parameters. Finally, there are different strategies for non-deterministic modal superposition that can be applied to estimate the variation in the FRF. The latter are discussed in detail in Chapter 7. The use of modal sensitivities and the application of perturbational relations within the CMS framework are discussed in Section 5.5 and Chapter 6.

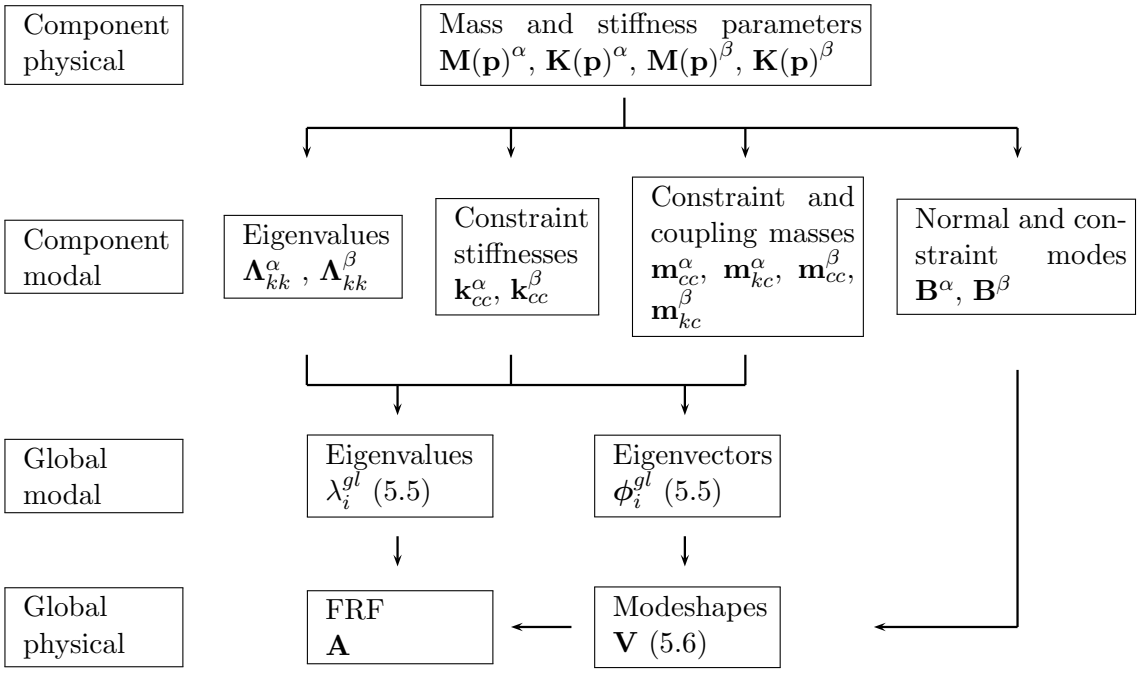

Figure 5.3: *Outline of uncertainty propagation in the fixed-interface CMS method.*

5.2.3 Influence of random parameters

In this section, the propagation of uncertainties through the various coordinate systems will be examined to investigate the influence of individual parameters in the fixed-interface CMS method. A model with two components α and β is used for simplicity. Parametric uncertainty is assumed to be present in the physical mass and stiffness matrices, denoted by a vector $\mathbf{p}$ in the form $\mathbf{M}(\mathbf{p}), \mathbf{K}(\mathbf{p})$. The objective is to calculate the resulting variation in the global eigenfrequencies λ_i^{gl} and the frequency response $\mathbf{A}$ of the whole structure. In Figure 5.3, the four coordinate levels, the corresponding parameters and the paths of uncertainty propagation are outlined. At the component modal level, uncertainty exists in the component eigenvalues and eigenvectors. Additionally, the terms associated with the static constraint modes are random as well. Therefore, at component modal level, uncertainty is present in elements of the modal mass and stiffness matrices and the component mode matrix $\mathbf{B}$.

The global eigenvalues λ_i^{gl} and eigenvectors $\boldsymbol{\phi}_i^{gl}$ are calculated from Equation 5.5 and depend on the component eigenvalues $\mathbf{\Lambda}^{\alpha}_{kk}$, $\mathbf{\Lambda}^{\beta}_{kk}$, the constraint mass and stiffness matrices $\mathbf{k}^{\alpha}_{cc} + \mathbf{k}^{\beta}_{cc}$, $\mathbf{m}^{\alpha}_{cc} + \mathbf{m}^{\beta}_{cc}$ and the coupling mass matrices $\mathbf{m}^{\alpha}_{kc}$, $\mathbf{m}^{\beta}_{kc}$. In order to calculate the frequency response, the physical mode shapes are needed, which depend on the transformation $\mathbf{V} = \mathbf{BCD}$. This also involves the component

Simulation	Uncertainty considered in:			
Exact	global stiffness and mass matrices component mode matrices	$\mathbf{K}^{gl}$	$\mathbf{M}^{gl}$	$\mathbf{B}$
A	global stiffness matrix component mode matrix	$\mathbf{K}^{gl}$	$\overline{\mathbf{M}^{gl}}$	$\mathbf{B}$
B	component eigenvalues component modal matrix	$\widetilde{\mathbf{K}^{gl}}$ $(\mathbf{\Lambda}, \overline{k_{cc}})$	$\overline{\mathbf{M}^{gl}}$	$\mathbf{B}$
C	global stiffness and mass matrices	$\mathbf{K}^{gl}$	$\mathbf{M}^{gl}$	$\overline{\mathbf{B}}$
D	component eigenvalues	$\widetilde{\mathbf{K}^{gl}}$ $(\mathbf{\Lambda}, \overline{k_{cc}})$	$\overline{\mathbf{M}^{gl}}$	$\overline{\mathbf{B}}$
$\overline{x}$ - baseline value of x				

Table 5.1: *Definition of different cases for a numerical analysis, where uncertainty is neglected in various component modal properties.*

mode matrix $\mathbf{B}$.

In the following analysis, the error caused by neglecting component constraint terms on uncertainty propagation is investigated. In Table 5.1, four different simulation cases are defined. For the exact solution, randomness in all component modal properties is considered. In case A, randomness in the global mass matrix $\mathbf{M}^{gl}$ is neglected and is replaced by its baseline matrix $\overline{\mathbf{M}^{gl}}$. In the next case, the random constraint terms in the global stiffness matrix $\widetilde{\mathbf{K}^{gl}}$ are neglected and replaced with their baseline values $\overline{k_{cc}}$, leaving only the component eigenvalues $\mathbf{\Lambda}$ as random variables. Finally, in cases C and D, the baseline component mode matrix $\overline{\mathbf{B}}$ is used. The results for all cases and a numerical example are presented in Section 5.3. The next two sections are concerned with the method of uncertainty propagation and the choice between probabilistic and possibilistic approaches.

5.3 Numerical example

The numerical example is a two-component beam structure as shown in Figure 5.4. The components are rigidly connected to each other and clamped at the ends. The structure is modelled using standard FE matrices for Euler-Bernoulli beam theory [9], including transverse and rotational DOFs. The beams are governed by bending stiffness EI and mass per unit length ρA. Each component is divided into 10 identical beam elements over the length L. The baseline values are given in Figure

5.4. Damping is included by a modal loss factor of 3%. A fixed-interface CMS model is constructed and component normal modes corresponding to a frequency higher than 150 Hz are neglected. The transfer accelerance between two points, each $0.4m$ from the clamped ends, for a frequency range from $0Hz$ to $50Hz$ will be considered. Figure 5.5 shows the baseline FRF for the exact solution and a fixed-interface CMS approximation, where the total number of DOFs is reduced from 38 to 20. In the following simulations, a frequency range from 0Hz to 50Hz, including the first 10 resonances, will be of interest. The error from model reduction can be neglected for at least up to the 10th mode, because there are twice as many DOFs retained.

Uncertainty is introduced in the thickness h and the Young's modulus E of each component. The Young's modulus contributes linearly to the stiffness matrix, but the thickness h appears as a cubic term in the bending stiffness and a linear term in the mass per unit length. In the following, both a possibilistic and a probabilistic analysis are performed.

5.3.1 Possibilistic analysis

In this analysis, the Young's modulus E and the thickness h of each component α and β can vary by $\pm 8.2\%$ around the baseline value. They are assumed to be constant over the length of each component. Therefore, there are 4 random variables in the whole structure and a vertex analysis with $2^4 = 16$ deterministic solutions of the original eigenvalue problem is performed as a reference analysis. For the CMS model, there are 2 random variables in each component and $2^2 = 4$ vertex solutions are performed for each component. When the components are assembled, there are a total of $4^2 = 16$ combinations to be considered for the solution of the reduced global eigenvalue problem. However, this is only the case if the individual solutions for each deterministic calculation are traced, i.e. the correlations between component eigen-

	L $[m]$	h $[m]$	b $[m]$	E $[N/m^2]$	ρ $[kg/m^3]$	$I = \frac{bh^3}{10}$, $A = bh$
component α	1	0.01	0.1	$1e8$	1000	
component β	1	0.015	0.1	$1e8$	1000	

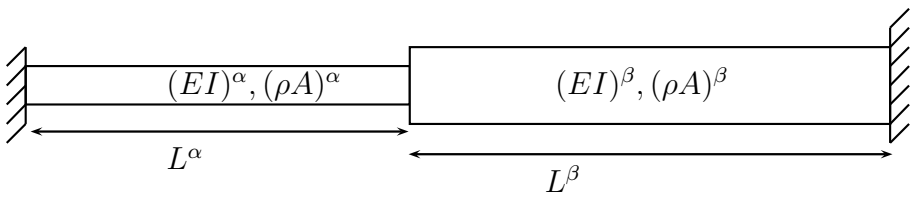

Figure 5.4: *Two component beam structure and baseline properties.*

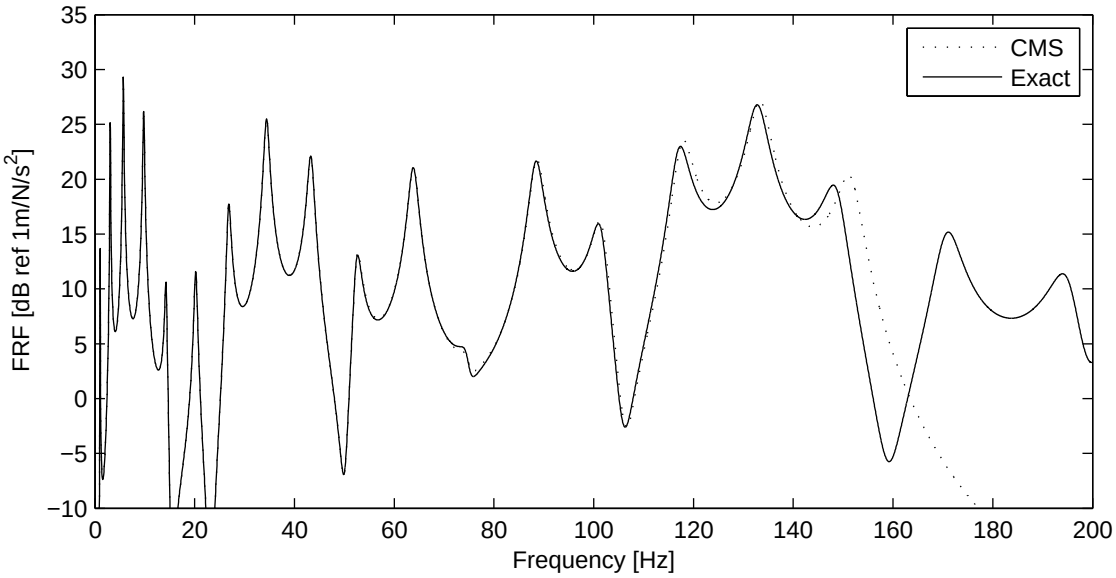

Figure 5.5: *Baseline FRF: exact solution (*38 *DOFs) and CMS (*16 *DOFs).*

values are known. The lower and upper limits of variation of the eigenfrequencies are found as the minimum and maximum values of the vertex combinations.

First, the influence of neglecting various component modal parameters will be investigated. The upper limit of global eigenfrequencies ω_i^U is computed for cases A and B as defined in Table 5.1. In Figure 5.6 the difference from the exact solution is shown for the first 10 eigenfrequencies. It can be seen that the approximation is inaccurate for the first two eigenfrequencies but improves for higher modes. In case A, where uncertainty in the global mass matrix is neglected, the eigenfrequencies are overestimated. This is possible because the interdependency between the mass and stiffness matrices is not considered. However, if the uncertainty in stiffness constraint terms is neglected too and only the component eigenvalues are considered, the exact results are underestimated. For the third and higher eigenfrequencies, the approximation error introduced by neglecting all constraint terms in the mass and stiffness matrices is less than 2%.

In case B the component eigenvalues are the only uncertain parameters at component level, which are in general correlated within one component. If those correlations are neglected, there is a set of $n_\Lambda = 18$ independent uncertain variables, where n_Λ is the total number of kept fixed-interface component modes. If interdependencies between variables are neglected, the results of the analysis will be conservative. However, a vertex analysis requires $2^{18} = 262144$ deterministic solutions of the global eigenvalue problem, which is often infeasible. Therefore, a reduction in the number

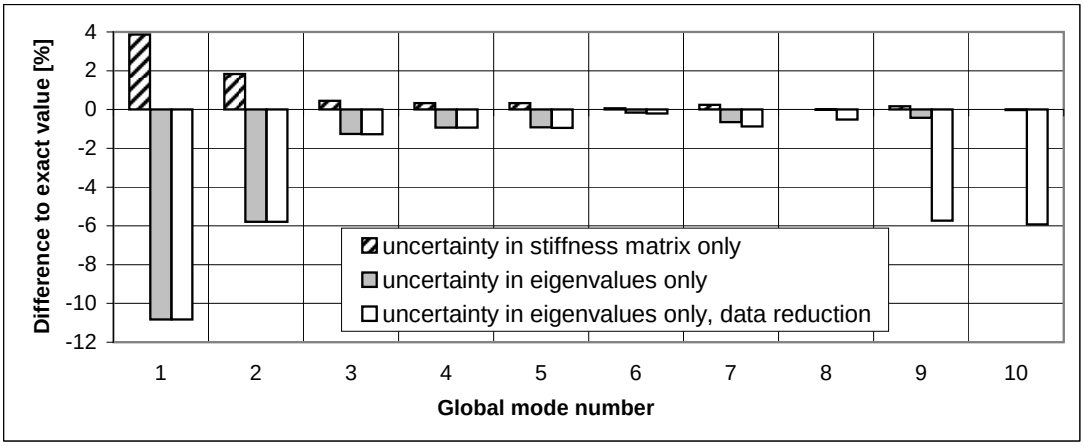

Figure 5.6: *Approximation error* $\left((\omega_i^U - \overline{\omega_i})/\overline{\omega_i} x 100\%\right)$ *for the upper limit of global eigenfrequencies for cases A and B.*

of uncertain parameters could be considered. Figure 5.6 also shows results for the case, where the number of independent uncertain component eigenvalues has been reduced to $n_\Lambda = 8$. It can be seen that this introduces non-conservative errors for higher frequencies. Alternatively, total correlation could be assumed for the eigenvalues within one component. In this case, only $2^{n_{comp}} = 4$ deterministic solution have to be performed, where $n_{comp} = 2$ is the number of components. However, in general the upper limits of all component eigenvalues correspond to the upper limits of all global eigenvalues. This can also be seen by the special structure of the CMS matrices. Therefore, only two deterministic solutions of the global eigenvalue problem are required. For the current numerical example, the results for case B are identical for any description of the correlation of component eigenvalues.

A FRF is calculated for every solution using deterministic modal superposition. A FRF envelope is then obtained as the maximum and minimum value of the magnitude, for every frequency, from the results of the vertex analysis. The magnitude over a resonance range is approximated by the maximum value in this range (non-deterministic modal superposition is the subject of Chapter 7). In Figure 5.7 the pseudo-exact FRF envelope is compared with several approximations. The results for cases A and B, where uncertainties are neglected in constraint terms of the global system matrices, are presented in Figure 5.7a. It can be seen that this mostly affects the resonance range at lower frequencies. Figure 5.7b concerns the influence of uncertainties in the component mode matrix $\mathbf{B}$. The whole frequency range is affected, but only to a very limited degree. Finally, the results based on the approach to consider uncertainty only in the component eigenvalues are shown in Figure 5.7c. The

differences are small except for low frequencies, which are governed by the constraint terms. In addition, the results are shown for the approach where component eigenvalue intervals are considered as independent. In this case, the resonance ranges remain unchanged, but there is more conservatism in the approximation of the FRF magnitude.

5.3.2 Probabilistic analysis

For the probabilistic analysis, the thickness h and Young's modulus E are modelled by a one-dimensional homogenous Gaussian random field with a CV of 5% and correlation length $0.5m$. The CV is linked to the possibilistic analysis by the criterion that 90% of the realisations lie between the lower and upper limits. The random field is discretised at element level so that there is a constant value for each of the 10 finite elements. A Monte Carlo (MC) approach with 10000 deterministic runs is applied to estimate eigenfrequency and FRF statistics. For the reference solution, the original eigenvalue problem is solved directly each run. In the CMS approach, first the component models are solved independently and then the reduced global problem is solved. The standard deviation of the global eigenfrequencies is computed for cases A and B, where uncertainty is neglected in constraint terms in the global system matrices. The corresponding errors are presented in Figure 5.8. The results show the same tendencies as those described for the possibilistic analysis. There are large differences for the first two eigenfrequencies, but results improve for higher modes.

In contrast to the possibilistic analysis, the number of solutions does not depend on the number of uncertain parameters or if correlations are considered or not. It can be different for the propagation at component level and the propagation to global modal level. In case B the component eigenvalues are the only random parameters. They are given by pdfs and are in general correlated. The correlations can be considered, if the sequence of the deterministic solutions in a MC simulation approach is traced. If only the pdf of each component eigenvalue is known, further errors are introduced in the MC propagation to the global eigenvalues. The results for this case are also shown in Figure 5.8. The statistics are underestimated, because the likelihood that certain combinations of the component eigenvalues occur is lower. The results presented here relate to the real distribution discretised by 10000 samples. However, in many cases it might be reasonable to propagate only the mean values and variances of probabilistic properties.

A FRF is calculated for every MC solution and FRF statistics are evaluated from a sample of 1000 MC results. In Figure 5.9, the 5 and 95 percentiles of the

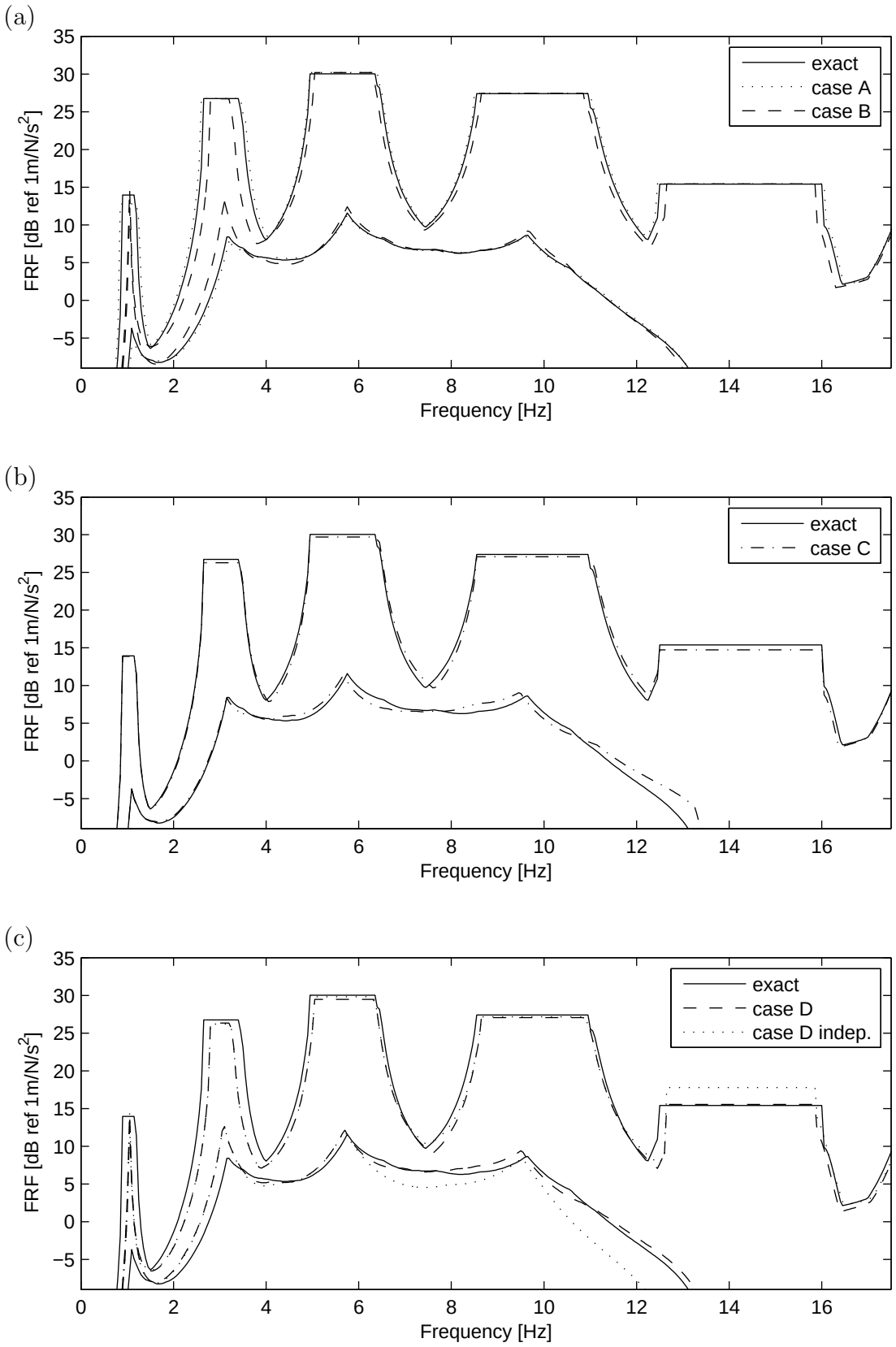

Figure 5.7: *FRF envelope: exact solution and approximations from cases A,B,C and D.*

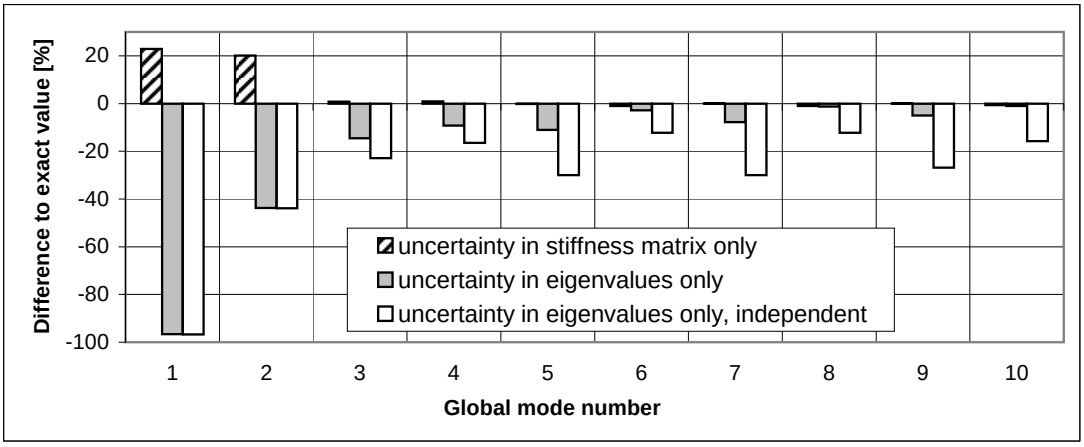

Figure 5.8: *Approximation error for the standard deviation of global eigenfrequencies for cases A and B.*

FRF magnitude are shown for the exact FRF and various approximations, where uncertainty is neglected in certain modal properties. The variation at lower modes is strongly dependent on the constraint terms. The modal matrix B has a limited influence in the whole frequency range (case C). The approximation considering variation only in the component eigenvalues (case D) is reasonably good for frequencies above the second mode. In Figure 5.9c, it is also shown that neglecting the correlations between component eigenvalues leads to errors, especially to an underestimation of the resonance range statistics. These observations are qualitatively similar for general systems, but the frequency above which the influence of uncertainty in the constraint terms can be neglected depends strongly on the coupling of the components.

5.4 Combined possibilistic and probabilistic approaches

Most non-deterministic analyses follow either a probabilistic or a possibilistic approach. The main criteria for this choice are the available information about the input uncertainty and the objective of the analysis. However, there are several reasons which can make the selection of the correct approach problematic. The results of a possibilistic method might be associated with a very low likelihood and therefore of little practical use in an application. Probabilistic approaches often suffer from the lack of accurate data and many assumptions have to be made concerning probabilistic distributions etc. A further problem arises if different qualitative and

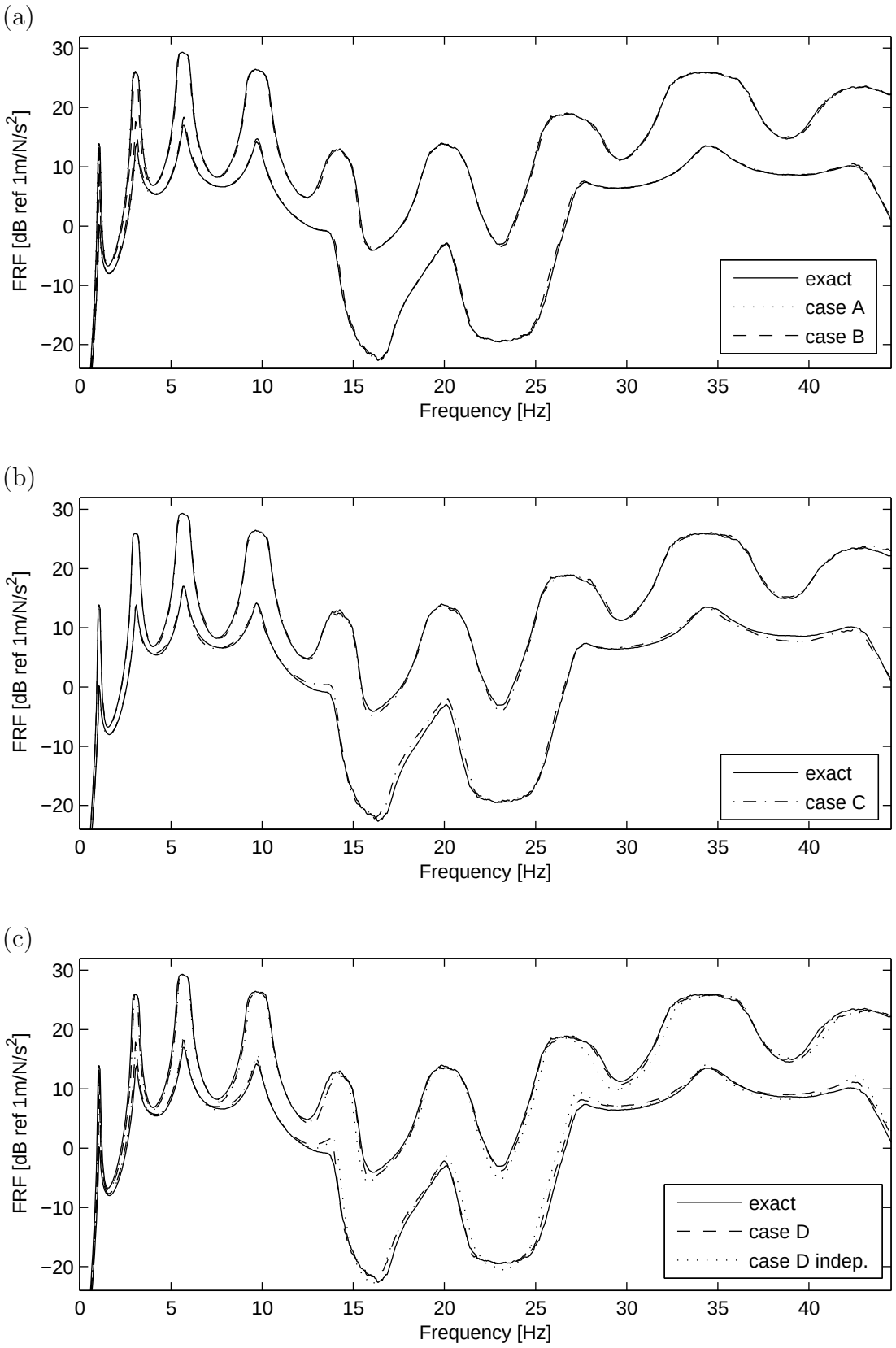

Figure 5.9: 5 *and* 95 *percentiles of FRF: exact solution and approximations by cases A,B,C and D.*

quantitative descriptions of non-deterministic input data are given for one structure. In this case the combination of possibilistic and probabilistic approaches has to be considered. In terms of pdf and interval descriptions, two principle techniques are apparent. A distribution can be assumed for the possibilistic results, where the lower and upper bounds are replaced with specified percentiles of the pdf. However, this involves further assumptions and can introduce errors. On the other hand, the probabilistic results can be transformed into an interval by using percentiles of the pdf as lower and upper limits. In this case, no assumptions have to be made, but valuable information is lost and bounds are no longer strict bounds.

The CMS framework is appropriate for the combination of probabilistic and possibilistic approaches, which will be discussed in this section. Options and advantages arise from the fact that the propagation at component level can be treated independently of the propagation to the global modal level. In the following, two numerical examples are given to illustrate the combination of possibilistic and probabilistic approaches in CMS.

5.4.1 Change from a probabilistic to a possibilistic uncertainty description

Consider the numerical example shown in Figure 5.4, where the input data is modelled by a probabilistic random field as presented in Section 5.3.2. The goal of the analysis is to estimate a FRF envelope based on 5 and 95 percentiles. However, in theory the percentiles could be applied at any of the four coordinate systems in CMS, as outlined in Figure 5.2. A standard option is to apply a sampling approach and estimate percentiles for a FRF sample. This analysis has been shown in Section 5.3.2. Alternatively, an interval approach can be followed, if the percentiles are applied already to the pdf at the component physical level. This equals the analysis performed in Section 5.3.2. Furthermore, a hybrid approach is possible, where a probabilistic approach is applied for the component level and a possibilistic approach for the subsequent propagation. The results for these three described analyses are shown in Figure 5.10. In each case uncertainty is considered only in the component eigenvalues and correlations are neglected. The probabilistic steps are based on 10000 runs and the vertex method is applied for possibilistic steps. As expected, the percentiles of the FRF sample look qualitatively different to the FRF envelopes. In each of those three cases, bounds are put to the pdf of a fundamentally different property and any of them could be a valid approach for a specific application. However, it can be noted that if the change from a probabilistic to a possibilistic description is done in a later propagation step, the resulting FRF

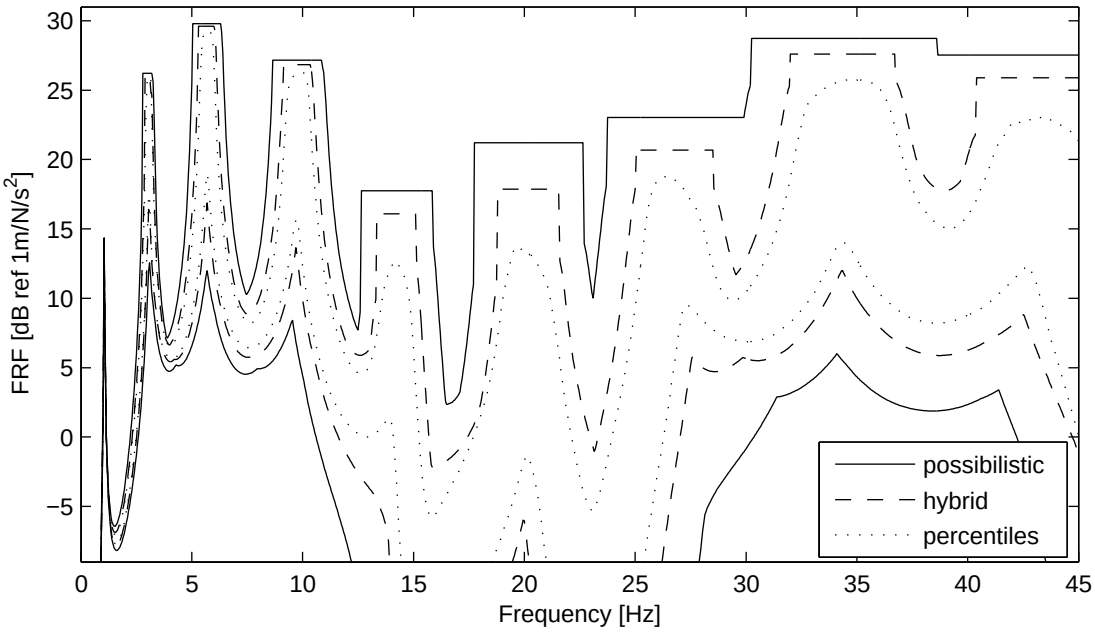

Figure 5.10: *FRF envelopes based on a possibilistic, probabilistic and hybrid approach.*

envelope will be narrower.

Similar concepts in relation to non-deterministic modal superposition are also discussed in more detail in Chapter 7.

5.4.2 Combination of a probabilistic and a possibilistic uncertainty description

It is possible that parametric uncertainty in one component is given an interval, whereas sample statistics or distributions are known for others. In this case, both descriptions have to be unified at some stage and it seems appropriate to do it at the component modal level. Figure 5.11 outlines this strategy, where the appropriate propagation method is used at component level and subsequently the qualitatively different results are combined at component modal level. Considering the numerical example shown in Figure 5.4. Uncertainty in component α is now modelled possibilistically, as described in Section 5.3.1, whereas uncertainty in component β is modelled probabilistically, as described in Section 5.3.2. Figure 5.12 shows the results for the estimated FRF envelopes. For the possibilistic approach, the uncertain data was unified at the component physical level and for the hybrid approach, it was unified at the component modal level. It can be seen that the hybrid method gives much closer bounds to the FRF than a classical possibilistic approach. Therefore,

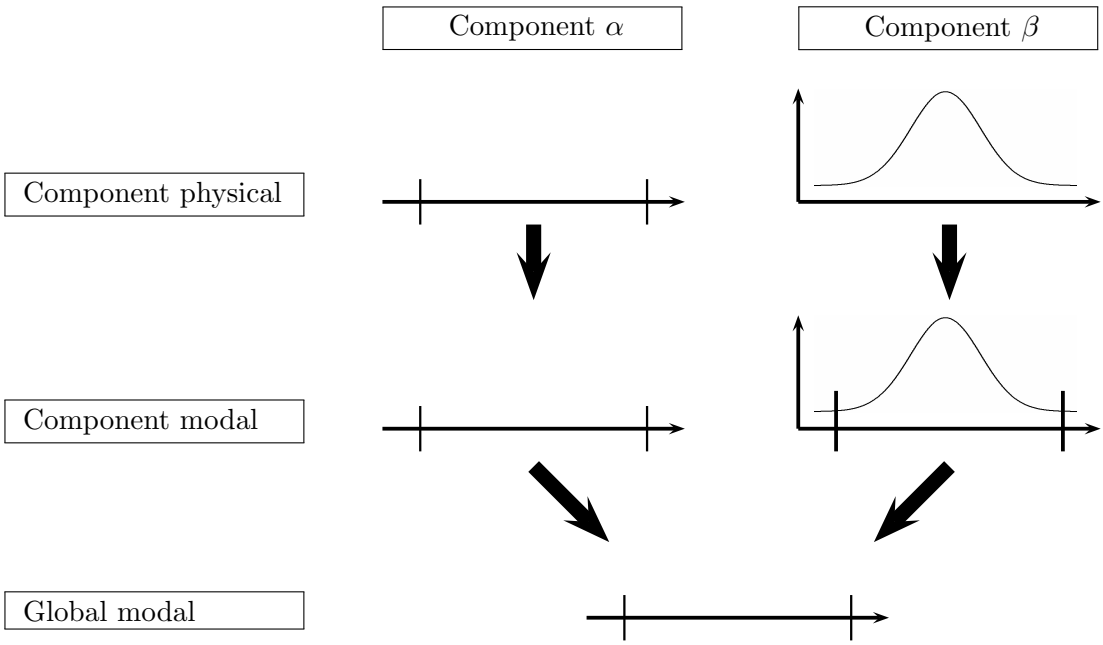

Figure 5.11: *Outline of a combined probabilistic and possibilistic analysis in CMS.*

conservatism could be reduced and the available information is used as much as possible. However, bounds are not strict possibilistic bounds nor can they be associated with distinct probabilities. The combination of possibilistic and probabilistic data remains a mathematical and philosophical challenge.

5.5 Modal sensitivities and perturbation in CMS

This section concerns modal sensitivities and the use of perturbational relations for the propagation of non-deterministic data within the CMS framework. Perturbation methods can be used to replace numerically expensive operations, such as solving an eigenvalue problem. The propagation problem is then reduced to an algebraic equation, which is numerically very cheap. In general, the accuracy of first order perturbation methods is reasonable if the variations in input parameters are small. However, in the context of calculations involving uncertain properties, the accuracy that can be achieved is limited by the level of uncertainty in the input data. Therefore, exact or highly accurate propagation methods are often unnecessary and approximate techniques might be appropriate.

The coordinate systems and uncertain parameters that will be considered for uncertainty propagation in this section are shown in Figure 5.13. At the component physical level, uncertainty is present in parameters p. At component modal level, uncertainty is only considered in terms of the component eigenvalues, which can be

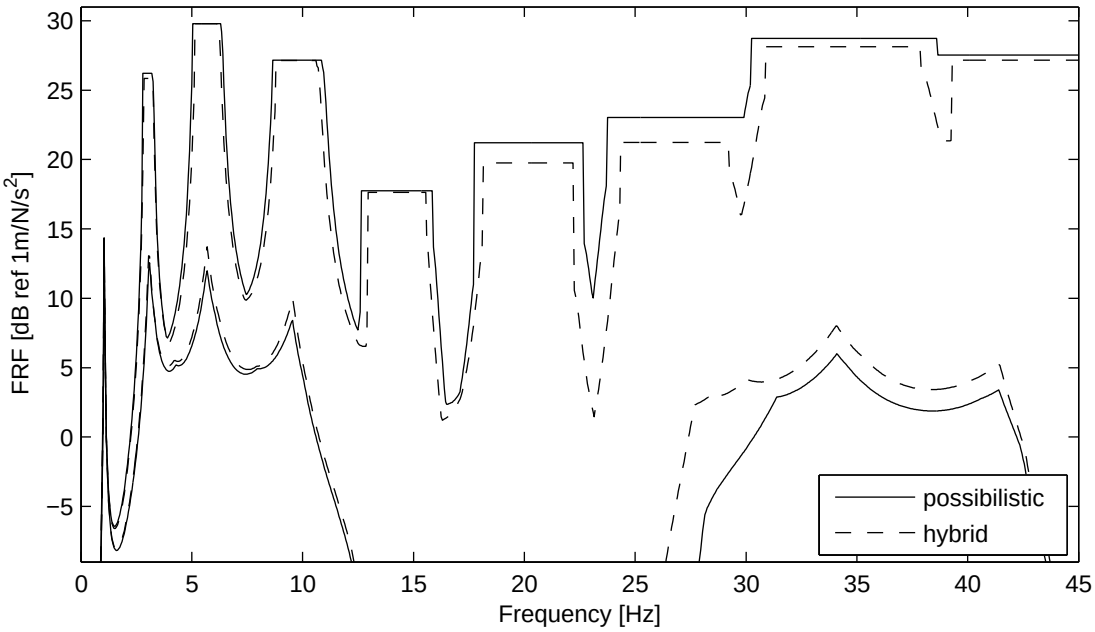

Figure 5.12: *FRF envelopes based on a possibilistic and a hybrid approach.*

fixed or free-interface eigenvalues. The arising inaccuracies and errors have been discussed previously. At global modal level, the variation in eigenvalues and eigenvectors is included. The propagation to the global physical level by non-deterministic modal superposition is discussed in Chapter 7.

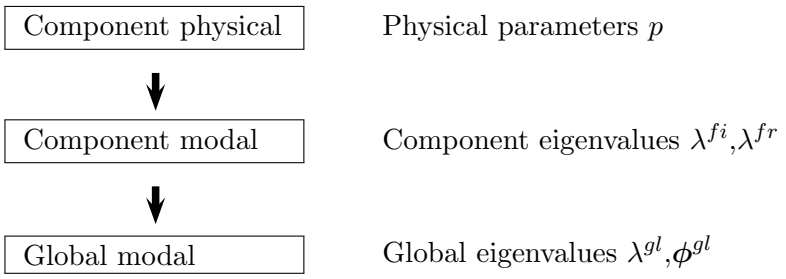

Figure 5.13: *Outline of coordinate levels and parameters considered for uncertainty propagation by perturbation.*

5.5.1 Perturbation from physical to modal properties

The rate of change of an eigenvalue λ_i with respect to a parameter p_j is given by [64]

$$\frac{\partial \lambda_i}{\partial p_j} = \boldsymbol{\phi}_i^T \left(\frac{\partial \mathbf{K}}{\partial p_j} - \lambda_i \frac{\partial \mathbf{M}}{\partial p_j} \right) \boldsymbol{\phi}_i \tag{5.7}$$

where $\mathbf{M}$ and $\mathbf{K}$ are the mass and stiffness matrices respectively and $\boldsymbol{\phi}$ is the ith eigenvector. Similar expressions exist for the first order sensitivity of the ith eigenvectors, as shown in Chapter 2. The baseline modal properties are given by the deterministic solution and only the derivatives of the stiffness and mass matrices with respect to the uncertain physical parameters have to be obtained. If a sensitivity matrix $\mathbf{R}$ is defined such that $r_{ji} = \frac{\partial \lambda_i}{\partial p_j}$, a change in component eigenvalues can be approximated from a change in parameters as

$$\Delta \boldsymbol{\Lambda} = \mathbf{R} \Delta \mathbf{p} \tag{5.8}$$

It follows that the covariance matrix of the eigenvalues can be approximated from the covariance matrix of the physical parameters as

$$COV(\boldsymbol{\Lambda}) = \mathbf{R} \quad COV(\mathbf{p}) \quad \mathbf{R}^T \tag{5.9}$$

In practice, spatially varying physical properties can be modelled by random fields. In FE methods, these are discretised using the existing mesh. In this case, $\mathbf{p}$ is a vector of correlated finite element properties and $COV(\mathbf{p})$ is the covariance matrix as used in the representation of random fields. The gradients r_{ji} depend on the FE model and their calculation might not be trivial.

In a classical approach, this perturbation can be used for uncertainty propagation from component physical to global modal properties. In the CMS framework, it describes propagation from component physical to component modal properties. It is valid for both fixed-interface and free-interface methods. The subsequent propagation to the global modal level, which concerns the synthesis of components, is addressed next.

5.5.2 Perturbation from component modal to global modal properties

A local modal/perturbational propagation method from the component modal to the global modal level has been presented in [95]. It makes use of the special structure of the global system matrices, Equation 5.4 where the component eigenvalues appear

uncoupled on the diagonal of the stiffness matrix. If Equation 5.7 is applied, where the uncertain parameters are now the component eigenvalues ($p_j = \lambda_j^c$), it follows that

$$\frac{\partial \lambda_i^{gl}}{\partial \lambda_j^{fi}} = \left(\boldsymbol{\phi}_i^{gl}\right)_j \left(\boldsymbol{\phi}_i^{gl}\right)_j \tag{5.10}$$

where λ_i^{gl} and λ_j^{fi} are the ith global and jth component eigenvalue respectively and $\boldsymbol{\phi}_i^{gl}$is the ith baseline global eigenvector. Thus changes in the component eigenvalues can be related to changes in the global eigenvalues by

$$\Delta\boldsymbol{\Lambda}^{gl} = \mathbf{S}\Delta\boldsymbol{\Lambda}^{fi} \tag{5.11}$$

where a sensitivity matrix $\mathbf{S}$ has been defined such that $s_{ji} = \left((\boldsymbol{\phi}_i^{gl})_j\right)^2$.

If the covariance matrix of the component eigenvalues is known, the covariance matrix of the global eigenvalues can be estimated by

$$COV(\Lambda^{gl}) = \mathbf{S}COV(\Lambda^{fi})\mathbf{S}^T \tag{5.12}$$

This sensitivity approach can be extended to the propagation of uncertainties in the component and constraint mode shapes, but is less straightforward if these submatrices are not diagonal. The constraint mode shapes in particular seem to affect the FRF variability primarily for the lowest few modes, where the static constraint terms are more important. An approach considering the variation in component modes was suggested in [96], although quantifying the uncertainty in a practical situation might be problematical.

5.5.3 Numerical example

Consider the numerical example in Figure 5.4, with a probabilistic description of uncertainties as described in section 5.3.2. A Monte Carlo approach with 10000 runs was applied in order to estimate the statistics of the global eigenvalues for the case that uncertainty at component modal level is only considered in the component eigenvalues. Equation 5.9 can be used to estimate the covariance matrices of the component eigenvalues from the covariance matrices of the random fields. Subsequently, Equation 5.10 can be used to estimate the covariance matrix of the global eigenvalues. The corresponding first order sensitivities for both relations are obtained from the baseline solution. In Figure 5.14, the errors in the estimated standard deviation of the first 10 global eigenvalues due to the use of a perturbation are shown. In one case, perturbation is applied to both propagation steps, i.e. from component physical to global modal properties. In the other case, perturbation is

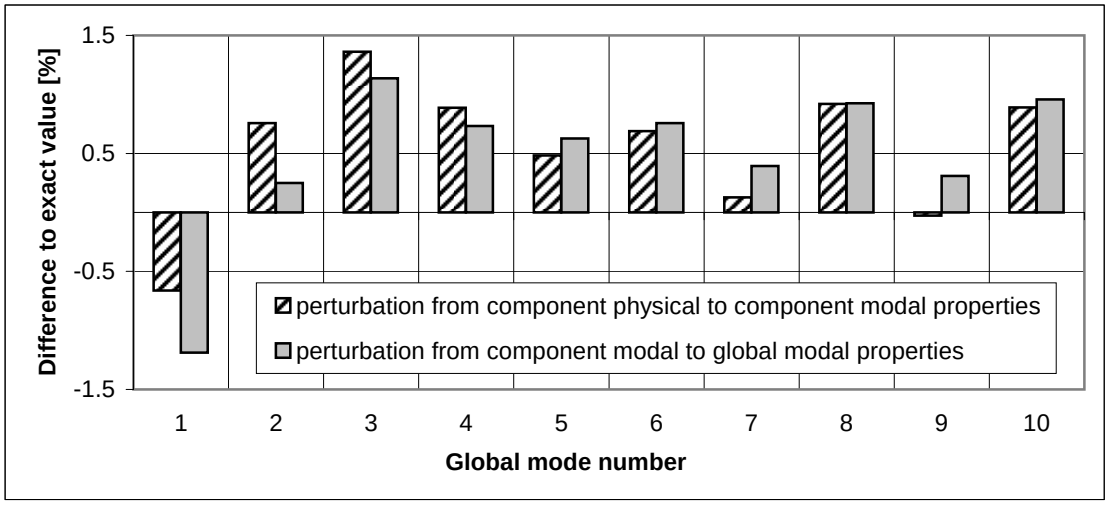

Figure 5.14: *Errors in standard deviation of the global eigenvalues due to perturbation.*

only considered for the propagation from component modal to global modal properties. The maximum error is about 1.5% which is very satisfactory, especially in the context of other inaccuracies in the analysis and the level of uncertainty in general.

In practice the modal/perturbational relation from component modal to global modal properties is highly relevant. It concerns, in general, the numerically most expensive propagation step. However, the required modal sensitivities are automatically obtained by the baseline solution of CMS. It can be used if uncertainty is directly quantified in the component eigenvalues, if quantitatively different data descriptions are unified or if correlations are neglected. Figure 5.15 shows the results for FRF percentiles, where a perturbation has been used from component modal to global modal properties. Similarly, Figure 5.16 presents the results for a possibilistic uncertainty description.

In both cases the agreement between the results for the exact and approximate propagations is reasonably good.

5.6 Discussion and concluding remarks

Component mode synthesis is a well-established method for the deterministic analysis of built-up structures. CMS also provides an appealing framework for the analysis of structures with non-deterministic properties. The computational cost of a non-deterministic analysis can already be reduced drastically by model reduction. Several advantages arise from the fact that CMS introduces the component

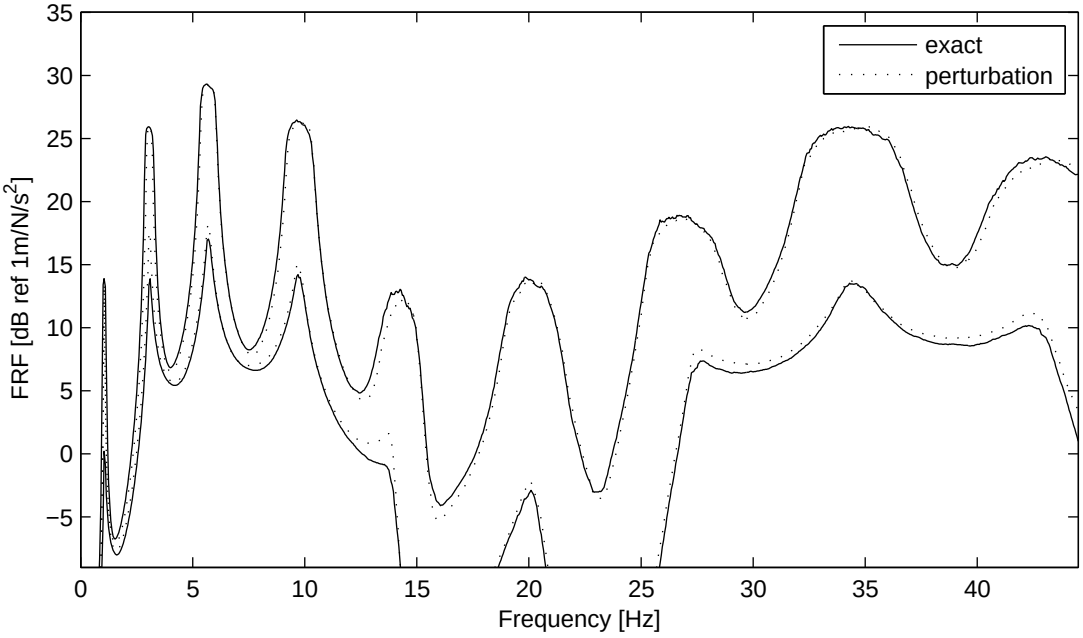

Figure 5.15: 5 *and* 95 *FRF percentiles: exact propagation and perturbation from component modal to global modal level.*

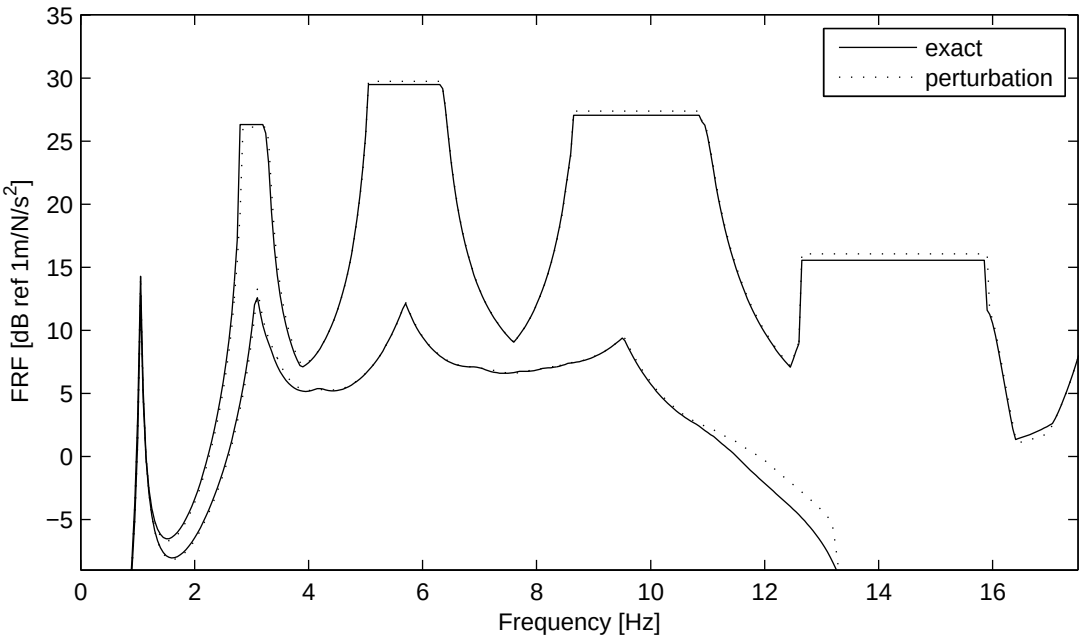

Figure 5.16: *FRF envelope: exact propagation and perturbation from component modal to global modal level.*

modal level as an additional coordinate system. Uncertainty can be straightforwardly introduced at the component level, either in physical or modal coordinates. The propagation of uncertainties from physical to component modal coordinates and from component modal to global modal coordinates can be treated independently. The application of perturbational relations is most appropriate and has been shown to be reasonable accurate and numerically very cheap.

The fixed-interface CMS method has further advantages for the analysis of structures with uncertain properties, because the global mass and stiffness matrices possess a special structure. The global mass and stiffness matrices are governed by the component eigenvalues and the constraint terms. Quantifying the uncertainty in component eigenfrequencies experimentally is straightforward, for example from repeated hammer tests on an ensemble of structures. In contrast it is much more difficult to quantify the variation in normal and constraint modes experimentally, as is the case for spatial variation of physical properties. Similarly, for the numerical propagation of uncertainties several benefits arise if the variations in the constraint terms, especially the off-diagonal terms, are neglected. However, this introduces approximation errors, particularly for the lower modes. For higher frequencies, the approximation gives good results. Other errors in the FRF magnitude arise if the variations in the component modal matrices are neglected. Overall the approximation of considering uncertainty only in component eigenvalues seems reasonable for a frequency range where the lower limit is determined by the influence of the constraint terms. If this approximation is made, the analysis simplifies greatly. The perturbational relations discussed can be implemented, with the required sensitivities already being known from the baseline eigenvector matrix. The perturbation can be performed at very little cost and can be combined with probabilistic or possibilistic approaches. Statistics such as the variance can be computed directly. It is worth noting that the approximation errors introduced may well be comparable to errors in the quantification of uncertainty in the component physical properties. A core strength of CMS is the ability to combine component models with qualitatively and quantitatively different deterministic FE models. Similarly, different descriptions of uncertain properties can be considered at component level. This includes the combination of probabilistic and possibilistic data, which can be a realistic requirement. Uncertainty in damping mainly affects the magnitude of the FRF and could be included independent of the eigenvalue and eigenvector analysis at little extra cost. Similarly, uncertainties in joints can be included through the constraint matrices, although this has not been considered here.

Chapter 6

Uncertainty propagation using free- and fixed-interface methodologies in CMS

This chapter mainly concerns a perturbational relation between free- and fixed-interface component eigenvalues, which has potential applications for the experimental quantification of uncertainties. Measurements on components are most easily performed in a free configuration, which can easily be realised and leads to relatively accurate results. Each component of a structure may be tested in a free configuration and the statistics of the free-interface natural frequencies can be determined straightforwardly. For numerical analysis, however, fixed-interface methods are preferable for various reasons, as discussed before. Therefore, an approximate approach will be discussed where free-interface data is used to estimate fixed-interface data, which is then used in fixed-interface analysis to predict response statistics.

6.1 Fixed and free-interface methodology for one component

Considering a component model in free configuration, described by the mass and stiffness matrices $\mathbf{M}$ and $\mathbf{K}$ respectively, the free-interface eigenvalues λ_i^{fr} can be found by solving the eigenvalue problem

$$\left(\mathbf{K} - \lambda_i^{fr}\mathbf{M}\right)\boldsymbol{\psi}_i^{fr} = \mathbf{0} \tag{6.1}$$

If there are fixed-interface conditions, the fixed-interface eigenvalues λ_i^{fi} can be calculated from the eigenvalue problem associated with the internal coordinates,

given by

$$(\mathbf{K}_{II} - \lambda_j^{fi}\mathbf{M}_{II})\boldsymbol{\psi}_j^{fi} = \mathbf{0} \tag{6.2}$$

Introducing a transformation in the form

$$\boldsymbol{\mu} = \mathbf{B}^T\mathbf{M}\mathbf{B} \quad \text{and} \quad \boldsymbol{\kappa} = \mathbf{B}^T\mathbf{K}\mathbf{B} \tag{6.3}$$

where $\mathbf{B}$ is the component mode matrix, the modal mass and stiffness matrices take the form

$$\boldsymbol{\kappa} = \begin{bmatrix} diag(\boldsymbol{\Lambda}^{fi}) & \mathbf{0} \\ \mathbf{0} & \mathbf{k}_{cc} \end{bmatrix} \quad \boldsymbol{\mu} = \begin{bmatrix} \mathbf{I} & \mathbf{m}_c \\ \mathbf{m}_c^T & \mathbf{m}_{cc} \end{bmatrix} \tag{6.4}$$

where $\boldsymbol{\Lambda}^{fi}$ is a vector of fixed-interface eigenvalues λ_i^{fi}. The eigenvalue problem

$$\left(\boldsymbol{\kappa} - \lambda_i^{fr}\boldsymbol{\mu}\right)\boldsymbol{\phi}_i^{fr} = \mathbf{0} \tag{6.5}$$

yields the free-interface eigenvalues λ^{fr}. Therefore, the free-interface eigenvalues depend on the fixed-interface eigenvalues and the constraint stiffness and mass terms in the matrices $\boldsymbol{\kappa}$ and $\boldsymbol{\mu}$. The constraint stiffness matrix $\mathbf{k}_{cc}$ is in general not diagonal, but can be made diagonal by a transformation that follows from solving the eigenvalue problem associated with the constraint coordinates. A diagonal matrix of characteristic constraint stiffnesses, the eigenvalues of $\mathbf{k}_{cc}$, and characteristic constraint modes are obtained [89].

If the model has n_{fr} DOFs, the free-interface solution will have n_{RB} zero-valued rigid-body eigenvalues and $n_{fr} - n_{RB}$ nonzero eigenvalues. In the fixed-interface CMS model, there are n_{fi} fixed-interface eigenvalues, n_{RB} zero-valued characteristic constraint stiffnesses and $n_{fr} - n_{fi} - n_{RB}$ nonzero characteristic constraint stiffnesses. As expected, the number of nonzero free-interface eigenvalues is equal to the number of nonzero elements in the diagonal of the modal stiffness matrix $\boldsymbol{\kappa}$. However, if there are more than the necessary interface conditions to constrain all DOFs, then the number of fixed-interface eigenvalues is less than the number of nonzero free-interface eigenvalues.

The derivative of the ith free-interface eigenvalue with respect to the jth fixed-interface eigenvalue is given by elements of the free-interface eigenvectors in the form

$$\frac{\partial\lambda_i^{fr}}{\partial\lambda_j^{fi}} = (\phi_i)_j(\phi_i)_j \tag{6.6}$$

This sensitivity approach can be extended to the characteristic constraint terms, but is less straightforward if these submatrices are not diagonal. In practice, it is also not feasible to quantify variation in the constraint terms experimentally. There-

fore, only variation in the component eigenvalues will be considered. A sensitivity matrix $\mathbf{T}$ relating changes in fixed-interface eigenvalues to changes in free-interface eigenvalues can be defined as

$$\Delta\mathbf{\Lambda}_m^{fr} = \mathbf{T}_{mp} \quad \Delta\mathbf{\Lambda}_p^{fi} \tag{6.7}$$

where $t_{ji} = ((\phi_i)_j)^2$ and $\mathbf{T}_{mn}$ is a submatrix of $\mathbf{T}$ corresponding to selected sets m and p of fixed and free-interface eigenvalues. A change in fixed-interface eigenvalues can be related to a change in free-interface eigenvalues using the inverse formulation

$$\Delta\mathbf{\Lambda}_p^{fi} = \mathbf{T}_{mp}^{-1} \quad \Delta\mathbf{\Lambda}_m^{fr} \tag{6.8}$$

The number of selected eigenvalues in the sets m and p is important for the inverse formulation. If $\mathbf{T}_{mp}$ is a square matrix, the problem is determined and the matrix can be inverted normally. If it is a rectangular matrix, the problem is under-determined or over-determined and methods such as singular value decomposition or the pseudoinverse have to be employed. In general, problems such as ill-conditioning have to be addressed.

Equation 6.8 could be used in a model updating procedure in order to update the fixed-interface eigenvalues directly from experimental free-interface eigenvalue data. An example is given in the next section. However, in practice it is more appropriate to update the free-interface eigenvalues and subsequently include the interface conditions in the model.

The sensitivity matrix $\mathbf{T}_{mp}$ can be used to estimate the covariance matrix of the free-interface eigenvalues from the covariance matrix of the fixed-interface eigenvalues by

$$COV(\mathbf{\Lambda}_m^{fr}) = \mathbf{T}_{mp} \quad COV(\mathbf{\Lambda}_p^{fi}) \quad \mathbf{T}_{mp}^T \tag{6.9}$$

In practice, it is preferable to quantify free-interface statistics of eigenvalues experimentally, but fixed-interface statistics are often preferred in a numerical analysis. Therefore, the inverse formulation of Equation 6.9 is of interest, which is given by

$$COV(\mathbf{\Lambda}_p^{fi}) = \mathbf{T}_{mp}^{-1} \quad COV(\mathbf{\Lambda}_m^{fr}) \quad \mathbf{T}_{mp}^{-T} \tag{6.10}$$

In the next section, a numerical example is used to illustrate this approach.

6.1.1 Numerical example: cantilever beam

The numerical example is a cantilever beam with rectangular cross-section as shown in Figure 6.1. It is modelled by 11 finite elements using standard Euler-Bernoulli

beam theory [9]. To include variation, the beam thickness is modelled by a one-dimensional random field [42] with a Gaussian distribution. The coefficient of variation is 10% and the correlation length is $0.5m$, half the length of the beam. Monte Carlo simulation with 10000 runs is used to estimate sample statistics of the eigenvalues. The free-interface eigenvalue statistics are considered as experimental data and form the input for the estimation of the fixed-interface eigenvalue statistics. The exact fixed-interface eigenvalues are used as the reference solution.

First, a theoretical approach is demonstrated, where the mean free-interface eigenvalues are used to update mean fixed-interface eigenvalues. In order to create start values to be updated, the exact fixed-interface eigenvalues are perturbed by 10%. Equation 6.8 is then employed in an iterative scheme, where the sensitivity matrix is updated each step when the eigenvalue problem is solved. This approach is not exact, if the static constraint mass and stiffnesses are not considered. In Figure 6.2, the error before and after updating is shown for the first 10 modes. The error for the first mode could not be reduced, the error for the second mode is about half and for higher modes it gradually reduces towards zero. This shows the general effect in approaches were static constraint terms are neglected in the CMS formulation, where a lower frequency limit can be observed, below which the results are not particularly accurate. In practice, the free-interface eigenvalues would be updated directly, subsequently the interface conditions would be imposed and finally the fixed-interface eigenvalue problem solved to obtain exact results.

L $[m]$	h $[m]$	b $[m]$	E $[N/m^2]$	ρ $[kg]$
1	0.02	0.1	2.1e11	7850

$I = \frac{bh^3}{12}$

$A = bh$

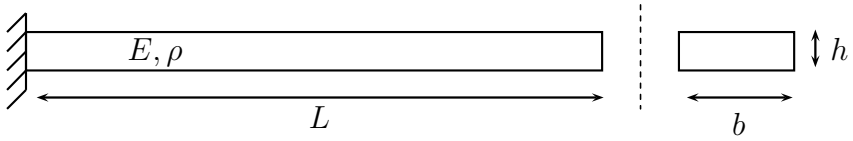

Figure 6.1: *One component beam structure and baseline properties.*

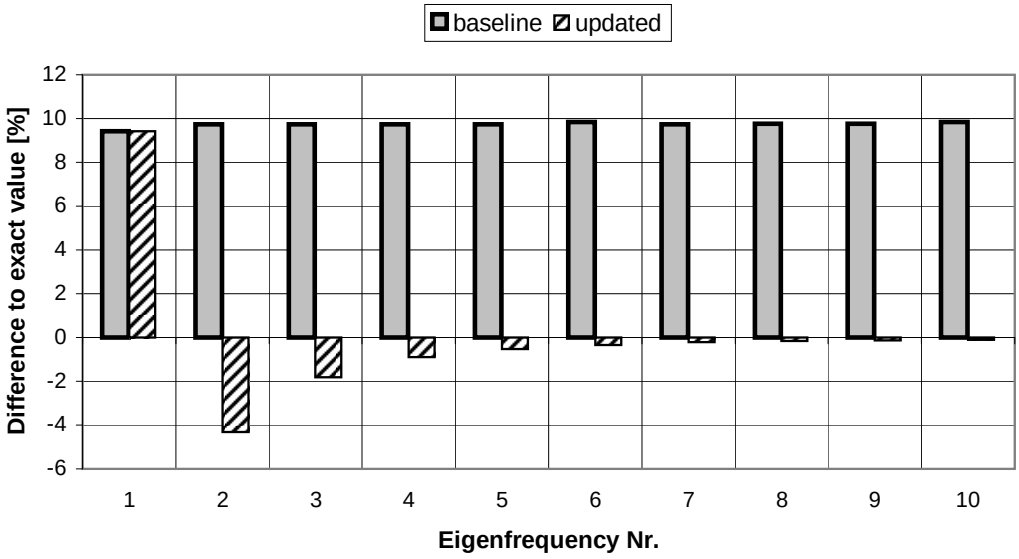

Figure 6.2: *Mean value of component eigenfrequencies: error before and after updating of fixed-interface eigenvalues using data on free-interface eigenvalues.*

Next, the standard deviations of the fixed-interface eigenvalues are estimated from the covariance matrix of the free-interface eigenvalues using Equation 6.10. The estimated results are compared with the exact solution and the difference is shown in Figure 6.3. In this case, all nonzero free-interface eigenvalue statistics have been considered to estimate the covariance matrix of all except the first fixed-interface eigenvalues. The error is large for the lowest modes, but gradually decreases for higher modes and is less than 1% above the 8th mode. The condition number of the sensitivity matrix depends on the selected sets of eigenvalues. If the first fixed-interface eigenvalue is neglected, the condition number of the sensitivity matrix is lower and the results for the other modes improves. This and other issues will also be addressed in the discussion section.

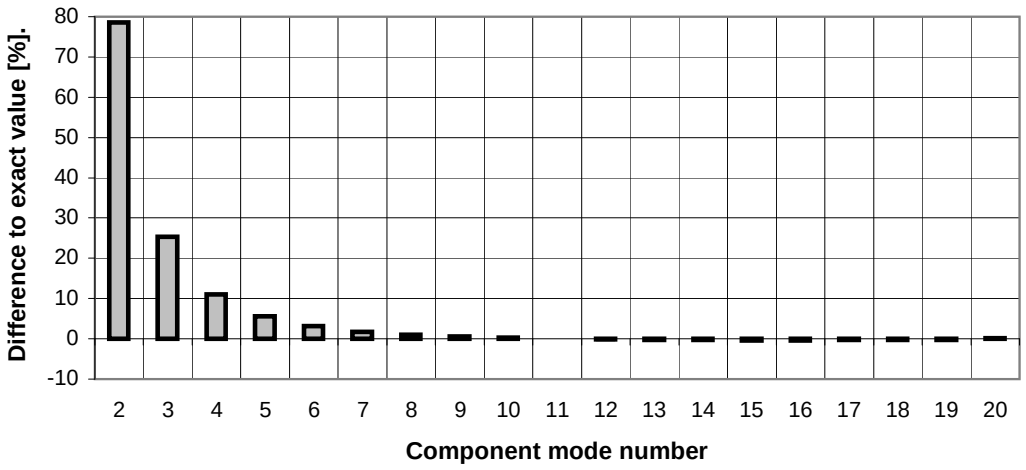

Figure 6.3: *Standard deviation of fixed-interface component eigenvalues: approximation error for estimation from free-interface statistics.*

6.2 Built-up structure

The propagation of non-deterministic data in a built-up structure has been discussed in the previous chapter. A perturbational relation between fixed-interface component modal and global modal eigenvalues was discussed, where $\mathbf{S}$ is the sensitivity matrix given by

$$\frac{\partial \lambda_i^{gl}}{\partial \lambda_j^{fi}} = s_{ji} \tag{6.11}$$

If the covariance matrix of the fixed-interface component eigenvalues is known, the covariance matrix of the global eigenvalues can be estimated by

$$COV(\mathbf{\Lambda}_r^{gl}) = \mathbf{S}_{rs} \quad COV(\mathbf{\Lambda}_s^{fi}) \quad \mathbf{S}_{rs}^T \tag{6.12}$$

where r refers to the set of selected global eigenvalues ($\mathbf{\Lambda}_r^{gl}$) and s refers to the set of selected fixed-interface eigenvalues of components α and β.

If Equations 6.10 and 6.12 are combined, a relation between the statistics of the global eigenvalues of the built-up structure and the statistics of the free-interface eigenvalues of individual components can be written as

$$COV(\mathbf{\Lambda}_r^{gl}) = \quad \mathbf{S}_{rs} \quad \mathbf{T}_{mp}^{-1} \quad COV(\mathbf{\Lambda}_m^{fr}) \quad \mathbf{T}_{mp}^{-T} \quad \mathbf{S}_{rs}^T \tag{6.13}$$

where

$$COV(\mathbf{\Lambda}_m^{fr}) = \begin{bmatrix} COV({}^{\alpha}\mathbf{\Lambda}_{m_\alpha}^{fr}) & \mathbf{0} \\ \mathbf{0} & COV({}^{\beta}\mathbf{\Lambda}_{m_\beta}^{fr}) \end{bmatrix} \tag{6.14}$$

is the matrix containing the covariance matrices for selected sets m_α and m_β of free-interface eigenvalues for components α and β respectively. The corresponding component sensitivity matrices are arranged as

$$\mathbf{T}_{mp} = \begin{bmatrix} {}^{\alpha}\mathbf{T}_{m_\alpha p_\alpha} & \mathbf{0} \\ \mathbf{0} & {}^{\beta}\mathbf{T}_{m_\beta p_\beta} \end{bmatrix} \tag{6.15}$$

Equation 6.13 involves first an inverse calculation at component level, where fixed-interface eigenvalue statistics are estimated from free-interface eigenvalue statistics independently for each component, and secondly a forward approach to estimate global eigenvalue statistics from fixed-interface component eigenvalue statistics. In the formulation of Equation 6.13, all component statistics estimated by the inverse step are also used in the forward step and therefore sizes of the matrices correspond (index p = index s). In practice, both steps can be treated independently. A numerical example is presented in the next section.

6.2.1 Numerical example: two component beam structure

	L $[m]$	h $[m]$	b $[m]$	E $[N/m^2]$	ρ $[kg]$	$I = \frac{bh^3}{12}$
component α	1	0.02	0.1	2.1e11	7850	$A = bh$
component β	0.8	0.01	0.1	2.1e11	7850	

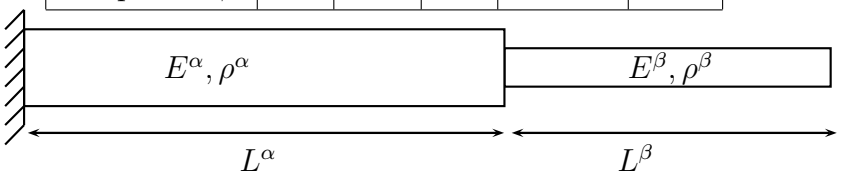

Figure 6.4: *Two component beam structure and baseline properties.*

The two-component structure in Figure 6.4 is used as a numerical example for a built-up structure. The model consists of two connected Euler-Bernoulli beam components and the built-up structure is fixed at one side. The baseline values are given in Figure 6.4, where the components differ in length and thickness. To simulate experimental data, a random field model for the thicknesses of the beams is

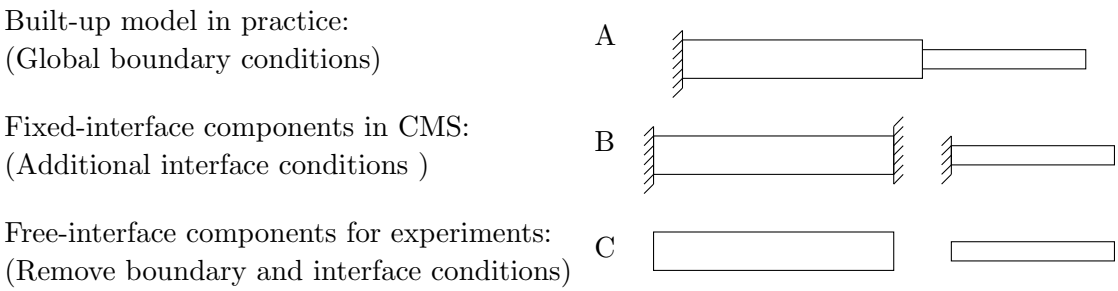

Figure 6.5: *Different interface conditions for components.*

used. A Gaussian distribution with a coefficient of variation of 10% is assumed and the correlation length is chosen as $0.5m$. A standard Monte Carlo simulation approach with 10000 runs is used to calculate mean values and the covariance matrix of eigenvalues.

In Figure 6.5, different interface conditions for the components are illustrated. Case A shows the global built-up structure, which will be used to obtain reference results. In case B, the independent fixed-interface components are shown as they are used in the CMS formulation. Case C refers to the components under free-interface conditions, which is the preferred situation to perform experimental measurements.

In this analysis, first Equation 6.10 is used to estimate the covariance matrix of the fixed-interface eigenvalues from the free-interface statistics, independently for both components. In the second step, the global covariance matrix is estimated by Equation 6.12. The variation in the first fixed-interface eigenvalues of both components has been neglected in both steps. The results can be compared with the reference solution obtained for case A. The differences for the standard deviations of the first 30 modes is shown in Figure 6.6. There is no variation estimated for the first two global modes. For higher frequencies up to the 10th mode, the error is up to about 40%. For higher modes, the error is less than 10% and decreasing. A discussion of the results and alternative approaches follows in the next section.

6.3 Discussion

The fixed-interface CMS method was used to relate free-interface modal properties to fixed-interface eigenvalues and constraint terms. It is convenient for the analysis to neglect variation in the constraint terms. The sensitivities between free and fixed-interface eigenvalues are directly given by terms of the eigenvectors found by solving the component eigenvalue problem. In order to estimate fixed-interface eigenvalue

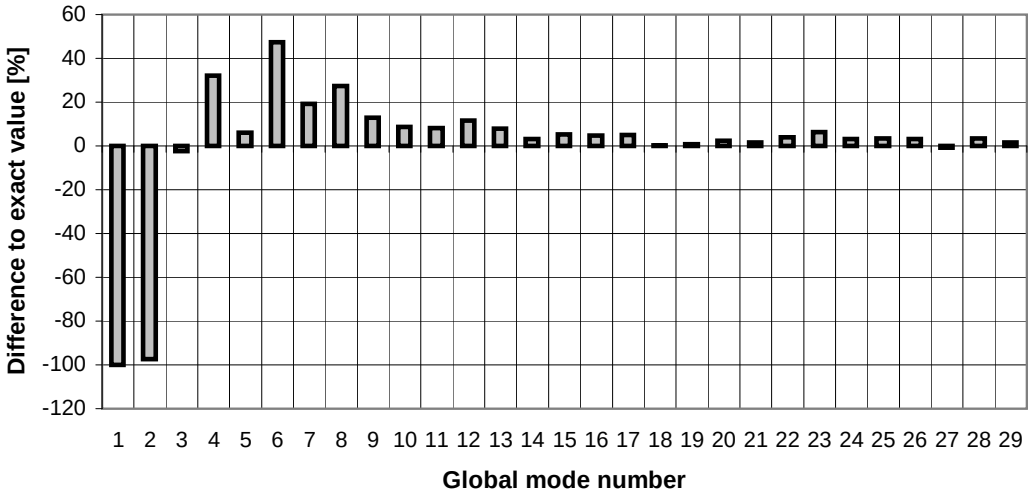

Figure 6.6: *Standard deviation of global eigenvalues: approximation error for proposed approach.*

statistics from free-interface statistics, the sensitivity matrix has to be inverted. This is related to problems such as ill-conditioning. The sensitivity matrix is well conditioned if it is square and the fixed and free-interface eigenvalues involved have about the same magnitude. In the simple case of a beam that is clamped at both ends, the fixed-interface eigenvalues correspond well to the nonzero free-interface eigenvalues. For a cantilever beam, the results are similar, but there is a shift by one mode. In general, the eigenfrequencies for fixed and free-interface conditions will match very well for higher modes, but can be shifted by a certain number of modes. For lower modes, fixed and free-interface results are in general very different. The transition depends on the characteristics of the boundary conditions and how they change the mode shapes of the structure. The results for the lowest fixed-interface eigenvalues have the largest errors. Numerically, this overestimation seems to compensate for neglecting the variations in the static constraint terms.

The forward propagation of component statistics to global statistics does not impose any numerical problems. The perturbation approach for CMS is known to yield reasonably accurate results and the sensitivity matrix is directly obtained from the global modal eigenvectors. The component statistics appear independently in the assembled model, since the variations in the coupling constraint terms are neglected. There are no variations predicted in the lowest eigenvalues, because these are governed by the static constraint terms. The largest error for the other modes, which is about 40%, is due to overestimations in the lower fixed-interface component modes. For higher frequencies, the errors gradually reduce.

The numerical framework discussed here aims at predicting the statistics of individual modal properties at component and global level. However, in practice it may be sufficient to consider an average coefficient of variation for eigenfrequencies at component level and neglect any correlations. Additionally, in some cases the difference between free and fixed-interface component statistics is small and can be neglected within a given accuracy.

Chapter 7

Non-deterministic modal superposition

7.1 Introduction

This chapter concerns the estimation of the frequency response function (FRF) and its variations based on the modal superposition principle. This constitutes the final step in a component mode synthesis analysis or general finite element analysis, where uncertainty is propagated from the global modal level to the global physical level. The FRF is a function of frequency ω and can be calculated from the eigenvalues λ_i and eigenvectors $\boldsymbol{\phi}_i$. The receptance FRF between two coordinates q_1 and q_2 can be written as a summation of contributions from individual modes as

$$\alpha(\omega, q_1, q_2) = \sum_{i=1}^{n} \alpha_i(\omega, q_1, q_2) = \sum_{i=1}^{n} \frac{(\boldsymbol{\phi}_i)_{q_1} (\boldsymbol{\phi}_i)_{q_2}}{\lambda_i - \omega^2 + j d_i} \tag{7.1}$$

where α_i is the modal receptance of mode i and n is the number of modes. Contributions from the modal displacements of the ith eigenvector at coordinates q_1 and q_2 appear in the numerator. The term $j\, d_i$ represents modal damping, which could be viscous or structural damping.

In a non-deterministic analysis, the modal parameters are random or interval variables, which are generally correlated. An analysis with uncertain parameters has to be performed for each frequency, especially since the FRF magnitude varies non-monotonically. The number of required deterministic solutions of Equation 7.1 can therefore be high, but the computational cost in solving this algebraic equation is very small. Another advantage of the modal superposition approach is that only a limited number of modes have to be considered according to the frequency range of interest, therefore further reducing numerical costs. However, the non-deterministic

eigenvalue problem has to be solved first to obtain the modal properties.

The first part of this chapter concerns a possibilistic approach, where the variation in modal properties is specified by intervals. The goal of the analysis is to obtain the FRF envelope, consisting of lower and upper bounds. A numerically efficient approach is discussed, where first the FRF envelopes for each mode are found and subsequently combined to obtain the total FRF envelope. In this context, the often-used definition of modal mass and stiffness as modal space parameters [59] is compared with a new formulation using a modal constant and the eigenvalue. The benefits of this novel family of methods are shown using a numerical example.

In the second part of this chapter, probabilistic uncertainties are considered and FRF percentiles are calculated. A Monte Carlo sampling approach, considering distribution functions and correlations of modal parameters, can be applied to obtain an ensemble of FRFs, from which FRF statistics can be estimated. However, the input data available in practice is often limited. Therefore, the effects of neglecting various correlations and assuming distribution functions are investigated. Furthermore, a hybrid probabilistic/possibilistic approach to quantify variations in the FRF is presented. In this method, a FRF envelope is calculated based on bounds of the probability distribution functions at the modal level.

7.2 Possibilistic approach

In this section, uncertainty is specified by intervals and the goal of the analysis is to calculate the global FRF envelope, denoted by $\overline{\underline{\alpha}}$. The undamped single mode FRF is given by

$$\alpha_i(\omega, q_1, q_2) = \frac{(\boldsymbol{\phi}_i)_{q_1} \, (\boldsymbol{\phi}_i)_{q_2}}{\lambda_i - \omega^2} \tag{7.2}$$

In the approach presented here, damping is initially neglected for simplicity. It can be shown [59] that the combination of single mode FRF envelopes yields a conservative approximation to the global FRF envelope, written as

$$\overline{\underline{\alpha}}(\omega, q_1, q_2) \subseteq \bigoplus_{i=1}^{n} \overline{\underline{\alpha_i}}(\omega, q_1, q_2) \tag{7.3}$$

where $\bigoplus$ denotes a summation where the uncertain parameters are considered independent between all modes. The calculation of a single mode FRF $\overline{\underline{\alpha_i}}$ from Equation 7.2 is not trivial, because it constitutes an interval problem as a function of frequency and with correlated parameters. Several methods have been developed in order to make conservative approximations of the single mode FRF envelope in a systematic way and potentially at a lower cost. In the following, different modal space

formulations and approximation methods will be investigated.

7.2.1 Modal spaces

The single mode FRF (Equation 7.2) can be written as

$$\alpha_i(\omega, q_1, q_2) = \frac{A_i}{\lambda_i - \omega^2} \tag{7.4}$$

where

$$A_i = (\boldsymbol{\phi}_i)_{q_1} \, (\boldsymbol{\phi}_i)_{q_2} \tag{7.5}$$

is the modal constant. Alternatively, it can be written in the form

$$\alpha_i(\omega, q_1, q_2) = \frac{1}{\hat{k}_i - \omega^2 \hat{m}_i} \tag{7.6}$$

where

$$\hat{k}_i = \frac{\lambda_i}{(\boldsymbol{\phi}_i)_{q_1} \, (\boldsymbol{\phi}_i)_{q_2}} \quad , \quad \hat{m}_i = \frac{1}{(\boldsymbol{\phi}_i)_{q_1} \, (\boldsymbol{\phi}_i)_{q_2}} \tag{7.7}$$

are the specific modal stiffness and mass, respectively, defined in terms of a pair of excitation and response coordinates. The modal parameters defined in Equation 7.5 and Equation 7.7 describe different modal spaces, which will be referred to as the the A - λ space and the $\hat{m}$ - $\hat{k}$ space. The transformation between the two spaces is given by

$$\lambda_i = \frac{\hat{k}_i}{\hat{m}_i} \quad , \quad A_i = \frac{1}{\hat{m}_i} \tag{7.8}$$

The mode index i will be omitted for convenience for the remainder of this section.

7.2.2 Uncertain modal space

If the system is deterministic, there are unique values $\hat{m_0}, \hat{k_0}, A_0$ and λ_0 describing a point in both modal spaces for each mode. However, if the modal space parameters are uncertain variables, they describe a region in the $\hat{m}$ - $\hat{k}$ and A - λ modal spaces. In Figure 7.1, the region described by the uncertain modal parameters is represented qualitatively by an ellipse. In a possibilistic analysis, the boundary of this region represents the envelope of all possible parameter realisations.

In the $\hat{m}$ - $\hat{k}$ space, the equation $\hat{k} = \omega^2 \hat{m} + \frac{1}{\alpha}$ describes straight lines with gradient ω^2. In Figure 7.1a, two lines, which bound the region, are fitted for a particular frequency ω_a and hence two intersections with the $\hat{k}$-axis are found. The magnitude of the single mode FRF corresponds to the inverse of these values. If both

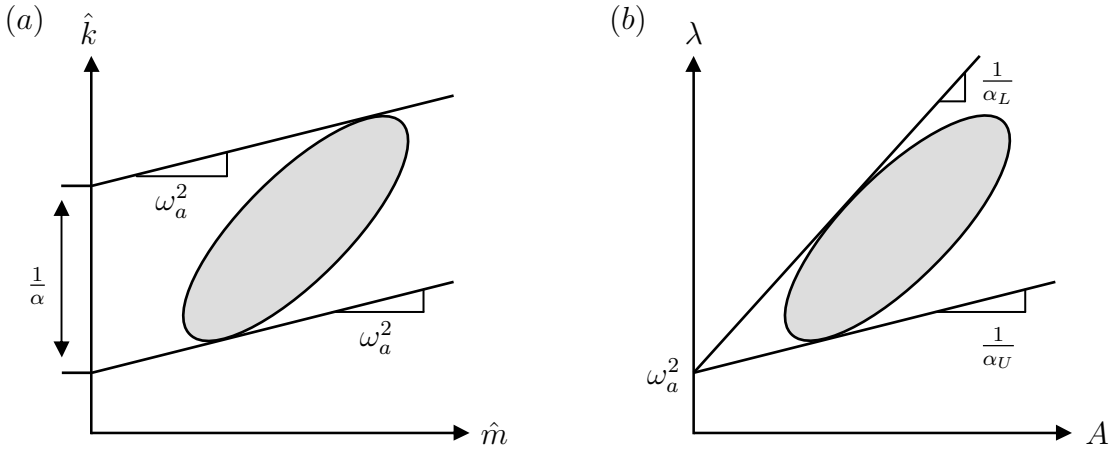

Figure 7.1: *Qualitative representation of the region due to uncertainty and construction of bounds on the FRF in different modal spaces.*

intersections lie either on the positive or on the negative part of the $\hat{k}$-axis, then they represent the upper and lower bounds of the single mode FRF. If one intersection lies on the positive part and the other on the negative part of the $\hat{k}$-axis, then the range of the FRF magnitude is not monotonic and includes resonance. In this case, the upper bound of the single mode FRF is infinite, if no damping is considered, and the lower bound is found as the smaller value of the two intersections.

In the A - λ space, the equation $\lambda = \frac{1}{\alpha}A + \omega^2$ describes straight lines that cross the λ-axis at ω^2. In Figure 7.1b, two lines are fitted to the uncertain region for the frequency ω_a and the magnitude of the single mode FRF corresponds to the inverse value of the gradient. If both gradients are either positive or negative, then they represent the upper and lower bounds of the single mode FRF. If one gradient is positive and the other is negative, then the range between them includes a line with zero gradient, which represents resonance.

7.2.3 Modal space approximation

In general, it is computationally expensive to determine the boundary of the uncertain region exactly, because the modal space parameters are correlated and a large number of data points is required. A conservative approximation to the bounds of the uncertain region can be made if the interdependency between the modal space parameters is neglected. In this case, the lower and upper bounds, denoted by indices L and U respectively, of the parameters are determined individually, which implies only four different values for the two modal parameters. In Figure 7.2, this approximation is illustrated by a rectangular boundary surrounding the region. This approach has been referred to as the modal rectangle (MR) method [59, 97]. Furthermore, it has been shown that the approximation in the $\hat{m}$ - $\hat{k}$ space can be

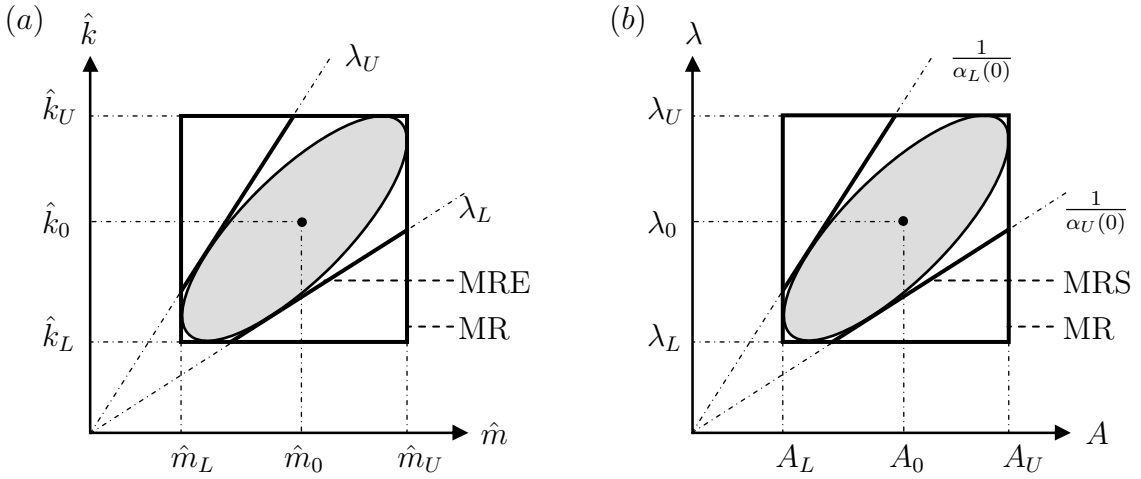

Figure 7.2: *Approximations by the modal rectangle (MR) method and appropriate corrections: (a) $\hat{m}$ - $\hat{k}$ space and (b) A - λ space.*

improved if the bounds on the eigenvalue, which are given by straight lines from the origin, are included. This approach is referred to as the modal rectangle method with eigenvalue correction (MRE) [59, 97]. The same approaches can be applied to the A - λ space, where the modal rectangle is described by the bounds on the modal constant A and the eigenvalue λ. Similarly to the $\hat{m}$ - $\hat{k}$ space, lines from the origin also improve the approximation, but in the A - λ space they relate to the bounds of the static solution. Therefore, this approach will be called the modal rectangle method with static correction (MRS).

In Figure 7.3, the estimation of the single mode FRF envelope based on the different approximations is compared qualitatively for the $\hat{m}$ - $\hat{k}$ and A - λ spaces. Lines are shown that refer to frequencies ω_a and ω_b, below and above the resonance range, respectively. The points used ($\triangle$, $\circ$) are bounds on the parameters from which the upper bound of the FRF is calculated. In the $\hat{m}$ - $\hat{k}$ space, only the upper left and lower right corners ($\triangle$) of the modal rectangle are used in the calculations. If the eigenvalue correction is implemented, these two points are replaced by four points ($\circ$) defined by the bounds of the eigenvalue. For very low and very high frequencies, the MR and MRE methods give similar results. For frequencies close to resonance (e.g. ω_a, ω_b), the MRE method gives much better results than the MR method. This can be seen by a closer fit of the frequency lines to the uncertain area in Figure 7.3. It has been shown that the correction using the eigenvalue bounds is essential to give not overly conservative results for approximations in the $\hat{m}$ - $\hat{k}$ space. In the A - λ space, all four corners ($\triangle$) of the modal rectangle are considered. If the static correction is used, two of them are replaced by other points ($\circ$), but two corner points remain unchanged. It can be seen that for frequencies above the resonance range (e.g. ω_b), the results from the MR and MRS methods are the same,

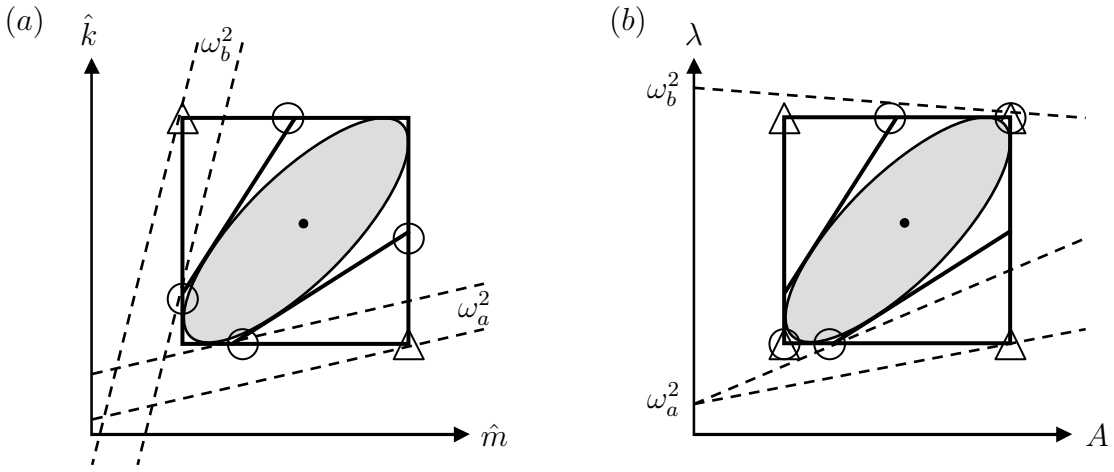

Figure 7.3: *Construction of points to calculate the upper bound of the FRF for two frequencies ω_a and ω_b using the standard and improved modal rectangle methods: $\triangle$ - points used by MR method; $\bigcirc$ - points used by MRE or MRS methods; (a) $\hat{m}$ - $\hat{k}$ space and (b) A - λ space.*

because the same point ($\triangle \equiv \circ$) is used. The MRS method gives better results then the MR method in the A - λ space only for low frequencies (e.g. ω_a).

7.2.4 Damping

It is straightforward to include either viscous or structural damping in the form of a modal damping ratio ζ or modal loss factor η, respectively. Table 7.1 shows the corresponding equations governing the single mode FRF for the $\hat{m}$ - $\hat{k}$ and A - λ spaces. The FRF is now a complex function and it has been shown [97] that the bounds on the real and the imaginary parts can be evaluated separately for all modes and combined in the final stage. If the damping constants are deterministic, only the two-parametric modal space has to be evaluated and the approximations discussed in the previous section are still valid. For the $\hat{m}$ - $\hat{k}$ space, it has been shown [97] that only the horizontal and vertical lines of the approximation have to be considered in order to find the extreme values of the real and imaginary parts. In the A - λ space, only the vertical lines (A=constant) which describe the range of the eigenvalue, have to be considered, since the influence of the modal constant is monotonic.

For the numerical example presented in the next section, a simple approximation of the effects of damping will be used. Damping is only considered over the eigenfrequency range related to possible resonance, where the magnitude of the FRF will be bounded by a constant value. If the damping is small and the modal overlap is low, the magnitude of the FRF at resonance is dominated by the resonant mode.

$\alpha(\omega, q_1, q_2)$	$\hat{m}$ - $\hat{k}$ space	A - λ space
Rayleigh damping Modal damping ratio ζ	$1/(\hat{k} - \omega^2\hat{m} + j2\omega\sqrt{\hat{k}\hat{m}}\zeta)$	$A/(\lambda - \omega^2 + j2\omega\sqrt{\lambda}\zeta)$
Structural damping Modal loss factor η	$1/(\hat{k} - \omega^2\hat{m} + j\hat{k}\eta)$	$A/(\lambda - \omega^2 + j\lambda\eta))$

Table 7.1: *Complex single mode FRF expressions for different damping models.*

The maximum magnitude of the single mode FRF can be approximated for $\omega^2 = \lambda$ and is then given by the imaginary part of the FRF. It can be calculated from the interval problem

$$\alpha_i(\omega^2 \in [\lambda], q_1, q_2) = \frac{A}{\lambda\eta} = \frac{1}{\hat{k}\eta} \tag{7.9}$$

The results are identical for both Rayleigh and structural damping if $\zeta = 2\eta$. The approximations of the modal parameters can be used to find a conservative approximation to the FRF magnitude. In general, the MRE and MRS methods give best results. In the $\hat{m}$ - $\hat{k}$ space, the FRF magnitude depends on the specific modal stiffness only and the modal rectangle approximation is sufficient.

7.3 Comparison of modal space formulations

In this section a numerical example, a simple four-DOF spring-mass system with eight independent parameters as shown in Figure 7.4, is considered to compare the accuracy of the above approaches. An uncertainty interval of $\pm 10\%$ for each parameter is considered and possibilistic results are sought. Structural damping has been included by a modal loss factor of 0.2%. In the following, first the approximations in the non-deterministic modal spaces are compared and then the uncertain FRF envelopes are shown.

7.3.1 Modal spaces

In Figure 7.5, the region described by the uncertain parameters is plotted for all four modes in the $\hat{m}$ - $\hat{k}$ modal space. In each figure (a-d), there are $2^8 = 256$ points representing the results from calculations using the vertex combinations, which depict the shape of the uncertain area. The boundary of the region is approximated by the modal rectangle method with eigenvalue correction. It can be seen that the specific modal mass and stiffness parameters are distributed almost uniformly for the first

N/m	k_1 1025	k_2 1575	k_3 3025	k_4 2325
kg	m_1 5.5	m_2 13	m_3 9.5	m_4 17

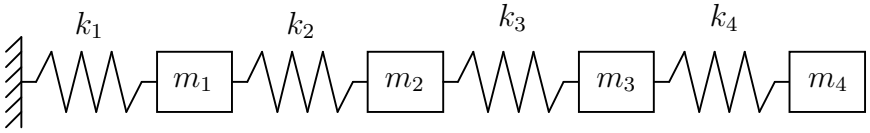

Figure 7.4: *Four degree of freedom model for analysis.*

mode. Therefore, the MR approximation can be expected to yield accurate results. The improvement achieved by using the eigenvalue bounds is small. In contrast, the vertex points for the higher modes are spread out around a line corresponding to the baseline eigenvalue. There is interdependency between the specific modal mass and stiffness and therefore the approximation by the MR method gives very conservative results. The bounds on the eigenvalue range provide a distinct improvement of the approximation. It can be noted that the distribution of the points about the baseline solution is non-symmetric.

In Figure 7.6, the same data is plotted in the A - λ modal space. For the first mode, there is clear interdependency between the modal constant and the eigenvalue and the rectangle approximation method is improved by using the bounds provided by the static solution. For the higher modes, the vertex points are distributed more uniformly in the parameter space and the MR method may be sufficient. It can be noted that the points also extend uniformly about the baseline solution.

7.3.2 Frequency response functions

The receptance FRF between masses 3 and 4, α_{34}, will be considered. In Figure 7.7, the baseline FRF, the pseudo-exact FRF envelope and a conservative FRF envelope approximation are shown. The pseudo-exact reference solution for the FRF envelope is computed by considering all 256 vertex combinations of the uncertain mass and stiffness parameters in a direct analysis. It can be considered as exact, due to the monotonic behaviour in this numerical example, except around resonance or antiresonance. The conservative approximation to the total FRF envelope was obtained by combining the exact single mode FRF envelopes according to Equation 7.3. In this case, interdependencies between the modes are neglected and conservatism is intro-

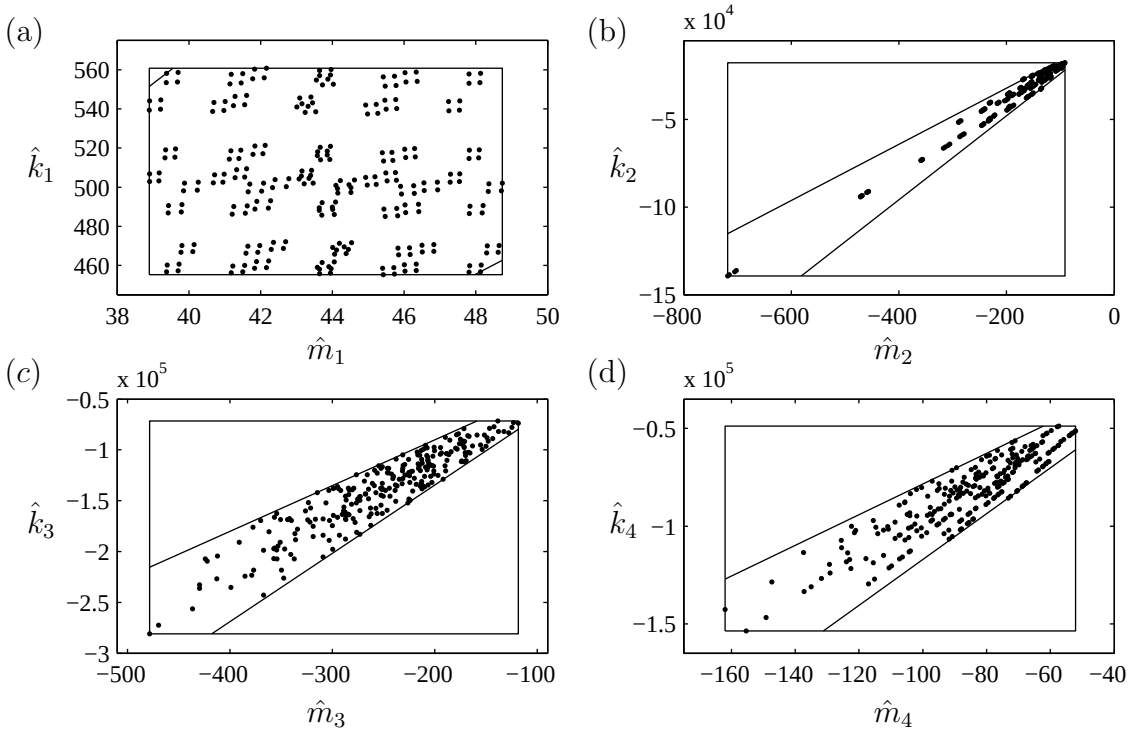

Figure 7.5: *Vertex points and approximations in the $\hat{k}$ - $\hat{m}$ modal space.*

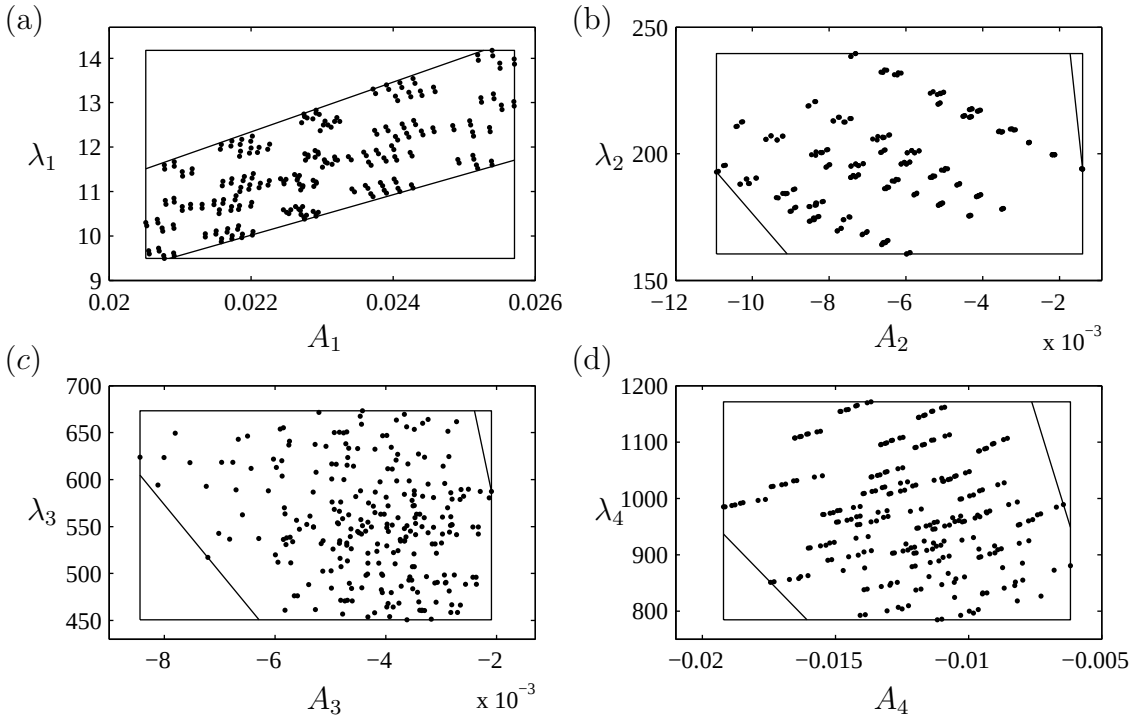

Figure 7.6: *Vertex points and approximations in the A - λ modal space.*

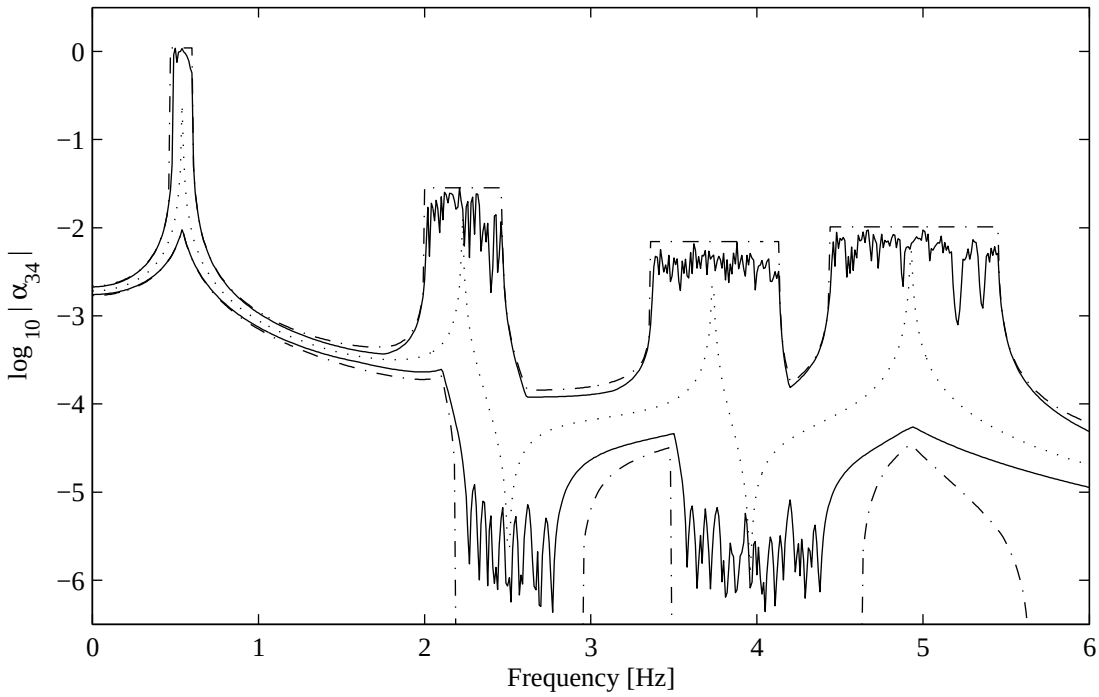

Figure 7.7: *Four-DOF system: baseline FRF (. . . .) and FRF envelopes for* ±10% *uncertainty:* ____ *pseudo-exact FRF envelope;* _ _ _ *approximate FRF envelope by summation of single mode FRF envelopes.*

duced to the total FRF envelope. Damping is only included to bound the upper FRF envelope over each eigenfrequency range, using the model presented earlier. Outside the eigenfrequency range, the effect of the modal damping is negligible in this example and does not affect the outcome of this analysis.

In Figure 7.8, results obtained from the MR and MRE methods in the $\hat{m}$ - $\hat{k}$ space are compared with the FRF envelope obtained by summation of exact single mode FRFs. The MR method is only able to capture the first resonance of the FRF envelope and is far too conservative. The reason is that the bandwidths of the resonance ranges are substantially overpredicted and begin to overlap from a frequency of about 1Hz onwards. If the exact bounds to the eigenvalues are used, the approximation of the FRF envelope clearly improves and compares very well with the reference solution. The upper bound to the magnitude of the FRF envelope over a eigenfrequency range is calculated from the bounds of the specific modal stiffness of the corresponding mode.

Figure 7.9 shows the same results for the case that approximations are made in the A - λ space. The MR method is now capable of capturing the complete FRF reasonably accurately. The resonant regions are predicted exactly, since the eigenvalue is one of the parameters of the modal space. The approximation is more conservative between resonances and for the static solution. The magnitude at

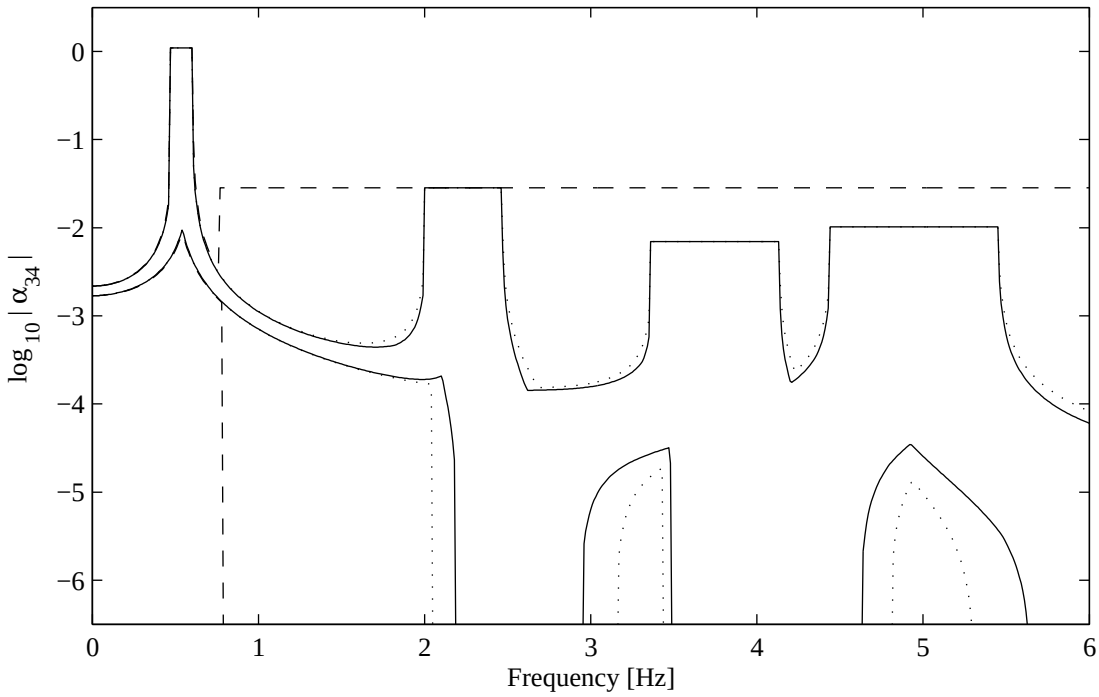

Figure 7.8: *FRF envelopes for* $\pm 10\%$ *uncertainty, different approximations:* ___ *approximate FRF envelope by summation of single mode FRF envelopes;* . . . . *MRE method in* $\hat{m}$ - $\hat{k}$ *space;* _ _ _ *MR method in* $\hat{m}$ - $\hat{k}$ *space.*

resonance is slightly overpredicted, because the interdependency between the modal parameters is neglected. Using the MRS method, the conservatism can be reduced in all frequency regions, except immediately above a resonant frequency. This is in line with the findings in the last section.

Finally, for comparison, the results of both modal space formulations are shown in Figure 7.10. The MRS and MRE methods yield identical results. The MR method applied in the A - λ space clearly provides better results than the MR method applied in the $\hat{m}$ - $\hat{k}$ space.

7.3.3 Perturbation

The application of perturbation methods can reduce the numerical costs drastically, but also introduces inaccuracies. In the context of non-deterministic modal-superposition it can be used to estimate the lower and upper bounds on the modal space parameters by a first order perturbation about the nominal values. Figure 7.11 and Figure 7.12 show the uncertain modal space using exact and approximate bounds in the $\hat{m}$ - $\hat{k}$ and A - λ spaces, respectively. The inaccuracies are relatively small, except for the third mode in both spaces. However, in the A - λ space, the errors can be assessed more easily. The lower and upper bounds of the eigenvalues

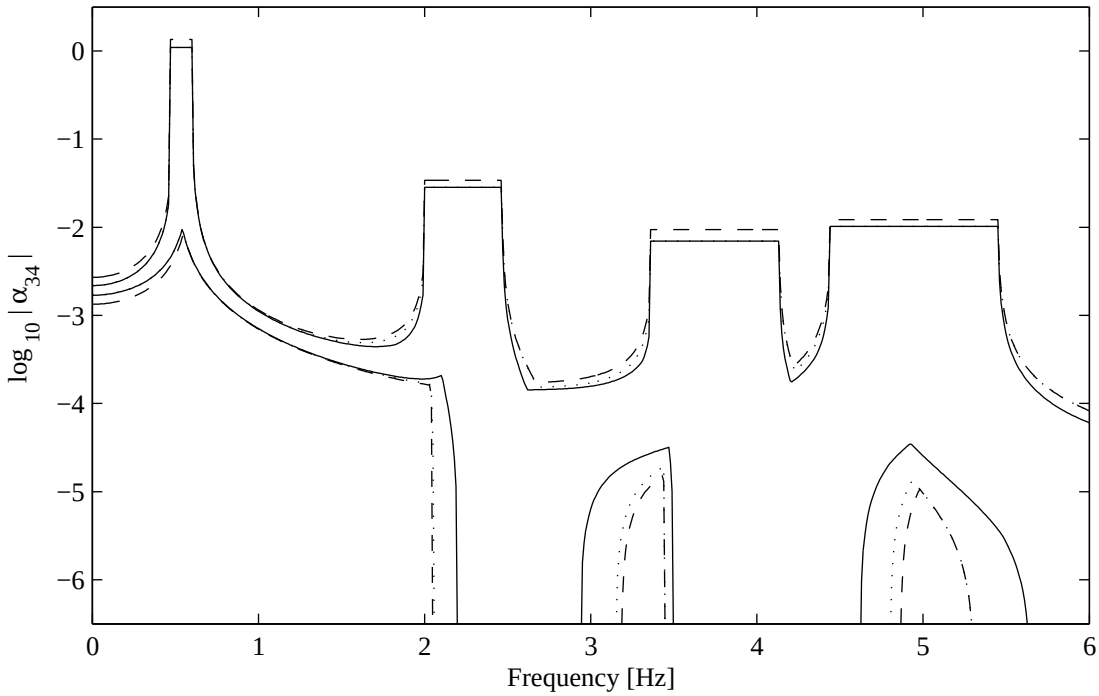

Figure 7.9: *FRF envelopes for* $\pm 10\%$ *uncertainty, different approximations:* ___ *approximate FRF envelope by summation of single mode FRF envelopes;* . . . . *MRS method in* A - λ *space;* _ _ _ *MR method in* A - λ *space.*

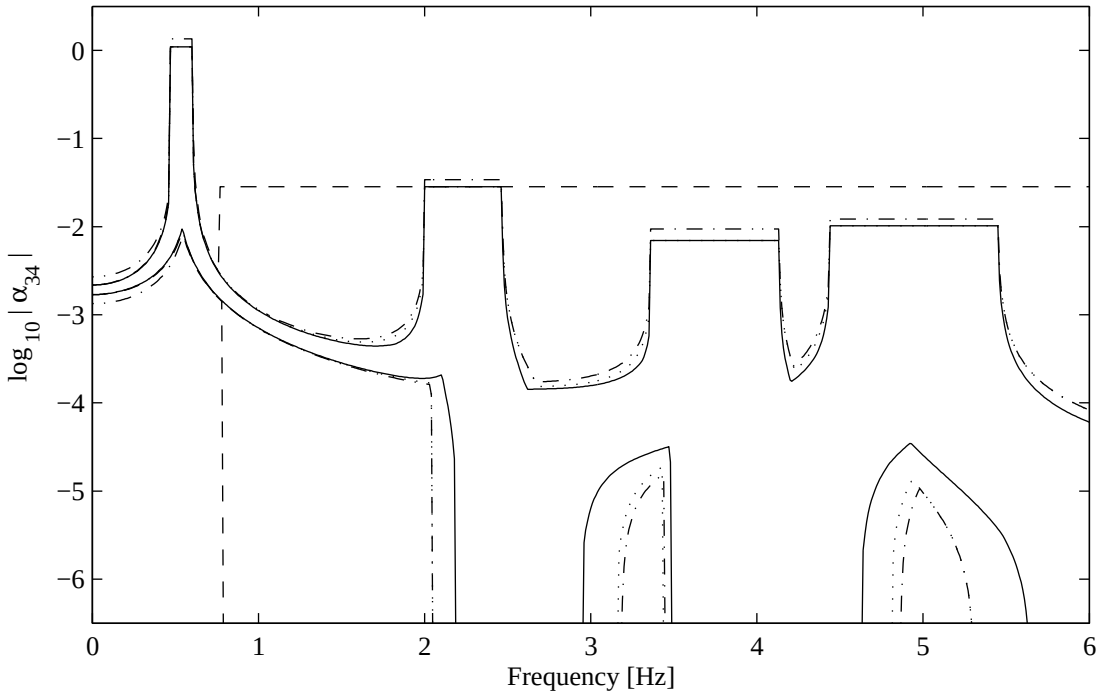

Figure 7.10: *FRF envelopes for* $\pm 10\%$ *uncertainty, comparison of approximations in different modal spaces:* ___ *approximate FRF envelope by summation of single mode FRF envelopes;* . . . . *MRE/MRS methods;* _ _ _ *MR method in* $\hat{m}$ - $\hat{k}$ *space;* _ . _ . *MR method in* A - λ *space.*

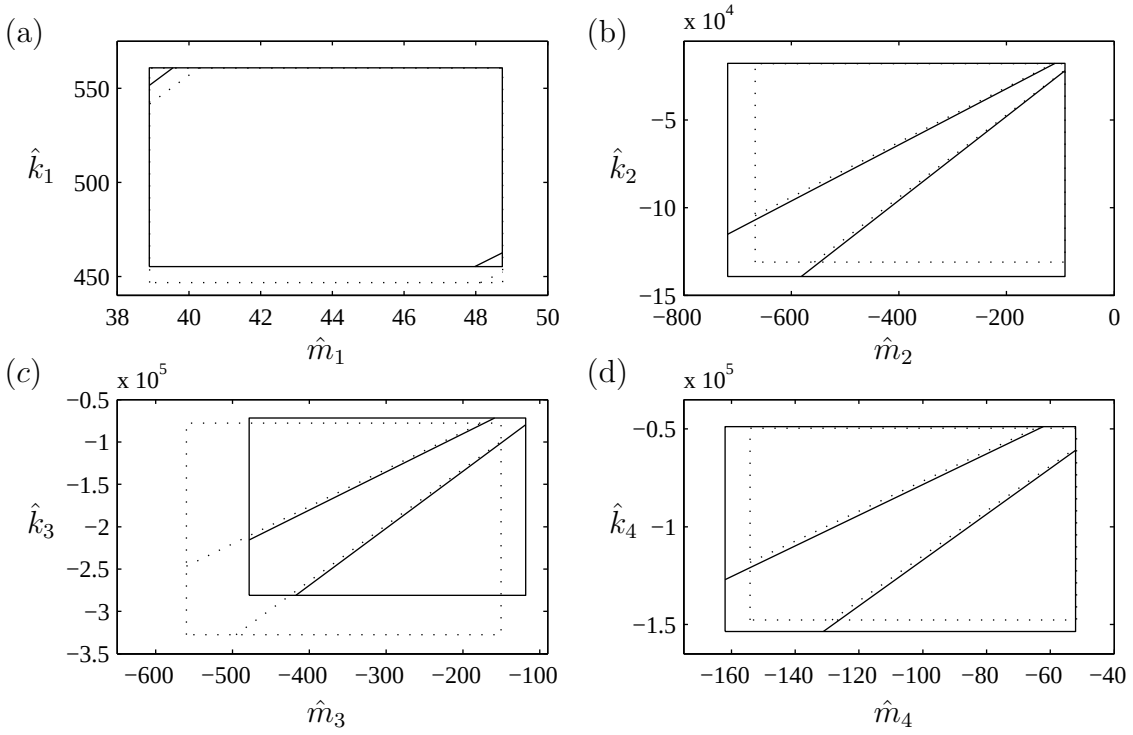

Figure 7.11: *Perturbation of bounds of modal parameters in $\hat{m}$ - $\hat{k}$ space: ____ exact and .... perturbation about nominal values.*

are consistently approximated with smaller values as a effect of the perturbation. There is a larger inaccuracy in the approximation of the modal constant in the third mode. In contrast, in the $\hat{m}$ - $\hat{k}$ space, the errors in the modal constants affect the accuracy of both modal space parameters, which makes the interpretation more difficult.

Finally, the FRF envelopes are calculated using the MR method in the A - λ space. Figure 7.13 compares the results based on exact and approximated bounds on the modal parameters. A shift of the eigenfrequency ranges and a difference in the resonance magnitude of the third mode can be seen.

7.3.4 Discussion

Both the $\hat{m}$ - $\hat{k}$ and A - λ spaces can be used to make safe approximations for the modal parameters and single mode FRFs. However, for some applications the A - λ formulation might be advantageous. In the $\hat{m}$ - $\hat{k}$ space, the MR method alone is highly conservative and the eigenvalue corrections are essential to obtain meaningful results. In the A - λ space, the theory and the numerical example show that the MR method can be sufficient. First of all, the important eigenvalue is one of the parameters and the static correction only improves the approximation for low frequencies. Furthermore, it seems that the region converges to a rectangular shape for higher frequencies, which is also advantageous for the MR method.

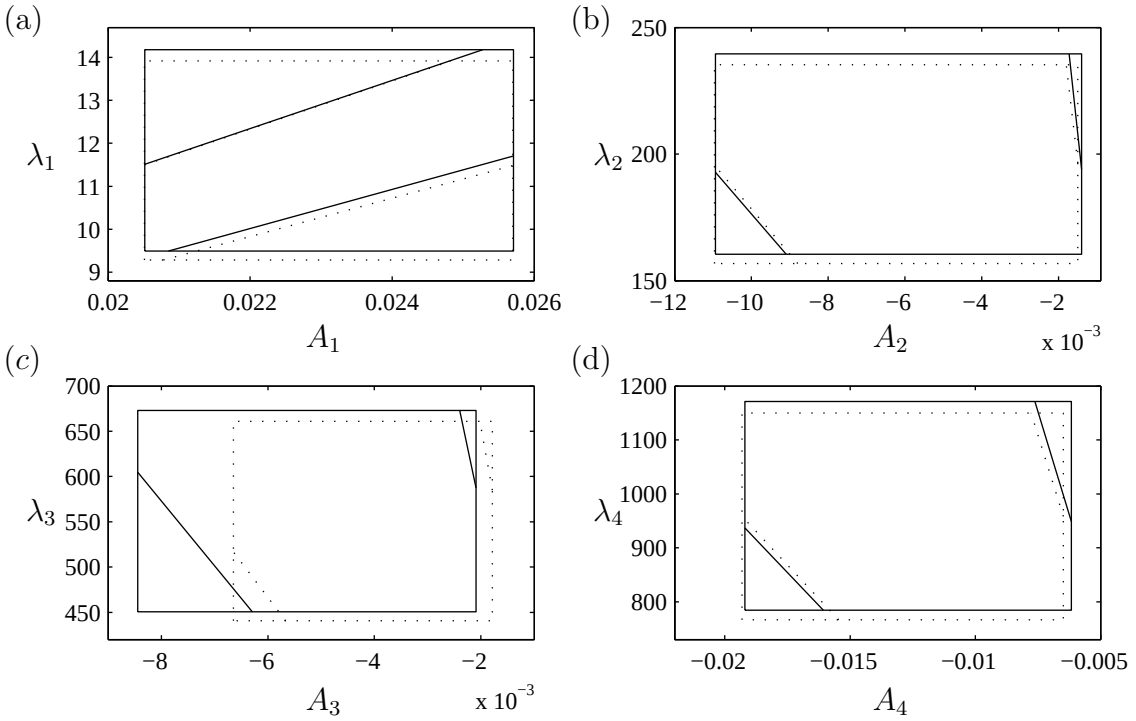

Figure 7.12: *Perturbation of bounds of modal parameters in A - λ space:* ___ *exact and . . . . perturbation about nominal values.*

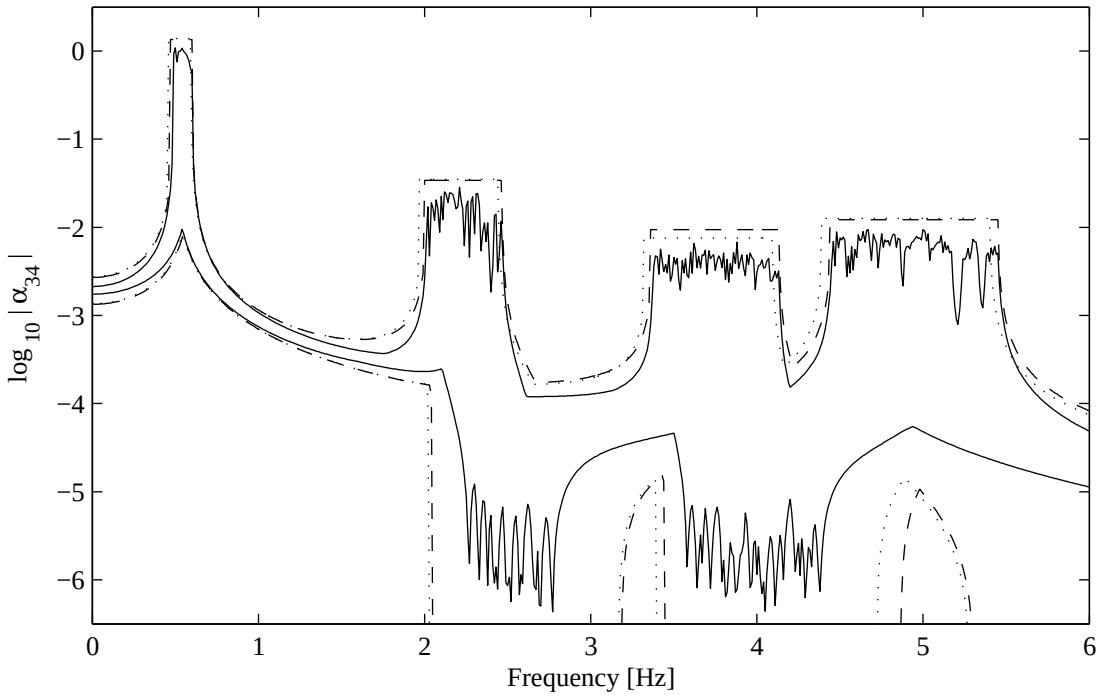

Figure 7.13: *FRF envelopes for ±10% uncertainty; comparison of perturbation and exact methods:* ___ *pseudo-exact FRF envelope;* _ _ _ *MR method in A - λ space; . . . . MR method in A - λ space with perturbation.*

In many implementations, optimisation is used to calculate the bounds on the modal parameters. This requires four optimisations to be carried out for the MR method and two more for the MRE method per mode. Therefore, the use of the MR method in the A - λ space is numerically cheaper and gives adequate results. Additionally, the bounds on the static solution required for the MRS method may be obtained at a lower cost compared to dynamic properties. If different FRFs are of interest, the modal parameters have to be computed several times, except the eigenvalues, which are shared by all FRFs. Therefore, only the modal constant has to be recalculated in the A - λ space. This is a major advantage of the A - λ space. In practice, it is also relatively easy to measure the bounds on resonance frequencies, which could then be used in the numerical model.

Different exact and approximate methods can be used to estimate the bounds of some or all modal parameters. In this context the use of a modal constant and the eigenvalue seems more convenient than using the specific modal mass and stiffness. In the $\hat{m}$ - $\hat{k}$ space, the distribution of the vertex points around the baseline value is non-symmetric for some modes. This is because the inverse is taken of a modal constant that might be close to zero. Therefore, this formulation is more sensitive to approximations. Overall, the eigenvalue and the modal constant show different physical characteristics and it seems sensible to keep them separate.

7.4 Probabilistic approaches

In this section, various aspects of a probabilistic approach to estimate the FRF variation are discussed. The use of modal superposition and the effects of correlations between modal parameters are addressed. Furthermore, approaches based on the variance of random modal parameters are presented, including the application of the Karhunen-Loève (KL) decomposition.

7.4.1 FRF statistics

The goal of the analysis is to obtain statistics of the FRF, such as the 10 and 90 percentiles. A standard approach is to use Monte Carlo sampling to obtain an ensemble of FRFs, from which the statistics can be estimated. The numerical example shown in Figure 7.4 will be used, where the uncertainty in all eight parameters is now modelled by normal distributions with a coefficient of variation of 7.8%. The baseline values are taken as mean values. Figure 7.14 shows the 10 and 90 percentiles of the magnitude, which were calculated from $n = 10^4$ samples. It is a classical approach to evaluate statistics of the FRF magnitude at a given frequency. However,

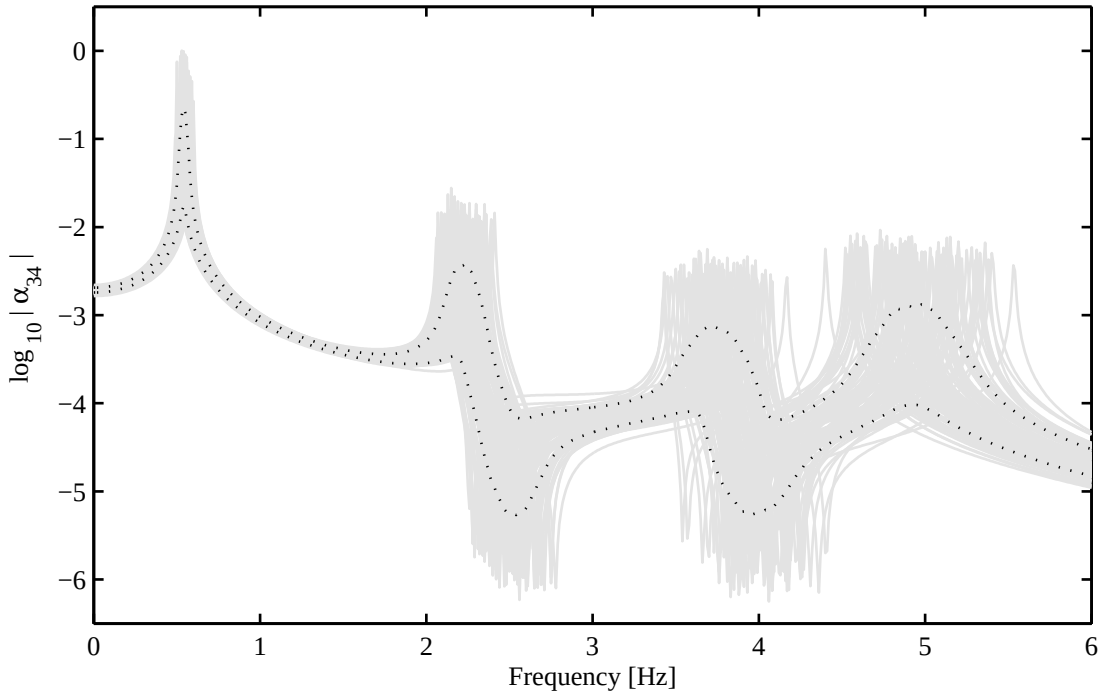

Figure 7.14: *FRF of four-DOF system:* ▬ 100 *realisations and* .... 10/90 *percentiles.*

variation in damping is mainly responsible for a variation in the magnitude around resonance or antiresonance. A change in mass or stiffness properties mainly causes a shift of the FRF along the frequency axis. Therefore, statistics of the FRF along the frequency axis, such as percentiles of natural frequencies, are also important. Information about the FRF magnitude statistics at a specific frequency are useful if a deterministic excitation frequency is considered. In many cases, however, the statistics of the magnitude of a resonance peak, independent of its frequency, can be more useful. In Figure 7.14 it becomes evident that the classical approach does not provide this information, because the 90 percentile of the FRF magnitude is drastically lower than the magnitude of the baseline FRF. In fact, since the damping is considered deterministic, the magnitude at resonance is almost identical for all realisations. Every FRF realisation is resonant and lies above the 90 percentiles at some frequency. Therefore, the percentiles shown in Figure 7.14 are not representative of any realisation.

Another possible approach to quantify the FRF variation would be to evaluate the statistics of the FRF in a direction perpendicular to the locus of the baseline FRF. Alternatively, the FRF magnitude statistics can be calculated using a sliding frequency window, where the maximum and minimum values within this specified frequency window for each realisation are considered. Figure 7.15 shows the 10 and 90 percentiles of both the maximum and minimum FRF magnitudes for two

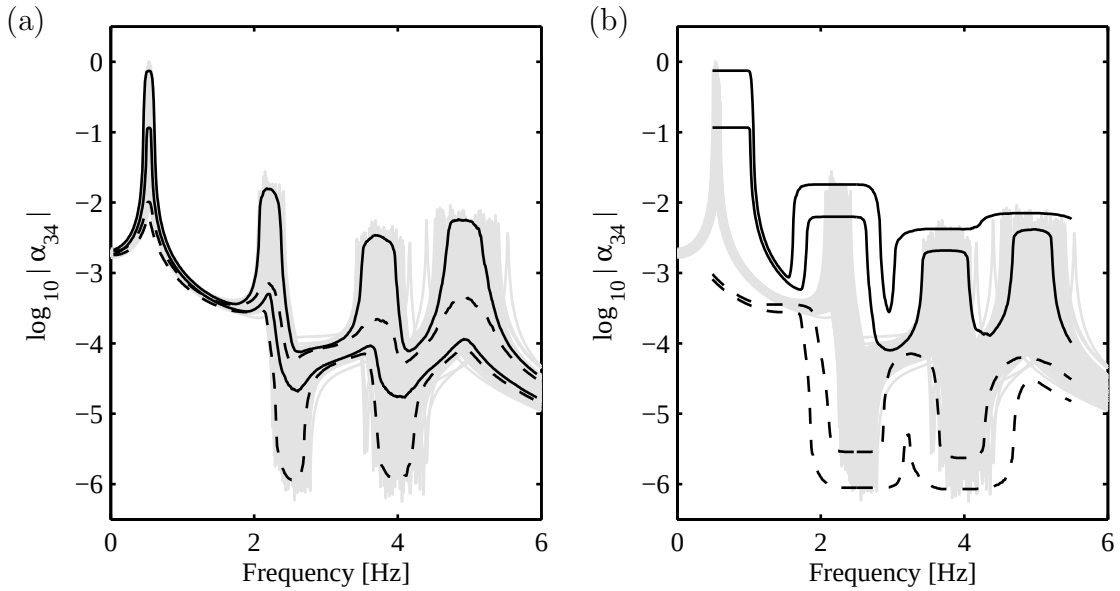

Figure 7.15: *FRF realisations and* 10/90 *percentiles of four DOF-system based on maximum (___) and minimum (_ _ _) values in a sliding frequency window with a width of* $0.1Hz$ *(a) and* $1Hz$ *(b).*

different frequency window widths. For example, the 90 percentile of the maximum FRF magnitude at a specific frequency is the value that will not be exceeded, with a probability of 90%, in a frequency band centered about that frequency, i.e. 90% of the ensemble members do not exceed this value. However, the results depend greatly on the width chosen for the frequency window. This approach is therefore especially useful if the excitation frequency is non-deterministic and can be specified by an interval.

7.4.2 Modal superposition and correlations

In a direct approach, a large number of deterministic solutions must be found for each frequency at which the FRF is evaluated. This might be infeasible due to the large computational cost. In a modal approach, first the non-deterministic eigenvalue problem is solved independent of frequency. Subsequently, Monte Carlo simulation is applied to the numerically cheap modal superposition equation for each selected frequency.

The receptance FRF can be calculated by

$$\alpha(\omega, q_1, q_2) = \sum_{i=1}^{n} \frac{A_i}{\lambda_i - \omega^2 + jd_i} \tag{7.10}$$

where A_i and λ_i are now correlated random variables. In practice, the probability distribution functions of modal constants and eigenvalues may be given, but some

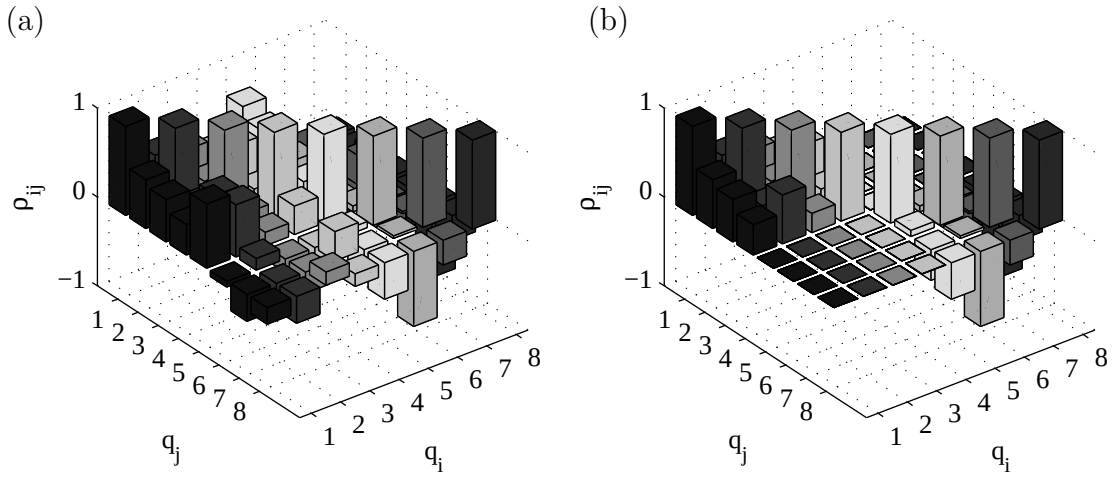

Figure 7.16: *Correlation coefficient matrices: (a) full correlation, (b) A - λ correlation neglected;* $v_i = \lambda_i, \quad v_{4+i} = A_i, \quad i = 1 \ldots 4.$

of the correlations might not be known. In the following, the effects of neglecting various correlations are illustrated. Figure 7.16(a) shows the correlation coefficient matrix $\boldsymbol{\rho}$ for the numerical example, where the eight modal parameters are arranged as

$$v_i = \lambda_i, \quad v_{4+i} = A_i, \quad i = 1 \ldots 4 \tag{7.11}$$

Figure 7.16(b) shows the case where the correlations between eigenvalues and modal constant are neglected. If all correlations are neglected, only the autocorrelations, located on the diagonal of the correlation coefficient matrix, are considered. Figure 7.17 compares the 10 and 90 percentiles for these approximations with the exact solution. The differences are negligible. The correlations between different modes are not influential, because the modal overlap is low. The correlation between the eigenvalue and the modal constant of one mode is small, as shown in Figure 7.16, and the resulting differences in the FRF are not significant.

7.4.3 Variance-based approaches

The results in the previous section were based on the real distribution of the modal parameters. However, in practice, the variation is often only characterised by the variance and the mean value. In that case, the variance can be propagated or a distribution can be assumed to facilitate Monte Carlo simulation. A first order approximation for the variance of the FRF is given by

$$VAR(\alpha(\omega)) = \mathbf{S}(\omega) \quad COV(\mathbf{v}) \quad \mathbf{S}(\omega)^T \tag{7.12}$$

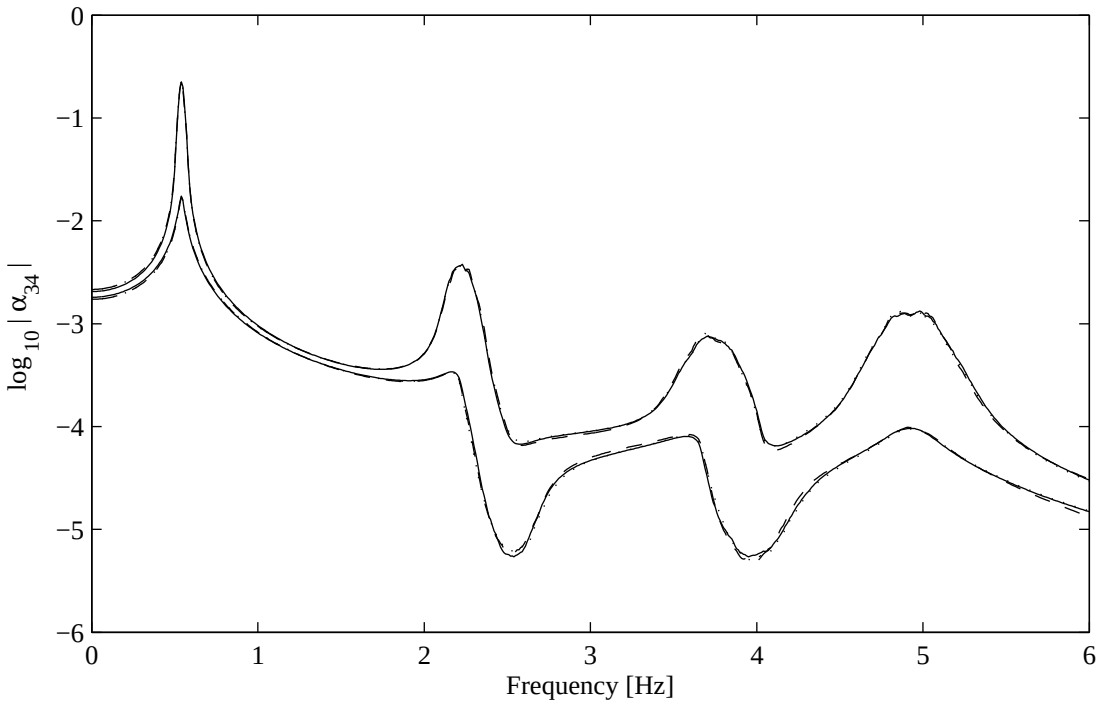

Figure 7.17: *FRF* 10/90 *percentiles of four-DOF system for different correlations:* ____ *all correlations considered;* _ _ _ *correlation between A and* λ *neglected;* . . . . *all correlations neglected.*

where $s_i = \frac{\partial \alpha}{\partial v_i}$ is the derivative of the FRF with respect to the modal parameter v_i and $COV(\mathbf{v})$ is the covariance matrix of modal parameters. Expressions for the FRF sensitivity, a complex function of frequency if damping is considered, can be found by differentiating Equation 7.10 [98]. In general the approximation is reasonably good for frequencies outside the resonance range. There are inaccuracies near resonance, due to the highly non-monotonic behaviour of the FRF. It is possible to extend the first order approximation by using a series expansion based on Equation 7.10.

A Monte Carlo sampling technique in combination with modal superposition seems to be a reasonable approach to estimate statistics of the FRF. It allows all correlations to be considered and is very robust, but requires distribution functions. If these are not known, distribution functions have to be assumed. A normal distribution, for example, which can be quantified by the variance and the mean, is often a good estimate for the eigenvalues. In contrast, the FRF magnitude is known not to be normally distributed, especially near resonance. Figure 7.18 compares the real distribution of the eigenvalue and modal constant for the second mode with a normal distribution with the same mean and variance. For this simple numerical example, the agreement is very good. Therefore, it can be expected that the agreement for the FRF is also very good. Figure 7.19 shows a comparison of FRF percentiles based on the real distribution and a distribution assumed to be normal.

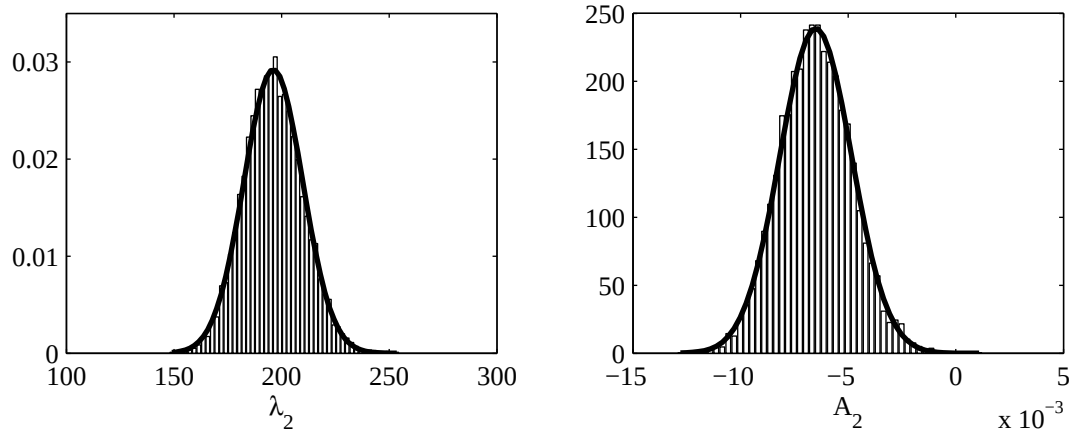

Figure 7.18: *Comparison of histogram for real distribution with normal distribution model for modal parameters.*

The differences are negligible.

7.4.4 Characteristic variation of modal parameters

If the full covariance matrix of the modal parameters is given, the correlations can be considered by using the KL expansion [40]. Assuming a normal distribution, it provides a relation between the correlated random modal properties $\mathbf{v}$ and uncorrelated random variables $\boldsymbol{\zeta}$ in the form

$$\mathbf{v} = \mathbf{v}_0 + \sum_{i=1}^{r \leq n} \boldsymbol{\psi}_i \sqrt{\mu_i} \zeta_i \tag{7.13}$$

where $\boldsymbol{\psi}_j$ and $\sqrt{\mu_j}$ are the eigenvectors and eigenvalues of the covariance matrix $COV(\mathbf{q})$ respectively. Monte Carlo sampling can then be applied in the uncorrelated standard normal random variables. The eigenvectors of the covariance matrix give characteristic variations of the modal space parameters. The corresponding eigenvalue is a measure of their contribution to the expansion. Therefore, it is possible to reduce the number of terms in the summation of Equation 7.13 by considering only the terms associated with largest eigenvalues. However, the modal parameters constitute an inhomogeneous discrete random field problem, because the mean and variance values vary between them. It is therefore appropriate to use the eigenvalues μ_i^* and eigenvectors $\boldsymbol{\psi}_i^*$ that can be obtained from the correlation coefficient matrix $\boldsymbol{\rho}$. In this case the expansion becomes

$$\mathbf{v} = \mathbf{v}_0 + diag(\boldsymbol{\sigma_v}) \sum_{i=1}^{r \leq n} \boldsymbol{\psi}_i^* \sqrt{\mu_i^*} \zeta_i \tag{7.14}$$

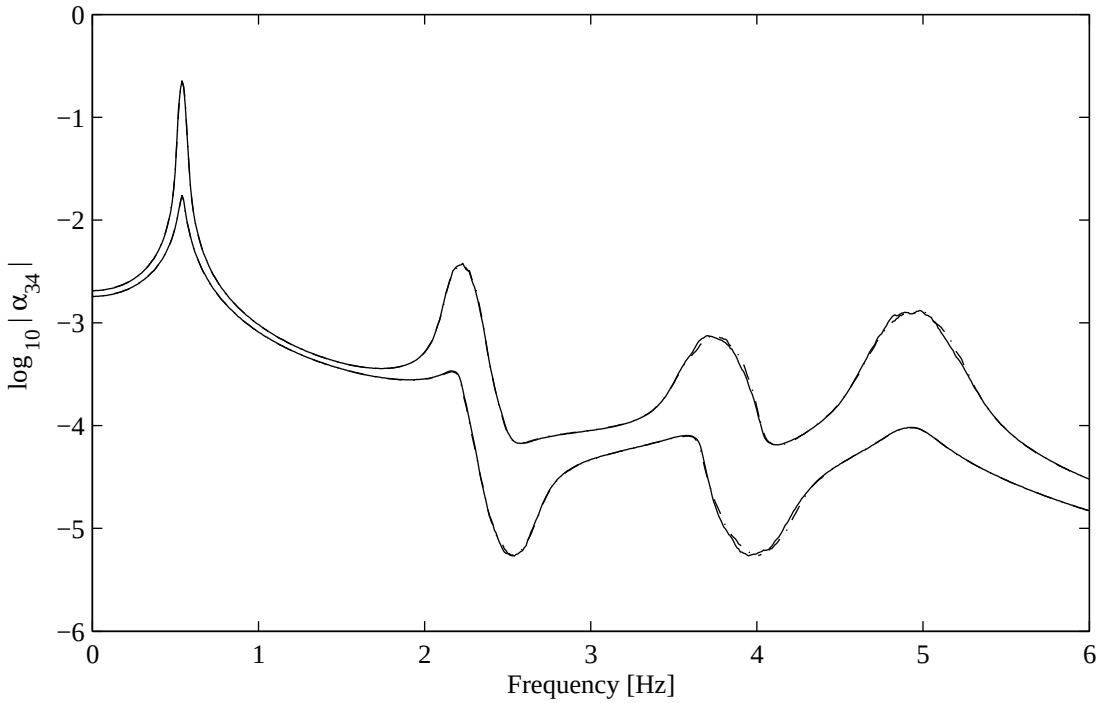

Figure 7.19: *FRF* 10/90 *percentiles of four-DOF system based on real (___) and assumed normal (_ _ _) distributions for the modal parameters.*

Figure 7.20 shows the estimation of the FRF percentiles, where only a few terms of the KL expansion are retained. If the first characteristic variation of modal parameters considered, there are considerable differences, especially around the third mode. However, if the first three terms, out of a total of eight, are taken into account, the agreement is reasonably good. In practice, all contributions can be considered and in this case, both Equation 7.13 and Equation 7.14 yield the exact results.

A second numerical example will be considered to illustrate the physical meaning of characteristic variations of modal space parameters. Figure 7.21 shows a cantilever beam with rectangular cross-section. It is modelled by 10 uniform finite elements using standard Euler-Bernoulli beam theory [9]. The thickness h and Young's modulus E are modelled by random fields with a coefficient of variation of 5% and a correlation length of $0.5m$.

Figure 7.22 shows the 10 and 90 percentiles of the FRF obtained from a Monte Carlo simulation with 10^4 samples. In addition, the approximate percentiles based on retaining only the most important term in the KL expansion, is given. The results agree very well, except for a few frequency regions for the lower FRF percentile and at the antiresonance around 55Hz. The approximate FRF percentiles depend only on one standard normal random parameter, which facilitates the application of various analytical methods. The good agreement is mainly due to the fact that, for

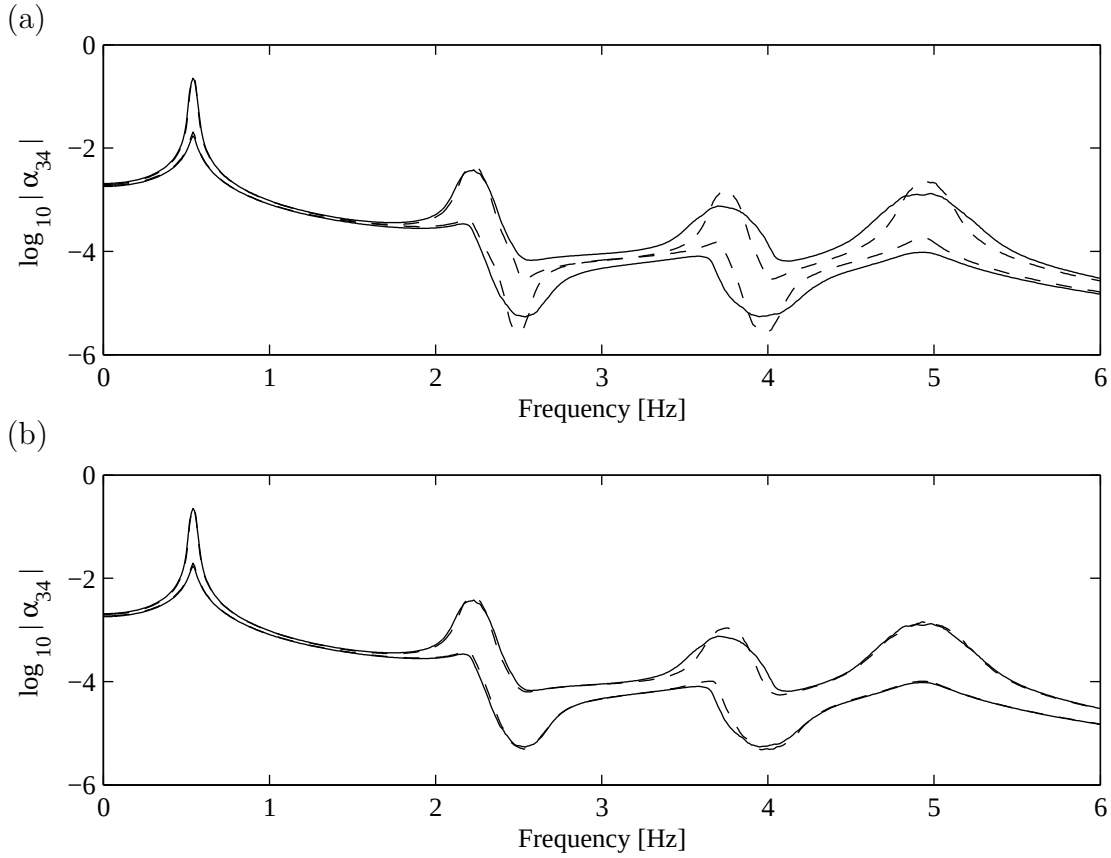

Figure 7.20: *FRF* 10/90 *percentiles of four-DOF system based on characteristic variations of modal parameters: exact results (___), (a) first characteristic vector (- - -); (b) first three characteristic vectors (- - -).*

L $[m]$	h $[m]$	b $[m]$	E $[N/m^2]$	ρ $[kg]$
1	0.02	0.1	1e8	1000

$I = \frac{bh^3}{12}$

$A = bh$

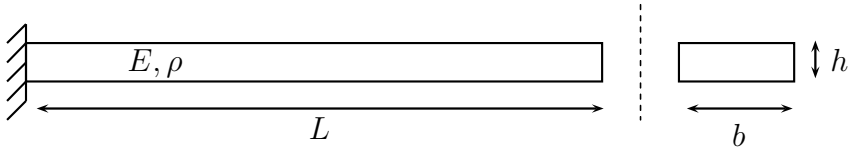

Figure 7.21: *One component beam structure and baseline properties.*

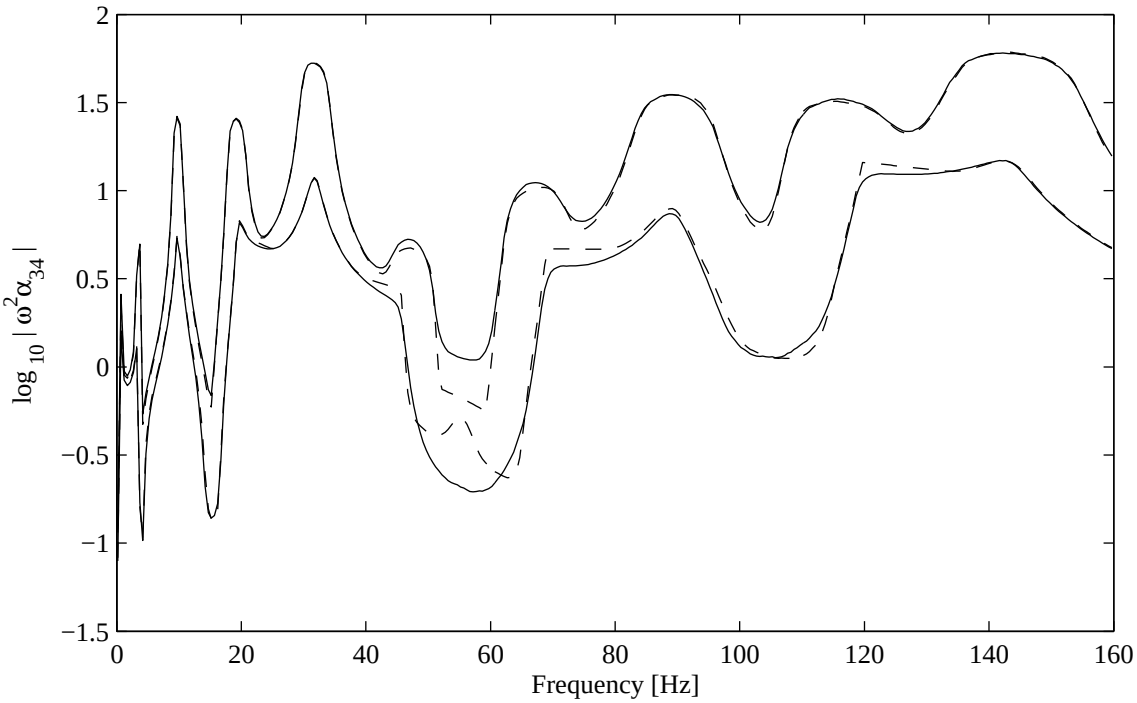

Figure 7.22: *FRF* 10/90 *percentiles for cantilever beam based on the first characteristic variation of modal parameters (_ _ _) and exact results (___).*

this numerical example, the first characteristic variation of the eigenvalues is very dominant. It corresponds to the case of total correlation between the eigenvalues and the KL expansion simplifies to

$$\boldsymbol{\lambda} = \boldsymbol{\lambda}_0 + \boldsymbol{\sigma}_{\boldsymbol{\lambda}} \zeta_1 \tag{7.15}$$

if only this component is retained.

7.5 Hybrid probabilistic/possibilistic approach

In this section, a hybrid approach, which uses the modal space as an intermediate level between the physical parameters and the FRF, is presented. In the first step, the percentiles of modal constants and eigenvalues are evaluated. Subsequently, the distributions are truncated to form possibilistic bounds at a chosen level to calculate a FRF envelope. The evaluation of statistics in the A - λ modal space seems appropriate, because the physical effects are clearly distinguished. The effects of a shift in frequency, due to varying mass and stiffness, is captured predominantly in the variation of the eigenfrequency λ. The effects of uncertain damping in general does not affect the eigenvalues and modal constants significantly. For the numerical example, a Monte Carlo approach with $n = 10^4$ samples is used to estimate the

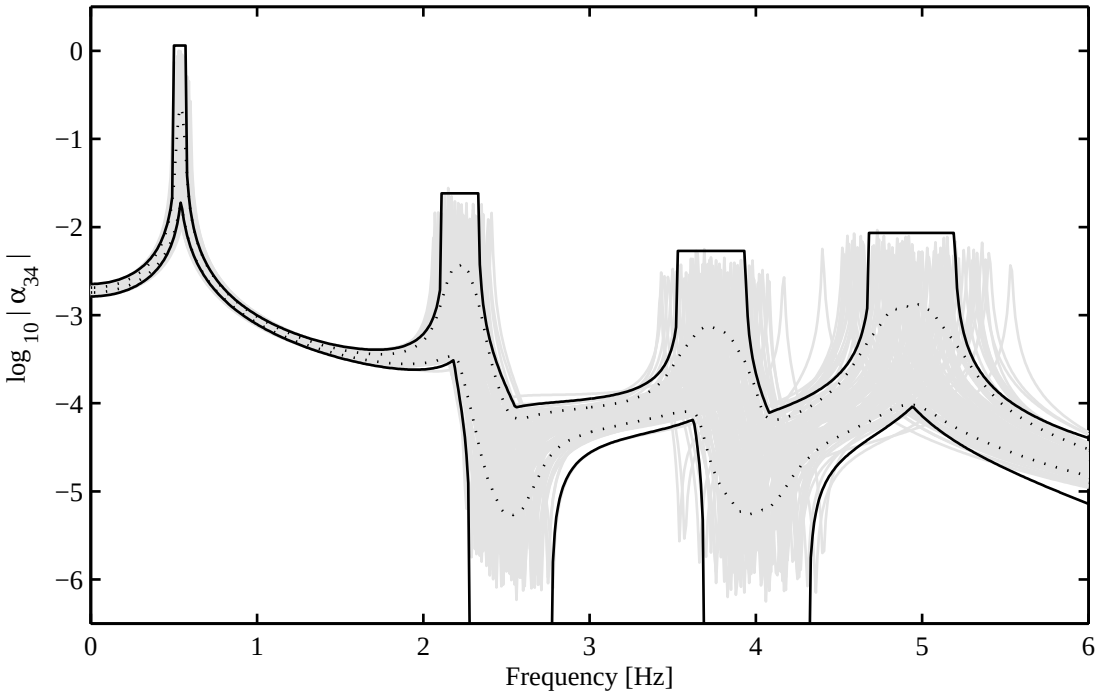

Figure 7.23: *FRF for four-DOF system:* 100 *realisations (* ▬ *),* 10/90 *percentiles (. . . .) and hybrid FRF envelope (*▬*).*

10 and 90 percentiles of the modal space parameters. These are then considered as lower and upper bounds of the modal space parameters and a conservative FRF envelope, using the MR method discussed in Section 7.2, is calculated. The FRF envelope obtained from this hybrid method is shown in Figure 7.23 together with the exact FRF percentiles. Statistics on the width of the resonance range as well as on the magnitude of the resonance peak are included. However, there is some conservatism due to the approximations in the modal space and the superposition of independent single mode FRF envelopes.

Next, the hybrid envelope method will be compared with an approach where the possibilistic bounds are already introduced in the physical parameter space. The 10 and 90 percentiles of the physical parameters are evaluated and the FRF envelope is calculated using the MR method. The results for this direct method are shown in Figure 7.24. The direct envelope, which is based on statistics in the physical parameter space, is clearly broader then the hybrid FRF envelope, as expected. The difference is due to the conservatism introduced by the possibilistic propagation from the physical to the modal space.

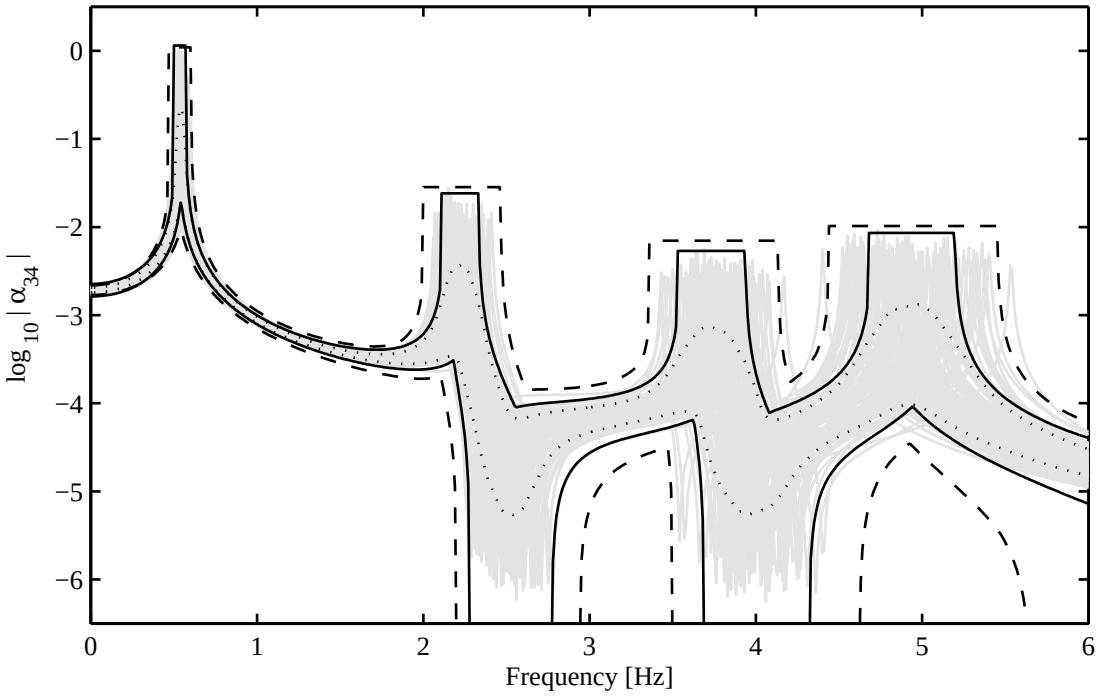

Figure 7.24: *FRF for four-DOF system:* 100 *realisations (* ▬ *),* 10/90 *percentiles (. . . .), hybrid (*▬▬*) and direct (- - -) FRF envelopes.*

7.6 Conclusions

Different approaches to estimate response variations using non-deterministic modal superposition have been discussed. A possibilistic approach was considered and the effects of the choice of modal space parameters were investigated. It was shown that, for some applications, a formulation using a modal constant and the eigenvalue has advantages compared to the often-used definition of a specific modal mass and stiffness. Monte Carlo simulation is the most appropriate approach in a probabilistic analysis. The errors introduced by neglecting correlations or assuming a normal distribution for the modal parameters are often reasonably small compared to the required accuracy of the results. A general advantage of modal superposition methods is that the system response is decomposed into modal contributions, which introduces an intermediate step in the propagation of uncertainties. First, the numerically expensive non-deterministic eigenvalue problem is solved and subsequently the FRF variation as a function of frequency is calculated based on an algebraic relation. A two-step approach can be used to apply a hybrid technique, where a probabilistic method is used to estimate the variation in modal properties and a possibilistic method is used to propagate it to the physical FRF. This approach offers a qualitatively different way to quantify response variations compared to traditional concepts.

Chapter 8

Application of Line-Sampling to structural dynamics

8.1 Introduction

In a probabilistic approach [39, 40], Monte Carlo (MC) simulation [99] can be applied to estimate the statistics of response properties. In the standard MC simulation method, parameter values are randomly drawn from their distributions and a number of deterministic problems are solved. The method is very robust and converges to the exact solution if the sample size tends to infinity. However, in practice a large sample size can often not be realised, due to time and computing restrictions. Therefore, advanced MC simulation methods, that can achieve the same accuracy with a lower number of deterministic solutions, have been developed.

There are advanced MC methods to estimate the mean and variance of a distribution using a low number of samples, such as Latin Hypercube sampling [58]. It is a version of stratified sampling, where it is ensured that the samples are taken more evenly from the input parameter distribution. A different class of advanced MC methods concerns the efficient estimation of low probability events [53, 100], which is addressed in Section 8.1.1. In this context, Line-Sampling (LS) has been developed, amongst others, to calculate a small probability of failure in high-dimensional systems.

This chapter concerns the application of the LS simulation method to the dynamic analysis of structures with non-deterministic properties. In particular, LS is applied to efficiently estimate the distribution functions of natural frequencies and frequency response functions (FRFs) of a system. In the following section, the theory of LS is reviewed. Subsequently, the application of the LS method to estimate distribution functions is presented. In Section 8.4, various numerical examples are

given based on a structural dynamic model. Finally, the application of LS to random field models is investigated. The efficiency of the LS approach is compared with the standard MC simulation method.

8.1.1 Low probability events

The probability of occurrence of an event E can be expressed as

$$p_E = \int 1_E(\boldsymbol{\theta}) h(\boldsymbol{\theta}) d\boldsymbol{\theta} \tag{8.1}$$

where $1_E(\boldsymbol{\theta})$ is the indicator function of the event, $\boldsymbol{\theta}$ is the vector of random parameters and $h(\boldsymbol{\theta})$ is the joint probability density function (pdf). A performance function $g(\boldsymbol{\theta})$ can be defined such that $g(\boldsymbol{\theta}) < g_0$ describes the event domain E where $1_E(\boldsymbol{\theta}) = 1$, $g(\boldsymbol{\theta}) > g_0$ is associated with $1_E(\boldsymbol{\theta}) = 0$ and $g(\boldsymbol{\theta}) = g_0$ is the limit state function. The often high dimensionality of $\boldsymbol{\theta}$ makes analytical integration infeasible. Furthermore, the indicator function is in general not known in closed form, because it is often connected with the response of the system. Therefore, the response of the structure is typically calculated repeatedly for different values of $\boldsymbol{\theta}$, according to their distributions, to obtain information about the response. The number of calculations required to achieve a certain accuracy is the criterion for the efficiency of the solution method.

Standard MC simulation uses an estimator for Equation 8.1 in the form

$$\hat{p}_E = \frac{1}{N} \sum_{i=1}^{N} 1_E(\boldsymbol{\theta^{(i)}}) = \frac{N_E}{N} \tag{8.2}$$

where N is the total number of samples, N_E is the number of samples associated with event E. The realisations of parameters $\boldsymbol{\theta^{(i)}}$ are independent and identically distributed (i.i.d.) with respect to $h(\boldsymbol{\theta})$. The variance of the estimator $\hat{p}_E$ is a measure of the accuracy of this approach and the coefficient of variation (CV) is given as [53]

$$CV_{MC} = \frac{\sqrt{Var[\hat{p}_E]}}{p_E} = \sqrt{\frac{1 - \hat{p}_E}{N_E}} \tag{8.3}$$

The disadvantage of this approach is that for small probabilities $p_E << 1$ a very large number of samples is required in order to obtain a reasonable number N_E of hits in the event domain. The required sample size is typically inversely proportional to the target probability.

Several methods have been developed to reduce the variance of the estimator and to achieve the same accuracy with a lower number of samples. These include

Importance Sampling [54], Directional Sampling [55], Subset Simulation [56] and Line Sampling [53, 57, 101]. In this chapter the LS technique and its application in structural dynamic analyses with non-deterministic properties will be considered. After a review of the theoretical background, the application of the method to estimate statistics and distribution functions of response parameters of structural dynamics systems will be discussed. Finally, the combination of LS with other non-deterministic modelling approaches is considered.

8.2 Theory of Line-Sampling

LS [53, 57, 101] has been developed for problems in high dimension and where small failure event probabilities are of interest. It involves sampling along a line in an important direction in the parameter space towards the event domain. If the formulation is made in the standard normal space, the random parameters $\boldsymbol{\theta}^{(i)}$ are independent and Gaussian distributed with zero mean and unit variance. In this case the joint probability density function can be written as

$$h(\boldsymbol{\theta}) = \prod_{i=1}^{d} \phi(\theta_i) \tag{8.4}$$

where d is the number of random parameters and $\phi(\theta_i) = (1/\sqrt{2\pi})e^{-(\theta_i^2/2)}$. Equation 8.1 can now be written in the form

$$p_E = \int_d 1_E(\boldsymbol{\theta}) \prod_{i=1}^{d} \phi(\theta_i) d\boldsymbol{\theta} \tag{8.5}$$

The event domain E can be alternatively expressed as

$$E := \{\theta_1 \in E_1(\boldsymbol{\theta}_{-1})\} \tag{8.6}$$

which defines occurrence of the event for the case that the parameter θ_1 lies in a subset event domain E_1 of dimension $d-1$ and where $\boldsymbol{\theta}_{-1}$ denotes all parameters except θ_1. The indicator function is then written as $1_{E_1}(\boldsymbol{\theta}_{-1})$ and Equation 8.5

becomes

$$p_E = \int_d 1_{E_1}(\boldsymbol{\theta}_{-1}) \prod_{i=1}^{d} \phi(\theta_i) d\boldsymbol{\theta} \tag{8.7}$$

$$p_E = \int_{d-1} \left(\int 1_{E_1}(\boldsymbol{\theta}_{-1}) \phi(\theta_1) d\theta_1 \right) \prod_{i=2}^{d} \phi(\theta_i) d\boldsymbol{\theta}_{-1} \tag{8.8}$$

$$p_E = \int_{d-1} \quad \Phi(E_1(\boldsymbol{\theta}_{-1})) \quad h(\boldsymbol{\theta}_{-1}) d\boldsymbol{\theta}_{-1} \tag{8.9}$$

where

$$\Phi(E_1(\boldsymbol{\theta}_{-1})) = \int 1_{E_1}(\boldsymbol{\theta}_{-1}) \phi(\theta_1) d\theta_1 = p_{E_1}(\boldsymbol{\theta}_{-1}) \tag{8.10}$$

is the probability of event E for a given set of parameters $\boldsymbol{\theta}_{-1}$. The LS estimator for the probability of event E is

$$\overline{p}_E = \frac{1}{N} \sum_{i=1}^{N} \Phi(E_1(\boldsymbol{\theta}_{-1}^{(i)})) = \frac{1}{N} \sum_{i=1}^{N} p_{E_1}(\boldsymbol{\theta}_{-1}^{(i)}) \tag{8.11}$$

where $\boldsymbol{\theta}_{-1}^{(i)}$ are independent and identically distributed with respect to $h(\boldsymbol{\theta}_{-1})$. For each sample of the parameters $\boldsymbol{\theta}_{-1}^{(i)}$ the probability of the event $p_{E_1}(\boldsymbol{\theta}_{-1}^{(i)})$ is calculated as a one-dimensional problem in terms of parameter θ_1. The variance of this estimator is

$$Var[\overline{p}_E] = \frac{1}{N(N-1)} \sum_{i=1}^{N} (p_{E_1}^{(i)} - \overline{p}_E)^2 \tag{8.12}$$

and the CV for LS is

$$CV_{LS} = \frac{\sqrt{Var[p_{E_1}^{(i)}]}}{\sqrt{N}\overline{p}_E} \tag{8.13}$$

In Equation 8.1, the probability p_E is expressed as the expectation of the indicator function $1_E(\boldsymbol{\theta})$, but in Equation 8.9 it is expressed as the expectation of the random variable $\Phi(E_1(\boldsymbol{\theta}_{-1})) = p_{E_1}(\boldsymbol{\theta}_{-1})$. It has been shown that [57]

$$Var[\Phi(E_1(\boldsymbol{\theta}_{-1}))] \leq Var[1_E(\boldsymbol{\theta})] \tag{8.14}$$

and therefore the variance of the LS estimator is always less than, or equal to, the variance of the standard MC estimator. In fact, the variance of the standard MC estimator depends on the value of the event probability, whereas the variance of the LS estimator depends only on the variability of the event probabilities $p_{E_1}(\boldsymbol{\theta}_{-1}^{(i)})$. Therefore the accuracy of the LS estimator is better, the more dominant the influence of the direction given by parameter θ_1 and the less important the influence of all other

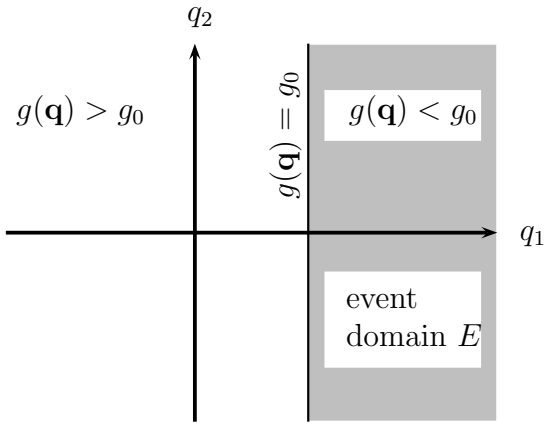

Figure 8.1: *Example of a two-dimensional parameter space with event domain.*

directions $\boldsymbol{\theta}_{-1}$ are on the performance function. Similarly, gains in computational cost using LS depend on whether or not a parameter θ_1 can be identified for which the integral in Equation 8.10 can be evaluated efficiently, i.e. if the response is relatively insensitive to the remaining parameters $\boldsymbol{\theta}_{-1}$. The variation between realisations of $\Phi(E_1(\boldsymbol{\theta}_{-1}^{(i)}))$ is an indication of this. The next paragraph concerns a simple example.

Consider the two-dimensional space in Figure 8.1 with parameters q_1, q_2 and failure domain F. If the LS direction is perpendicular to the failure domain, $\theta_1 = q_1$, then $Var[\Phi(F_1(\theta_2))]$ is zero and the CV of the probability estimator is zero. In contrast, if the sampling direction is parallel to the failure domain, $\theta_1 = q_2$, then $Var[\Phi(F_1(\theta_2)) = Var[1_F(\boldsymbol{\theta})]$ and the CV for LS is the same as for the standard MC estimator.

The implementation of LS is illustrated in Figure 8.2, considering a d-dimensional space with parameters $\mathbf{q}$ ($d = k+m$). If an important direction α, given by the unit vector e_α, is known, a new set of coordinates $\boldsymbol{\theta}$ can be introduced, where θ_1 points in the direction of α and $\boldsymbol{\theta}_{-1}$ denotes the $d-1$ dimensional space perpendicular to α. A sample $\boldsymbol{\theta}_{-1}^{(i)}$ describes a point on the $\boldsymbol{\theta}_{-1}$ axis and the one dimensional probability problem of parameter θ_1 in direction α has to be solved. In the most simple case, as shown in Figure 8.2a, the limit state function $g(\mathbf{q}) = g_0$ is intersected only once and the probability of an event E is given by $p_{E_1}^{(i)} = \Phi(\beta^{(i)})$, where Φ is the cumulative density function and $\beta^{(i)}$ is the shortest distance in the standard normal space between the point $\boldsymbol{\theta}_{-1}^{(i)}$ and the limit state function $g(\mathbf{q}) = g_0$. Figure 8.2b illustrates an approach to approximate the distance $\beta^{(i)}$. The performance function $g(\mathbf{q})$ is evaluated at predefined values β_j and the distance $\beta^{(i)}$ for $g(\mathbf{q}) = g_0$ is found by linear interpolation. Therefore, for n_i samples and n_j predefined values β_j, the performance function has to be evaluated at $n_i \times n_j$ points to describe $g_j^{(i)}$. The

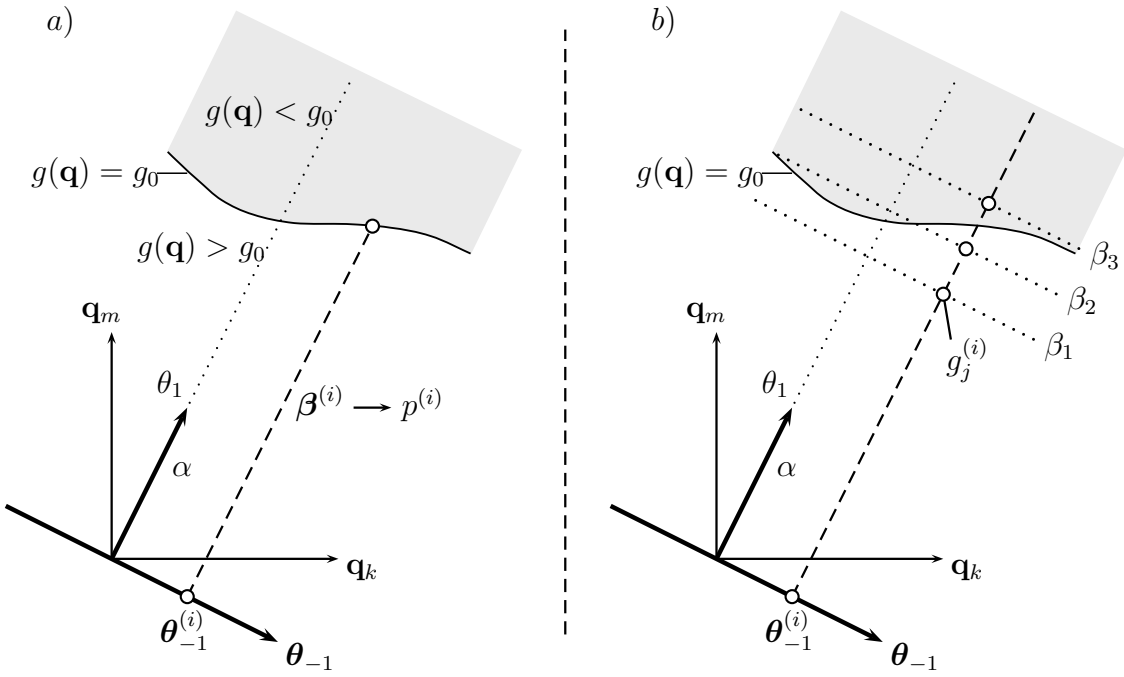

Figure 8.2: *Implementation of Line-Sampling.*

sampling vector in terms of coordinates $\mathbf{q}$ is defined as

$$\mathbf{q}_S^{(i)}(j) = \beta_j \mathbf{e}_\alpha + (\mathbf{q}^{(i)} - < \mathbf{e}_\alpha, \mathbf{q}^{(i)} > \mathbf{e}_\alpha) \tag{8.15}$$

where $(\mathbf{q}^{(i)} - < \mathbf{e}_\alpha, \mathbf{q}^{(i)} > \mathbf{e}_\alpha) = \boldsymbol{\theta}_{-1}^{(i)}$ is the projection on the $d-1$ dimensional plane perpendicular to α and $<,>$ denotes the scalar product.

LS is a robust method and especially suited for high dimensional problems. It can deal with irregular limit state functions and several event domains. However, it is most advantageous if an important sampling direction can be identified and if the limit state function is simple. Compared to other sampling methods it is not affected by low event probabilities or a large number of random parameters. A common choice for the important direction is the gradient at a point in the parameter space, for example at the baseline solution. However, the gradient should be weighted by the variances of the random variables. In general, gradient estimation requires some additional calculation and can be numerically expensive, but efficient methods for high dimensions exist [102].

8.3 Application of the LS method to the estimation of response parameter statistics and distribution functions

In this section, the application of the LS simulation method to estimate distribution functions and other statistics is examined. First, a simple analytical example is used to illustrate the concept. Subsequently, LS is applied to a structural dynamic model to estimate the distribution functions of natural frequencies and FRF magnitudes. The numerical efficiency of the LS approach is compared with the standard MC simulation method.

8.3.1 Analytical example

Considering the function

$$g = 5q_1 + q_2 \tag{8.16}$$

where q_1 and q_2 are normally distributed independent random variables with a mean value of 10 and variance 1. The function g is then normally distributed as well, with a mean value of 60 and variance 26. This analytical problem can be used to illustrate the application of LS to estimate the distribution of g. A standard MC approach and the proposed LS approach with $n = 10$ samples each are compared. The important direction is defined by parameter q_1, such that $\theta_1 = q_1$ and $\theta_2 = q_2$. Therefore, the parameter q_1 is varied corresponding to the distance β and samples are taken for parameter q_2. In Figure 8.3a, the values $g_j^{(i)}$ are plotted for $n_i = 5$ samples and values $\beta_j = [-5, 5]$. For each sample, the data points are connected by a straight line. In this simple example, the linear interpolation is exact for all levels of β. For a given value g_0, $n_i = 5$ corresponding values of β_0 are found. Using the standard normal space, the associated probabilities $p_0^{(i)}$ can be calculated. Finally, the mean probability $\overline{p_0}$ for the given value g_0 is calculated and can be plotted in the normal probability plot in Figure 8.3b. If this is done systematically for a number of values g_0 covering the whole range of g, then the complete distribution can be estimated. Alternatively, a given probability p_0 could be used to estimate a corresponding mean value $\overline{g_0}$. In Figure 8.3b, the results of the LS approach show a very good estimation of the exact distribution, especially at the tails, which is a straight line. The number of deterministic solutions required for the LS approach is given by the number of evaluations $g_j^{(i)}$, which is the number of samples ($n_i = 5$) multiplied by the number of levels β_j ($n_j = 2$). The number of data points used to describe the distribution function is independent of the total sample size and

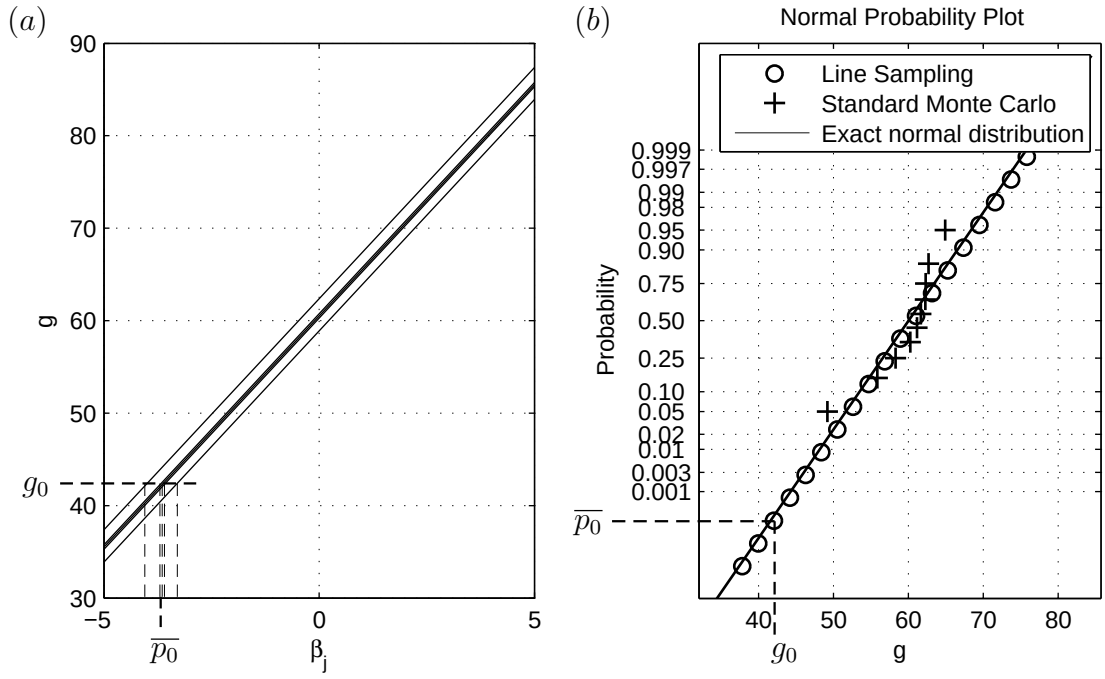

Figure 8.3: *(a) Evaluation of function $g_j^{(i)}$ at levels β_j along the important direction for $n_i = 5$ samples; (b) estimation of the normal distribution by the LS approach ($n = 10$) and the MC method ($n = 10$).*

can be increased with little numerical cost. The accuracy of the LS approach is also independent of the probability and only depends on the discretisation of the performance function $g(\beta)$ and the sample size. In Figure 8.3b, the results of a MC simulation with $n = 10$ samples are also shown. The data points are spread around the mean value and no estimate is given for the tails of the distribution. Both approaches estimate the mean value of g reasonably well. However, a sample size of $n = 10$ is not enough to estimate the variance of g accurately using the standard sampling approach. A sampling approach with 1000 samples was used to estimate the variance of the variance estimator for both approaches. Based on a probability of 90%, the standard MC method predicts an interval for the variance of $[10 : 51]$ whereas the LS approach predicts an interval of $[23 : 30]$, the exact value being 26. In this simple example of a normal distribution it is sufficient to approximate the function $g(\beta)$ for two values β_j. In general, the number of levels β_j required and the numerical cost depend on the characteristics of the function $g(\beta)$. However, if the shape of the output distribution is known, then the number of LS solutions required is equal to the number of independent parameters in that distribution.

Other statistics, such as the mean, variance and percentiles, can be deduced from the distribution function. For the estimation of percentiles, values of the distribu-

tion function only have to be calculated in the corresponding probability region. However, an iterative process has to be followed to calculate a given percentile with the required accuracy. A qualitatively different approach is to calculate a percentile directly, which will be referred to as the LSp approach later. For a given value of probability p corresponding values of g can be found. However, the mean value of them in general does not correspond to the correct result for the percentile. In the special case of a linear performance function, as given by Equation 8.16, the result is exact. For non-linear functions g, the result is not exact, but it can be useful in the case monotonic functions. This will be investigated further using the numerical example in the next section.

8.4 Structural dynamics example

k_1	k_2	m_1	m_1
16	12	3.5	2.5

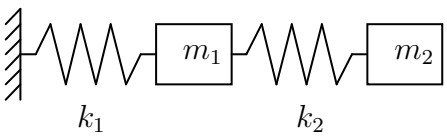

Case	Vector in $k_1 - k_2$ space	Important direction
A	$(0, 1)$	k_2, one parameter
B	$(1, 1)$	k_1, k_2, diagonal
C	$(1, 0)$	k_2, one parameter
D	$(1, 0.45)$	gradient of λ_1

Figure 8.4: *Spring-mass system; baseline parameter values; definition of important directions for LS.*

The numerical example considered is a spring-mass system as shown in Figure 1. Both stiffnesses are treated as random variables and modelled by a normal distribution with a coefficient of variation of 10%. Damping is included by a modal loss factor of 0.1.

8.4.1 Eigenvalue distribution

The LS approach is used to estimate the distribution function of the first eigenvalue of the system. As a reference, a standard MC approach with a sample size of $n = 10^6$ is used. The random parameter space is two-dimensional, given by the parameters k_1 and k_2. Four different cases are defined for the selection of the important direction as listed in Figure 8.4. In Figure 8.5 the evaluations of the performance function $\lambda_j^{(i)}$ are shown for $n_i = 5$ samples and n_j=5 values β_j. According to the direction of

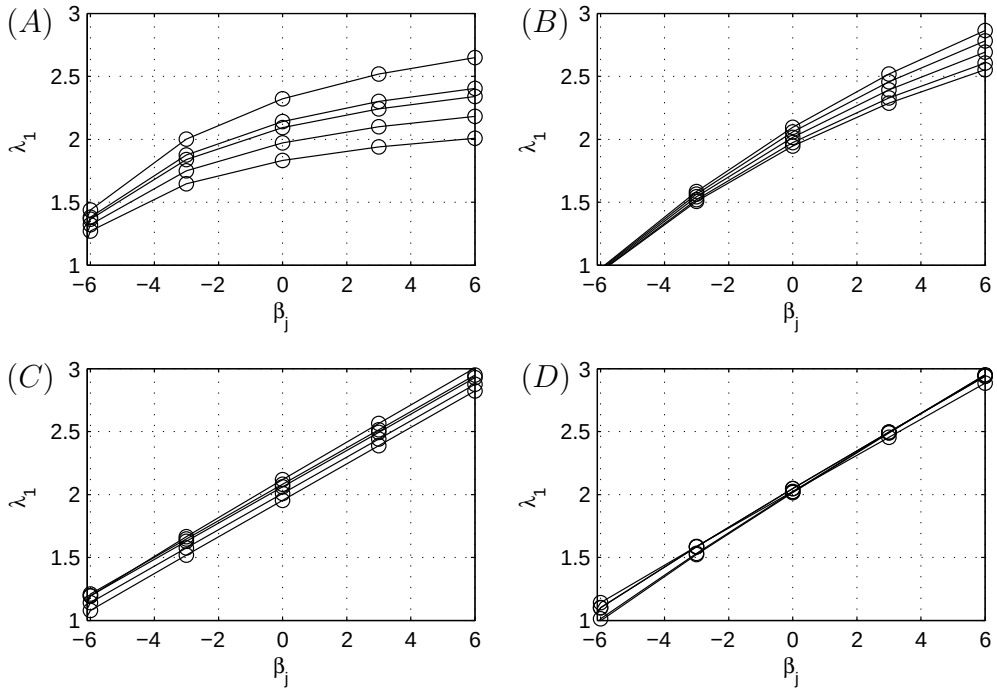

Figure 8.5: *Evaluation of the performance function λ_1 at given values β_j along four different important directions (A,B,C,D) using the same sample of size $n_i = 5$ at all points (LSa).*

LS (cases A,B,C,D), the paths of the curves and the variation between them varies. The best result for the LS approach can be achieved using direction D (gradient), because the variation between the samples is small and the graph is almost linear. The sample size of $n_i = 5$ and the discretisation at $n_j = 5$ points are sufficient, and only $n = 25$ deterministic solutions of the eigenvalue problem are required. For the results shown in Figure 8.5, the same sample has been used for the evaluation of the performance function at different values β_j, which will be denoted as the LSa approach. However, a different sample can also be used at each step (LSb), which is illustrated by the performance functions shown in Figure 8.6, where the lines cross at various points. The numerical cost is the same, but the approach is based on more independent samples, which can increase the robustness. A further approach (LSc) is to order the independent samples such that the lines do not cross, as shown in Figure 8.7. However, it has to be noted that these approaches (LSb,LSc) are not theoretically rigorous. The influence of these different implementations will be investigated.

In Figure 8.8, the estimates of the cumulative density function (cdf) of the first eigenvalue λ_1 for the MC method and the LS approach ($n = 25$ each) are compared with the reference distribution function. The data is shown using a normal proba-

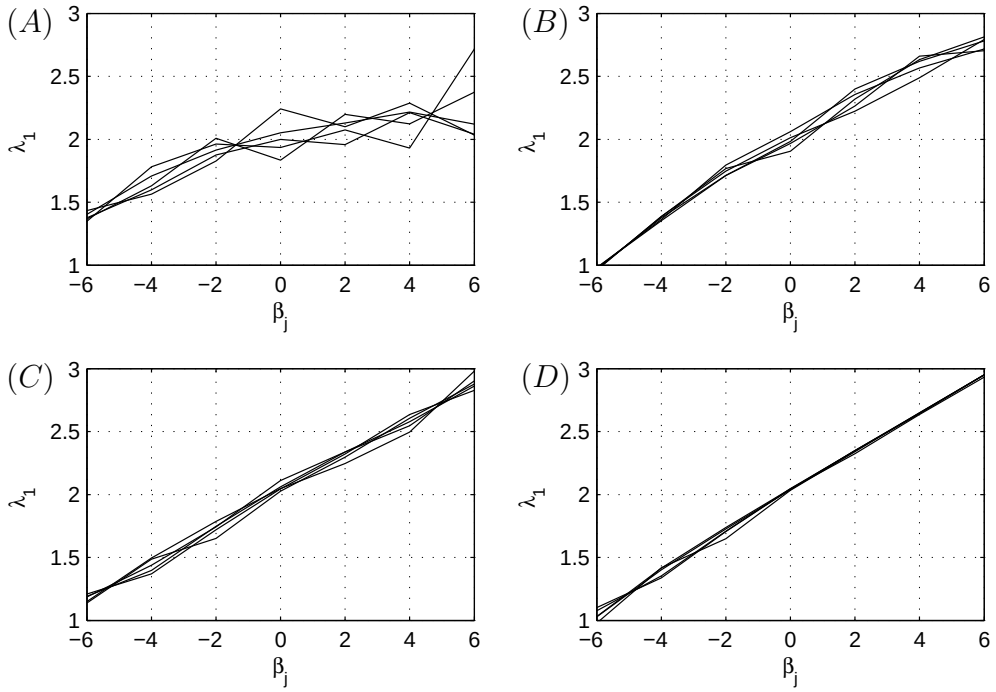

Figure 8.6: *Evaluation of the performance function* λ_1 *at given values* β_j *along four different important directions (A,B,C,D) using different samples of size* $n_i = 5$ *at all points (LSb).*

bility plot to emphasise the tails of the distribution. The $n = 25$ MC samples are plotted separately as data points. The LS results can be shown as a line, because the number of points (found by interpolation) is independent of the number of solutions of the eigenvalue problem. The MC estimate is the same in all four cases, but the LS estimate depends on the chosen important direction. While the MC data points only give a reasonable estimate of the distribution around the mean, the LS approach is able to capture the tails of the distribution at no extra numerical cost. As expected from Figure8.5, the results in case D are best and are clear improvements compared to the standard MC estimate. Figure 8.9 concerns the comparison of the different LS implementations (LSa, LSb, LSc) regarding the use of independent samples for the evaluation of the performance function (see Figures 8.5, 8.6, 8.7). Furthermore, results for the LSp approach, where percentiles are calculated directly from given probabilities, are shown. For directions B and C, LS gives good results and there is no clear advantage for the LSa, LSb or LSc approaches. Direction D seems to be most appropriate for LS and there is no significant difference for the various approaches. Results for direction A are not considered because of numerical problems due to the introduced non-monotonicity. The approach based on calculating percentiles directly (LSp) gives good results in this case of a monotonic behaviour

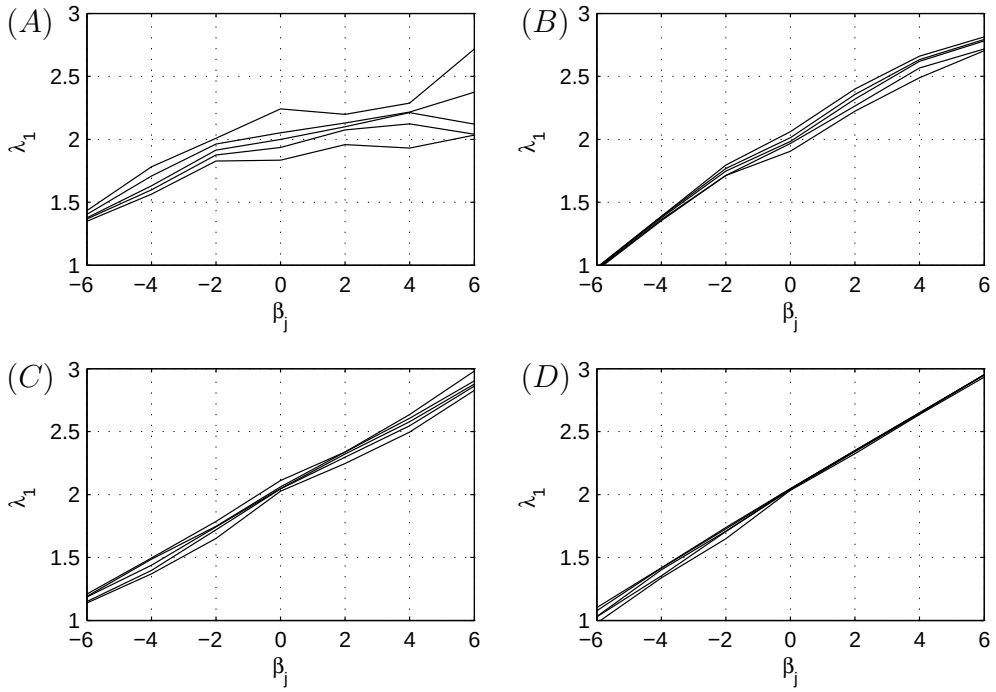

Figure 8.7: *Evaluation of the performance function* λ_1 *at given values* β_j *along four different important directions (A,B,C,D) using different, but sorted, samples of size* $n_i = 5$ *at all points (LSc).*

of the performance function. Therefore, it might constitute an alternative approach for special applications, but future work is required.

The estimated distributions are compared with the reference distribution using two different criteria related to distribution tests. A mean-absolute-error test of the cdf and a mean-square-normalised error test of the pdf (similar to a χ^2-test), each using 200 evenly distributed points over the range of values g are used. The mean-absolute-error test puts a large emphasis on the centre of the distribution, whereas the mean-square-normalised-error test considers the tails of the distribution as well. If there is no data for any of the approaches towards the lower or upper tail of the distribution, the probabilities 0 and 1 have been assigned, respectively. Figure 8.10 shows the results for the MC method and the three different implementations of LS, each for four different important directions and with the same numerical cost. The errors shown are mean values from 30 samples. The LS approaches give better results than the standard MC method. The accuracy of the LS approaches is best in the case of the gradient direction. The differences between the three implementations of LS are small and inconclusive. Future work is required in that area.

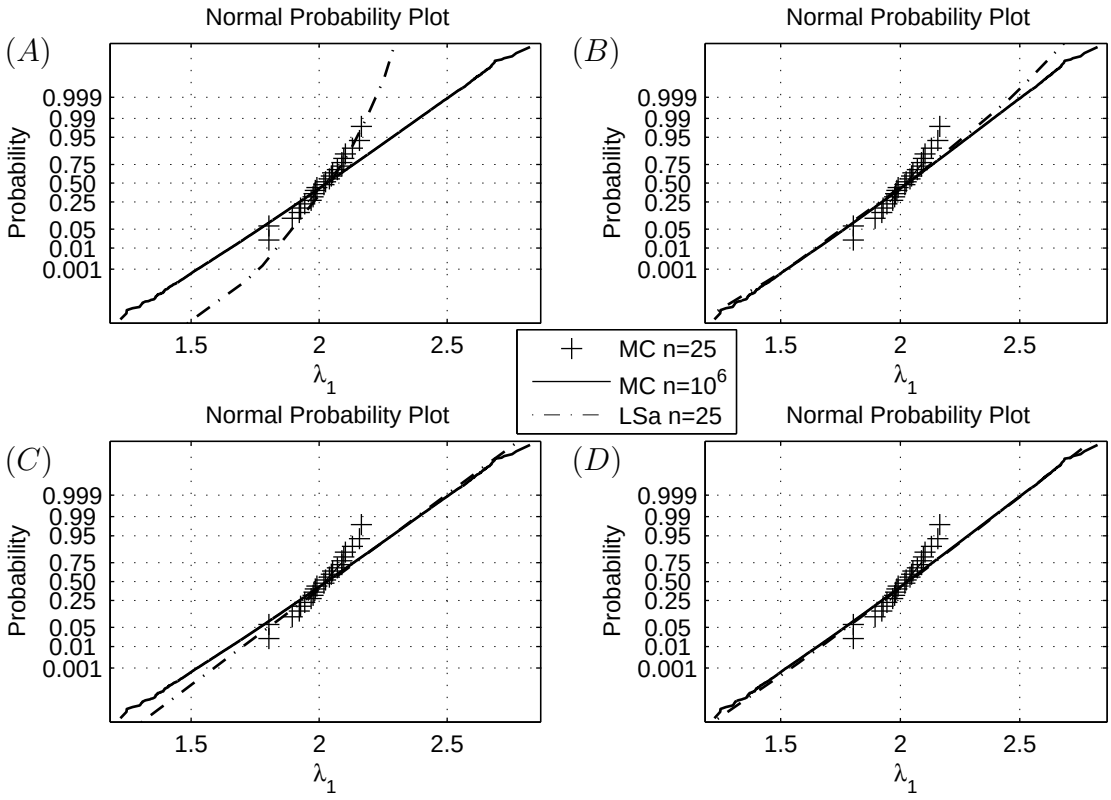

Figure 8.8: *CDF of λ_1: comparison of the LS approach ($n = 25$, using four different directions A,B,C,D) with the standard MC method ($n = 25$ and $n = 10^6$).*

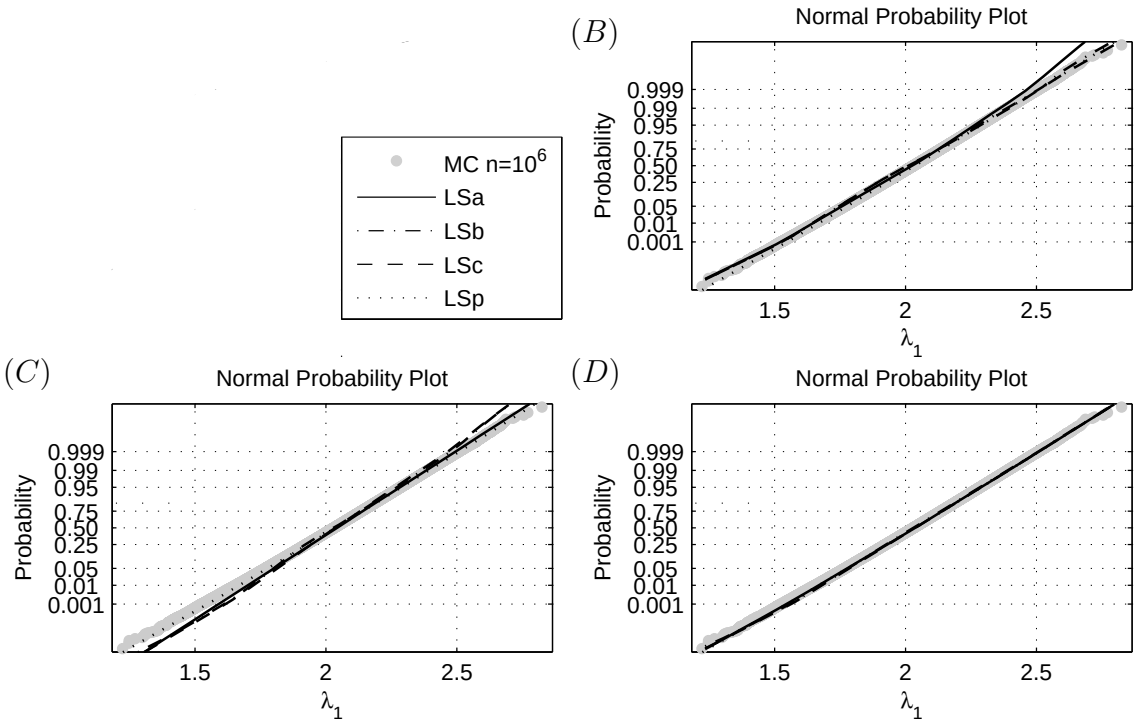

Figure 8.9: *CDF of λ_1: comparison of different implementations (a,b,c,p) of the LS approach ($n = 25$, using different important directions B,C,D) with the standard MC method ($n = 10^6$).*

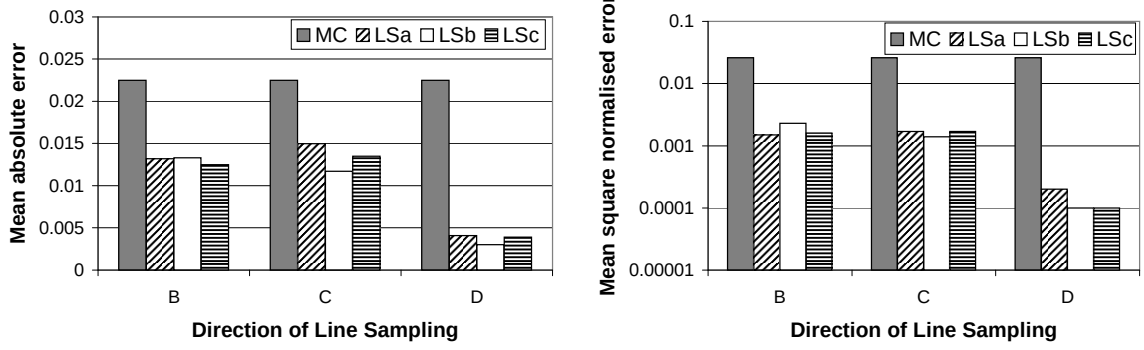

Figure 8.10: *Comparison of the estimated eigenvalue distributions ($n = 25$) with the reference distribution ($n = 10^6$): differences (mean values based on 30 samples) for the standard MC method and the LS approaches (using three different implementations a,b,c and different important directions B,C,D).*

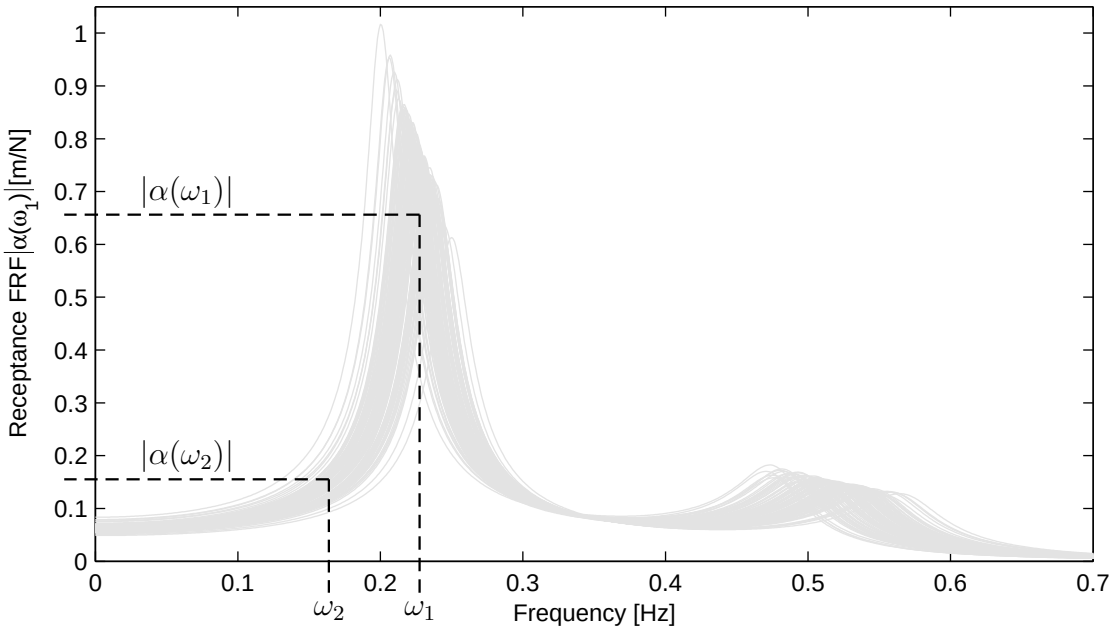

Figure 8.11: *FRF of two-DOF system with uncertain parameters:* 100 *realisations.*

8.4.2 FRF magnitude distribution at baseline resonance frequency

The transfer FRF α between the two masses is now considered and the LS approach is used to estimate the distribution of the FRF magnitude at the first baseline eigenfrequency $|\alpha(\omega_1)|$ as shown in Figure 8.11. Two different cases are defined for the selection of the important direction in the two-dimensional parameter space. In case F the direction is given by the gradient of the baseline response magnitude with respect to the stiffnesses k_1,k_2 and in case E it is arbitrarily chosen to be at an angle of 30 degrees to this gradient. Figure 8.12 shows the performance function $|\alpha(\omega_1)|^{(i)}$ for $n_i = 5$ samples and the two different important directions. The performance function is non-monotonic and sharply varying, similar to the resonance peak in the frequency domain. The variation between the 5 samples is less for the gradient direction F and therefore a higher accuracy can be expected for LS.

For the implementation within the LS approach, the performance function has to be discretised. Figure 8.13a shows a discretisation using $n_j = 20$ values β_j, which were chosen such that a linear interpolation gives a good approximation. If a linear spacing is used, the number of levels required would be much higher. Furthermore, for one value $|\alpha_0|$, two mean probabilities $\overline{p}_1$ and $\overline{p}_2$ are obtained. The probability of occurrence for a magnitude greater than $|\alpha_0|$ is given by $\overline{p} = \overline{p}_2 - \overline{p}_1$.

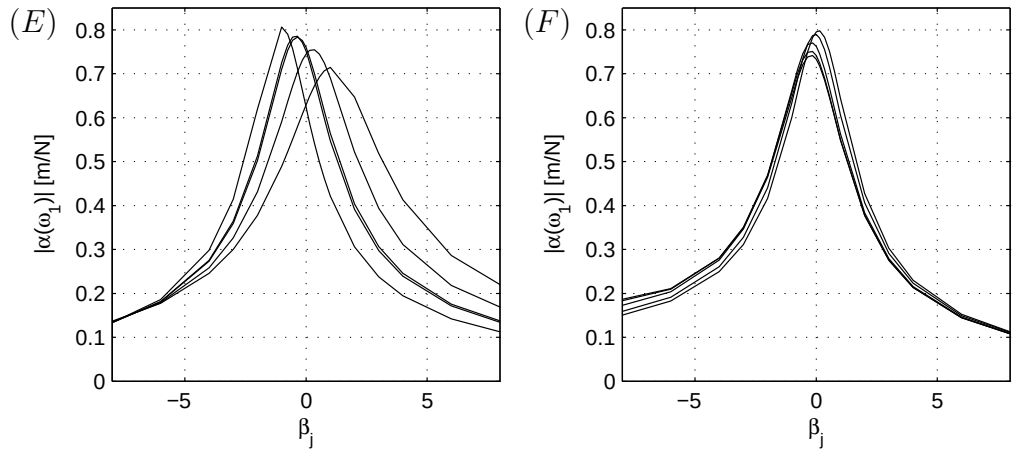

Figure 8.12: *Evaluation of the performance function* $|\alpha(\omega_1)|$ *at given values* β_j *along two different important directions (E,F) using the same sample of size* $n_i = 5$.

The discretisation of the performance function is numerically costly and the total number of calculations required is now $n = 100$.

In Figure 8.14, the estimated distribution is compared with the reference distribution (MC with 10^6 samples) in the normal probability plot. The results for case F are slightly better than for case E. The tail of the distribution for smaller values of the FRF magnitude is estimated well. The tail including the highest magnitudes is only covered up to a level of about 99%. This is due to the fact that the performance function is parallel to the important direction around the peak, which limits the efficiency of LS. In this case, the maximum value of the peak is highly dependent on the sampling and less dependent on a change along the important direction.

In order to reduce the numerical cost of LS, it is possible to parameterise the performance function. The shape of the performance function is related to the FRF of a 1-DOF system, given by

$$|\alpha| = \frac{a}{\sqrt{(1-(\omega/b)^2)^2 + c\omega^2/b^2}} \tag{8.17}$$

However, this model leads to numerical difficulties, because of the symmetry with respect to ω. Instead, a similar 3-parameter model, given by

$$|\alpha| = \frac{1}{\sqrt{a(\beta-b)^2 + c}} \tag{8.18}$$

where the distance β has been substituted for the angular frequency can be used. There are 3 independent parameters a, b, c, which control the spread, position and height of the peak, respectively. This approximates the correct form of $|\alpha|$ and is

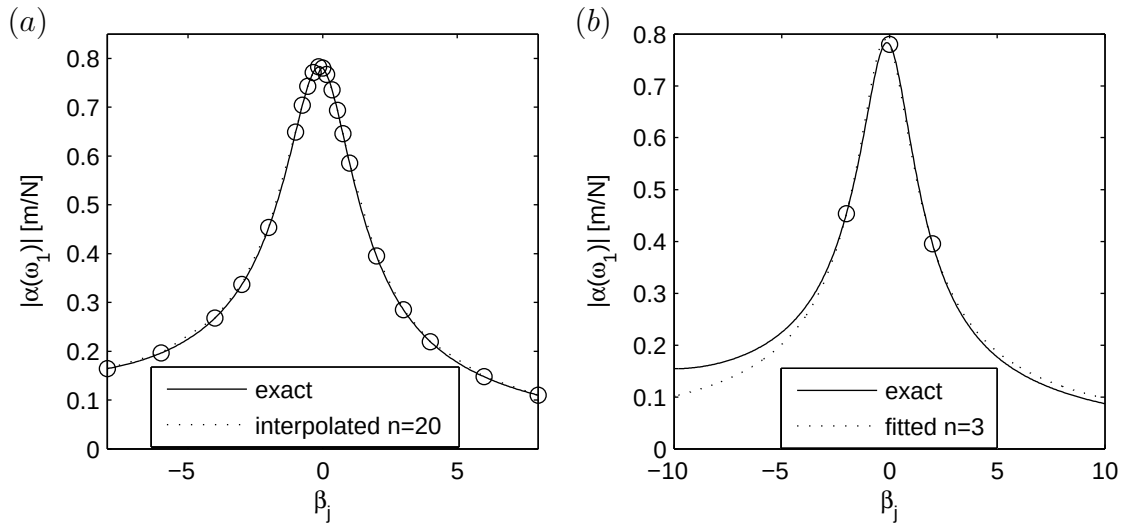

Figure 8.13: *Comparison of the exact performance function with approximations: a) linear interpolation with* 20 *data points, b) fit of a* 3*-parameter model (Equation 8.18) using* 3 *data points.*

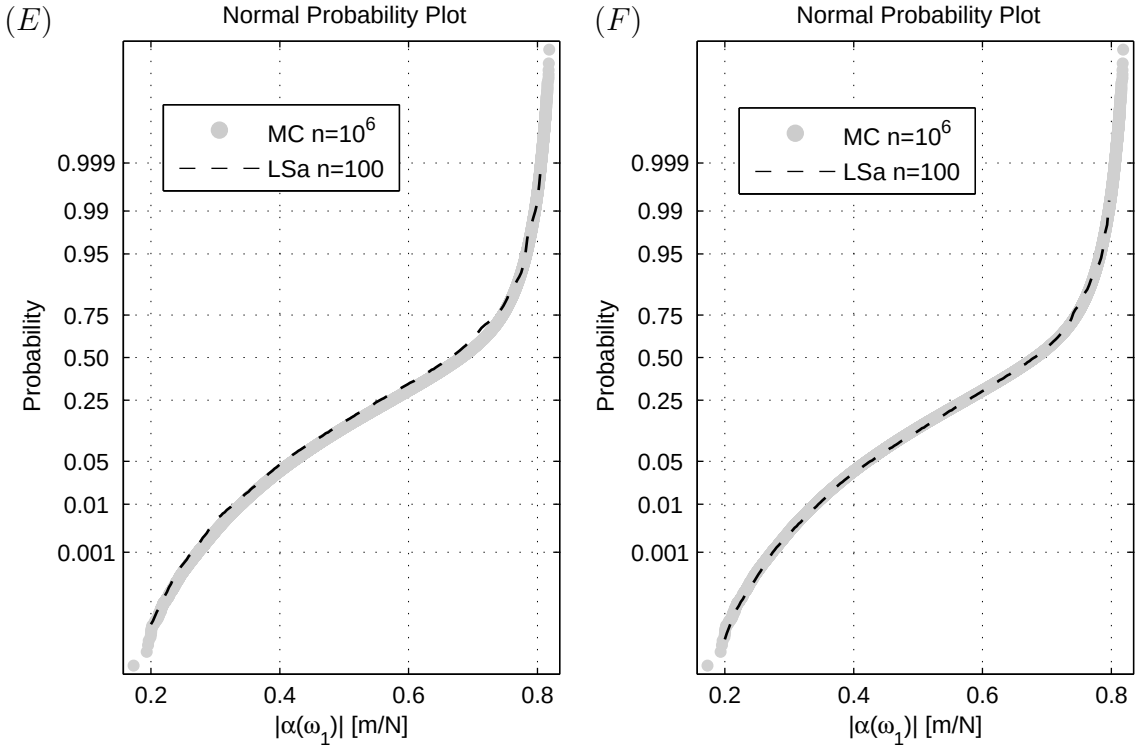

Figure 8.14: *CDF of* $|\alpha(\omega_1)|$*: comparison of the LS approach (*$n = 100$*, using two different directions E,F) with the standard MC method (*$n = 10^6$*).*

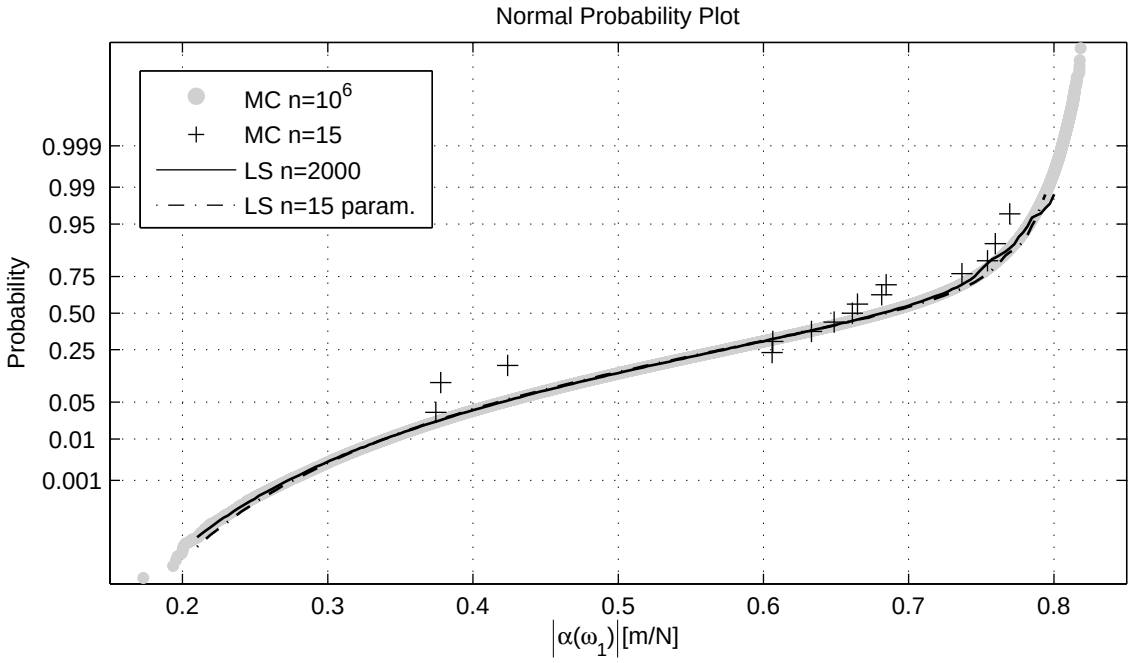

Figure 8.15: *CDF of* $|\alpha(\omega_1)|$*: comparison of the LS approach* ($n = 2000$ *with linear interpolation and* $n = 15$ *with parameterised (param.) model) with the standard MC method* ($n = 10^6$ *and* $n = 15$*).*

particularly good around the resonance, where an accurate approximation is most important and $|\alpha|$ changes most rapidly. Alternatively, a higher order polynomial model can be used, but the 3-parameter model is robust and has the lowest associated computational cost. Figure 8.13b shows the exact performance function and the result using the model in Equation 8.18. The graphs compare very well in the region around the peak. There are increasing differences for values further away from the peak, which correspond to the lower magnitudes.

The results for the estimation of the cdf are shown in Figure 8.15. A Monte Carlo simulation with $n = 10^6$ samples is used as reference. LS has been performed with 5 samples using two different methods for the discretisation of the performance function. A pseudo-exact approach uses 400 data points and linear interpolation, which corresponds to an overall numerical cost of $n = 2000$ evaluations. The proposed approach based on parameterisation uses 3 data points and the model given by Equation 8.18, therefore requiring a total of $n = 15$ calculations. For comparison, the results from 15 Monte Carlo simulations are plotted as well. The agreement between the LS solutions is reasonably good, there are only small differences in the tails of the distribution. Overall, the parameterisation approach works very well for this specific application.

The estimated distributions from the various approaches can be compared using

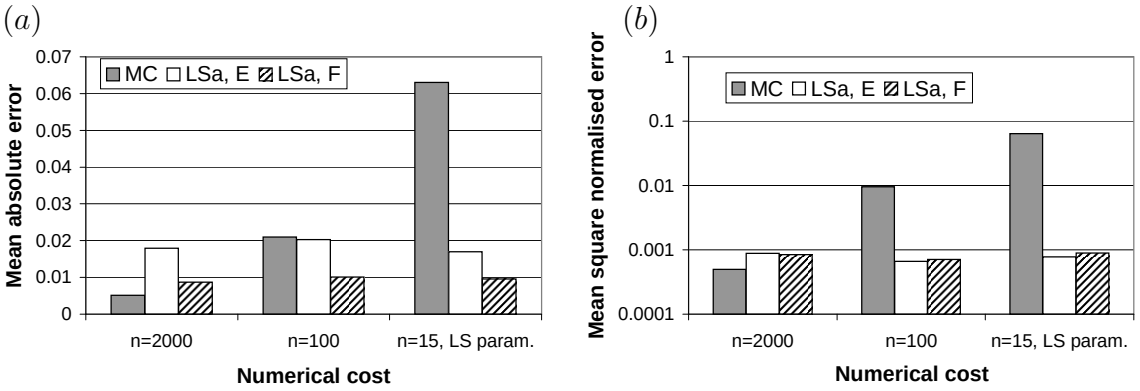

Figure 8.16: *Comparison of the estimated FRF magnitude distributions ($n = 100$) with the reference distribution ($n = 10^6$): differences (mean values based on 30 samples) for the standard MC method and the LS approaches (using two different directions E,F).*

the mean-absolute-error and mean-square-normalised-error tests, respectively. The calculated mean values from 30 samples are shown in Figure 8.16 according to the numerical cost. LS has been performed using the important directions (E,F) and with the same sample of size $n_i = 5$ (LSa) in all cases. The difference in numerical cost of the LS approaches is only due to the different number of data points used to evaluate the performance function. For the standard MC method, the numerical cost shown corresponds directly to the number of samples. It can be seen that, if the performance function is discretised accurately using 400 points, the numerical cost ($n = 2000$) is so high that the standard Monte Carlo method achieves a better accuracy. If the performance function is discretised using 20 points, the numerical cost corresponds to $n = 100$ calculations and LS achieves a better accuracy then the standard MC method. In the case of the parameterisation of Equation 8.18, LS only requires $n = 15$ solutions of the model and the accuracy is much better then the standard MC method with that number of samples. Comparing the LS approaches amongst each other, Figure 8.16a shows that the gradient direction F gives better results than direction E. However, the results shown in Figure 8.16b do not show that difference. Overall, as might be expected, the LS solutions achieve about the same accuracy for all numerical costs. The differences are small compared to the coefficients of variation of the mean values, which are around 45%. This means that the parameterisation using 3 data points and the discretisation using 20 data points give comparable results to the discretisation using 400 data points.

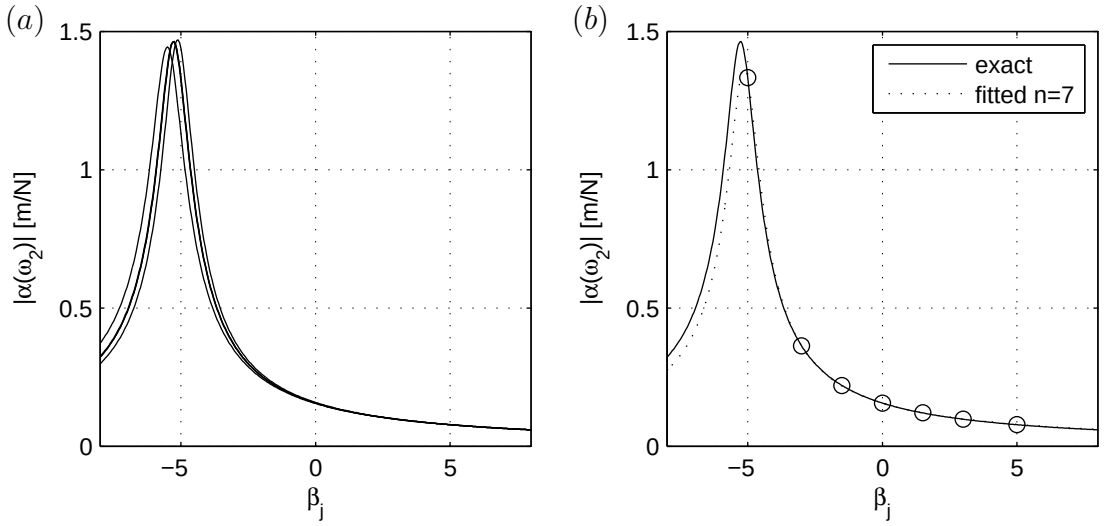

Figure 8.17: *Comparison of the exact performance function* $|\alpha(\omega_2)|$ *with approximations: a) linear interpolation with* 400 *data points, b) fit of a* 3*-parameter model (Equation 8.18) using* 7 *data points.*

8.4.3 FRF magnitude distribution off resonance

This section concerns the distribution of the transfer FRF magnitude away from the resonance peak, at the frequency $\omega_2 = 0.17Hz$ as shown in Figure 8.11. Figure 8.17a shows the evaluation of the performance function $|\alpha(\omega_2)|$ for $n_i = 5$ samples using the gradient direction. The performance function shows the same behaviour as discussed in the previous section, but the peak is shifted by a distance of 5 along the important direction. This corresponds to the probability that the resonance occurs at the specified frequency ω_2. In order to use the most efficient LS approach, the performance function will be parameterised using the model given by Equation 8.18. A reasonable number of 7 data points are used and a fit based on a nonlinear-least-square approach is performed. The total numerical cost is therefore given by $n = 35$ calculations. Figure 8.17b shows the pseudo-exact performance function and the results from the parameterisation. The agreement is reasonably good. The 7 data points have been spread about the origin such that they could be used for a parameterisation of the performance function at different frequencies including resonance.

The estimated distribution is compared with the reference solution in Figure 8.18. For comparison, the results of the LS approach, using the pseudo-exact evaluation of the performance function with $n_j = 400$ data points, and the standard MC method with $n = 35$ samples are shown. The shape of the distribution function has changed and is still non-Gaussian. The LS approaches give very accurate results in both tails

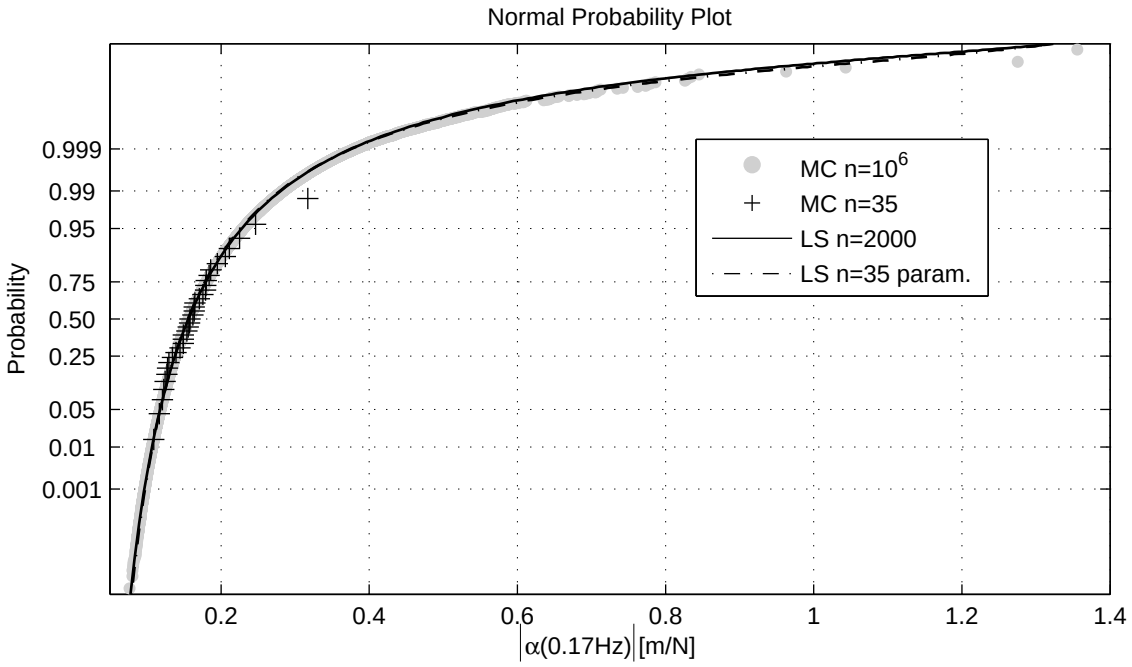

Figure 8.18: *CDF of* $|\alpha(\omega_2)|$*: comparison of the LS approach* ($n = 2000$ *with linear interpolation and* $n = 15$ *with parameterised model) with the standard MC method* ($n = 10^6$ *and* $n = 15$*).*

of the distribution. The influence of the resonance peak, which caused problems in the previous example, can not be seen on the graph, because it is associated with very low probabilities. The FRF magnitude below resonance at ω_2 is stiffness dominated and hence the FRF magnitude distribution is proportional to the distribution of $1/(k_1)$.

8.4.4 FRF magnitude distribution at resonance and uncertainty in damping

This analysis focuses on the transfer FRF magnitude distribution at resonance and considers uncertainty in damping in addition to uncertainty in the stiffnesses. The modal loss factor (η) is modelled by a normal distribution with a coefficient of variation of 10%. Three different important directions will be considered as shown in Table 8.1, where case F is the same as in the previous section. Case G defines the important direction with respect to damping only case H used the gradient with respect to all uncertain parameters.

Figure 8.19 shows the evaluation of the performance function for $n_i = 10$ samples and three different important directions. For case F, the important direction is given by the gradient of the FRF magnitude with respect to both stiffnesses. The shape

Case	Vector in $k_1 - k_2 - mlf$ space	Important direction
F	$(1, 0.54, 0)$	gradient with respect to stiffnesses
G	$(0, 0, 1)$	damping
H	$(1, 0.54, 2.17)$	gradient with respect to all parameters

Table 8.1: *Definition of important directions for LS.*

of the performance function is the same as in the previous section and the effect of the uncertainty in damping can only be seen in a larger variation in the magnitude of the peak. In case G, the variation between the 10 samples is relatively large. The FRF magnitude depends inverse proportionally on the damping, which is reflected in asymptotic curves ($g \sim 1/\beta$). However, the shift of the resonance peak due to uncertainties in the stiffnesses introduces the non-monotonic behaviour as seen in case G. The latter effect is seen more clearly in case H as a combination of the asymptotic and the resonance peak behaviour. In the following, the performance functions have been discretised with a very large number of data points ($n_j = 400$) so that the errors in this part of the approximation can be neglected. The focus is on interpreting the influence of the important direction and the variability between the samples.

Figure 8.20 compares the calculated distribution functions with the reference solution. For cases F and G, the lower tail or the upper tail of the distribution is estimated very well, respectively. There is either no data or larger differences in the opposite tail. In case H, based on the gradient direction, data for all parts of the distribution is available, but with slightly lower accuracy. It seems that a combination of cases F and G would result in the best estimation of the distribution function. In order to implement this idea, it is possible to use two important directions, one given by the gradient with respect to the uncertain stiffnesses and another given by the gradient with respect to the uncertain damping. This seems logical, since these uncertainties have qualitatively different effects on the FRF. The implementation of two important directions β^1 and β^2 would require that the performance function $g(\beta^1, \beta^2)$ is evaluated in a two-dimensional domain. This concept of multi-level LS is a subject for future work.

In many applications, it might be more important to know the FRF magnitude distribution of the first resonance instead of the FRF magnitude distribution at the baseline resonance frequency. The difference lies in the effect of the frequency shift that is caused by the uncertainty in the stiffnesses. For the evaluation of statistics

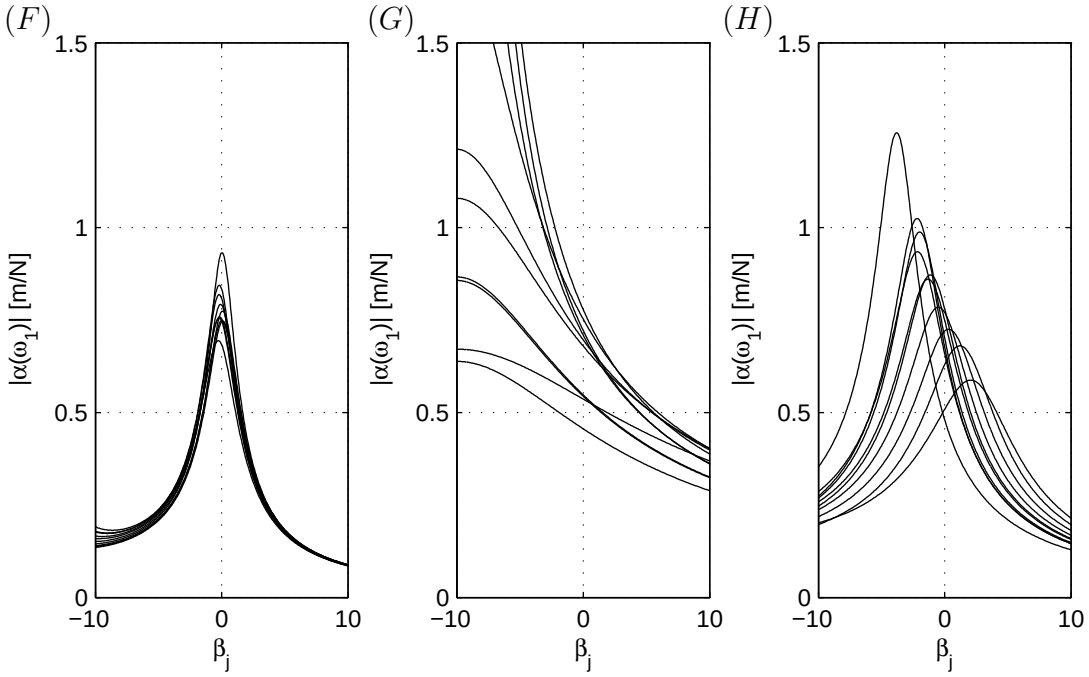

Figure 8.19: *Evaluation of the performance function* $|\alpha(\omega_1)|$ *at given values* β_j *along three different important directions (F,G,H) using the same sample of size* $n_i = 10$.

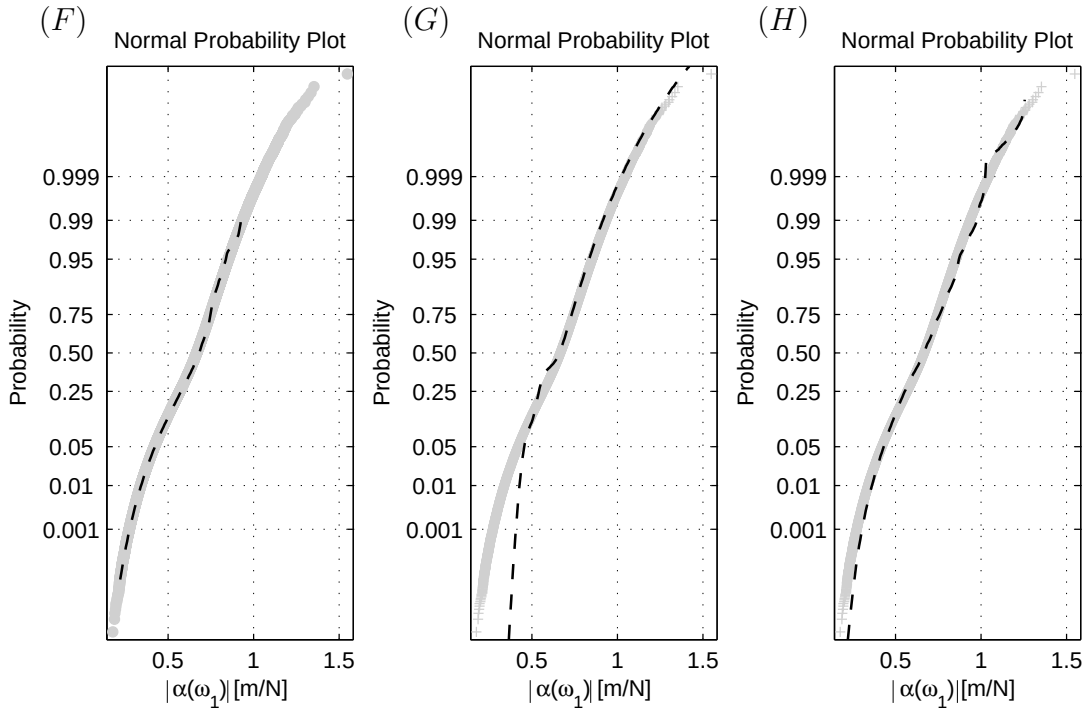

Figure 8.20: *CDF of* $|\alpha(\omega_1)|$*: comparison of the LS approach (___* $n = 4000$ *with linear interpolation) with the standard MC method (____* $n = 10^6$*).*

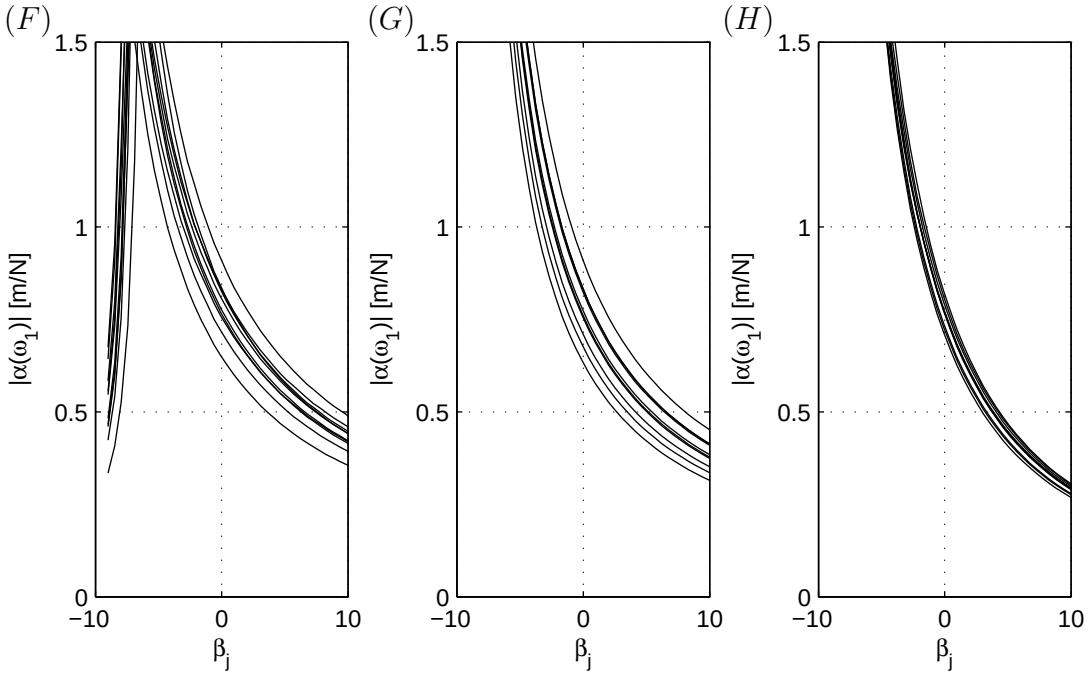

Figure 8.21: *Evaluation of the performance function* $|\alpha_1|$ *at given values* β_j *along three different important directions (F,G,H) using the same sample of size* $n_i = 10$.

at a fixed frequency, a shift of the FRF along the frequency axis greatly affects the results. In comparison, if only the magnitude of the resonance peak is considered, independent of its frequency, any shift of the FRF along the frequency axis has little effect. The following analysis follows the same lines as the previous one, except that the magnitude of the resonance peak is considered. Figure 8.21 shows the evaluation of the performance function in this case for $n_i = 10$ samples and the three different important directions. It can be seen that the graphs follow the asymptotic behaviour, which corresponds to the effect of uncertainty in damping. Only for case F, there is non-monotonic behaviour within the considered range of values. For cases G and H, the performance function varies monotonically for the considered range of values β.

Figure 8.22 shows the corresponding results for the estimated FRF distribution functions. The magnitude of the resonance peak is dominated by the damping and hence the cdf is proportional to the cdf of $1/\eta$.

The results show reasonable agreement for case G and very good agreement for case H. The errors in case F are due to the fact that the important direction does not consider the effect of uncertainty in damping. The discretisation of the performance function in cases G and H can be performed with a few data points only, which makes the LS approach very efficient.

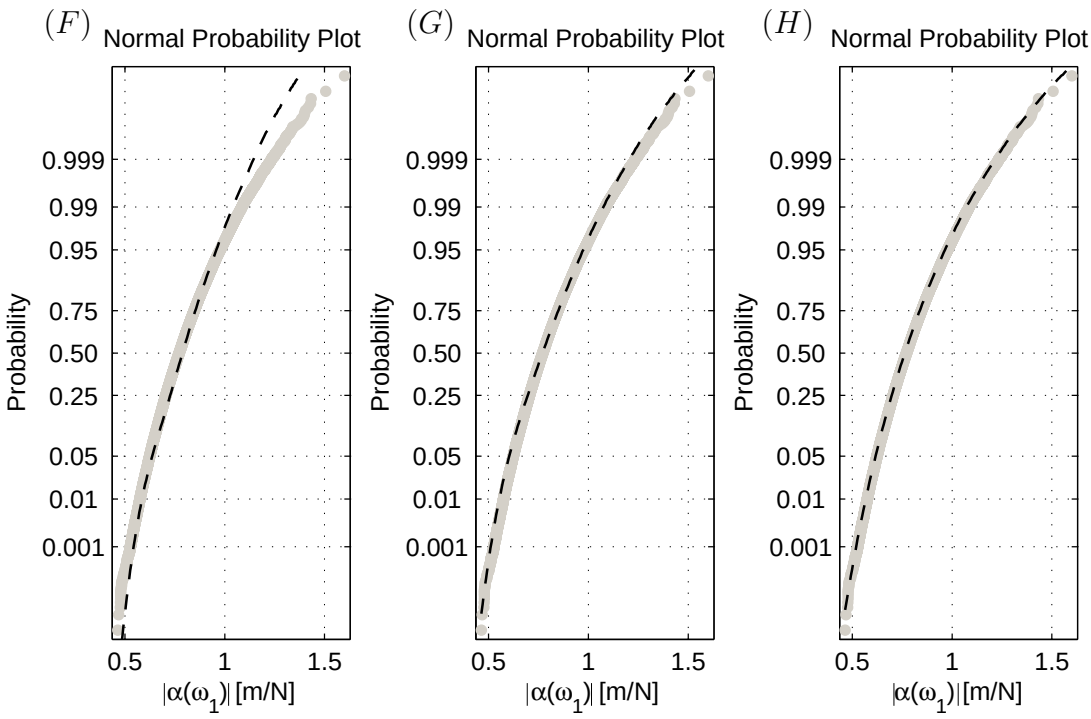

Figure 8.22: *CDF of* $|\alpha_1|$*: comparison of the LS approach* ($n = 4000$ *with linear interpolation) with the standard MC method* ($n = 10^6$*).*

8.5 Discussion

The LS simulation method is known to be an effective method to estimate small probability events, such as a probability of failure of a structure. It is robust and independent of the number of random variables. If an important sampling direction can be identified and the limit state function is simple, a reduction in the numerical cost by a factor of 100 or more can be achieved.

In the application of the LS method to estimate a complete distribution function, the limit state value is moved through the range of possible values of the performance function and a number of subsequent LS problems are solved. Compared to the standard MC method, where the solutions concentrate around the mean, the LS approach basically allows one to choose the probability of the individual solutions. Therefore, there is no difference in the numerical cost for estimating the tails of a distribution compared to the area around the mean. The LS approach is in general more efficient than the standard MC approach, especially if the performance function can be approximated along the important direction by a reasonably small number of points. If the shape of the distribution function is known a priori, only as many LS solutions are required as there are independent parameters to describe the distribution. In this case mean values and variances can be estimated with high

accuracy at very low numerical cost.

The LS approach works well for the estimation of the distribution of natural frequencies in structural dynamic systems with uncertain mass and stiffness properties, because in this case the performance function varies smoothly and monotonically along the important direction and only a few points are required to estimate it. The performance function of frequency response magnitudes varies sharply and non-monotonically along the important direction and a larger number of discretisation points is required, which reduces the efficiency of the LS approach in this case. In the region around the resonance peak, which is responsible for the upper tail of the magnitude distribution, the accuracy of the estimate is limited. This is due to the interpolation and the fact that the gradient is zero at the peak. The performance function has a shape similar to that of the FRF of a single degree-of-freedom system and can be parameterised to further reduce numerical costs.

8.6 Application of Line-Sampling to random field models

This section concerns the application of the LS method to random field models. The use of random fields to model spatial variations in mechanical structures has been discussed in Chapter 3. A simple model for a random field is a homogenous isotropic Gaussian field, where the random variables have a Gaussian distribution with parameters independent of direction and location. Therefore, the interdependency between two random variables defined at two points depends only on the distance between them. The correlation between two Gaussian random variables can be modelled by an exponential function of the form

$$R(d, L_c, \sigma) = \sigma^2 \exp\left(-\left|\frac{d}{L_c}\right|\right) \tag{8.19}$$

where σ is the standard deviation, d is the distance between two points and L_c is the correlation length. For n random variables, a nxn covariance matrix $\mathbf{C}$ can then be constructed. A random field in one dimension, given by a vector $\mathbf{p}$ of length n, can be represented by the Karhunen-Loève (KL) expansion in the form [40]

$$\mathbf{p} = \bar{\mathbf{p}} + \sum_{j=1}^{r \leq n} \boldsymbol{\psi}_j \sqrt{\mu_j} \zeta_j \tag{8.20}$$

where $\bar{\mathbf{p}}$ denotes the mean, ζ_j are uncorrelated standard normal (zero mean and unit variance) random variables and μ_j and $\boldsymbol{\psi}_j$ are the eigenvalues and eigenfunctions of

the covariance matrix respectively. The mean $\bar{\mathbf{p}}$ and the eigensolutions μ_j and $\boldsymbol{\psi}_j$ are deterministic. The randomness of the field is only included in ζ . There are n eigensolutions, but in general it is sufficient to consider only the r most important eigenfunctions, which give a good approximation of the random field. The parameters of the Gaussian random field are the mean value $\overline{p}$, the standard deviation σ and the correlation length L_c.

For the application of the LS approach, it seems reasonable to derive the important sampling direction α directly from the KL expansion. One possible approach is to associate the KL variables ζ_j directly with the LS variables θ_j such that $\boldsymbol{\theta} = \boldsymbol{\zeta}$ and $\zeta_1 = \theta_1$ is the coordinate in the important direction α. The advantages of this approach are that no additional calculations are needed to define an important direction and the parameters are already given in the required standard normal space. LS will then be most effective, if the variable ζ_1 in the important direction is dominant compared to all other variables $\boldsymbol{\zeta}_{-1}$. The influence of these variables is determined by the corresponding eigenvalues of the covariance matrix. For small correlation lengths all eigenvalues have a value of about 1 and for large correlation lengths all except one eigenvalue approach a value of 0. Therefore the larger the correlation lengths, the more efficient the LS procedure will be.

A cantilever beam as shown in Figure 3.1 is used as a numerical example. Standard finite element stiffness and mass matrices for Euler-Bernoulli beam theory [9] with transverse and rotational degrees of freedom are used. The beam of length $l = 1m$ is divided into 10 elements. A random field model is considered for the Young's modulus E with a CV of 10% and varying correlation length. It is discretised such that each element has a different but constant thickness. In order to compare the LS approach with the standard MC approach, a low probability event of the fundamental frequency f_1 will be calculated. First, the performance function f_1 is evaluated at arbitrarily chosen values $\boldsymbol{\beta_j} = [-6 : 2 : 4]$ along the important direction, which is defined by the first coordinate in the KL decomposition of the random field. Figure 8.24 shows the performance function for $n_i = 100$ samples and based on linear interpolation. In Figure 8.24a the correlation length is $10^{-6}m$, which is a theoretical value, in Figure 8.24b,c the correlation length is comparable to the length of the beam and in Figure 8.24d it is considerably larger than the length of the beam. The convergence rate of LS is better if the variance within the samples is small, which is shown as a narrow spread of lines in Figure 8.24. As expected, the variation clearly reduces for larger correlation lengths.

In Figure 8.25, the coefficient of variation of the probability estimator is compared for the two sampling methods and different correlations lengths. Standard MC simulations with $n = 10^4$ and $n = 10^3$ samples were performed and the lower

l $[m]$	h $[m]$	b $[m]$	ρ $[kg]$	E $[N/m^2]$
1	0.01	0.1	7850	$2.1e11$

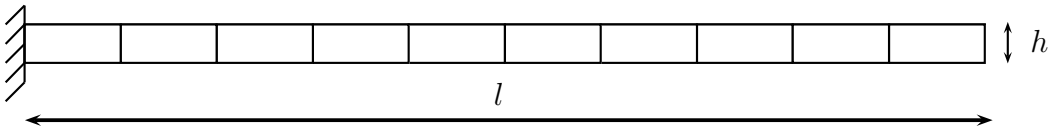

Figure 8.23: *Uniform cantilever beam with rectangular cross section and the baseline parameters.*

bound of the fundamental frequency corresponding to a probability of 5% was found. The corresponding CVs can be calculated from Equation 8.3 and are independent of the correlation length. Subsequently, LS was performed with $n = 100$ and $n = 10$ samples, respectively, and the CV was calculated from Equation 8.13. Figure 8.25 clearly shows that these results depend on the correlation length. In case of the LS method, the extra numerical cost required to evaluate the performance function has been neglected. In general, at least two points have to be evaluated for the approximate approach using linear interpolation. Any inaccuracies due to approximations to the performance function are not contained in the CV of the LS estimator. The results in Figure 8.25 show that for a correlation length of $L_c = 0.5m$, which is half the length of the beam, the standard MC approach requires about 10 times the number of samples as the LS approach. For larger correlation lengths, this ratio steadily increases. Similarly, the smaller the probability of the event the more effective LS performs compared to the standard MC approach.

8.7 Conclusions

The standard MC method is of widespread use in many fields of application and is often used to provide reference solutions for other approaches. The only disadvantage is the high numerical cost. Several advanced MC methods have been developed to reduce the numerical cost for specific problems, such as calculating a low probability of failure. It seems reasonable also to apply these successful methods to other areas, where standard MC methods are normally used.

In this chapter, the Line-Sampling method has been applied successfully to estimate distribution functions of structural dynamic systems. The emphasis was on low-cost approaches that require less than 100 solutions of a deterministic problem,

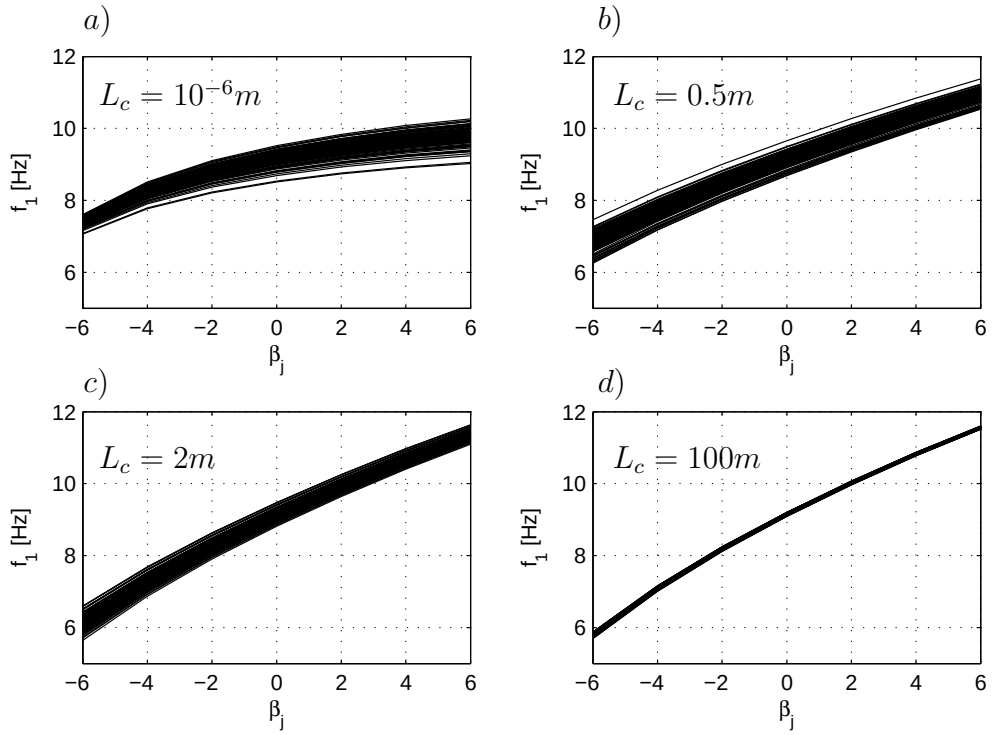

Figure 8.24: *Evaluation of the performance function f_1 for samples along the important direction, different correlation lengths.*

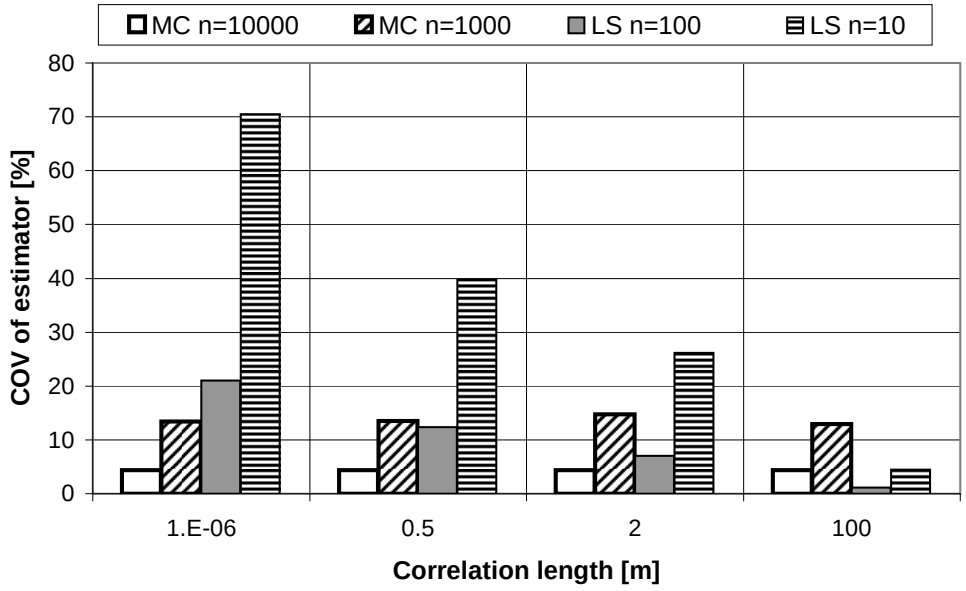

Figure 8.25: *Comparison of the variance of probability estimators, MC sampling ($n = 10^4, n = 10^3$)and LS ($n = 100, n = 10$), results based on a target probability of* 5%.

but are capable of capturing the complete distribution function up to probabilities of 10^{-5} or so. Furthermore, the efficient combination of LS with random field models of spatial variations has been presented. It is appropriate to define the important direction in LS according to the first random variable in the KL expansion.

Chapter 9

Numerical example: automotive windshield with uncertain properties

9.1 Introduction

This chapter concerns the vibration analysis of an automotive windshield with uncertain parameters. In particular, the modelling of spatial variations using random fields and the implementation within a finite element model are discussed. Spatial variations are considered for the thicknesses of the five layers of the laminate windshield and for the properties of the glue joint by which the windshield is mounted on the car. These spatially varying parameters can be modelled appropriately by random fields, as discussed in Chapter 3. The analysis is based on the FE model of the baseline system and information about parameter uncertainties. The variation in the frequency response of the windshield is investigated for the cases of a free and constrained configuration of the windshield. The Line-Sampling procedure, as described in Chapter 8, is applied to estimate statistics of the fundamental eigenfrequency of the windshield.

Continuous random fields are discretised using the existing FE mesh such that each finite element has a constant parameter value. A point discretisation method based on the geometric centre of each finite element is employed. The discrete random field for one windshield parameter is based on n correlated random variables, where n is the number of finite elements. The spatial correlation of the random variables mainly depends on the correlation length. If the spatial interdependencies are neglected, e.g. the correlation length is zero, then there are n uncorrelated random variables. If total spatial correlation is assumed, e.g. the correlation length

is infinite, then there is only one random variable covering all finite elements.

The next section concerns the analysis of the windshield in a free configuration. Subsequently, the windshield is considered in a constrained configuration as mounted on the car. Results from numerical and experimental studies of the windshield [103–105] are considered.

9.2 Windshield in free configuration

9.2.1 Windshield FE model

The windshield shown in Figure 9.1 is a laminate shell structure, slightly curved, consisting of five layers with different materials and thicknesses. Figure 9.2 shows a schematic of the cross-section of the laminate. The two external layers are made of glass and the intermediate layers of two different polymers, two PVB (poly vinyl butyral) layers and one further polymer (AP) in the middle. The windshield measures approximately 800mm in the vertical and 1500mm in the horizontal direction. Compared to the surface dimensions, the nominal thickness of 4.96mm is small. The structure has been modelling using planar shell elements with the capability of including multi-layered cross-sections (NASTRAN PCOMP element). The calculations are performed using a mesh consisting of 793 nodes (4758 degrees of freedom), 758 rectangular (NASTRAN CQUAD4) and triangular (NASTRAN CTRIA3) elements. It has to be noted that the current finite element model may not be sufficient to model the dynamic behaviour of the windshield accurately, but it is appropriate in regard to the objectives of this chapter. A more accurate finite element model of the windshield should comprise solid finite elements, allowing individual shear deformation in each layer, and a temperature and frequency dependent material model for the polymers. Overall, it can be shown that results from the finite element model compare qualitatively well to measured data. Therefore, the model of the windshield is appropriate to study the modelling and the effects of spatial variations in various properties.

9.2.2 Variability and uncertainty

In [103] two different sources of nondeterministic data for the windshield were identified. First, there is the change of material properties of one structure with temperature, which has been referred to as intra-variability and was considered in [103]. On the other hand, inter-variability refers to the variation between two or more structures, for example in the thickness of the individual layers. It is inevitable that

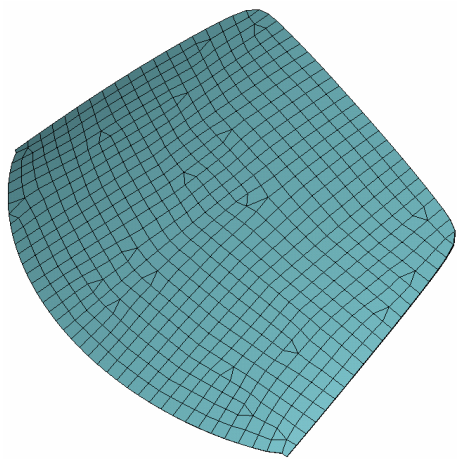

Figure 9.1: *Windshield FE mesh.*

1	Glass	2.1 mm
2	PVB - polymer (vinyl butyral)	0.33 mm
3	AP - acoustic polymer	0.1 mm
4	PVB - polymer	0.33 mm
5	Glass	2.1 mm

Figure 9.2: *Schematic view of cross-section and nominal thicknesses.*

Geometric variability	Nominal value	Tolerance
Sandwich thickness (1+2+3+4+5)	$4.96mm$	$(-0.2; +0.2)mm$
Polymers thickness (2+3+4)	$0.76mm$	$(-0.16; 0)mm$

Table 9.1: *Mean values and tolerances for thicknesses.*

the thickness of each individual layer will differ from the nominal value and vary over the layer, because neither an exact nor constant thickness can be achieved in manufacturing. The available information on mean values and expected bounds are listed in Table 9.1. In this work, the use of random field models to describe the variation in thicknesses is investigated.

9.2.3 Simulation

The simulations were carried out using the FE software NASTRAN. For the nominal FE model, the material parameters and modal damping ratios were selected according to a constant temperature of 5 °C according to [103].

For the random field model, a Gaussian distribution for the thicknesses was assumed. The mean value was calculated to lie in the centre of the given interval using the nominal and tolerance values in Table 9.1. The standard deviation was obtained by the criterion that a sample from the Gaussian distribution has a probability of 95% to fall within the specified interval. A constant coefficient of variation was calculated for all polymer layers. Furthermore, the random fields of the individual layers were treated independently and a correlation length of 500mm was assumed (no data). The parameter values used in the simulations are given in Table 9.2.

Parameter / Layer		Glass (1,5)	PVB (2,4)	AP(3)
Mean value	$[mm]$	2.14	0.29	0.1
Coefficient of variation (CV)	%	4	12	12
Correlation length	$[mm]$	500	500	500

Table 9.2: *Parameters of Gaussian random field for layer thickness.*

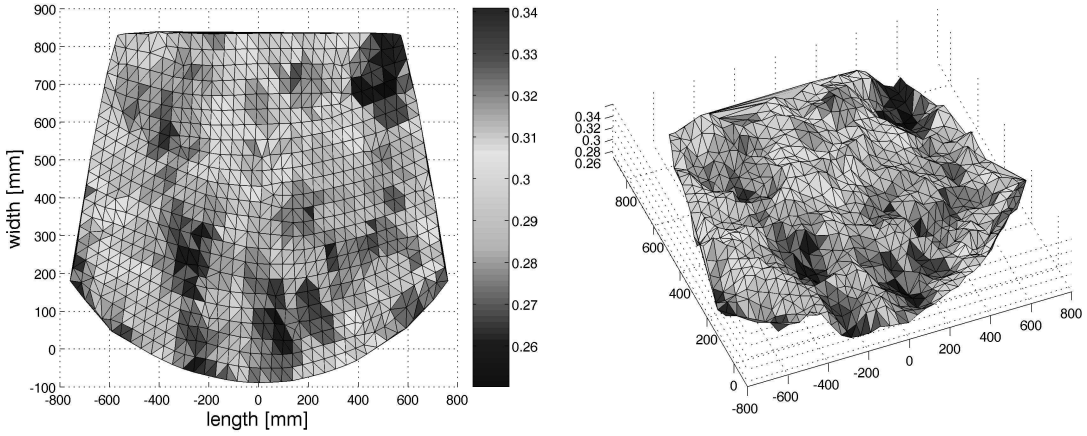

Figure 9.3: *Realisation of a homogenous isotropic Gaussian random field, 2D and 3D views; mean value* $0.29mm$*, coefficient of variation* 12%*, correlation length* $500mm$*.*

The application of the random field model is straightforward, if a discretisation at element level is chosen. The NASTRAN input file is changed accordingly by creating one property card for each element. The random field model is implemented in MATLAB. For the calculation of the distances between elements, information on element nodes and node coordinates is used to calculate the geometric centre of each element. The distance of two elements, which determines their correlation, should be the shortest connection on the surface. For simplification, the shortest distance in space was used, which however is expected to be a sufficiently accurate approximation. Figure 9.3 shows one realisation of the random field for a PVB layer.

A Monte Carlo simulation is applied to obtain a response sample. The procedure has been automated using a script in the programming language PERL. First, an input file is created, which specifies the parameters for the random field model (mean, standard deviation, correlation length) and the number of runs. Next, a file containing the thicknesses for all layers and all evaluations is created by MATLAB. In the main simulation loop, the PERL script updates the NASTRAN input files with the new thickness values, then submits them to the NASTRAN solver and subsequently extracts and saves the required results. All steps are automated by the script and the NASTRAN environment can be used unchanged.

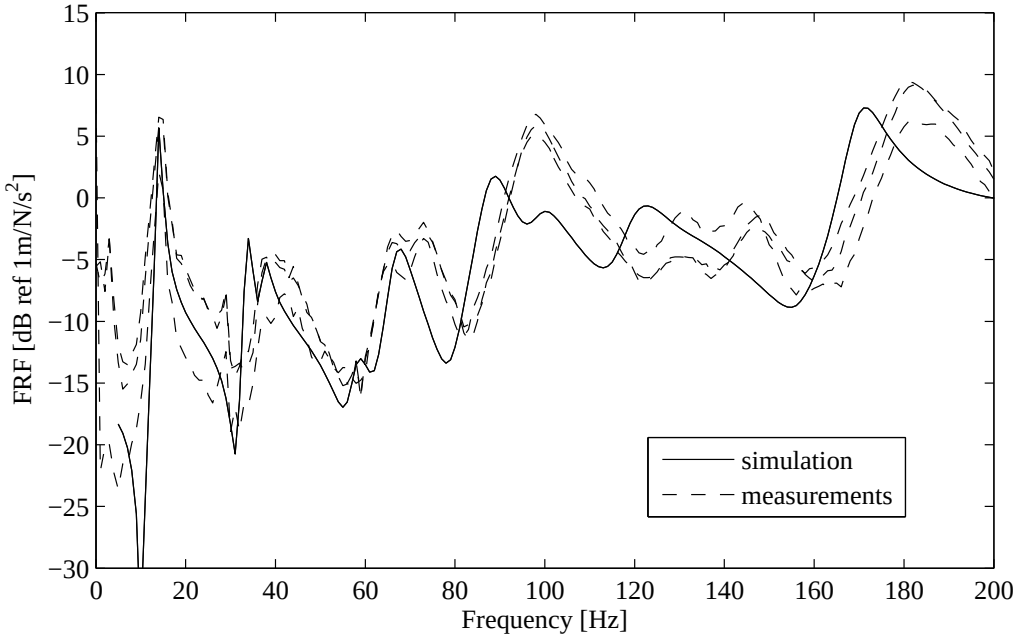

Figure 9.4: *Comparison of FRF measurements on three different windshields with deterministic simulation.*

9.2.4 Results

In Figure 9.4 the deterministic results from the nominal FE model are compared with the measured FRFs from three different windshields. The experimental campaign is described in [103]. The measurements were performed on three nominally identical acoustic windshields in a free configuration. An excitation by an impact hammer was used and the acceleration was measured by piezoelectric accelerometers at different locations. Furthermore, modal damping ratios have been estimated from the FRFs. All experimental data relate to the temperature of 5 °C and the same point FRF. In general, the simulations capture the characteristics of the dynamic response well. However, there is a shift to lower frequencies for the simulation results. This is mostly due to the fact that the frequency dependence of the elastic properties of the polymers was not modelled. For higher frequencies the dynamic stiffness of the polymers can be expected to increase.

Figure 9.5 shows the results from a Monte Carlo simulation with 500 samples including the 5 and 95 percentiles of the FRF magnitude. As expected, the variation increases with frequency and therefore predicts a larger range in magnitude for higher frequencies. In Figure 9.6, results are shown for two cases where the correlation length L_c of the random field is set to a very small and very high value, respectively. The changes in the FRF statistics are significant. A very large correlation length corresponds to the case that there is a constant but random value for all elements

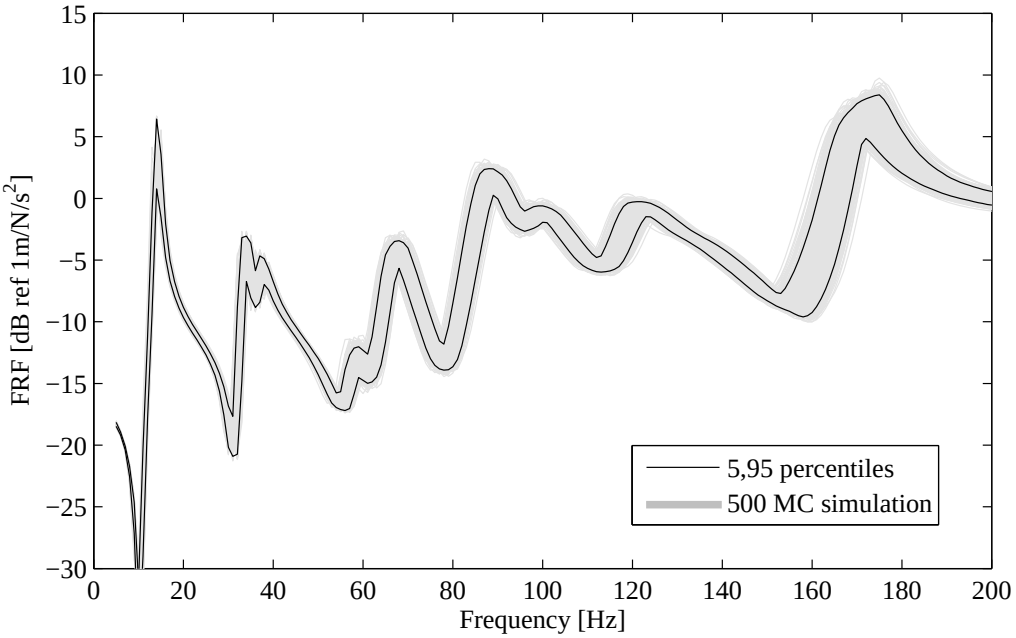

Figure 9.5: *FRFs from 500 MC simulations and statistics.*

and leads to increased FRF variation. The statistics for the case of zero correlation length, where all elements are nearly statistically independent, show a much smaller variation. This is because the effects due to uncorrelated variation in all finite elements is averaged out.

9.3 Windshield in constrained configuration

This section concerns the practical case where the windshield is mounted on the car. The glue joint and polymer seal, by which the windshield is connected to the car, have spatially varying material and geometric properties over their lengths. These inherent variations can have a considerable effect on the dynamic response of the system. For this analysis, the effects of the joint and the chassis on the dynamic behaviour of the windshield are approximated by translational stiffnesses in all directions at the 102 nodes along the edge of the windshield. A measurement campaign on the windshield in a constrained configuration has been conducted [103] and four resonance frequencies were identified. The nominal values of the joint stiffnesses were calculated such that the fundamental eigenfrequency from simulation and measurement are identical. The best results were achieved for the case where in-plane motions are effectively constrained and the out-of plane stiffness has a value of $2500\,N/mm$. The comparison between the first four simulated eigenfrequencies and measured resonance frequencies is shown in Table 9.3. The agreement is good. However, uncertainties were neglected in this step, because the baseline joint stiffness

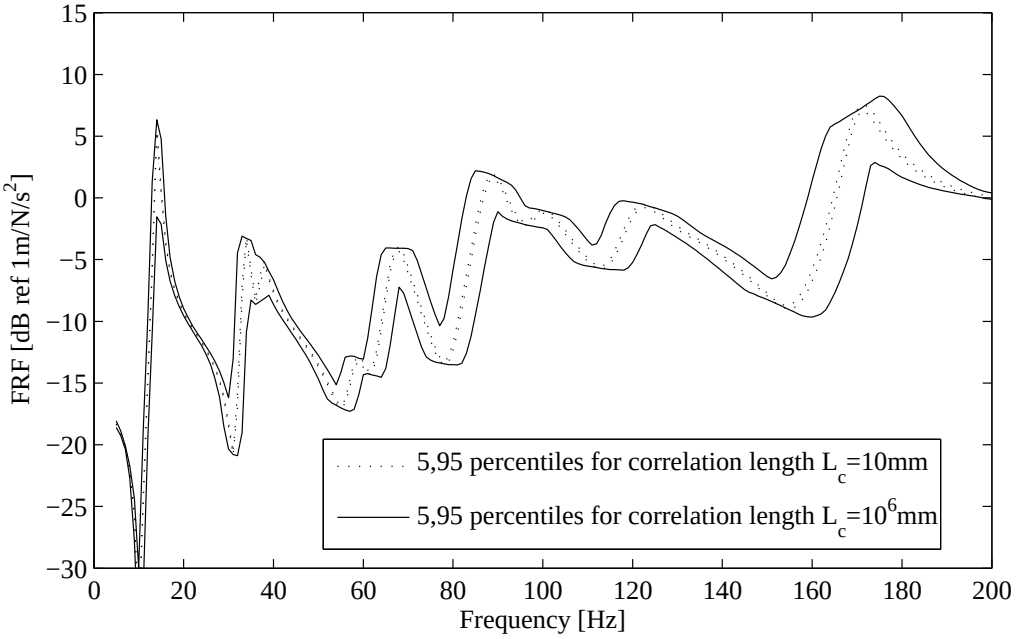

Figure 9.6: *5 and 95 FRF percentiles for very small and very large correlation lengths, 500 MC simulations.*

Eigenfrequencies [Hz] / Mode	1	2	3	4
Simulation	58	106	162	226
Measurement	58	109	163	227

Table 9.3: *Comparison of eigenfrequencies for simulation and measurement.*

was updated using one available measurement of the fundamental eigenfrequency only.

Variability data on the joint properties [103] indicates that a CV of 30% is realistic for the joint stiffness. A correlation length of $L_c = 500mm$ has been assumed. 500 Monte Carlo simulations have been performed considering the random field models for the individual thicknesses, as described before, and the out-of-plane stiffness of the joint. The FRFs and statistics are shown in Figure 9.7. The frequency response is characteristically different to the free configuration case. There is very large variation around the fundamental resonance and much less variation for higher frequencies. It is clear that the joint properties mainly affect the lower frequencies. In addition to the variation of the FRF magnitude, the variation in the frequency of resonance peaks can be of interest. Figure 9.8 shows a histogram of the fundamental eigenfrequency of the windshield based on 2000 MC simulations. The shape is close to a Gaussian distribution, but is skewed somewhat. In practice various statistics of the fundamental frequency can be of interest, for example the 5 and 95 percentiles or

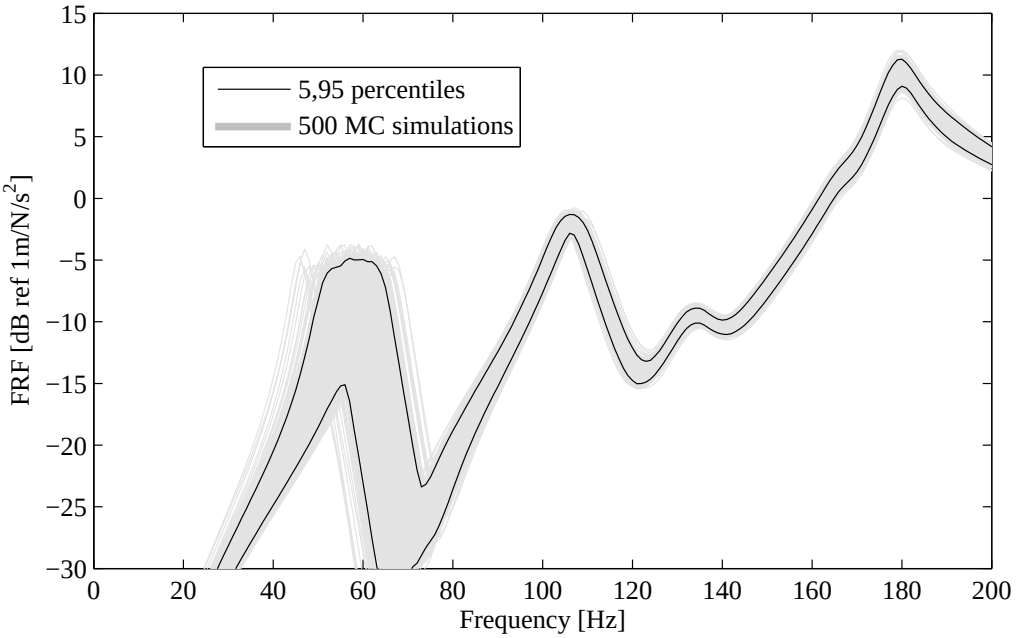

Figure 9.7: *FRFs from 500 MC simulations and statistics.*

the probability of the fundamental frequency being below a certain value. In general the numerical cost for such an analysis can be relatively large. In the next section, the application of a simple Line-Sampling procedure to estimate the distribution and statistics of the fundamental eigenfrequency will be considered.

9.4 Line-Sampling

This section concerns the application of the Line-Sampling method to the random field model in order to increase computational efficiency, as discussed in Chapter 8. The Karhunen-Loève (KL) expansion of the spatially varying discretised joint stiffnesses can be written as

$$\mathbf{k} = \bar{\mathbf{k}} + \boldsymbol{\psi}_1 \sqrt{\mu_1} \zeta_1 + \sum_{j=2}^{r \leq n} \boldsymbol{\psi}_j \sqrt{\mu_j} \zeta_j \tag{9.1}$$

where the term associated with the largest eigenvalue μ_1 of the covariance matrix has been explicitly separated from the sum. The term associated with the largest eigenvalue makes the largest contribution to the expansion and therefore has the largest effect on the variation in the fundamental eigenfrequency. The Line-Sampling technique is based on an important direction in the parameter space, along which a performance function is evaluated at predefined values, and MC samples taken in the perpendicular direction. If this concept is applied to Equation 9.1 then the

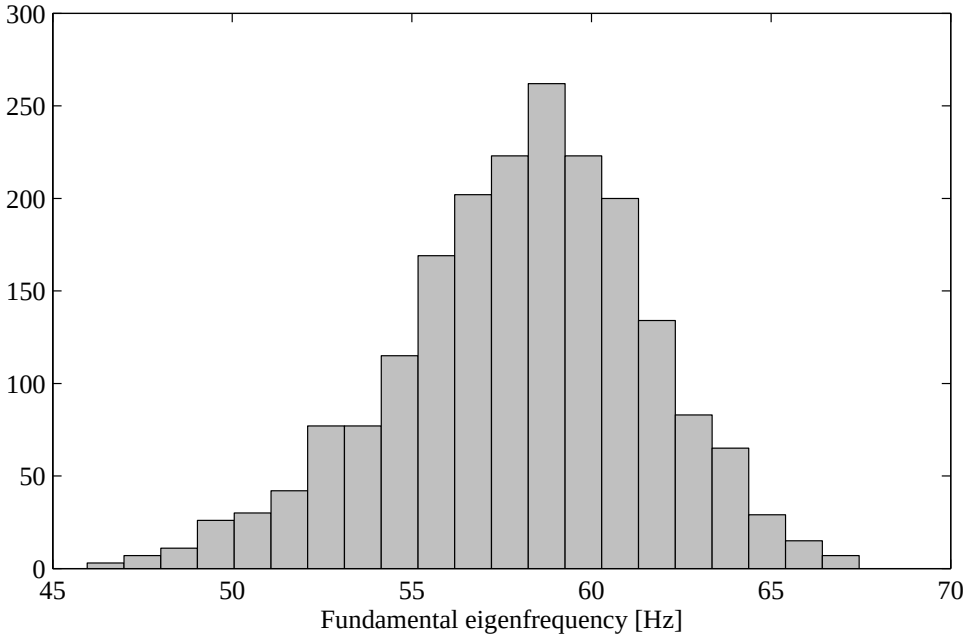

Figure 9.8: *Histogram of fundamental eigenfrequency of constrained windshield.*

parameter ζ_1 can be used to define the important direction. The parameters ζ_i are already standard normal (zero mean unit variance) random variables as used in the Line-Sampling procedure. First, a vector of discrete values for ζ_1 is defined arbitrarily, for example as $\zeta_1 = [-3 : 0.5 : 3]$ with a total of 13 values. Subsequently, for each value of ζ_1, a standard MC simulation with 5 runs is performed considering the $n - 1$ random variables $\zeta_i, i \neq 1$. Overall, the fundamental eigenfrequency is calculated for 13 x 5 = 65 realisations. The results are shown in Figure 9.9, where four different correlation lengths have been considered. The further analysis can be performed using any chosen correlation length, but the accuracy of the results will be different. The highest accuracy can be expected for the case of the largest correlation length (D), because the variation between the MC samples is small and the gradient of the curves is large.

The data in Figure 9.9 can be used to estimate the cdfs, which are shown in Figure 9.10. It can be seen that all cdfs have the same mean value (58 Hz), but the spread depends on the correlation length. For larger correlation lengths, the standard deviation of the fundamental eigenfrequency is larger and more extreme realisations are likely. This indicates that an extreme value of the fundamental eigenfrequency occurs if the stiffnesses are either high or low for all locations around the edge of the windshield.

The accuracy of these cdf estimates depends on the correlation length as discussed before. Figure 9.11 shows the CV of the LS estimator for an event with a probability of 5% based on $n = 10$ deterministic solutions, calculated from Equation

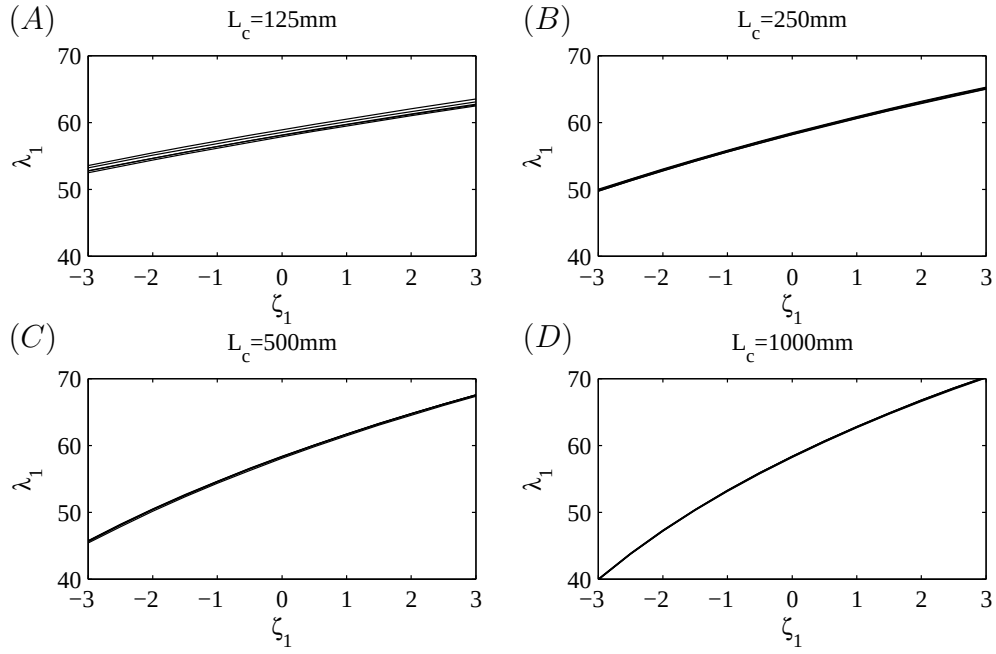

Figure 9.9: *Evaluation of the fundamental eigenfrequency along important direction* ζ_1 *for different correlation lengths.*

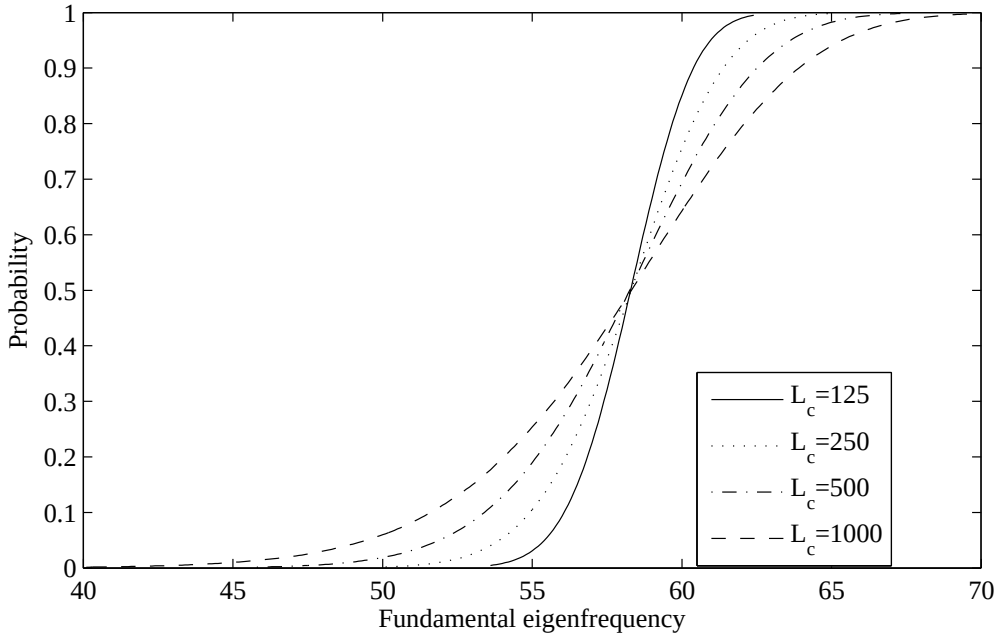

Figure 9.10: *Cumulative density functions of fundamental eigenfrequency estimated by LS approach, different correlation lengths.*

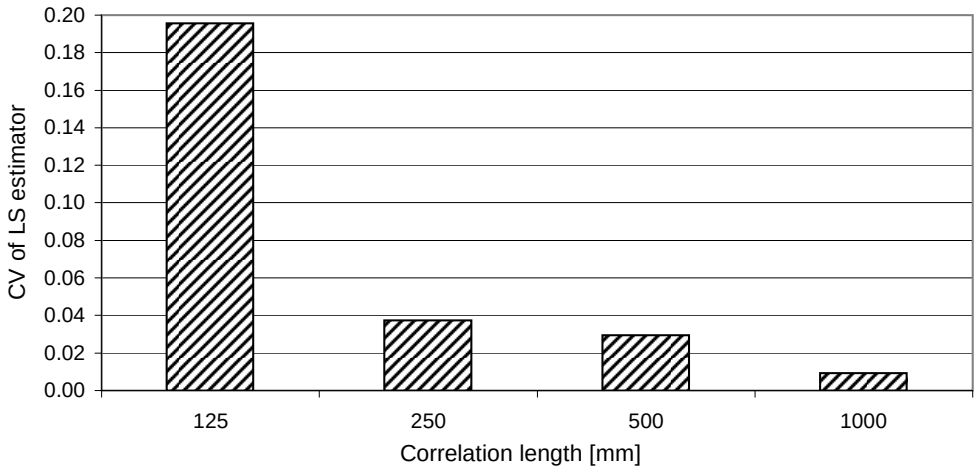

Figure 9.11: *Coefficient of variation of LS estimator for different correlation lengths based on 5% event and $n = 5$ samples.*

8.13. The accuracy increases with larger correlation lengths. The CV of the MC estimator for a 5% event is independent of the correlation length and about 9% based on $n = 2000$ samples. Figure 9.12 shows a comparison of the cdf estimates from the MC and LS approaches with $n = 2000$ and $n = 65$ required deterministic solutions respectively. The agreement is very good and it can be expected that the LS approach provides better results towards the tails of the distribution.

9.5 Discussion and concluding remarks

The use of a random field model for the spatial variation of thicknesses of a laminate windshield has been discussed. The theory of a simple Gaussian random field and its realisation using the KL representation was reviewed. The implementation within an existing deterministic FE model and standard FE software was shown to be straightforward. Experimental and numerical results were compared and the influence of the random field parameters was investigated. A Monte Carlo simulation approach is most appropriate to obtain the statistics of a response sample. The numerical cost can be reduced by using advanced sampling techniques.

The discretisation of the random field at the element level is convenient for implementation within existing FE models and software. This approximation is justified if the correlation length is large compared to the element size. Since a refinement of the FE mesh is in general easily done, this approach seems suitable for many applications.

The quantification of the random field suffers from the lack of experimental data. In particular, information about the correlation length is not known, which has been shown to be much more important than the type of correlation function (exponential,

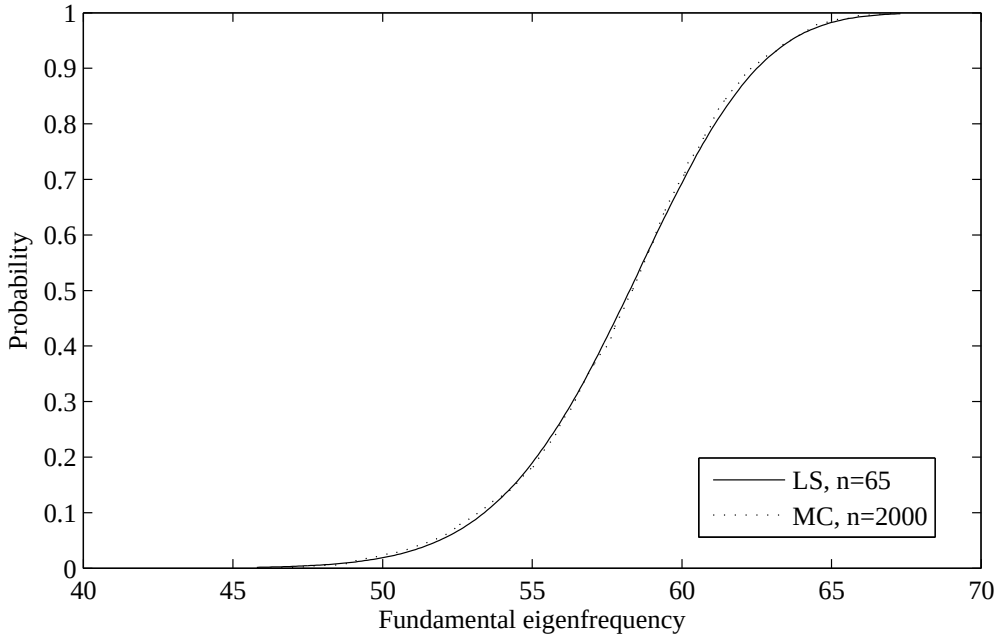

Figure 9.12: *Cumulative density function of fundamental eigenfrequency: comparison of MC (n=2000) and LS (n=65) approaches, same correlation length.*

triangular, Gaussian) [75]. A zero correlation length implies that the elements are statistically independent. For a large correlation length, the results converge to the case of total correlation, where all elements have the same properties. The influence of the correlation length on the dynamic response of the windshield can be fundamental. The maximum variation in the FRF is obtained if the thicknesses of elements are all at a maximum or minimum. If the correlation between elements is small, the probability that all thicknesses are near a maximum or minimum for the same realisation of the random field is very low. If the correlation length is large then the element thicknesses are all similar and it is more likely that all of them are large or small for the same realisation. The sample statistics in Figure 9.6 show the differences in the predicted response variation. If the correlation length is small enough, the effect of variation in thicknesses can be neglected.

The assumption of a homogenous isotropic random field is reasonable, if no other information about the manufacturing process is available. A Gaussian distribution has been assumed for convenience, which seems reasonable for the nature of the manufacturing process. The polymer layers mainly influence the acoustic properties of the automotive windshield and also introduce a substantial amount of uncertainty and variability. The change of material properties with temperature was not considered in this work. There are well-established relations for temperature and frequency dependent elastic properties of viscoelastic materials, which should be included. The spatial variation of material properties is due to product variability

and should be considered as well.

The use of a Monte Carlo simulation approach is often limited by the resources available (especially time), because the deterministic model has to be solved repeatedly. If events with small probability of occurrence are of concern, for example in a reliability analysis, the required number of evaluations can be much higher. In this context the LS technique was applied, which achieves the same accuracy as the standard MC approach in a lower number of runs. It was shown that the term associated with the largest contribution to the KL expansion is an appropriate choice for the important direction. However, it has to be noted that in this case the convergence of the LS estimator depends on the correlation length.

Chapter 10

Concluding remarks

This thesis concerned modelling approaches for the low-frequency analysis of built-up structures with non-deterministic properties. The uncertainties due to a lack of knowledge or the naturally inherent variation of properties in a numerical model are of growing concern in industry and research. It is recognised that these effects have to be taken into account in order to satisfy the increasing requirements towards product performance. The challenges for an analysis with non-deterministic properties were identified to be mainly the high numerical costs and the applicability and practicality of the approaches. The high numerical costs are due to the repeated analysis of a deterministic problem in most cases. The computational cost for one deterministic solution is already high, because at low frequencies detailed information about the response variation of the system is desired, which in turn requires a large finite element model. In this work various strategies to reduce the number of deterministic solutions and the computational cost for one deterministic solution were discussed.

First of all, any model reduction method is beneficial and can in general be combined with other probabilistic or possibilistic approaches. In the context of built-up structures, as is often the case in practice, the component mode synthesis method is most appropriate, and a comprehensive review of deterministic component mode synthesis approaches has been given. A number of original contributions were made regarding component mode synthesis as a framework for the analysis of built-up structures with non-deterministic properties. It has been shown that various possibilities and advantages arise from the multi-level quantification and propagation of uncertainties and the substructuring itself. These include the numerical costs as well as issues of applicability and practicality. Overall, the component mode synthesis method offers some physical insight in the analysis and can be effectively combined with other non-deterministic approaches.

The second class of methods to reduce the numerical costs concerns the application of approximate propagation methods. In a linear modal analysis, the eigenvalue

problem is often the computationally most expensive operation. For the reanalysis of the eigenvalue problem, it is often appropriate to replace it with perturbation or interpolation methods. Within this work, perturbational relations have been considered mostly within the component mode synthesis framework, which can in some cases reduce the numerical cost of an uncertainty analysis to that of a deterministic analysis. The accuracy of such numerically cheap approaches has to be seen in context with the level of uncertainty in the statistics of the input data and is therefore often acceptable.

The frequency response function in linear structural dynamic problems is often found by modal superposition. The numerical cost of deterministic modal superposition is very small. However, if there is uncertainty or variation in the modal properties, a non-deterministic problem has to be solved for every frequency considered. In this work novel contributions have been made to non-deterministic modal superposition, where the modal parameters are described either by probability density functions or intervals. In the latter case, it is appropriate to make conservative approximations in the modal space, independent of frequency, in order to calculate frequency response function envelops efficiently.

Finally, a reduction in the number of required reanalyses for probabilistic approaches has been considered. The Monte Carlo simulation method is often used as a reference solution, because it is robust and the Monte Carlo estimator converges to the exact results for a larger sample size. The numerical cost of such an analysis can be drastically reduced if advanced Monte Carlo methods are employed. In this thesis, the Line-Sampling technique has been reviewed and original contributions have been made for its application in structural dynamics. In general, the Line-Sampling method is as robust as the standard Monte Carlo method and the Line-Sampling estimator also converges to the exact solution for a large enough sample size. However, if some additional information about the system, such as parameter sensitivities, is known, then Line-Sampling achieves the same accuracy at a much smaller number of deterministic solutions.

Many non-deterministic properties in mechanical structures are varying spatially and can be appropriately modelled by random fields. The quantification of spatially varying uncertain properties in existing finite element models and software has been addressed in various applications.

All modelling approaches discussed in this thesis can be applied together. Component mode synthesis is applicable to the linear analysis of built-up structures and can be used to reduce the size of the model. At component level, spatially varying properties can be quantified by random field models. Alternatively, uncertainties can be quantified directly in terms of modal properties, for example from

experimental data. The influence of neglecting uncertainty in various properties, for example in component mode shapes, has been investigated. Perturbational relations can be applied at any level of the component mode synthesis framework, but seem most appropriate from component modal to component global properties. Subsequently, non-deterministic modal superposition is applied to estimate the variation in the physical frequency response of the structure. Finally, for most probabilistic propagations, the Line-Sampling method can be applied. The known characteristics of structural dynamic properties allow Line-Sampling to work very efficiently. Overall, all methods discussed provide some physical insight into the quantification and propagation of non-deterministic properties. The main focus is on reducing the computational costs and increasing the applicability. The introduced approximations and errors are transparent and can often be neglected in view of the level of uncertainty in the input parameters. In any case, the results of the baseline analysis are still available and have been enhanced with information concerning the more complex behaviour of the system.

10.1 Conclusions

The specific conclusions of this thesis are:

- The high numerical cost is a major challenge in the low-frequency uncertainty analysis of structures using the FE method.
- Approximate propagation methods based on perturbation and interpolation are appropriate to reduce the numerical cost.
  - Perturbation and linear sensitivity approaches are useful techniques if the change in a parameter is small and the change in the quantity of interest is small as well.
  - Approximation errors can often be neglected with respect to the level of uncertainty in the statistics of input data.
- Spatial variations of properties should be considered and can be appropriately modelled by random fields and the KL expansion.
  - A discretisation of the continuous random field at the element mesh using point discretisation methods is convenient for implementation within existing FE models and software.
  - The correlation length is the most important parameter of the random field model and influences the results and their accuracy in many applications.

- Deterministic model reduction can be used in an uncertainty analysis to reduce the numerical cost.
  - It is often an essential step in a low-frequency non-deterministic analysis, where the models are in general large.
  - The CMS method is appropriate for the modelling of built-up structures and their components.
- The CMS method provides a suitable framework for uncertainty quantification and propagation.
  - Several advantages arise from the fact that CMS introduces the component modal level as an additional coordinate system.
  - Each substructure can be treated independently.
  - The fixed-interface CMS method has further advantages due to the special structure of the global mass and stiffness matrices.
- The modal superposition method can be applied to non-deterministic modal data.
  - A definition of the modal space using a modal constant and the eigenvalue has advantages compared to the often-used definition of a specific modal mass and stiffness.
- LS is a numerically efficient approach that can often be applied instead of the MC method.
  - Its accuracy depends on the existence and identification of an important direction.
  - It can be applied efficiently to structural dynamics, e.g. for the evaluation of eigenfrequency and FRF distribution functions and statistics.

10.2 Suggestions for future work

Future work in order to extend the contents of this thesis should first of all concern the effects of further sources of uncertainty, such as damping and the properties of joints. The modelling of the effects of deterministic damping in structural dynamic models is a difficult problem and still a subject of basic research. Therefore, the uncertainty and variability in damping is often neglected and simple deterministic damping models are employed. However, for some cases the variation in damping

might be the most decisive factor for the variation in the response. In a modal analysis, it can be assumed that a change in damping only causes a change in response magnitude. Therefore, variability and uncertainty in damping could be considered independent of variations in eigenfrequencies and modeshapes at little extra cost. However, non-classical damping approaches have to be used for joints and other complex components. Most mechanical structures comprise some sort of joints and often the effects of the uncertainty in joints can be more important than other sources of uncertainty in a structure. There is a wide range of dynamic characteristics between different joints and the behaviour of joints often differs greatly from the behaviour of the rest of the structure. Furthermore, the influence of the joint properties depends on many factors such as the frequency of vibration. Novel approaches are required to assess the influence of joint uncertainty and include them in the modelling. A promising idea is to define characteristic joint properties, which are different from the physical properties, and to model the variation in the most important of them.

An important task for future work is the assessment of the numerical approaches in regards to their application to realistic engineering problems. Existing and newly developed methods have to be validated and tested. This could include benchmarks against other numerical methods and a comparison with experimental data. In this context it is important to assess what experimental data are likely or possible to be obtained in connection with an application case. Some theories and models for the quantification of non-deterministic effects (e.g. random fields) have been around for many decades, but the experimental data required to define them is often not available.

In a practical situation various sources and types of uncertainty are present in general. Therefore, a comprehensive framework for uncertainty modelling that makes used of all available individual methods should be provided. In this context, the full frequency range has to be considered. The combination of probabilistic and possibilistic data remains a challenge and further research is required regarding the modelling of hybrid data and the use of hybrid methods.

The work in this thesis concerns the forward propagation of non-deterministic data. In order to achieve the overall goal of a robust design of structures, this can be complemented with inverse propagation methods and optimisation techniques. In this context, it can be the case that the variation in the response is given and the corresponding variation in input parameters has to be found, which conforms to model updating under uncertainties. Similarly, the objective function in reliability-based design optimisation takes account of the variation in the properties of interest.

References

[1] Fahy, F. J., "Statistical energy analysis : a wolf in sheep's clothing?" *Inter-Noise 93*, Leuven, 1993.

[2] Kompella, M. and Bernhard, R. J., "Measurement of the statistical variation of structural-acoustic characteristics of automotive vehicles," *SAE Noise and Vibration Conference*, 1993.

[3] Hinke, L., Mace, B. R., and Waters, T. P., "Modelling uncertainty using non-deterministic modal superposition," *Ninth International Conference on Recent Advances in Structural Dynamics - RASD*, Southampton, UK, 2006.

[4] Hinke, L., Mace, B. R., and Waters, T. P., "Analysis of structures with uncertain parameters using component mode synthesis," *ISMA 2006*, Leuven, Belgium, 2006.

[5] Hinke, L., Pichler, L., Pradlwarter, H. J., Mace, B. R., and Waters, T. P., "A random field model for a laminate windshield," *Ninth International Conference on Recent Advances in Structural Dynamics - RASD*, Southampton, UK, 2006.

[6] Hinke, L., Mace, B. R., and Ferguson, N. S., "Uncertainty quantification and CMS: free and fixed-interface methodologies," *International Modal Analysis Conference - IMAC XXV*, Orlando, USA, 2007.

[7] Hinke, L., Mace, B. R., and Waters, T. P., "Estimating response distributions of uncertain dynamical systems using Line-Sampling," *First International Conference on Uncertainty in Structural Dynamics USD*, Sheffield, UK, 2007.

[8] Hinke, L., Mace, B. R., and Waters, T. P., "Propagation of Uncertainty in Structural Dynamics Using Component Mode Synthesis Methods," *NATO Advanced Vehicle Technology Symposium on Computational Uncertainty in Military Vehicle Design*, Athens, Greece, 2007.

[9] Petyt, M., *Introduction to Finite Element Vibration Analysis*, Cambridge University Press, 1990.

[10] Bathe, K. J., *Finite Element Procedures*, Prentice-Hall, Englewood Cliffs, 1997.

[11] Craig, R. R. J. and Kurdila, A. J., *Fundamentals of Structural Dynamics*, Wiley, 2006.

[12] Chopra, A. K., *Dynamics of Structures*, Prentice-Hall, 2001.

[13] Friswell, M. I. and Mottershead, J. E., *Finite Element Model Updating in Structural Dynamics*, Kluwer Academic Publishers, 1995.

[14] Oberkampf, W., DeLand, S., Rutherford, B., Diegert, K., and Alvin, K., "A new methodology for the estimation of total uncertainty in computational simulation," *40th AIAA/ASME/ASCE/AHS/ASC Structures, Structural Dynamics and Materials Conference*, 1999.

[15] Alvin, K., Oberkampf, W., Diegert, K., and Rutherford, B., "Uncertainty quantification in computational structural dynamics: a new paradigm for model validation," *16th International Modal Analysis Conference IMAC XVI*, 1998.

[16] Langley, R. S., "Natural frequency statistics and universality," *ICSV12*, Lisbon, 2005.

[17] Soize, C., "Random matrix theory and non-parametric model of random uncertainties in vibration analysis," *Journal of Sound and Vibration*, Vol. 263, 2003, pp. 893–916.

[18] Adhikari, S., "Matrix variate distributions for probabilistic structural dynamics," *AIAA Journal*, Vol. 45, No. 7, 2007.

[19] Soize, C., "A nonparametric model of random uncertainties for reduced matrix models in structural dynamics," *Probabilistic Engineering Mechanics*, Vol. 15, 2000, pp. 277–294.

[20] Soize, C., "A comprehensive overview of a non-parametric probabilistic approach of model uncertainties for predictive models in structural dynamics," *Journal of Sound and Vibration*, Vol. 288, 2005, pp. 623–652.

[21] Adhikari, S., "Uncertainty quantification and propagation using matrix variate distributions," *First International Conference on Uncertainty in Structural Dynamics USD*, Sheffield, UK, 2007.

[22] Hills, E., Mace, B. R., and Ferguson, N. S., "Response statistics of stochastic built-up structures," *ISMA*, Leuven, 2004.

[23] Hills, E., Mace, B. R., and Ferguson, N. S., "Response statistics of uncertain structures," *Inst. Acoustics Spring Conf*, Southampton, 2004.

[24] Brown, R. and Gear, J., "Dynamic variations within nominally identical product lines," Tech. rep., University of Auckland, 1999.

[25] Fahy, F. J. and Walker, J. G., *Advanced Applications in Acoustics, Noise and Vibration*, Spon Press, 2004.

[26] Lyon, R. H. and DeJong, R. G., *Theory and Application of Statistical Energy Analysis*, Butterworth-Heinemann, Newton, MA, USA, 2nd ed., 1995.

[27] Keane, A. J. and Price, W. G., *Statistical Energy Analysis: An Overview with Applications in Structural Dynamics*, Cambridge University Press, Cambridge, UK, 1997.

[28] Shorter, P. J. and Langley, R. S., "Vibro-acoustic analysis of complex systems," *Journal of Sound and Vibration*, Vol. 288, 2005, pp. 669–699.

[29] Langley, R. S., Lande, R., Shorter, P. J., and Cotoni, V., "Hybrid deterministic-statistical modelling of built-up structures," *ICSV12*, Lisbon, 2005.

[30] Moens, D., De Gersem, H., Desmet, W., and Vandepitte, D., "An overview of novel non-probabilistic approaches for non-deterministic dynamic analysis," *NOVEM*, 2005.

[31] Dong, W. M., Chiang, W. L., and Wong, F. S., "Propagation of uncertainties in deterministic systems," *Computers and Structures*, Vol. 25, No. 3, 1987, pp. 415–423.

[32] Dong, W. and Shah, H., "Vertex method for computing functions of fuzzy variables," *Fuzzy Sets and Systems*, Vol. 24, 1987, pp. 65–78.

[33] Manson, G., "Calculating frequency response functions for uncertain systems using complex affine analysis," *Journal of Sound and Vibration*, Vol. 288, 2005, pp. 487–521.

[34] Box, G. E. P., Hunter, W., and Hunter, U., *Statistics for experiments*, Series in Probability and Statistics, Wiley, 1978.

[35] Zadeh, L., "Fuzzy sets," *Information and Control*, Vol. 8, 1965, pp. 338–353.

[36] Möller, B. and Beer, M., *Fuzzy Randomness - Uncertainty in Civil Engineering and Computational Mechanics*, Springer Verlag, Berlin, 2004.

[37] Hanss, M., *Applied Fuzzy Arithmetic*, Springer, 2005.

[38] Hanss, M., "The transformation method for the simulation and analysis of systems with uncertain parameters," *Fuzzy Sets and Systems*, Vol. 130, 2002.

[39] Schuëller, G. I., "Computational stochastic mechanics - recent advances," *Computers and Structures*, Vol. 79, 2001, pp. 2225–2234.

[40] Schuëller, G. I., "A state of-the-art report on computational stochastic mechanics," *Probabilistic Engineering Mechanics*, Vol. 12, No. 4, 1997, pp. 197–321.

[41] Upton, G. and Cook, I., *Dictionary of statistics*, Oxford Paperback Reference, Oxford University Press, 2004.

[42] Vanmarcke, E., *Random fields: Analysis and Synthesis*, The M.I.T. Press, 1983.

[43] Ghanem, R. G. and Spanos, P. D., *Stochastic Finite Elements: A Spectral Approach*, Dover Publications, 2003.

[44] Loeve, M., *Probability Theory*, Springer-Verlag, 1977.

[45] Hammersley, J. M. and Handscomb, D. C., *Monte Carlo Methods*, Fletcher and Son Ltd., Norwich, 1967.

[46] Rubinstein, R. Y., *Simulation and the Monte Carlo Method*, Wiley, New York, 1981.

[47] Fishman, G. S., *Monte Carlo: Concepts, algorithms, and applications*, Springer Series in Operations Research, Springer-Verlag, Berlin, 1996.

[48] Sachdeva, S. K., Nair, P. B., and Keane, A. J., "Comparative study of projection schemes for stochastic finite element analysis," *Comput. Methods Appl. Mech. Engrg.*, Vol. 195, 2006, pp. 2371–2392.

[49] Nair, P. B. and Keane, A. J., "Stochastic reduced basis methods," *AIAA Journal*, Vol. 40, No. 8, 2002.

[50] Bae, H. R., Grandhi, R. V., and Canfield, R. A., "Uncertainty quantification of structural response using evidence theory," *43rd AIAA/ASME/ASCE/AHS/ASC Structures, Structural Dynamics, and Materials Conference*, Denver, Colorado, 2002.

[51] Worden, K., Manson, G., and Denoeux, T., "Evidence-based damage classification for an aircraft structure," *First International Conference on Uncertainty in Structural Dynamics USD*, Sheffield, UK, 2007.

[52] Lucas, C. and Araabi, B. N., "Generalization of the Dempster-Shafer theory: a fuzzy-valued measure," *IEEE Transactions on Fuzzy Systems*, Vol. 7, No. 3, 1999, pp. 255–270.

[53] Schuëller, G. I., Pradlwarter, H. J., and Koutsourelakis, P. S., "A critical appraisal of reliability estimation procedures for high dimensions," *Probabilistic Engineering Mechanics*, Vol. 19, 2004, pp. 463–474.

[54] Au, S. K. and Beck, J. L., "Important sampling in high dimensions," *Journal of Structural Safety*, Vol. 25, No. 2, 2003, pp. 139–163.

[55] Nie, J. and Ellingwood, R., "Directional methods for structural reliability," *Journal of Structural Safety*, Vol. 22, 2000, pp. 233.

[56] Au, S. K. and Beck, J. L., "Estimation of small failure probabilities in high dimensions by subset simulation," *Probabilistic Engineering Mechanics*, Vol. 16, 2001, pp. 263–277.

[57] Koutsourelakis, P. S., Pradlwarter, H. J., and Schuëller, G. I., "Reliability of structures in high dimensions, part I: algorithms and applications," *Probabilistic Engineering Mechanics*, Vol. 19, 2004, pp. 409–417.

[58] McKay, M. D., Beckman, R. J., and Conover, W. J., "A comparision of three methods for selecting values of input variables in the analysis of output from a computer code," *Technometrics*, Vol. 42, No. 1, 2000.

[59] Moens, D. and Vandepitte, D., "Fuzzy finite element method for frequency response function analysis of uncertain structures," *AIAA Journal*, Vol. 40, No. 1, 2002, pp. 126–136.

[60] Guyan, R. J., "Reduction of stiffness and mass matrices," *AIAA Journal*, Vol. 3, No. 2, 1965, pp. 380.

[61] Craig, R. R., J. and Bampton, M., "Coupling of substructures for dynamic analysis," *AIAA Journal*, Vol. 6, 1968, pp. 1313–1319.

[62] Saltelli, A., Chan, K., and Scott, E. M., *Sensitivity Analysis*, Wiley, 2000.

[63] Schuëller, G. I., Bucher, C. G., and Pradlwarter, H. J., "The response surface method - an efficient tool to determine the failure probability of large structural systems," *International Conference on Spacecraft Structures and Mechanical Testing*, Noordwijk, The Netherlands, 1991.

[64] Fox, R. L. and Kapoor, M. P., "Rate of change of eigenvalues and eigenvectors," *AIAA Journal*, Vol. 6, No. 12, 1968, pp. 2426–2429.

[65] Nelson, R. B., "Simplified calculation of eigenvector derivatives," *AIAA Journal*, Vol. 14, No. 9, 1976.

[66] Alvin, K. F., "Efficient computation of eigenvector sensitivities for structural dynamics," *AIAA Journal*, Vol. 35, No. 11, 1997.

[67] Adhikari, S. and Friswell, M. I., "Eigenderivative analysis of asymmetric non-conservative systems," *International Journal for Numerical Methods in Engineering*, Vol. 51, 2001, pp. 709–733.

[68] Mills-Curran, W. C., "Calculation of eigenvector derivatives for structures with repeated eigenvalues," *AIAA Journal*, Vol. 26, No. 7, 1988, pp. 867 – 871.

[69] Vessel, K., Ram, Y., and Pang, S.-S., "Sensitivity of repeated eigenvalues to perturbations," *AIAA Journal*, Vol. 43, No. 3, 2005, pp. 582 – 5.

[70] Adhikari, S., "Rates of change of eigenvalues and eigenvectors in damped dynamic system," *AIAA Journal*, Vol. 39, No. 11, 1999.

[71] Adhikari, S., "Derivative of eigensolutions of nonviscously damped linear systems," *AIAA Journal*, Vol. 40, No. 10, 2002.

[72] Bhaskar, A., "Gross modifications in structural dynamics via interpolated modes," *Seventh International Conference of Recent Advances in Structural Dynamics*, Southampton, UK, 2000.

[73] Bhaskar, A., Sahu, S. S., and Nakra, B. C., "Approximations and reanalysis over a parameter interval for dynamic design," *Journal of Sound and Vibration*, Vol. 248, No. 1, 2001, pp. 178–186.

[74] Brenner, C., *Ein Beitrag zur Zuverlässigkeitsanalyse von Strukturen unter Berücksichtigung von Systemunsicherheiten mit Hilfe der Methode der Stochastischen Finiten Elemente*, Ph.D. thesis, University of Innsbruck, 1995.

[75] Charmpis, D. C. and Schuëller, G. I., "The need for linking micromechanics of materials with stochastic finite elements: a challenge for material science." *NSF Workshop "Probability and Materials: From Nano- to Macro-Scale"*, Baltimore, 2005.

[76] Bah, M. T., Nair, P. B., Bhaskar, A., and Keane, A. J., "Stochastic component mode synthesis," *44th AIAA/ASME/ASCE/AHS Structures, Structural Dynamics, and Materials Conference, AIAA-2003-1750, Norfolk*, 2003.

[77] Sunar, M., "Encyclopedia of Vibration," Vol. 3, Academic Press, 2002, pp. 1332–1335.

[78] Bennighof, J. and Kim, C., "Adaptive multilevel substructuring method for efficient modeling of complex structures," *33rd AIAA/ASME/AHS/ASC Structures, Structural Dynamics, and Materials Conference*, 1993.

[79] Hurty, W. C., "Dynamic analysis of structural systems using component modes," *AIAA Journal*, Vol. 3, 1965, pp. 678–685.

[80] Craig, R. R., J. and Chang, C. J., "Free-interface methods of substructure coupling for dynamic analysis," *AIAA Journal*, Vol. 14, 1976, pp. 1633–1635.

[81] Craig, R. R., J., "Methods of component mode synthesis," *Shock and Vib. Digest*, Vol. 9, 1977, pp. 3–10.

[82] Craig, R. R., J., *Structural Dynamics - An Introduction to Computer Methods*, Wiley, 1981.

[83] Meirovitch, L., *Computational Methods in Structural Dynamics*, Sijthoff and Noordhoff, Alphen aan der Rijn, Netherlands, 1980.

[84] Hintz, R. B., "Analytical methods in component modal synthesis," *AIAA Journal*, Vol. 13, No. 8, 1975, pp. 1007–1016.

[85] Craig, R. R., J. and Chang, C. J., "On the use of attachment modes in substructure coupling for dynamic analysis," *AIAA/ASME 18th Struc., Struc. Dyn. and Materials Conf.*, San Diego, CA, 1977.

[86] Craig, R. R., J., "A review of time-domain and frequency-domain component mode synthesis methods," *Journal of Modal Analysis*, Vol. 2, No. 2, 1987, pp. 59–72.

[87] Craig, R. R., J., "Substructure methods in vibration," *Transactions of ASME*, 1995.

[88] Craig, R. R., J. and Chang, C. J., "A review of substructure coupling methods for dynamic analysis," *NASA CP-2001, National Aeronautics and Space Admin.*, Washington, DC, 1976.

[89] Castanier, M. P., Tan, Y. C., and Pierre, C., "Characteristic constraint modes for component mode synthesis," *AIAA Journal*, Vol. 39, No. 6, 2001.

[90] Tran, D. M., "Component mode synthesis methods using interface modes. Application to structures with cyclic symmetry." *Computers and Structures*, Vol. 79, 2001, pp. 209–222.

[91] Balmes, E., "Use of generalized interface degrees of freedom in component mode synthesis." *International Modal Analysis Conference - IMAC*, 1996.

[92] Cuppens, K., Sas, P., and Hermans, L., "Evaluation of the FRF based substructuring and modal synthesis technique applied to vehicle FE data," *ISMA 25*, Leuven, 2000.

[93] Iankov, R., Moens, D., Sas, P., and Hermans, L., "Propagation of variances of FRFs through FRF-based coupling calculations," *ISMA*, Leuven, 2002.

[94] Lim, T. C. and Li, J., "A theoretical and computational study of the FRF-based substructuring technique applying enhanced least square and TSVD approaches." *Journal of Sound and Vibration*, Vol. 231, No. 4, 2000, pp. 1135–1157.

[95] Mace, B. R. and Shorter, P. J., "A local modal/perturbational method for estimating frequency response statistics of built-up structures with uncertain properties," *Journal of Sound and Vibration*, Vol. 5, No. 242, 2001, pp. 793–811.

[96] De Gersem, H., Moens, D., Desmet, W., and Vandepitte, D., "On the use of deviatoric component modes for the assessment of uncertainty in component mode synthesis." *First International Conference on Uncertainty in Structural Dynamics USD*, Sheffield, UK, 2007.

[97] Moens, D. and Vandepitte, D., "A fuzzy finite element procedure for the calculation of uncertain frequency response functions of damped structures: Part 1 - Procedure." *Journal of Sound and Vibration*, Vol. 288, 2005, pp. 431–462.

[98] Ewins, D. J., *Modal Testing - Theory, Practice and Applications, Second Edition*, Research Studies Press Ltd., 2001.

[99] Metropolis, N. and Ulam, S., "The Monte Carlo method," *Journal of the American Statistical Society*, Vol. 44, 1949, pp. 335–41.

[100] Schuëller, G. I. and Stix, R., "A critical appraisal of methods to determine failure probabilities," *Structural Safety*, Vol. 4, 1987, pp. 293–309.

[101] Pellissetti, M. F., Pradlwarter, H. J., and Schuëller, G. I., "Reliability analysis of large FE-systems using Line Sampling," *ICOSSAR 2005*, 2005.

[102] Pradlwarter, H. J., Pellissetti, M. F., and Schuëller, G. I., "Sensitivity and uncertainty in complex FE-models," *ICOSSAR 2005*, 2005.

[103] Scionti, M. and Lardeur, P., "Experimental and numerical study of the intra/inter variability of an acoustic windscreen," *International Conference on Noise and Vibration - ISMA 2006*, Leuven, Belgium, 2006.

[104] Scigliano, R., Scionti, M., and Lardeur, P., "Intra variability and predictive capability of windscreen finite element models in structural dynamics," *First International Conference on Uncertainty in Structural Dynamics USD*, Sheffield, UK, 2007.

[105] Lardeur, P. and Scionti, M., "Verification and validation of finite element models for the vibrational behaviour of a windscreen in presence of variability," *International Conference on Noise and Vibration - ISMA 2006*, Leuven, Belgium, 2006.